აჭარის ავტონომიური რესპუბლიკის განათლების, კულტურისა და სპორტის სამინისტრო
MINISTRY OF EDUCATION, CULTURE AND SPORT OF AJARA AUTONOMOUS REPUBLIC

JAPMED' 11 BATUMI-2019

BATUMI SHOTA RUSTAVELI STATE UNIVERSITY

11th Japanese-Mediterranean Workshop Applied Electromagnetic Engineering for Magnetic, Superconducting, Multifunctional and Nanomaterials

BOOK OF ABSTRACTS

16-19 JULY, 2019

BATUMI SHOTA RUSTAVELI STATE UNIVERSITY

JAPMED' 11

11th Japanese-Mediterranean Workshop Applied Electromagnetic Engineering for Magnetic, Superconducting, Multifunctional and Nanomaterials

BOOK OF ABSTRACTS

16-19 JULY, 2019

ISBN 978-9941-462-97-9

CALL FOR PAPERS

CALL FOR PAPERS

Prospective authors are invited to submit electronically previously unpublished papers relevant to the workshop topics.

Papers will be reviewed upon two page extended abstracts, to be included in the Workshop Proceedings.

Authors of accepted extended abstracts will be encouraged to submit a full version (up to 6 pages) of the papers at the Workshop, which will be reviewed for inclusion in special Issues of “Nanotechnology Perceptions” and “Journal of Biological Physics and Chemistry”.

For instructions on preparation of extended abstracts please consult the Workshop Web site:

http://japmed11.bsu.edu.ge

For further information, please contact the Conference Secretariat.

CONFERENCE SECRETARIAT

L.Kalandadze (Batumi Shota Rustaveli State University, Batumi, Georgia)
I. Jabnidze (Batumi Shota Rustaveli State University, Batumi, Georgia)
N. Japaridze (Batumi Shota Rustaveli State University, Batumi, Georgia)

Tel: +995 422 271797
Fax/Tel: +995 422 271797
Email: japmed11@bsu.edu.ge
gomidze@bsu.edu.ge

TOPICS

The scope of the Workshop includes: Advances in Analysis, Characterization and Manufacturing of Advanced Materials (Magnetic, Superconducting, Multifunctional and Nanostructured Materials).

The topics related to new developments are:

• Computational electromagnetics
• Generation by renewable energy sources
• Magnetohydrodynamics
• Losses analysis
• Devices (magnetic circuits, transformers, electrical machines, micro-machines)
• Magnetic material processing
• Magnetic material characterization
• Perspectives of high -Tc superconductors
• Modelling of superconductive properties
• Characterization techniques
• Processing of bulk superconductors
• Processing of thin and thick film superconductors
• Applications in energy (electricity/electronics, green energy), environment and transportation (levitation, electrical/ magnetic machines, flywheels, HTS/metal junctions, shielding, SQUIDS)
• Computational materials science
• Multifunctional materials for energy conversion
• Nanotechnology
• Nanostructured materials, nanocomposites
• Ultraprecision engineering (static to shock loading)
• Biomedical engineering
• Modern advanced industrial technologies (Problems of “Industry-4.0”)
• Mathematics and it’s Applications

PRESENTATION

The Eleventh Japanese-Mediterranean Workshop on Applied Electromagnetic Engineering for Magnetic, Superconducting, Multifunctional and Nanomaterials (JAPMED’10) is continuing and extending the successful previous events: two Japanese-Greek Joint Workshops held in Athens, Greece (1999) and Oita, Japan (2001), followed by seven Japanese-Mediterranean Joint Workshops

held in Athens, Greece (2003), Cairo, Egypt (2005), Larnaca, Cyprus (2007), Bucharest, Romania (2009), Budapest, Hungary (2011), Athens, Greece (2013), Sofia, Bulgaria (2015) and Izmir, Turkey (2017), respectively.

The aim of this Conference is to create a link for the participants to share knowledge and experience and for the cross-fertilization of new ideas and developments in applied electromagnetics, design, analysis, new material (magnetic, superconducting, multifunctional, nanomaterials) utilization, static- to shock-processing from macro-, micro-, to nanoscale and optimization techniques, including applications related to advanced manufacturing, ultraprecision engineering, nanotechnology, biomedical engineering, transport, energy and environment. Topics related to practical applications, operation, maintenance are also highly encouraged.

The JAPMED'11 will be jointly organized by the: Japan Society of Applied Electromagnetics and Mechanics (JSAEM); Project Center for Nanotechnology and Advanced Engineering (PC-NAE), a joint initiative of the Greek National Center for Scientific Research "Demokritos" and the Russian Research Center "Kurchatov Institute"; National Technical University of Athens (NTUA), Greece; Texas A&M University (TAMU), USA; University of Nevada, Reno (UNR), USA; Izmir Institute of Technology (IZTECH), Turkey; Beijing Institute of Technology (BIT), P.R. China; Batumi State University (BSU) and Georgian Technical University (GTU).

EXECUTIVE COMMITTEE

INTERNATIONAL ADVISORY COMMITTEE MEMBERS

A. Taşdemirci (Izmir Institute of Technology, Turkey)
N. Thadhani (Georgia Institute of Technology, USA)
R. Tomoshige (Sojo University, Japan)
V. Tonkonogy (Odessa Nacional Technical Universitet., Ukraine)
L. Tovazhnyansky (NTU “Kharkov Polytechnic Institute”, Ukraine)
Ç. Vakıfahmetoglu (Izmir Institute of Technology, Turkey)
I. Yatchev (Technical University of Sofia, Bulgaria)
Q. Zhou (Beijing Institute of Technology, P.R. China)
X. Zhu (University of Nevada, Reno, USA)

TECHNICAL PROGRAM COMMITTEE

Chairman
T. Sawada (Keio University, Japan)

Members
A. Kladas (National Technical University of Athens, Greece)
E. Hristoforou (National Technical University of Athens, Greece)
P. Kervalishvili (Georgian Technical University, Georgia)
R. Turmanidze (Georgian Technical University, Georgia)
K. Spentzas (Euro-Mediterranean Academy, Greece)

LOCAL ORGANIZING COMMITTEE

Chairman
N. Gomidze (Batumi Shota Rustaveli State University, Georgia)

Members
T. Siradze (Batumi Shota Rustaveli State University, Georgia)
N. Tsiklashvili (Batumi Shota Rustaveli State University, Georgia)
Z. Sikharulidze (Batumi Shota Rustaveli State University,Georgia)
M. Metreveli (Batumi Shota Rustaveli State University, Georgia)
L. Turmanidze (Batumi Shota Rustaveli State University,Georgia)
M. Giorgadze (Batumi Shota Rustaveli State University, Georgia)

Opening Welcoming Address

ძვირფასო Rector of the Batumi Shota Rustaveli State University Professor Merab Khalvashi, ბატონო Chairman of the Government of the Ajara Autonomous Republic Mr.Tornike Rizhvadze, ქალბატონო Minister of Education, Culture and Sport, Ms. Maia Khajishvili, Distinguished Colleagues and Dear Undergraduate and Graduate Students. As Honorary Chairman of the Executive Committee, it is my great pleasure to warmly welcome all of you to the 11th Japanese-Mediterranean Workshop on Applied Electromagnetic Engineering for Magnetic, Superconducting, Multifunctional and Nano Materials a landmark in development of materials, advanced manufacturing and electrical engineering. This Conference, held every two years, is jointly organized this year by the Project Center for Nanotechnology and Advanced Engineering, a joint initiative of the Greek National Center for Scientific Research "Demokritos" and the Russian Research Center "Kurchatov Institute", the Japan Society of Applied Electromagnetics and Mechanics, the two high level American Universities Texas A&M and University of Nevada Reno, the Faculty of Electrical Engineering and Electronics of the National Technical University of Athens, the Izmir Institute of Technology, Turkey, the Beijing Institute of Technology, P.R. of China and the two leading Georgian Universities, the Batumi Shota Rustaveli State University and the Georgian Technical University.

The JAPMED has been originated in the late 90's, actually we celebrate this year its 20th Anniversary, from the previous, very successful, *1st and 2nd Japanese - Greek Joint Workshops*, held in Athens, Greece in May 1999 and Oita, Japan in May 2001, respectively. Subsequently, it was extended to further wide International participation and cooperation, with the 3rd Event hosted in Athens, Greece in May 2003, the 4th in Cairo, Egypt in September 2005, the 5th in Larnaca, Cyprus in September 2007, the 6th in Bucharest, Romania in July 2009, the 7th in Budapest, Hungary in July 2011, the 8th in Athens, Greece in June 2013, the 9th in Sofia, Bulgaria in July 2015 and the 10th in Izmir, Turkey in July 2017. This Conference provides a forum for specialists from *Universities*,*Research Centers* and *Industry* of various Countries worldwide to establish cooperation, to share knowledge and experience and the cross-fertilization of new ideas and developments in the *design, analysis, new materials utilization and optimization techniques* in the broad areas of *electromagnetics and advanced manufacturing of advanced materials and their industrial sustainable applications*, in the modern technological sectors: *precision / ultraprecision engineering, nanotechnology, powder production* and processing associated *with high strain-rate phenomena, electricity and electronics, bioengineering, transportation, safety and defense, energy and environment*. From the very beginning, the *high- and low-temperature superconductivity* constituted the first preferential subject of the Conference, focusing on the recent progress in physics, mechanics, materials and applications of high- and low- temperature superconductors, with a projection to the emerging and future areas in science and technology. *Magnetic materials*, such as *magneto-resistance and ferroelectric materials*, as well as

conventional ferromagnetic materials and electromagnetics, constitute the second preferential subject, with results that appear to exhibit a breakthrough either conceptually or in the applications they generate. The scope of the Conference has been further expanded over the years towards *advanced manufacturing* to include the modern advanced technological fields: *nanotechnology, precision / ultraprecision manufacturing, biomedical engineering and transport*, whilst, six years ago, two additional topics have been included, namely: the *multifunctional materials*, in relation also to *computational mechanics*, i.e. the interests of the then International Institute for Multifunctional Materials for Energy Conversion (IIMEC) of the Texas A&M University, and the *shock loading of materials and structures*, as a part of the that time established *Shockwaves Cluster*, involving cooperation between Greece, Russia, USA, Germany, Japan, China, Hungary, Ukraine, Turkey and India. The purpose of this international cooperation is the strong belief that we have to enhance our efforts and cooperation towards these advanced technologies, which may greatly affect our lives in the future.

Since *sustainability* prevails in science, technology, industry and many other parts of human life, as a follow-up of my *Sustainability Award* for the *SIPS 2018 Mamalis International Symposium on Advanced Manufacturing of Advanced Materials and Structures with Sustainable Industrial Applications* last November in Rio de Janeiro, I have incorporated it in the JAPMED topics, with the aim to further enhancing our international collaboration.

Although the world financial crisis has also affected the much higher expected participation in this Conference, my Georgian Colleagues and I will do our best to demonstrate the famous Georgian and Balkan hospitality, not sparing any effort to make your stay in this beautiful Country memorable. I am sure that your participation in this Conference is going to be an exciting experience with many benefits to all of us.

დიდი მადლობა	Arigato	Xièxiè	Спасибо
Teşekkür Ederim	Danke Schön	Thank you	Ευχαριστώ

Academician Prof. Dr-ing, Dr.h.c. Prof.h.c. A.G. Mamalis
Honorary Chairman of the JAPMED'11

PROGRAM

PROGRAM OF THE ELEVENTH JAPANESE-MEDITERRANEAN WORKSHOP ON APPLIED ELECTROMAGNETIC ENGINEERING FOR MAGNETIC, SUPERCONDUCTING, MULTIFUNCTIONAL AND NANO MATERIALS (JAPMED'11)

TUESDAY, JULY 16th

14:00 – 16:00 **Registration**

16:00 – 17:00 Opening Session
Chair: N. Gomidze

16:00 – 16:30 **Welcome Address:** Honorary Chairman of the JAPMED'11, Prof. A.G. Mamalis
Welcome Address: Chairman of the JAPMED'11, Prof. M. Enokizono
Welcome Address: President of the JSAEM, Prof. Y. Ido
Welcome Address: Rector of the Batumi Shota Rustaveli State University, Prof. M. Khalvashi
Welcome Address: Government Chairman of the Ajara Autonomous Republic, Mr.T. Rizhvadze
Welcome Address: Minister of Education, Culture and Sport, Ms. M. Khajishvili
Welcome Address: Chairman of FLOGEN Star OUTREACH, Dr. F. Kongoli

16:30 – 17:00 **Plenary Presentation (111): Advanced Manufacturing of Advanced Materials from Macro- to Nanoscale under Static to Shock Loading: Principles and Industrial Sustainable Applications**
A.G. Mamalis
PC-NAE, NCSR "Demokritos", Athens, Greece

17:00 – 18:30 Oral Session A: High Strain-Rate Phenomena / Impact to Shock Loading
Chair: E. Maragakis

17:00 – 17:30 **Keynote Presentation (35): The Effect of Velocity, Imperfection and Material Models on the Crushing of Aluminum Corrugated Structure**
M. Güden, M. Sarıkaya, İ. Canbaz, A. Taşdemirci
Izmir Institute of Technology, Turkey

17:30 – 17:50 **A1 (87): Structure and Mechanical Properties of Multilayer Metal-Intermetallic Composites Fabricated by Explosive Welding and Annealing**
Z. Sheng, PW Chen, Q. Zhou
Beijing Institute of Technology, PR of China

17:50 – 18:10 **A2 (101): Advanced Explosive Metalworking Industrial Technologies**
A. Szalay, A.G. Mamalis, I. Zador
S-Metalltech 98 Materials R&D Ltd., Budapest, Hungary

18:10 – 18:30 **A3 (33): Syntheses of Ti-Al-Si-B-C Nanocomposites by Mechanical Alloying and Explosive Compaction**
M. Chikhradze, F D.S Marquis, N. Chikhradze, G. Abashidze, A. Gigineishvili, T. Bzhalava
Georgian Technical University, Tbilisi, Georgia

19:30 – 22:00 **Welcome Informal Dinner and Entertainment (Beachfront)**

WEDNESDAY, JULY 17th

08:00 – 08:30 **Registration**

08:30 – 10.40 Oral Session B: Electromagnetic Engineering
Chair: T. Prikhna

08:30 – 09:00 **Keynote Presentation (85): Vector Magnetic Hysteresis Characteristics of Electrical Steel Sheet**
M. Enokizono, D. Wakabayashi, Y. Kai
Vector Magnetic Characteristic Technical Laboratory, Usa-city, Japan

09:00 – 09:20 **B1 (12): Diagnosis of Dynamic Eccentricity Fault in Inverter-Fed Permanent Magnet Synchronous Motor Based on Zero Sequence Voltage Component**

J. Faiz, M.S. Bozorgian, E. Mazaheri-tehrani
University of Tehran, Tehran, Iran

09:20 – 09:40 **B2 (99): Noncontact Iron Loss Measurement of Motor Stator Core Using Radiation Thermometer in the Atmosphere**
D. Wakabayashi, M. Oka, M. Enokizono
Nippon Bunri University, Oita, Japan

09:40 – 10:00 **B3 (23): Simple Method for Micro Flow Generation Using Magnetic Fluid and Small Cubic Permanent Magnet**
S.Sudo, M.Ito
Akita Prefectural University, Japan

10.00 – 10:20 **B4 (40): Iron Loss Evaluation for a Small High-Efficiency Motor Stator Core Made of an Ultrathin Electrical Steel Sheet under PWM Inverter Excitation Using the Stator Windings Excitation Method**
M. Oka, M.Enokizono, D. Wakabayashi, H. Kiyotake
National Institute of Technology, Oita, Japan

10.20 – 10.40 **B5 (27): Characteristics Comparison of Self-Propelled Rotary Actuator in Consideration of Shape and Rolling Direction of Steel Sheets**
N. Soda, T. Kawano, M. Enokizono
Ibaraki University, Japan

10:40 – 11:10 Coffee Break

11:10 – 13:20 Oral Session C: Applications in Energy and Transportation - I
Chair: M. Enokizono

11:10 – 11:40 **Keynote Presentation (64): Structure and Pinning Centers in MgB2 Bulks, Wires, Thin Films and MT-YBCO**
T. Prikhna, M. Eisterer, V. V. Romaka, A. G. Mamalis, A. Jouline, J. Rabier, S. S. Ponomaryov, M. V. Karpets, M. Rindfleisch, M. Tomsic, A.V. Kozyrev, V.E. Moshcchil, A.V. Shaternik
Bakul Institute for Superhard Materials of the National Academy of Sciences of Ukraine (NASU), Kiev, Ukraine.

11:40 – 12:00 **C1 (100): Oscillation Amplitude Reduction of a High-Tc Superconducting Levitation System by an Electromagnetic Shunt Damper Coupled Nonlinearly**
T. Sugiura
Keio University, Yokohama, Japan

12:00 – 12:20 **C2 (66): Estimation Scintillation Index on a Superconductor Receiver for Gaussian Laser Beam Propagated Trough Random Phase Screen**
N. Kh. Gomidze, I. N.Jabnidze, K.A.Makharadze, M.R.Khajishvili, L.G.Kalandadze, O.Nakashidze, E.N.Mskhaladze
Batumi Shota Rustaveli State University, Batumi, Georgia

12:20 – 12:40 **C3 (115): Parameter Identification of Nonlinear Dynamic Systems of Industrial Processes**
B. Shanshiashvili, N. Kavlashvili
Georgian Technical University, Tbilisi, Georgia

12:40 – 13:00 **C4 (36): Novel Electrical Approach to Protect PV Modules under Various Partial shading situations**
H. Hanifi, M. Pander, B. Jaeckel, J. Schneider, A. Bakhtiari, W. Maier
Fraunhofer Center for Silicon Photovoltaics CSP, Halle (Saale), Germany

13:00 – 13:20 **C5 (31): Investigation of Thermal Insulation for Static Cryostats of HTSC Devices**
L.I. Chubraeva, S.S. Timofeyev
Institute of Electrophysics and Electric Power Engineering of RAS, Saint-Petersburg, Russia

13:20 – 14:50 Lunch Break

14:50 – 16:30 Oral Session D: Applications in Energy and Transportation - II
Chair: P. Kervalishvili

14:50 – 15:20 **Keynote Presentation (60): Stress Distribution Monitoring and Rehabilitation in Ferrous Steels**

S. Aggelopoulos, X. Vourna, A. Ktena, A. G. Mamalis, E. Hristoforou
National Technical University of Athens, Greece

15:20 – 15:40 **D1 (98): Refunction Techniques of Electrical Steel Sheets by Secondary Current Heating for High Efficiency Motors**
Y. Tsuchida, M. Enokizono
Oita University, Oita, Japan

15:40 – 16:00 **D2 (55): Development of Travelling Wave Propulsion Mechanism with Permanent Magnet Vibration Motor**
K. Kasuga, I. Murakami, M. Ono, Y. Ando
Gunma University, Kiryu, Japan

16:00 – 16:20 **D3 (46): Transport Characteristics of a Transport DeviceComposed of Two Magnetically-Driven Systems Using a Temperature-sensitive Magnetic Fluid**
Y. Ido, Y. Iwamoto, G. Ichinose, K. Odai
Nagoya Institute of Technology, Japan

16:20 – 16:40 **D4 (26): Torque Properties Analysis of Magnetic Harmonic Gear with Stackable Structure**
L T. Kurahashi, Y. Ando, R. Takei, K. Yonezawa, I. Murakami, A. Tomura
Gunma University, Tenjin-cho, Kiryu, Japan

16:40 – 17:00 **D5 (57): Development of 2 DOF Linear Oscillatory Actuator for Vibration Control**
F. Kitayama, R. Kondo
Ibaraki University, Japan

17:00 – 17:30 Coffee Break

17:30 – 19:30 Oral Session E: Multifunctional, Composite and Magnetic Nanomaterials
Chair: M. Güden

17:30 – 17:50 **E1 (107): Fatigue Corrosion Behavior of NiTi Shape Memory Alloy**
M. Mohajeri, H. Castanedaa, D.C. Lagoudas
Texas A&M University, College Station, TX, USA

17:50 – 18:10 **E2 (105): Modeling of Internal Damage Evolution During Actuation Fatigue in Shape Memory Alloys**
F.R. Phillips, D.T. Martin, D.C. Lagoudas
Texas A&M University, College Station, TX, USA

18:10 – 18:30 **E3 (38): Ceramic Composites Based on Functionalized Graphene Oxide and Alumina**
G.G. Bokuchavaa, E.E. Sanaiab, T.N. Archuadzec, T.V. Kuchukhizded, N.T Jalagoniae
Ilia Vekua Sukhumi Institute of Physics and Technologies, Tbilisi, Georgia

18:30 – 18:50 **E4 (30): Studying Electro-Physical and Mechanical Properties of SNO_2- SB_2O_3-C Ceramic-Based Composite Material**
S. S. Dobromyslov, V. I. Kirko, V.A. Razumovskaya
Siberian Federal University, Krasnoyarsk, Russia

18:50 – 19:10 **E5 (39): Influence of the Size, Shape and Concentration of Magnetic Particles on the Optical Properties of Nano Nickel Thin Films**
L.G. Kalandadze, O.M. Nakashidze, N.KH. Gomidze, I.N. Jabnidze
Batumi Shota Rustaveli State University, Batumi, Georgia

19:10 – 19:30 **E6 (68): Rheological Properties of Magnetized Bidisperse Magnetorheological Fluids Containing Needle-Like Particles**
Y. Iwamoto, T. Koroki, Y. Ido, H. Yamamoto, H. Nishida, Y. Fujii, T. Deguchi
Nagoya Institute of Technology, Nagoya, Japan

THURSDAY, JULY 18th

09:00 – 11.00 Oral Session F: Advanced Industrial Technologies
Chair: N. Chikhradze

09:00 – 09:20 **F1 (108): Generating Analytical Fragility Curves for Gypsum Partition Walls with Different Aspect Ratios**
E. Maragakis
University of Nevada, Reno, Nevada, USA

09:20 – 09:40 **F2 (67): Electrical Consolidation under Pressure for Al_2O_3 and WC, SiC Nanodisperse Powders**
E.S. Gevorkyan, A.G. Mamalis, Y.G. Gutsalenko
Ukrainian State University of Railway Transport, Kharkov, Ukraine

09:40 – 10:00 **F3 (78): Design of High Speed Interior Permanent Magnet Type Motor for Turbo-Machinery**
Y. Okada, F. Kitayama R. Kondo
Ibaraki University, Hitachi, Japan

10:00 – 10:20 **F4 (44): Influence of Plasma Based Ion Implantation and Deposition Method on Structure, Internal Stress, Mechanical Properties of Nano-Crystalline Bioinert ZrN Coatings**
A. Taran, I. Garkusha, V. Taran, R. Muratov,V. Starikov, A. Baturin, S. Romaniuk, A.G. Mamalis
Institute of Plasma Physics of NSC KIPT, Kharkov, Ukraine

10:20 – 10:40 **F5 (13): Neutron Sensors Based on Silicon-Graphene Nanosystems Enriched by Boron10 Isotope**
P.Kervalishvili, R. Turmanidze, T. Berberashvili, L. Chakhvashvili
Georgian Technical University, Tbilisi, Georgia

10:40 – 11:00 **F6 (71): The Effect of Magnetic Field on the Destruction Petroleum Emulsion**
N. Mamulaishvili, G. Partskhaladze, G. Chavleshvili , O. Janelidze
Batumi Shota Rustaveli State University, Georgia

11:00 – 11:30 Coffee Break

11:30 – 12:40 Oral Session G: Material Synthesis, Measurements and Characterization
Chair: Y. Ido

11:30 – 12:00 **Keynote Presentation (25): Strong Effect of Multiplicity Fluctuations in Rare-Earth Cobaltites on Magnetic, Electronic and Crystal Structure Properties**
S.G. Ovchinnikov, V.A. Dudnikov, Yu.S. Orlov, M. V. Gorev
Kirensky Institute of Physics, Federal Research Center, Krasnoyarsk, Russia

12:00 – 12:20 **G1 (92): Polyvalent Iron Oxide Magnetic Nanopowders Synthesized by Electroerosion Dispersion for Microwave Absorbing Coatings**
T. Prikhna, M. Monastyrov, A.G. Mamalis, B. Halbedel, S.S. Ponomaryov, V. Moshchil, O. Prysiazhna
Bakul Institute for Superhard Materials of the National Academy of Sciences of Ukraine (NASU), Kiev, Ukraine

12:20 – 12:40 **G2 (15): Clusters – Particles Balance in Matter by Dynamic Fractals**
A. Bakhtiari, T. Berberashvili, P. Kervalishvili
Georgian Technical University, Tbilisi, Georgia

12:40 – 14:10 Lunch Break

14:10 – 15:50 Oral Session H: Sustainability: Principles and Applications
Chair: A.G. Mamalis

14:10 – 14:40 **Keynote Presentation (102): A Sustainable World Population**
J. Ramsden, A.A. Mamali, N.T. Athanassoulis
The University of Buckingham, England

14:40 – 15:10 **Keynote Presentation (91): Science and Technology–The Grand Disruptors and Solution Providers**

F. Kongoli
FLOGEN Star OUTREACH, Canada

15:10 – 15:30 **H1 (103): Prosumer Communities Piloting Smart Cities Development: The Case of the First Near-Zero Energy Smart Home of Greece**
N.T. Athanassoulis, A. Tsakanikas, D. Tzovaras
National Technical University of Athens, Greece

15:30 – 15:50 **H2 (104): Statistical Analysis of the Global Competitiveness Index (GCI) of Georgia**
R. Turmanidze, P. Dašić, G. Popkhadze
Georgian Technical University, Tbilisi, Georgia

15:50 – 16:30 Coffee Break / Conference Photo

16:30 – 18:30 Poster Session (P)
Chair: T. Sawada, R. Turmanidze, P. Kervalishvili

P1 (96): Overhead Transmission Lines Impact Evaluation on Human Presence
T. Damatopoulou, A.G. Kladas
National Technical University of Athens, Greece

P2 (95): Optimal Design Methodology Based on Sensitivity Analysis for Marine Electric Propulsion Salient Pole Synchronous Motors
A.P. Moschoudis, A. G. Kladas, G.J. Tsekouras
National Technical University of Athens, Greece

P3 (94): Development of Vehicle Detection System Using Geomagnetic Level Sensor
K. Oka, S. Kiyofuji, A. Harada, Y. Kumagai
Kochi University of Technology, Japan

P4 (86): C-V Characterization and Electric Parameters of ZrO_2 Received by UV Stimulated Plasma Anodizing
A. Bibilashvili, Z. Kushitashvili
Ivane Javakhishvili Tbilisi State University, Tbilisi, Georgia

P5 (83): Radiation Modified Ion-Implanted Balls of Ball Bearings
A.I. Guldamashvili, Yu.I. Nardaia, Ts.M. Nebierdze, E.E. Sanaia A.V. Sichinava
Ilia Vekua Sukhumi Institute of Physics and Technologies, Tbilisi, Georgia

P6 (82): Obtaining of Ultrafine Powder Composites of Tungsten, Molybdenum, Titanium and Boron Carbides Using Liquid Precursors
N. Barbakadze, K. Sarajishvili, R. Chedia, L. Chkhartishvili, O. Tsagareishvili, A. Mikeladze, M. Darchiashvili, V. Ugrekhelidze
Ivane Javakhishvili Tbilisi State University, Tbilisi, Georgia

P7 (81): Study of the Behavior of Polymer Concrete to Shock Loading
N. Chikhradze, G. Abashidze, D. Tsverava, S. Kvinikadze
LEPL Grigol Tsulukidze Mining Institute, Tbilisi, Georgia

P8 (62): Magnetic Particles Retaining on Open and Closed Systems
G. Banis, E. Mangiorou, P. Tselou, A. Ferraro, A. G. Mamalis, E. Hristoforou
National Technical University of Athens, Greece

P9 (61): A First Comparison Between the Microwave Assisted Co-Precipitation Technique and the Typical Solvothermal Method for the Preparation of Fe_3O_4/β-Cyclodextrin Core/Shell Type Nanoparticles
M. Kourinou, I. Kokkinopoulos, M.E. Kouli, A. Ferraro, A.G. Mamalis, E. Hristoforou
National Technical University of Athens, Greece

P10 (59): Visible MCD Spectroscopy and Nature of Room Temperature Ferromagnetism in Hydrogenated Co - and (Co+Al) - Doped ZnO Films
Yu.E. Samoshkina, I.S. Edelman, D.A. Petrov, Hsiung Chou, S.G. Ovchinnikov
Kirensky Institute of Physics, Federal Research Center KSC SB RAS, Krasnoyarsk, Russia

P11 (58): Development of Flexible Fingertip Using Magnetic Functional Fluid
N.Yamashita, I. Murakami, Y. Ando, Long Bui Si
Gunma University, Kiryu, Japan

P12 (56): Does Evolutionary Improvement of Cars is Sufficient to Neutralize their Impact in Pollution and Climate Change or Do We Need a Jump Toward New Technologies?
K. N. Spentzas
Chief Academician Secretary of the EuroMediterranean Academy of Arts and Sciences

P13 (54): Effect of Heat Treatment on the Structure, Magnetic and Thermoelectric Properties Dy0.2Sr0.8CoO3-δ
V. Dudnikov, Y. Orlov, L. Solovyov, S. Vereshchagin, S. Novikov, V. Kuznetsova, S. Gavrilkin, S. Ovchinnikov
Kirensky Institute of Physics, Federal Research Center KSC SB RAS, Krasnoyarsk, Russia

P14 (53): Study of Genetic Analysis of Mutations in BRAF, NRAS and HRAS Gene in Thyroid Cancer Patients of Georgia by Using Programming Language
S.A. Elmogheth Madani, I. Gotsiridze
Georgian Technical University, Tbilisi, Georgia

P15 (52): Sustainable Design of Mobile Transilluminator Vein Finder Device
T. Talebifar, I. Gotsiridze
Georgian Technical University, Tbilisi, Georgia

P16 (48): Medical Simulation Training System with Application of Unity
D. Kim, I.Gotsiridze, Z.Gurtskaia
Georgian Technical University, Tbilisi, Georgia

P17 (47): Estimation of Parameters for a Model of Polycrystalline Solar Cells
J.J. Shainidze, L.G. Kalandadze, O.M. Nakashidze, N.KH. Gomidze
Batumi Shota Rustaveli State University, Batumi, Georgia

P18 (45): Impact of Electrohydraulic Processes upon Lightning Protection of the Buildings Constructed on High Water Grounds and Onshore Facilities
M. Tugushi, G. Partskhaladze, M. Loria, G. Chavleshvili, B. Karasiev
Batumi Shota Rustaveli State University, Batumi, Georgia

P19 (42): Impact of Thin Nanotechnology Coatings on the Stress-Strain State of the Cylindrical Cladding Made from Zr-Based Alloys for Nuclear Fuel Elements
Yu. V. Romashov, E.V. Povolotskii, A.G. Mamalis
V.N. Karazin Kharkiv National University, Ukraine, Kharkiv

P20 (32): Electrodynamic Levitation Effect in Vertical HTSC Alternators with Axial Magnetic Flux
L.I. Chubraeva, S.S. Timofeyev, V.A. Lazerko
Institute of Electrophysics and Electric Power Engineering of RAS, Saint-Petersburg, Russia

P21 (29): Preparation and Relative Mechanical Strength of Erbium Monoselenide Films
Z. Jabua, A.Gigineishvili, K. Davitadze, T. Minashvili, G. Iluridze
Georgian Technical University, Tbilisi, Georgia

P22 (24): Ultrasonic Propagation Wave Velocity in MR Fluid at Magnetic Field Sweep Rates
R. Kanasashi, Y. Tanaka, T. Sawada
Keio University, Yokohama, Japan

20:00 – 22:30 Conference Dinner

FRIDAY, JULY 19th

09:00 – 10.50 Oral Session I: Biomedical Engineering / Biotechnology
Chair: J. Ramsden

09:00 – 09:30 **Keynote Presentation (73): Magnetic Nanoparticles and Nanosystems for Hyperthermy of Deseesed Cells**
P. Kervalishvili, T. Berberashvili, A.Papoyan, A. Manukyan
Georgian Technical University, Tbilisi, Georgia

09:30 – 09:50 **I1 (90): Dynamic Suspension Characteristics of a Compact Double Stator Axial Gap Motor with Full Magnetic Levitation During Rotary Blood Pump Operation**
M. Osa, T. Masuzawa, E. Tatsumi
Ibaraki University, Japan

09:50 – 10:10 **I2 (51): Genetic Analysis of Study Diagnose Mutations in a Gene BRAF, NRAS, KRAS and RET Gene in Thyroid Cancer Patients of Georgia by Matlab Environment**
S.A. Elmogheth Madani, I. Gotsiridze
Georgian Technical University, Tbilisi, Georgia

10:10 – 10:30 **I3 (34): Computer Simulation Study of Physical Properties of Nanosized Biostructures**

P.J. Kervalishvili, T.N. Bzhalava
Georgian Technical University, Tbilisi, Georgia

10:30 – 10:50 **I4 (63): Design and Thermal Management of Battery Pack for Medical Devices**
M. Yaghoobi, I. Gotsiridze
Georgian Technical University, Tbilisi, Georgia

10:50 – 11:20 Coffee Break

11:20 – 12:30 Closing Session

Chair: A.G. Mamalis

Closing Remarks

Paper Submission
Best Poster Award
Euro-Mediterranean Academy of Arts and Sciences (EMAAS) Ceremony
Shockwaves Cluster
SIPS 2019
JAPMED'12

13:00 – 19:00 Excursion

Batumi — Makhunceti — Keda (Including: Wine Testing / Lunch)

PLENARY PRESENTATION

ADVANCED MANUFACTURING OF ADVANCED MATERIALS FROM MACRO- TO NANOSCALE UNDER STATIC TO SHOCK LOADING: PRINCIPLES AND INDUSTRIAL SUSTAINABLE APPLICATIONS

Academician Prof. Dr.-Ing. Dr.h.c. Prof.h.c. Athanasios G. Mamalis
Project Center for Nanotechnology and Advanced Engineering (PC-NAE),
NCSR "Demokritos", Athens, Greece
a.mamalis@inn.demokritos.gr

Abstract

The *Principles* of *Advanced Manufacturing Technology* may be identified with six main elements, with the central one being the enforced *deformation t*o the material, i.e. the *processing* itself, brought about under consideration of the *interface between tool and workpiece*, introducing interdisciplinary features for lubrication and friction, tool materials properties and the surface integrity of the component. The *as-received material structure* is seriously altered through the deformation processing, subjected from *static* to *very high-strain phenomena / shock loading*, therefore, materials testing and quality control *before and after processing* are predominantly areas of interest to the mechanics, manufacturing and materials scientists. The performance of the *machine tools* together with the *tool design* are also very important, whilst, nowadays, the *techno-economical aspects*, like the notion of *manufacturing systems,* regarding automation, modeling and simulation, rapid prototyping, process planning, computer integrated manufacturing, *energy conservation* and *recycling*, as well as *environmental aspects* are important in *Advanced Manufacturing Engineering.*

Quality of manufactured parts is mainly determined by their dimensional and shape accuracy, the surface integrity, and the functional properties of the products. Development of manufacture engineering is related to the tendency to miniaturization and is accompanied by the continuous increasing of the accuracy of the manufactured parts. Note that, the two main trends towards a miniaturization of products are the *ultraprecision*, carried out by machine tools with very high accuracy, and the *nanotechnology processing*, defined as the fabrication of devices with atomic or molecular scale precision by employing new advanced energy beam processes that allow for atom manipulation, allowing, therefore, the design and manufacture of the *nanostructured materials*, having every atom or molecule in a designated location and exhibiting novel and significantly improved optical, chemical, mechanical and electrical properties. Furthermore, *Sustainability* nowadays is challenged on many fronts, among the most prominent ones, the *Advanced Manufacturing* may be considered. Some trends and developments in *Advanced Manufacturing from macro- to nanoscale* in the important engineering topics from industrial, research and academic point of view: nanotechnology/ultraprecision engineering and advanced materials (metals, ceramics, polymeric, composites/nanocomposites) under static, low/high speed impact and shock loading, with *sustainable industrial applications* to net-shape manufacturing, bioengineering, energy/environment and transport, an outcome of the very extensive academic and industrial work over 50 years on these fields performed by the author and his research international team, are briefly outlined in the present Plenary Lecture of the JAPMED'11.

KEYNOTE PRESENTATIONS

THE EFFECT OF VELOCİTY, İMPERFECTİON AND MATERİAL MODELS ON THE CRUSHİNG OF ALUMİNUM CORRUGATED STRUCTURE

M. Güden*, M. Sarıkaya, İ. Canbaz, Alper Taşdemirci

Mechanical Engineering Department, Dynamic Testing and Modelling Laboratory
Izmir Institute of Technology, Urla, Izmir, Turkey
*Dynamic Testing and Modeling Laboratory and Department of Mechanical Engineering, Izmir Institute of Technology, Gülbahçe Köyü, Urla, Izmir, Turkey

Abstract

The velocity dependent crushing stress of metallic cellular structures including Al foams, honeycombs and corrugated structures has been on the focus of scientific interest as their applications are widening into automobile and aerospace industries. They are widely used as core in sandwich structures to improve overall performance of sandwiches and also absorb part of impact energies. The strain dependent crushing stress of these materials is well known and the examples are found in refs. [1-5]. Briefly, the strain rate sensitivity of metallic cellular structures are due to compressed air in between crushed/bent/folded cells, the strain rate sensitivity of cell wall material, the micro-inertia of cell wall bending and inertia/shock formation [6]. The strain rate sensitivity of cell wall material increases the crushing stress of metallic cellular structures at increasing impact velocities [7, 8]. Similarly, the micro-inertia referred to as the delay of overall cell wall buckling increases cell wall buckling loads at increasing velocities [9, 10]. The shock mode of deformation however appears above a critical velocity with an indication of higher impact-end stress than distal-end stress. The difference between impact-end and distal-end stress increases as impact velocity increases above the critical velocity for shock formation [4, 5]. The velocity-dependent deformation behavior of Al closed and open-cell foams, Al honeycombs and Al single- and double-layer corrugated cores were previously determined experimentally and numerically [5, 11-21]. However, the effect of imperfections on cell walls and the cell-wall material mechanical behavior on the crushing behavior have not been fully investigated and fully understood, yet.

In this study the quasi-static compression (0.0048 m s-1) and direct and Taylor-like (20-200 m s-1) impact loading of a multilayer 1050 H14 aluminum corrugated core were investigated both experimentally and numerically in LS-DYNA using the perfect and imperfect sample models with perfect, strain hardening and strain rate hardening material models. In the imperfect sample models, one- or two- layer of corrugated fin structure were replaced by the fin layers made of bent-type cell walls.

The localized deformation in the quasi-static imperfect models of cylindrical sample started at the imperfect layers, the same as the tests, and the layers were compressed until about the densification strain in a step-wise fashion. The localized deformation in the perfect models; however, started at the layers at and near the top and bottom of the test sample. In the shock mode, the sample crushed sequentially starting at the impact end layer regardless the perfect or imperfect sample models were used. Furthermore, the perfect and imperfect models resulted in nearly the same initial crushing stresses in the shock mode. The layer strain histories revealed a velocity-dependent layer densification strain. Both model types, the imperfect and perfect, well approximated the stress-time histories and layer deformations of the shock mode. The r-p-p-l model based on the numerically determined densification strains also showed well agreements with the experimental and numerical plateau stresses of the shock mode.

The increase of velocity from quasi-static to 20 m s-1 also increased the numerical distal-end initial peak-stress in the direct impact tests, while it almost stayed constant between 20 and 250 m s-1 for all material models. The increased distal-end initial peak-stress of strain rate insensitive models from quasi-static to 20 m s-1 confirmed the effect of micro-inertia. The numerical models further indicated a negligible effect of used material models on the impact-end stress of investigated

structure. Finally, the contribution of strain rate to the distal-end initial peak-stress of cellular structures made of low strain rate sensitive Al alloys was shown to be relatively low as compared with that of strain hardening and micro-inertia, but it might be substantial for the structures constructed using relatively high strain rate sensitive alloys.

Keywords: Cellular structure, impact loading, imperfection, shock stress, modelling

References:

[1] Langseth, M. and O.S. Hopperstad, *Static and dynamic axial crushing of square thin-walled aluminium extrusions.* International Journal of Impact Engineering, 1996. **18**(7-8): p. 949-968.

[2] Paul, A. and U. Ramamurty, *Strain rate sensitivity of a closed-cell aluminum foam.* Materials Science and Engineering a-Structural Materials Properties Microstructure and Processing, 2000. **281**(1-2): p. 1-7.

[3] Zhao, H., I. Elnasri, and S. Abdennadher, *An experimental study on the behaviour under impact loading of metallic cellular materials.* International Journal of Mechanical Sciences, 2005. **47**(4-5): p. 757-774.

[4] Tan, P.J., et al., *Dynamic compressive strength properties of aluminium foams. Part I - experimental data and observations.* Journal of the Mechanics and Physics of Solids, 2005. **53**(10): p. 2174-2205.

[5] Zou, Z., et al., *Dynamic crushing of honeycombs and features of shock fronts.* International Journal of Impact Engineering, 2009. **36**(1): p. 165-176.

[6] Sun, Y.L. and Q.M. Li, *Dynamic compressive behaviour of cellular materials: A review of phenomenon, mechanism and modelling.* International Journal of Impact Engineering, 2018. **112**: p. 74-115.

[7] Alvandi-Tabrizi, Y., et al., *High strain rate behavior of composite metal foams.* Materials Science and Engineering a-Structural Materials Properties Microstructure and Processing, 2015. **631**: p. 248-257.

[8] Jung, A., A.D. Pullen, and W.G. Proud, *Strain-rate effects in Ni/Al composite metal foams from quasi-static to low-velocity impact behaviour.* Composites Part a-Applied Science and Manufacturing, 2016. **85**: p. 1-11.

[9] Tam, L.L. and C.R. Calladine, *INERTIA AND STRAIN-RATE EFFECTS IN A SIMPLE PLATE-STRUCTURE UNDER IMPACT LOADING.* International Journal of Impact Engineering, 1991. **11**(3): p. 349-377.

[10] Calladine, C.R. and R.W. English, *STRAIN-RATE AND INERTIA EFFECTS IN THE COLLAPSE OF 2 TYPES OF ENERGY-ABSORBING STRUCTURE.* International Journal of Mechanical Sciences, 1984. **26**(11-1): p. 689-&.

[11] Deshpande, V.S. and N.A. Fleck, *High strain rate compressive behaviour of aluminium alloy foams.* International Journal of Impact Engineering, 2000. **24**(3): p. 277-298.

[12] Lopatnikov, S.L., et al., *Dynamics of metal foam deformation during Taylor cylinder-Hopkinson bar impact experiment.* Composite Structures, 2003. **61**(1-2): p. 61-71.

[13] Radford, D.D., V.S. Deshpande, and N.A. Fleck, *The use of metal foam projectiles to simulate shock loading on a structure.* International Journal of Impact Engineering, 2005. **31**(9): p. 1152-1171.

[14] Tan, P.J., et al., *Dynamic compressive strength properties of aluminium foams. Part II - 'shock' theory and comparison with experimental data and numerical models.* Journal of the Mechanics and Physics of Solids, 2005. **53**(10): p. 2206-2230.

[15] Elnasri, I., et al., *Shock enhancement of cellular structures under impact loading: Part I experiments.* Journal of the Mechanics and Physics of Solids, 2007. **55**(12): p. 2652-2671.

[16] Liu, H., et al., *Performance of aluminum foam–steel panel sandwich composites subjected to blast loading.* Materials & Design, 2013. **47**(0): p. 483-488.

[17] Wang, S.L., et al., *Dynamic material parameters of closed-cell foams under high-velocity impact.* International Journal of Impact Engineering, 2017. **99**: p. 111-121.

[18] Kilicaslan, C., I.K. Odaci, and M. Gueden, *Single- and double-layer aluminum corrugated core sandwiches under quasi-static and dynamic loadings.* Journal of Sandwich Structures & Materials, 2016. **18**(6): p. 667-692.

[19] Gaitanaros, S. and S. Kyriakides, *Dynamic crushing of aluminum foams: Part II - Analysis.* International Journal of Solids and Structures, 2014. **51**(9): p. 1646-1661.

[20] Zhao, H. and G. Gary, *Crushing behaviour of aluminium honeycombs under impact loading.* International Journal of Impact Engineering, 1998. **21**(10): p. 827-836.

[21] Qiao, J.X. and C.Q. Chen, *In-plane crushing of a hierarchical honeycomb.* International Journal of Solids and Structures, 2016. **85-86**: p. 57-66.

VECTOR MAGNETIC HYSTERESIS CHARACTERISTICS OF ELECTRICAL STEEL SHEET

Masato Enokizono[1,a], Daisuke Wakabayashi[2,b], Yuichiro Kai[3,c]

[1]*Vector Magnetic Characteristic Technical Laboratory, 533 Joi, Usa-city 879-0442, Japan*
[2] *Department of Mechanical and Electrical Engineering, Nippon Bunri University, 1727 Ichigi,Oita,870-0397, Japan*
[3]*Graduate School of Science and Engineering, Kagoshima University, 1-21-40 Korimoto,Kagoshima, 890-0065,Japan*
[a]enoki@oita-u.ac.jp, [b]wakabayashids@nbu.ac.jp, [c]ykai@eee.kagoshima-u.ac.jp

Abstract. This paper describes the new expression of vector magnetic hysteresis loop characteristic of arbitrary direction. The conventional magnetic hysteresis loop characteristic was limited in the case of the magnetic flux density vector **B** parallel to magnetic field strength vector **H**, which can be named scalar characteristic. The vector magnetic hysteresis can be expressed □$_{BH}$-|**B**|-|**H**| characteristic. The □$_{BH}$ is the spatial difference phase angle between vector **B** and vector **H**.

Introduction

The magnetic characteristics of magnetic materials have vector relation on constitute equation generally. However, conventional hysteresis characteristic is only rolling direction of steel sheet and is not general characteristics. It is due to orientation, rolling anisotropy, and crystal anisotropy. Therefore, magnetic flux density vector **B** is not parallel to magnetic field strength vector **H** and difference phase angle between vector **B** and vector **H**, which can be definite spacific phase angle θ_{BH} . In this paper the magnetic characteristic from the viewpoint of the vector relation is reviewed.

Figures 1(a) and (b) show the $|\mathbf{B}|_{max}$-$|\mathbf{H}|_{max}$-θ_{BH} curve instead of conventional **B-H** curve about non-oriented electrical steel sheet and grain-oriented electrical steel sheet, respectively. This is possible to know the essence of the magnetic characteristic by showing vector hysteresis property by the 3D scatter diagram. Especially, handling of θ_{BH} is necessary. By being dependent on time-related phase angle and spatial phase angle, the hysteresis property changes [1], [2].

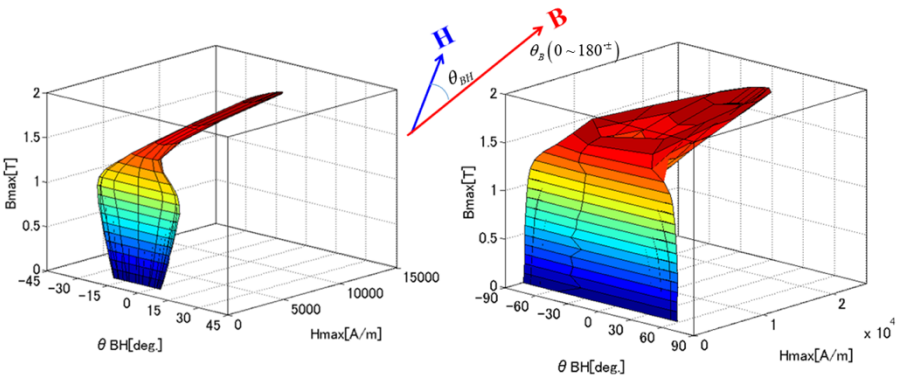

(a) Non-oriented electrical steel sheet (b) Grain-oriented electrical steel sheet.

Fig. 1 Vector magnetic charcteristics, $|\mathbf{B}|_{max}$-$|\mathbf{H}|_{max}$- ◤$_{BH}$ curve

What kind of hysteresis characteristic the vector magnetic characteristic is shown in this session. The waveform of each parameter of vector magnetic characteristic can be shown in order to draw two kinds of hysteresis property, as shown in B_x-H_x loop and B_y-H_y loop. Figure 2 described relationship between |**B**| and |**H**|, θ_{BH} and |**H**| independently. The θ_{BH}-|**H**| characterization, both rolling direction and transverse direction are described for 0 planes of θ_{BH} , because both vectors are parallel. Therefore, θ_{BH}-|**H**| hysteresis is not appearing. The characteristic of the optional direction except for the this shows the hysteresis property.

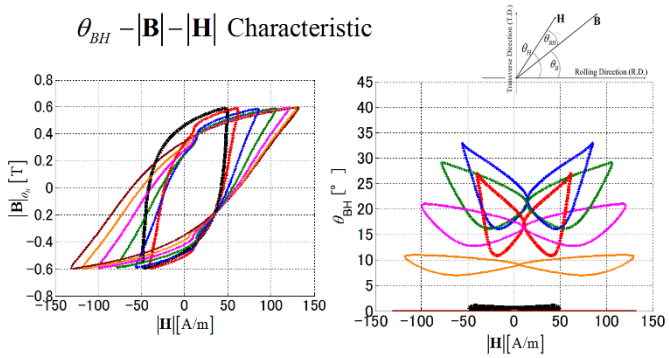

(a) |**B**|-|**H**| hystrsterssis characteristi (b) θ_{BH}-|**H**| hysteresis characteristic

Fig. 2. |**B**|-|**H**|-θ_{BH} characteristic of arbitrary direction

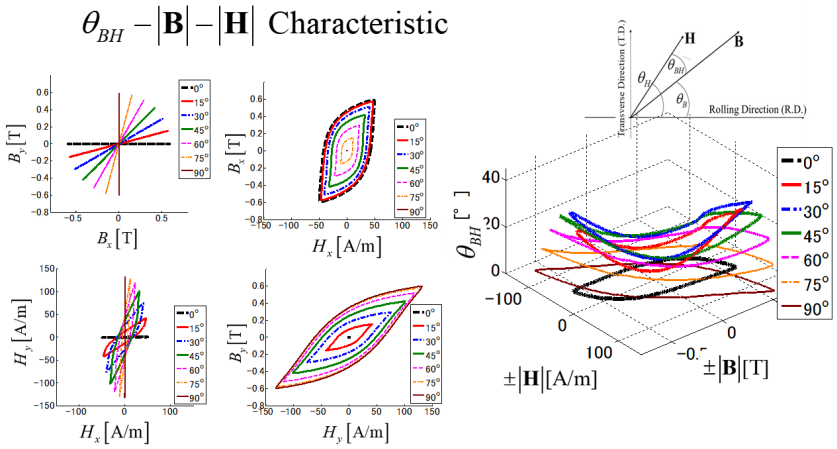

Fig. 3. Relation between vector locus and θ_{BH} -|**B**|-|**H**| - vector magnetic hystrsterssis characteristic

Figure 3 shows the hysteresisloop characteristics of vector magnetic property. This hysteresisloop characteristic of the curved surface shape is shown, when θ_{BH} increases. The increase of the surface area of hysteresis loop is connected with the increase in the magnetic power loss. Figure 4 shows the relationship between the vector locus characteristic both vector **B** and vector **H** and vector magnetic hysteresis characteristic. The expression of loss characteristic as W-θ_B-$|\mathbf{B}|_{max}$ as shown in Fig. 4.

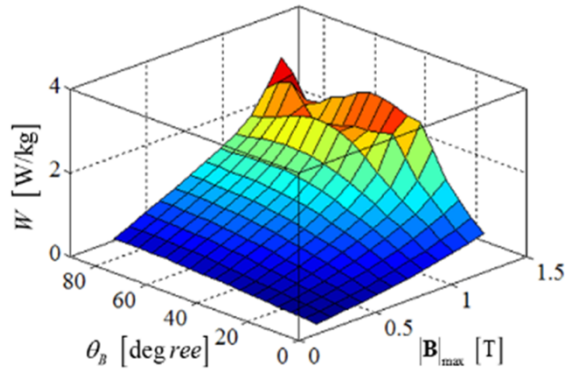

Fig. 4 W-θ_B-$|\mathbf{B}|_{max}$ characteristic

References

[1] Enokizono M. "Vector Magnetic Characteristic Technology and Design Method", Kagakujyoho shuppan Co.,Ltd., ISBN: 978-4-904774-36-6 (2015.4) 262 Japanese Book.

[2] URL http://www.vector-mgtec.

STRUCTURE AND PINNING CENTERS IN MgB_2 BULKS, WIRES, THIN FILMS AND MT-YBCO

T. Prikhna[1,a], M. Eisterer[2,b], V. V. Romaka[3,c], A. G. Mamalis[4,d], A. Jouline[5,e], J. Rabier[5,f], S. S. Ponomaryov[6,h], M. V. Karpets[1,i], M. Rindfleisch[7,j], M. Tomsic[7,k], A.V. Kozyrev[1,l], V.E. Moshcchil[1,m], A.V. Shaternik[1,n]

[1]*Bakul Institute for Superhard Materials of the National Academy of Sciences of Ukraine (NASU), 2 Avtozavodskaya Str., Kiev 07074, Ukraine.*
[2]*Atominstitut, TU Wien, Stadionallee 2, 1020 Vienna, Austria*
[3]*Lviv Polytechnic National University, 12 Bandera Str., Lviv, 79013, Ukraine*
[4]*Project Center for Nanotechnology and Advanced Engineering, NCSR "Demokritos", Greece*
[5]*Institute P', PHYMAT, UMR 6630, CNRS Université de Poitiers, SP2MI, BP 30179, F-86 962 Futuroscope, France*
[6]*Institute of Semiconductor Physics of the National Academy of Sciences of Ukraine (NASU), 41, Nauky Ave., Kyiv 03028, Ukraine*
[7]*Hyper Tech Research, Inc., 539 Industrial Mile Road, Columbus, OH, USA*
[a]prikhna@ukr.net.ua, [b]michael.eisterer@tuwien.ac.at, [c]vromaka@gmail.com, [d]mamalis@central.demokritos.gr, [e]anne.joulain@univ-poitiers.fr, [f] jacques.rabier@univ-poitiers.fr, [h]s.s.ponomaryov@gmail.com, [i]mkarpets@ukr.net, [j]mrindfleisch@hypertechresearch.com, [k]mtomsic@hypertechresearch.com, [l] artem.v.kozyrev@gmail.com, [m]vik_ism@ukr.net, [n]shanton855@gmail.com

Abstract. The structure and composition of MgB_2-based materials (wires, bulks, and thin films) prepared at different pressure (0.1 MPa - 2 GPa) – temperature (600 - 1050 °C) conditions and MT-YBCO oxidized in the gas flow at 440 °C under ambient pressure and under hydrostatic 16 MPa pressure at 800 °C witch demonstrated high critical current densities, j_c, were analyzed by X-ray, JAMP−9500F Auger spectrometer (after removing the oxidized layers at the sample surfaces by Ar ion etching performed directly in the vacuum chamber of microscope) and TEM. Regularly distributed inhomogeneities connected with Mg, B and admixture O content variation on the nanolevel were observed in all types of the MgB_2-based materials and are responsible for pinning. In MT-YBCO such defects as twins, dislocations and staking faults to high extent are responsible for pinning. Their densities are strongly correlated with the distances between dispersed Y_2BaCuO_5 inclusions. The correlations between the character of the materials inhomogeneities which can be pinning centers and the attained superconducting characteristics are discussed. The superconducting matrices of magnesium diboride bulks with AlB_2 structures contain some oxygen in their unite cells what has been shown experimentally by X-ray and Auger study and supported by ab-inito simulation.

1. Introduction

Magnezium diboride wires and bulks are promising for many different applications, for example, fault current limiters, magnetic resonance imaging, superconducting magnetic energy storage devices, transformers, electrical motors and generators, cryogenic pumps, adiabatic demagnetization refrigerators, magnetic separators, magnetic levitation transport and bearings, magnets for high-energy physics. Lightweight superconducting wires can be used for aviation and space applications and for powerful offshore wind generators, etc. Magnesium diboride wires and bulks compete to some extend with YBCO coated conductors and melt-textured ceramics. The working temperature of magnesium diboride can be chosen near liquid hydrogen or neon (20-30 K). It is easily produced and comparatively cheap, but prone to quenching during pulsed magnetization. This problem has to be solved in order not to restrict the material´s wide spread application. The working temperature of YBCO-based materials can be higher (e.g. around the temperature of liquid nitrogen, 77 K, or somewhat lower), but their production is much more expensive and complicated and the problems with ac losses and appropriate optimal twisting are not solved. A big risk of quenching and damaging powerful magnets is existing for coated conductors as well.

Many scientists are working on the improvement of the characteristics of MgB_2 –based materials and MT-YBCO and studying the positive effect of oxygen in their structures on superconducting characteristics.

2. Experimental procedure and sample preparation

Monofilamentary MgB_2 strands of round (0.83 mm in diameter) and quadratic (0.73×0.73 mm) shapes were fabricated by Hyper Tech Research Inc. The strand architecture consists of a Monel outer sheath and a Nb barrier surrounding the powder mixture. The starting powders were non doped and C-doped boron from Specialty Materials Inc. (SMI) or Pavezyum. The boron powders from Specialty Materials Inc. were mostly amorphous with a particle size of 10–100 nm. The C-doped powders contained 2 mol.%C. The MgB_2 bulk samples were prepared in MgB_2 stoichiometry (at the Institute for Superhard Materials NASU) without and

with carbon addition. The high pressure (2 GPa)-high temperature(600 and 1050 ºC) synthesis was performed in contact with pre-compacted hexagonal boron nitride powder in the recessed-anvil-type high pressure apparatus.

MT-YBCO after melt texturing was oxygenated at 440 ºC in O_2 flow for 14 days and at 800 ºC, 16 MPa for 3 days.

3. Results and conclusions

Despite magnesium diboride has a comparatively simple unit cell which contains only two elements, it is quite difficult to synthesize a uniform material and practically impossible to synthesize or sinter magnesium diboride without oxygen impurities. It is impossible to identify one main technological factor which will guarantee a high superconducting performance of magnesium diboride.

The study of different types of wires produced from boron without and with additions of carbon or using different initial types of boron allowed us to understand which factors are of primary importance for attaining high superconducting performance. First of all it is very important to obtain a stoichiomentry of matrix phase close to MgB_2 and a high density of the wire core. A significant deviation of the main superconducting phase from MgB_2 stoichiometry (i.e. Mg excess or deficiency) leads to a reduction of the critical current density, J_c, as well as a very non-uniform distribution of the elements. While regularly repeated nano– or micro-inhomogeneties in the material structure, can be the reason of J_c increase if their concentration is rather high. The wire with a round-shaped highly dense core (with a composition of its matrix phase near $MgB_{1.8\text{-}2.4}O_{0.04\text{-}0.71}C_{0.12\text{-}0.16}$) prepared from C-doped boron and with mostly homogeneously distributed (on the macrolevel) B, C, Mg, and O demonstrated the best superconducting characteristics: J_c(20 K, 2 T) = 10^5 A/cm^2 and J_c(20 K, 6 T) =2.7×10^3 A/cm ^{2}, J_c(4.2 K, 5 T) = 1.6×10^5 A/cm^2, J_c(4.2 K, 15 T) =2×10^3 A/cm ^{2} and B_{irr} (20 K) = 8 T, B_{irr} (12.5 K) = 15 T. The resolution of the used microscope was not enough to reveal the regularly repeated nano-inhomogeneties. Bulk magnesium diboride of Type 2 synthesized from the boron with carbon additions and regularly repeated inhomogeneties demonstrated J_c(10 K, 10 T)=4×10^3 A/cm ^{2} and J_c(20 K, 6 T)=4×10^3 A/cm ^{2}.

The critical current density, J_c, at 77 K of melt textured $YBa_2Cu_3O_{7\text{-}x}$ (MT-YBCO) oxygenated under 16 MPa at 800 ºC (the details of the manufacturing conditions are described in [1]), which is given for comparison, is rather high, but anisotropic. At 77 K in the *ab* plane $j_c=9\times10^4$ A/cm^2 (in a zero magnetic field), H_{irr}=9.7 T; in the direction of the *c*-axis $j_c=4\times10^4$ A/cm^2 (in the zero magnetic field), and in the magnetic field of 10 T j_c exceeds 2×10^3 A/cm^2. It has been shown that the J_c of the fully oxygenated MT-YBCO (up to $YBa_2Cu_3O_{6.9\text{-}7}$) depends to a high extend on the twin density (J_c increases with the twin density). The effect of dislocations is much smaller. The twin density is higher if the distance between the Y_2BaCuO_5 inclusions is smaller.

It has been shown experimentally that the stoichiometry of a superconducting magnesium diboride having AlB_2 structure with a high level of superconducting properties (transition temperature to superconducting state, critical current density, upper critical magnetic field, and field of irreversibility) is close to $MgB_{1.75}O_{0.25}$. The ab-inito simulation confirmed the possibility of the existence of solid substitution solutions (boron to oxygen) and the energy benefit of such stoichiometry, as well as the fact that the impurity oxygen with the high probability is included in each second plane of boron of the elemental atomic cell of magnesium diboride, while every second hexagonal plane of boron of the same unite cell remains unchanged.

References

[1] Prikhna T. A., Rabier J., Proult A., et al., *Supercond. Sci. Technol*., 2004, 17, 515–519.

STRESS DISTRIBUTION MONITORING AND REHABILITATION IN FERROUS STEELS

S. Aggelopoulos[1], X. Vourna[1], A. Ktena[1,2], A. G. Mamalis[3] and E. Hristoforou[1]

[1]Laboratory of Electronic Sensors, School of Electrical & Computer Engineering, National Technical University of Athens, Zografou Campus, Athens 1570, Greece
[2]National & Kapodistrian University Athens, Greece
[3]Project Centre for Nanotechnology and Advanced Engineering, NCSR "Demokritos", Athens, Greece

Abstract. Stress distribution monitoring and rehabilitation in ferrous steels, offering faultless steel production and manufacturing (FASTEP) represents a new method and technology for surface and bulk stress distribution monitoring and rehabilitation in steels. The quality of the steel and corresponding products depends on the distribution and level of stresses in its volume and surface, since stress gradient is responsible for steel cracking generation & failure.

The existing technology in stress monitoring concerns either surface stress distribution monitoring instruments with unacceptably high uncertainty, or point surface stress sensors, or surface and bulk laboratory techniques not able to operate in industrial environment. Therefore, a method to provide stress tensor distribution monitoring on the surface and in the bulk of steels would be the feedback system to not only monitor stresses but actually to achieve stress rehabilitation.

FASTEP solution in achieving stress distribution monitoring in steel production, manufacturing and use, is related to a new method and technology, currently pending for patent, offering stress tensor distribution monitoring on the surface and the bulk of steels, steel welds and products based on them. The achieved uncertainty has been <0.1% for surface or bulk stress measurements, with speeds as high as 10 □s per point of measurement, compared to ~10% uncertainty and speed of 1-10 s per point of the existing state of the art, thus opening a new era in diagnostics & therapeutics in steel industry. Such a technology can be the feedback system for automated stress rehabilitation (annihilation or strengthening) process in steel production and manufacturing, as well as in installed steel structures (end-user applications).

The research breakthroughs of FASTEP are related to the unique ability to monitor the stress tensor on the surface and in the bulk of ferromagnetic steels, as well as to rearrange the stress fluctuation on the surface and the bulk of the steel. This way, the steel producers (steel coil producers) and the steel manufacturers (shipyards, welding industry, etc.) will have a unique tool to:

- Control the quality of the raw materials for their production line. In other words, the shipyards will be able to control the stress distribution in the in-coming steel coils, point by point
- Control the stress distribution and non-uniformity in the produced steel coil or the manufactured steel product (pipeline, ship etc.)
- Test and possibly re-arrange the stress distribution in existing steel structures, like vessels under pressure, nuclear station domes, steel structures, ships, trains etc.

The problems to be solved in the steel industry are summarized as follows:

- Quality of boat manufacturing (shipyards) is not excellent yet. FASTEP can be used to provide a solution, like a portable or stationary welding machine, including welding, stress monitoring, stress rehabilitation by localized RF heating, and quenching strengthening when needed, as well as final total quality control and certification.
- Power losses in electric steels for transformers and motors are as high as 10k USD/W, after Prof Moses [1], an expert in electric steels. These losses are governed by the localized stresses and their distribution, affecting the magnetic properties and therefore the losses in the devices based on them, namely transformers and most importantly electrical machines, which are one of the key elements of electric cars.
- Furthermore, as the quality of heat exchangers should be holistically tested along the whole volume of the used steel, the stress distribution should be monitored along the whole length of the material. A company employed in pipeline manufacturing and welding processes will implement the FASTEP method for the faultless production of heat exchangers.
- Quality of the other steel production and manufacturing lines is not excellent yet. FASTEP is able to provide stress monitoring and rehabilitation in all steel production & manufacturing lines. The sensors and rehabilitation systems can have the shape of the steel product (flat or circular).

The mentioned sensors can be used in end-user applications, like constructions, ships, trains, railway rails, powder stations, bridges etc.

Figure 1 illustrates the excellent agreement between magnetic parameters (mainly magnetic permeability) and stresses monitored by X-Ray Diffraction Bragg-Brentano set-up. According to this inductive, contactless type of stress monitoring, the proper amount of induction heating can be locally applied to the steel under investigation in order to annihilate the local stresses.

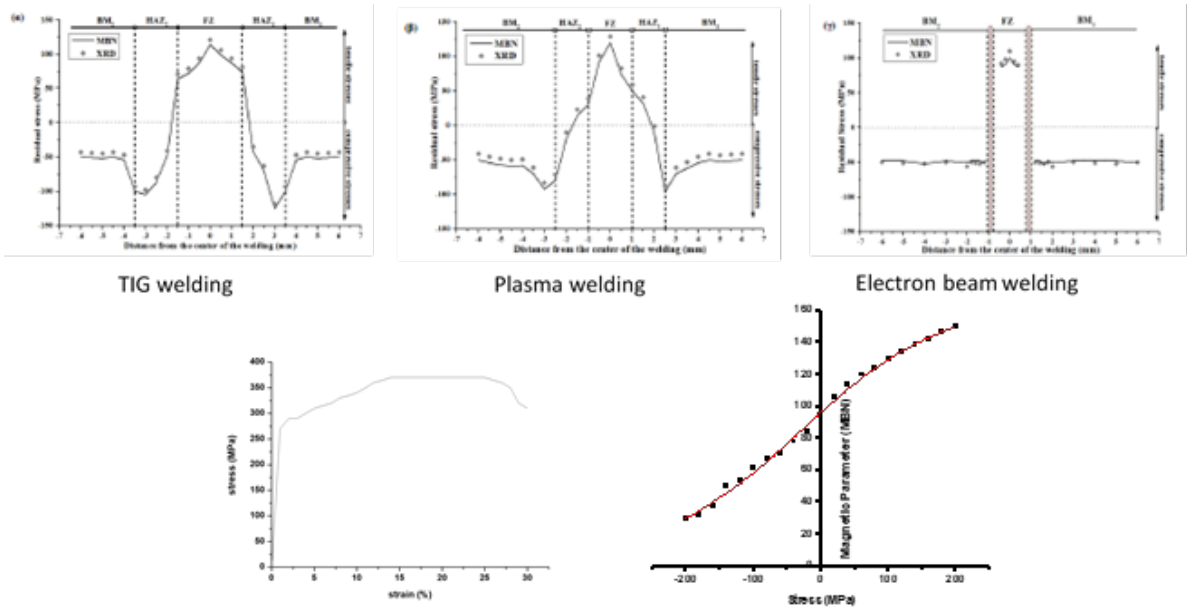

Figure 1: Example of comparison of stress components and magnetic permeability in autogenously welded steel (upper part). In this case steel has been AISI 1008, welded with TIG, Plasma and EBW. From these pairs of values the magnetic stress calibration curves are extracted.

References

[1] Shahrouzi H., Moses A. J., Anderson P.I., Li G., Hu Z. Comparison between measured and computed magnetic flux density distribution of simulated transformer core joints assembled from grain-oriented and non-oriented electrical steel, AIP Advances, Volume 8, Issue 4, 1 April 2018.

STRONG EFFECT OF MULTIPLICITY FLUCTUATIONS IN RARE-EARTH COBALTITES ON MAGNETIC, ELECTRONIC, AND CRYSTAL STRUCTURE PROPERTIES

S.G. Ovchinnikov [1,a], V.A. Dudnikov [1,b], Yu.S.Orlov [1,c], M. V. Gorev[1,d]

[1] *Kirensky Institute of Physics, Federal Research Center KSC SB RAS, Krasnoyarsk, Russia*
[a] sgo@iph.krasn.ru, [b]slad63@yandex.ru, [c]jso.krasn@mail.ru, [d]gorev@iph.krasn.ru

Abstract. The perovskite compounds $ReCoO_{3-y}$ (Re is Nd, Sm, Gd) have a number of unusual magnetic, electronic, and lattice properties related to the temperature induce spin state crossover from the low spin (LS) to the high spin (HS) states of the Co^{+3} ions. We have synthesized high quality polycrystalline samples and have measured temperature dependence of the X-ray diffraction, magnetic susceptibility, and lattice dilatation. All observed anomalies are related to the smooth increase of the concentration of the HS ions that are excited over the spin gap between HS and LS terms. Spin gap itself decreases with lattice expansion and goes to zero at the spin crossover temperature. The spin gap is determined by the Re ionic radii.

1. Introduction

Anomalous magnetic, electronic and lattice properties of LaCoO3 and other rare-earth cobaltites are known for a long time. It is known that the ground state of the Co^{+3} ions is the LS, and magnetic properties are thermally induced by the increasing occupation of the HS ions. The excitation from LS to HS ionic terms (the multiplicity fluctuations) occurs via the spin gap, its value is small ~100K for La and increases going from La to Y. For Gd we have estimated this gap 2000K at zero temperature. Due to lattice dilatation with heating the gap is decreasing, and tends to zero at the spin crossover temperature T*. We have demonstrated this behavior earlier for GdCoO3 where T*=800K [1]. The aim of this work is to prepare and study the complex of physical properties of Nd and Sm cobaltites where smaller spin gap is expected and the spin crossover temperature may be decreased to more convenient values.

2. Experimental procedure and sample preparation

Polycrystalline ceramic samples of SmCoO3 and NdCoO3 were prepared from a stoichiometric compositions of high quality oxides Co3O4 , Sm2O3, and Nd2O3 that were carefully mixed and heated at 1473 K in air during 24 h. After the annealing, the mixture was reground, and the powder was pressed to form pellets in the shape of bricks 5 × 10 × 2 mm^3. The pellets were annealed in air for 8 h at 1373 K, and then slowly cooled together with the furnace down to room temperature at the speed about 2 K/h.

Powder XRD patterns were recorded on a PANalytical X'Pert PRO diffractometer with a solid state detector PIXcel using Co Kα radiation. High temperature measurements were performed using an Anton Paar HTK 1200N stage.

The volume thermal expansion was measured in the temperature range 100−750 K with an induction dilatometer Netzsch DIL-402C calibrated with a silica glass as a standard in dynamic mode with heating and cooling rate 0.05 K/s in a flow of dry helium (O2 concentration is about 0.05% of volume).

Magnetic field and temperature dependences of magnetization in the temperature range 2−400 K were measured with the Physical Properties Measurement System (PPMS-9) by Quantum Design.

3. Experimental results

The XRD data has revealed single phase sample with the lattice parameters corresponding to the literature data. The experimental temperature dependences of the volumetric thermal expansion coefficient β, obtained in heating-cooling modes, do not show hysteresis differences and are shown in Fig. 1.

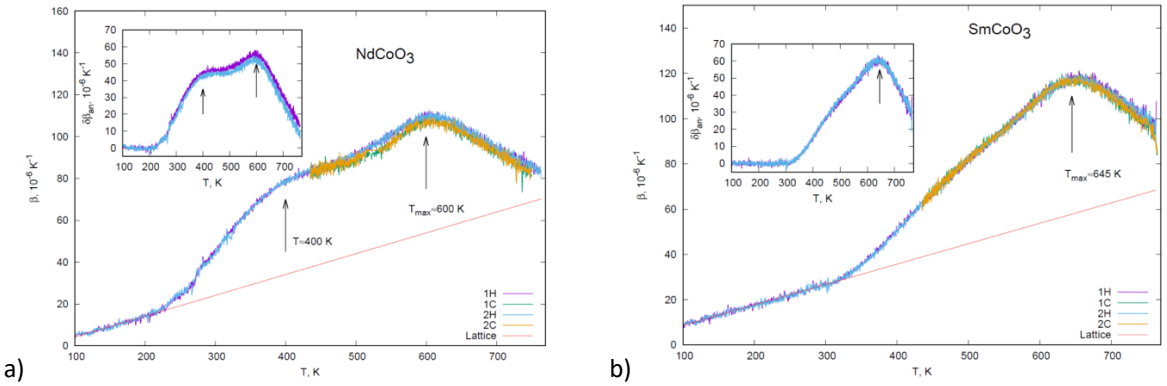

Fig. 1. Temperature dependences of the volumetric thermal expansion coefficient β for the samples ReCoO3 (Re = Nd (a), Sm(b)). The abnormal contributions to the thermal expansion coefficient are obtained by substracting linear contribution from the experimental values and are shown in the inset.

The high temperature maximum of the dilatation has been found earlier in LaCoO3, GdCoO3 and their solid solutions [2], it corresponds to the spin crossover temperature T*. It is larger in SmCoO3 vs NdCoO3 because zero temperature spin gap in SmCoO3 is ~1500K, while in NdCoO3 it is ~1000K [3]. The low temperature maximum for NdCoO3 corresponds to the maximal variation of HS concentration dn_{HS}/dT [2].For cobaltites with larger spin gap the maximal rate of the multiplicity fluctuations is achieved at higher temperatures and is close to T*. Similar two peak structure for NdCoO3 and single peak for SmCoO3 we have found in magnetic susceptibility temperature dependence.

Conclusions

The lattice dilatation with increasing temperature has the effect of the negative pressure that increases fluctuations of the multiplicity and results in the spin crossover of the LS state stable at low temperature into the HS state stable at high temperature. The average value of spin is temperature dependent, and reach its nominal for HS value S=2 only at temperature T>>T*. The physical origin of the strong deviations of the dilatation from the linear behavior is the large (about 10%) difference in the ionic radii of the LS and HS states of Co+3 ions. The characteristic spin crossover temperature T* is found to be 600K in NdCoO3, and 645K in SmCoO3.

Acknowledgment

This work is supported by the Russian Scientific Foundation grant 18-02-00022.

References

[1] Orlov Yu.S., Solovyev L.A., Dudnikov V.A., Fedorov A.S., Kuzubov A.A., Kazak N.V., Voronov V.N., Molokeev M.S., Vereshchagin S.N., Shishkina N.N., Perov N.S., Babkin R.Yu, Lamonova K.V., Pashkevich Yu.G., Anshits A.G., Ovchinnikov S.G. Electronic, magnetic and structural properties of GdCoO3 in wide temperature range: experiment and theory, Physical Review B, 2013,.88, 235105

[2] [Orlov Yu.S., Dudnikov V.A., Gorev M.V., Vereshchagin S.N., Solovyev L.A., Ovchinnikov S.G Thermal Properties of Rare Earth Cobalt Oxides and of La1 – xGdxCoO3 Solid Solutions, JETP Letters, 2016, 103, 607–612.

[3] Ovchinnikov S.G., Orlov Yu.S., Dudnikov V.A. Temperature and field dependent electronic structure and magnetic properties of LaC_oO_3 and GdC_oO_3, Journal of Magnetism and Magnetic Materials, 2012, **324**, 3584-3587.

A SUSTAINABLE WORLD POPULATION

Jeremy J. Ramsden[1,a], Alexandra A. Mamali[2,b] and **Nikolaos T. Athanassoulis[3,c]**

[1]*The University of Buckingham, England*

[2]*Cass Business School Alumni, Athens, Greece. e-mail:*

[3]*Laboratory of Energy and Industrial Economics (LIEE), National Technical University of Athens, Greece. e-mail:*

[a] j.ramsden@colbas.org, [b] a.mamali@hotmail.com, [c]nikos_athanasoulis@yahoo.gr

Indices of resource depletion and other indicators inimical to sustainability, such as pollution, atmospheric carbon dioxide concentration and mean temperature of the Earth's surface, are all proportional to population and mean gross domestic product (GDP) *per capita*. In order to combat the imminent threat of a catastrophic collapse of our present way of life, it would therefore appear that either population or mean GDP/capita must be drastically reduced. This paper focuses on the first possible remedy. A counterargument to population reduction is the notion that third way exists, namely a vast improvement in the effectiveness of resource utilization, an idea that certainly has merit; it is proposed that the more brains there are on Earth, the more abundant the emergence of new transformative technologies for achieving that third way. Evidence for the link between population and creativity is critically examined. One corollary of that link is the desirability of diminishing human body size. The appalling global epidemic of obesity scrutinized in this light.

SCIENCE AND TECHNOLOGY – THE GRAND DISRUPTORS AND SOLUTION PROVIDERS

Florian Kongoli[1,2.3,a]

[1]*CEO, FLOGEN Technologies Inc. Montreal, QC, Canada, H3P 2T1;*
[2]*Chairman, FLOGEN STAR OUTREACH, Montreal, QC, Canada, H3P 2T1;*
[3]*CEO, FLOGEN Technologies Inc., Wilmington, DE, 19808, USA;*
[a]*fkongoli@flogen.com*

Abstract

The role of science and technology as one of the most important pillars of sustainable development has been analysed within the new FLOGEN sustainability framework. Many distant and recent historical examples have been considered to make the point that science and technology are grand disruptors of boundaries, borders, and ways of life, and they have opened society's eyes to new serious problems and realities. The paper points out that science and technology are well credited for this great diagnostic role, but have been frequently ignored for their role as solution producers. Numerous examples illustrate the fact that usually solutions are sought far from science and technology, or without their close cooperation, and this has been in fact the cause of failures. It is shown that science and technology are grand solution providers, and this is clear from the distant, recent, and current realities, where they have proven wrong all non-scientific solutions or doomsday predictions. It is concluded that no sound long term solution can be found when science and technology are not considered as a solution provider as the pillar at the forefront of sustainable development, and this is even more so valid for the acute problems faced by the world today.

MAGNETIC NANOPARTICLES AND NANOSYSTEMS FOR HYPERTHERMY OF DESEESED CELLS

P.Kervalishvili[1a], T. Berberashvili[1b], A.Papoyan[2a], A. Manukyan[2b]

[1]Georgian Technical University, Tbilisi, Georgia; [2] Institute of Physical Research , Ashtarak, Armenia
[a]kerval@global-erty.net,, [b]t.berber@mail.com, [a] papoyan@ipr.sci.am , [b]manukyan.ipr@gmail.com

Abstract: Magnetic nanoparticle hyperthermia is based on a physical effect, where magnetic nanoparticles are introduced into the tumor tissue producing local heat when subjected to an alternating magnetic field. The destruction of cancer cells will occur at T = 42 - 44°C. However, higher temperatures can kill surrounding normal tissues. For a magnetic hyperthermia, it is necessary to receive magnetic nanoparticles with high values of specific absorption rate, as well as exercise control of heating temperature. The aim of the paper is elaboration of precise and minimally invasive heat mediators with high thermal energy transfer capability for magnetic hyperthermia treatment of cancer at the cellular level. This goal is achieved by using highly effective heating nanosystems of ferromagnetic nanoparticles encapsulated by carbon nanotubes or graphene nanostructures.

1. Introduction

Method of electromagnetic hyperthermia with magnetic nanoparticles have a strong potential to use as anticancer drugs [1]. It characterizing: by higher free-radical activity of magneto-sensitive nanocomplex due to the non-thermal magneto-spin effects ; The use of nanoparticles, which can combine both therapeutic and diagnostic capabilities in one dose, and has the potential to lead toward personalized oncology and better outcomes for patients. The method of magnetic nanotherapy can be used to treat tumors in all body parts without anesthesia[2]. At the same time the properties of nanoparticles of magnetic materials currently popular for the today's treatment technologies have: Weak surface selectivity of nanoparticles between malignant and normal cells; The need to create high local magnetic fields and appropriate thermal gradients for the treatment; Slow biodegradation of nanoparticles in the body and side effects of their accumulation in the liver, spleen, muscles, and other organs; Temperatures in the range of 41–50°C can be accompanied by the formation of thermal resistance at the cellular level; Targeted radio frequency therapy with magnetic nanoparticles is often not suitable [3].

2. Theoretical and experimental results

Depending on the parameters of the synthesis it is possible to prepare nanosystems with the necessary magnetic properties and frequency and amplitude of vibration plus size and structure of nanoparticles and carbon capsules.

Nowadays, there are several methods for obtaining metal nanoparticles such as solid-phase pyrolysis, chemical vapour and laser plasma deposition. In our work we mostly used the method of pyrolysis of organometallic compounds for the preparation of metal nanoparticles including Ni, Co, Cu, but also alloys and pure carbon micro and nano spheres [4,5]. Solid-phase pyrolysis is characterized by its simplicity and the ability to control the properties of the nanoparticles by pyrolysis parameters. In other words, using solid phase pyrolysis, it is possible to obtain materials with predetermined properties.

For development of high effective nanomaterials for hyperthermia process organization we consider to change the multi-domain ferromagnetic materials to single domain supermagnetic ones in connection with reducing the size of nanoparticles. For our works we choose the superparamagnetic and ferromagnetic (Ni-Cu)/C nanoalloys as well as Iron and Iron-oxide and Manganese based ferromagnetic and superparamagnetic nanocomposites. The important point is that the average size of the nanoparticles depends on the pyrolysis conditions and varies between 10 - 40 nm and 350 - 400 nm. This can be seen ar figure, where the bright spots correspond to the metal nanoparticles in a dark carbon matrix.

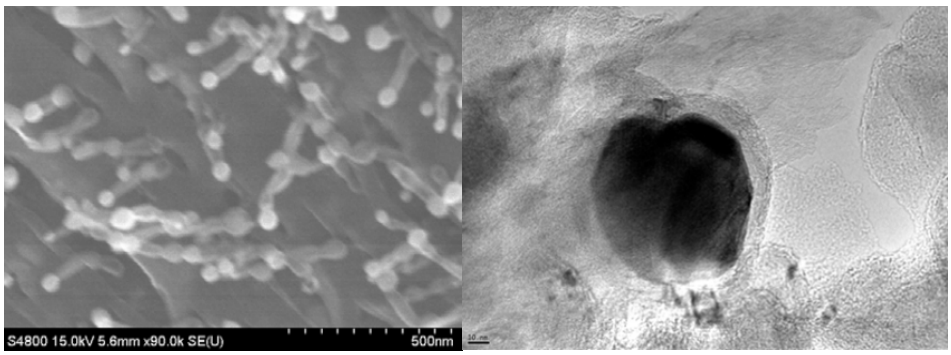

Fig. SEM and TEM images of nanocomposites Ni0.7Cu0.3/C, obtained by pyrolysis at Tpyr = 700 ° C and tpyr = 30 min. [4].

For obtaining the ferromagnet-graphene nanosystems we performed technological processes by using used laser plasma method of synthesis and deposition.

Modelling and simulation works we performed shown that carbon nanostructures (nanotubes, grapheme like systems) as coatings prevented the nano magnetic particles agglomeration, their protection of oxidation and biocompatibility.

Conclusions

Among the main results of our works aim farther development of hyperthermy methods and tools for cancer cells treatment it is necessary to underline: theoretical and experimental development and characterization (electron – optical analysis, electrical and magnetic measurements) of ferromagnet – carbon nanotube based nanosystems; elaboration, modeling and preparation of ferromagnet - graphene systems using laser plasma technologies.

References

[1] Thanos Mitrelias, Medical systems aimed at improving the outcome of cancer treatment. Cambridge, UK, The SECURE-R2I Project Final Dissemination and Brokerage Events – Presentations Septermber 29, 2015. Kiev Ukraine SECURE-R2I – Reinforcing cooperation with Eastern European Countries, secure-r2i.eu/index.php/en

[2] Kervalishvili P., Magnetic nanoparticles and nanomaterials for magnetic hyperthermia investigations, Presentation on Georgian medical society meeting, 11December, 2015.

[3] Berberashvili T., Buachidze Z., Chirakadze A., Chakhvashvili L., Jishiashvili D., Kervalishvili P., Aleqsanyan S., Gulasryan H., Manukyan A., Papoyan A., Saroyan E., Sajti L. Carbon coated Fe-FeC and Ag – doped Manganite (AgxLa1-xMnO3) nanocomposites for magnetic hyperthermia of cancer cells. 4th international conference "nanotechnologies" October 24-27, 2016 GTU Tbilisi, Georgia.

[4] Manukyan A.S., Mirzakhanyan A.A., Khachatryan T.K., Badalyan G.R., Abdulvakhidov K.G., Bugaev L.A., and Sharoyan E.G. Copper–Carbon Nanocomposites Prepared by Solid-Phase Pyrolysis of Copper Phthalocyanine, Journal of Contemporary Physics (Armenian Academy of Sciences), 47, 2012, p. 292–295

[5] Sajti L. Carbon coated Fe-FeC and Ag – doped Manganite (AgxLa1-xMnO3) nanocomposites for magnetic hyperthermia of cancer cells. 4th international conference "nanotechnologies" October 24-27, 2016, GTU Tbilisi, Georgia.

ORAL PRESENTATIONS

STRUCTURE AND MECHANICAL PROPERTIES OF MULTILAYER METAL-INTERMETALLIC COMPOSITES FABRICATED BY EXPLOSIVE WELDING AND ANNEALING

Zemin Sheng [1,a], Pengwan Chen[1,b], Qiang Zhou[1,c]

[1] *State Key Laboratory of Explosion Science and Technology, Beijing Institute of Technology, Beijing, China*
[a] m15090359861@163.com, [b] pwchen@bit.edu.cn, [c] zqpcgm@gmail.com

Abstract. To meet the demand of aerospace industry and anti-armor technique, scholars paid much attention to metallic–intermetallic laminate (MIL) composites to get some materials with higher properties like high performance and low specific gravity. In this work, Ti-$TiAl_3$-Ti multilayer composites were obtained using explosive weld method and annealing. The microstructure of the composites are investigated with optical microscopy, scanning electron microscopy (SEM) and X-ray diffraction (XRD). Microhardness measurement was carried out using a Vickers microindenter testing machine. Quasi-static tensile test and bending test were carried out with universal testing machine.

1. Introduction

Ti-$TiAl_3$ metallic–intermetallic laminate (MIL) composites have attracted many scholars attention for its advantages of low specific gravity, high strength, heat and corrosion resistance [1]. But many of the multilayer composites are obtained through sintering process which will take more time for the foils to react [2]. Explosive welding is an effective one-step welding method to fabricate multilayer composites. The aim of this work is to study the fabrication of Ti-$TiAl_3$ MIL by explosive welding and following annealing, and its microstructure and mechanical property is also investigated.

2. Experimental procedure

The Ti alloy (grade TA1) and pure Al plates in dimension of 150mm×100mm×0.5mm were used as initial materials in this study. The Ti and Al plates were stacked alternately in a parallel scheme. Two kinds of powder explosives were used; and the detonation velocities are 2.5 km/s and 3.2 km/s, respectively. The as-received composites were annealed at 640 °C for 4 h in the air atmosphere without pressing. The microstructures of the welded samples before and after heat treatment were observed using optical microscopy and scanning electron microscopy. The EDS tests were carried out to characterize the elements distribution and diffusion thickness at the interface between Ti and Al. The phase composition at the interface after heat treatment was analyzed by x-ray diffraction. The mechanical properties of Ti-$TiAl_3$ MIL were measured to estimate the effect of various microstructures and heat treatment. The microhardness distribution from top to bottom was investigated using a Vickers microindenter testing machine, with a loading of 50g and the dwell-time of 15 s. The tensile and three point bending tests were carried out using universal testing machine (INSTRON-5985) with a loading rate of 5mm/min.

3. Results and discussion

The microstructures of the cross-section of composites before and after heat treatment are shown in Fig.1. The morphology shown in Fig.1a presents that Ti-Al multilayers were successfully fabricated with a typical wavy interface [3]. The wavelength and amplitude decreased from the top to bottom and no voids or cracks were observed along the interfaces. Fig.1b shows the cross-section of Ti-$TiAl_3$ MIL, which was obtained from the heat treated Ti-Al multilayers. It shows that the Al layers have been completely consumed during the induced reaction between Ti and Al. Voids were observed at the intermetallic layers. The XRD result shows that only $TiAl_3$ phases were formed at the interface, as shown in Fig. 2.

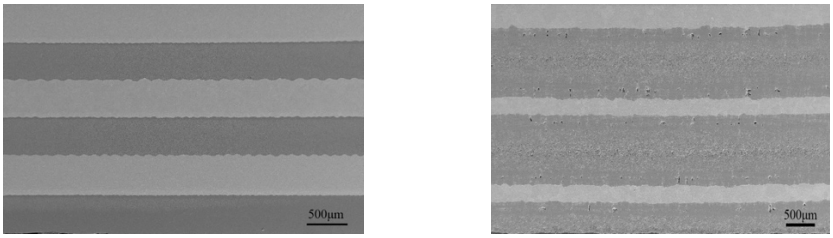

(a) (b)

Fig. 1 Microstructure observation images on the cross section of the composite obtained by SEM (a) TA1-Al composite after explosive weld; (b) composite after heat treatment at 640℃ for 4h

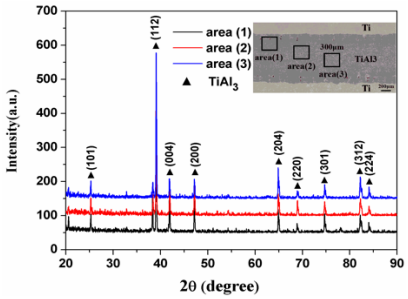

Fig. 2 XRD result of $TiAl_3$ from the top area to the middle area

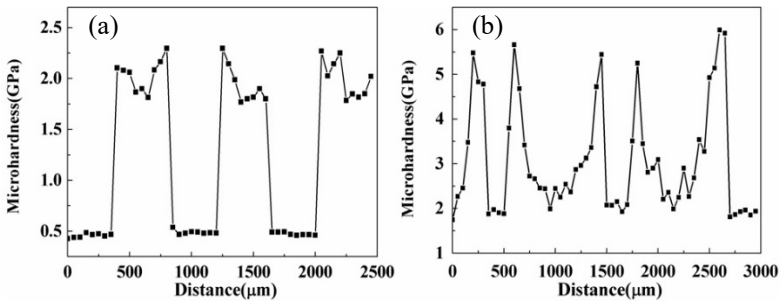

Fig. 3 Microhardness across the layers of the composite (a) TA1-Al composite after explosive weld; (b) composite after heat treatment at 640°C for 4h

The microhardness profiles at cross-section of Ti-Al multilayer was presented in Fig 3a. It shows that the hardness of Al plates throughout the cross-section is constant while the TA1 plates present higher hardness near the interface, which results from the dislocations and fine grains due to the extreme high pressure and severe deformation at the impact surface. The microhardness profiles at cross-section of Ti-$TiAl_3$ MIL, was presented in Fig. 3b. The distribution along each intermetallic layer is not uniform, showing a high hardness of 5.5 GPa at the interface and low one of 2 GPa at the center. The microstructure of intermetallic shows a dense morphology near the interface and voids at the center, which is mainly responsible for the low hardness. It is noticed that the grain size of $TiAl_3$ near the interface is smaller than the one at center; the reason for its formation will be discussed in detail.

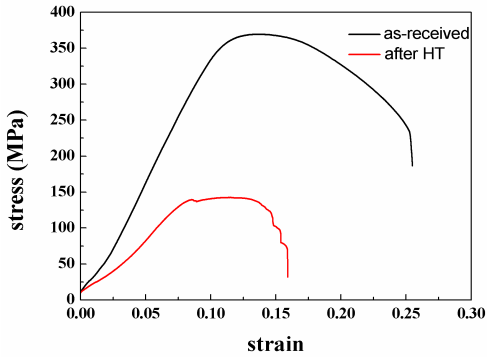

Fig. 4 Strain-stress curve of the sample before and after heat treatment

The tensile test result was presents in Fig.4. It shows that the tensile strength of this Ti-Al composite plate is 369MPa, with an elongation rate of 24%, and after heat treatment the tensile strength and elongation are lower than the sample without annealing.

Conclusions

The Ti-Al multilayer and Ti-$TiAl_3$ MIL were successfully fabricated by explosive welding and subsequent heat treatment. After heat treatment, all the Al were consumed and only TiAl3 were generated. The TiAl3 layers shows a high hardness of 5.5GP and an inhomogeneous structure due to the existence of voids. Tensile strength and elongation of the Ti-$TiAl_3$ MIL are lower than that of as received Ti-Al clad plate.

References

[1] Bataev I. A., Bataev A. A., Mali V. I. Structural and mechanical properties of metallic-intermetallic laminate composites produced by explosive welding and annealing. Materials & Design, 2012, 35, 225-234.
[2] YU, H. Preparation of Al-Al3Ti in situ composites by direct reaction method. Rare Metals, 2006, 25, 32-36.
[3] Lazurenko D.V., Bataev I.A. Explosively welded multilayer Ti-Al composites: Structure and transformation during heat treatment, *Materials and Design*, 2016, 102, 122-130

ADVANCED EXPLOSIVE METALWORKING INDUSTRIAL TECHNOLOGIES

A. Szalay[1,a], A. G. Mamalis[2,b], I. Zador[1,a]

[1] *S-Metalltech 98 Materials R&D Ltd (Budapest, Hungary)*
[2] *Project Center for Nanotechnology and Advanced Engineering, NCSR "Demokritos"*
[a]info@smet.hu, [b]agmamalis@yahoo.com

Abstract. Application of the High Energy Formings (HERF) technologies meets the principles of the Industry 4.0. The flexibile HERF technologies represent a new paradigm in the field of production of knowledge-based more components materials, furthermore manufacturing of special component parts: the processing of the materials is carried out directly, by high speed, high energy shock waves, without using energy transforming equipment as hydraulic presses etc. The energy sources of the HERF technologies, the high explosives can be utilized for many metalworking techniques. The three main type of the explosive metalworkings practised by us are the explosive welding and cladding, the explosive tubeforming and the explosive compaction of powders and granulates. The paper briefly introduces the principles, the practices furthermore the application possibilities of the three main types of the explosive metalworkings mentioned above.

1. Introduction

The term "Industry 4.0", originates from a project in the high-tech strategy of the German government. The characteristics given for the German government's Industry 4.0 strategy are: the strong customization of products under the conditions of highly flexible (mass-) production. Industry 4.0 fosters what has been called a "smart factory". Application of the High Energy Forming (HERF) technologies using the energy of high explosives meets these conditions.

A high explosive is a compound which, when subjected to heat, impact, friction, or shock, undergoes very rapid, self-propagating, heat- producing decomposition. This decomposition produces gases that exert tremendous pressures as they expand at the high temperature of the reaction. The work done by an explosive depends primarily on the amount of heat given off during the explosion. All commercial explosives except black powder are high explosives. The high explosives can be utilized for many metalworking techniques as the explosive welding/cladding, the explosive tubeforming and the explosive compaction of powders and granulates [1].

2. Explosive cladding

- ***What is the explosive cladding?***

Practically „explosive cladding" is the name of the technology serving for manufacturing two- or more layers plates and sheets by explosion.

- ***Principle of the explosive cladding***

Explosive cladding is a solid-state process in which controlled explosive detonations force two or more metals together at high pressures, resulting a high-quality metallurgical bond between the colliding surfaces (Fig.1). The bonding zone of the two metals has a characteristic wave-form.

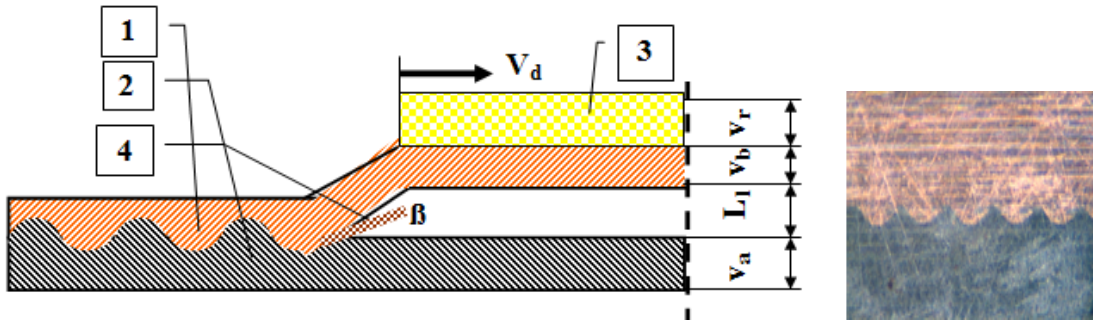

Fig.1: Principle of the explosive cladding: 1-clad plate, 2-base plate, 3-high explosive, 4-jet and the picture of the bonding zone (MgB superconductor + copper bimetallic)

The major advantages of the explosive cladding process in comparison the conventional ones are that bond can be created between normally incompatible metals (e.g. aluminum and steel).

- ***Possible applications of the explosive cladding***

The electrical industry, the vehicle production, the nuclear technique use many special multi-component materials, and component parts as two- or more-layer cladded plates, sheets, wires and component parts [2],

[3]. Applying conventional metal processing techniques as stamping, clamping, machining on explosively cladded two- or threelayer metals, different component parts can be manufactured as bimetallic washers, thermobimetals, superconducting joints etc.

3. Explosive tube forming

- ***What is the explosive tube forming?***

Technology where directed shock waves are used for manufacturing shaped parts of metallic tubes.

- ***Principle of the explosive tube forming***

The shock waves acting on the inner or outer surface of the tubes cause the plastic deformation of the metals, forcing them into the properly forms.

- ***Possible applications of the explosive tube formings***

Manufacture of formed heat exchanger tubes with elevated efficiency, where the pressure created by the detonation acts on the outer surface of the metal tube.

4. Explosive powder compaction

- ***What is the explosive powder compaction?***

The explosive compaction process is generally used for compacting ceramics and metal powders into various shapes. The shock wave generated by the detonation is transmitted to the material powder and generates two main effects, the joining effect of high shock pressure and the effect of high temperature, which lead to the increase of the sample density and cohesion [4].

- ***Principle of the explosive compaction***

The basic requirements for explosive compaction are a tube-form metal container filled with powder or granulate around which an explosive (powder-form, plastic, cord-form or liquid) is spread. Detonating the high explosive results in a shock wave acting on the metallic container, reducing its diameter which results the compaction of the powder or granulate.

- ***Possible applications of the explosive compaction***

The explosive compaction process is generally used for compacting ceramics and metal powders into various shapes. By applying the properly calculated and directed shock waves on powders or powder-mixtures special tasks can be realised as:

– preparation of metallic matrix composites reinforced with ceramic and carbide particles aiming at creation of reinforced structural materials
– special material composition can be manufactured by explosive powder compaction and subsequent processing as extrusion and wire drawing
– manufacture of aluminum sheathed boron carbide controlling rods for nuclear reactors

Conclusions

- The explosive metalworking technologies use the energy generated by an explosive detonation to form the metal workpiece. These processes can deliver a great deal of flexibility in the metal-forming processes.
- The explosive metalworkings can compete
  - with the roll cladding in the field of manufacturing two- or more layer metals
  - with the conventional hydro-forming, hot-stretch forming in the field of manufacturing special tubular form parts
  - with the static and isostatic pressing in the field of preparing special more component parts of powderform metals, ceramics and mixtures of those
- But we have to consider that the explosive metalformings serve not for replacement but for completion the conventional metalworking technologies.

References

[1] Prümmer R. *Explosive Welding, Forming and Compaction.* Ed. Blazynski T.Z. Applied Science, London 1983
[2] Gulbin, A.B., Thermobimetals mechanical properties produced by explosive welding with rolling*, J. de Phys. IV, v7 n 3,* Aug 1997
[3] www.emsclad.com, Clad metal from Engineered Materials Solutions
[4] Mamalis A.G. & Szalay A. & Rath, T. *Preparation of metal/metal and metal/ceramic component parts by explosive compaction* 5th EFEE World Conference 26-28 April 2009, Budapest, Hungary

SYNTHESES OF TI-AL-SI-B-C NANOCOMPOSITES BY MECHANICAL ALLOYING AND EXPLOSIVE COMPACTION

M. Chikhradze[1,a] , F.D.S Marquis[3], N. Chikhradze[1,2], G. Abashidze[2], A.Gigineishvili[1], T. Bzhalava[1]

[1]Georgian Technical University, 75 Kostava Str., Tbilisi 0175, Georgia
[2]G.Tsulukidze Mining Institute, 7 E.Mindeli str, Tbilisi 0186, Georgia
[3]San Diego State University, 5500 Campanile Drive San Diego, CA 92182-8010,USA
[a] m.chikhradze@gtu.ge

Abstract. Nanocomposites of Ti-Al-Si-B-C systems are characterized with unique physical and mechanical properties. They are attractive and can be used wide range of areas including aerospace, power engineering, machine and chemical fields. The coarse crystalline Ti, Al, C powders and amorphous B were used as initial elements. Different compositions of Ti, Al and C were prepared for mechanical alloying. Determination and selection of blend compositions was made on the base of phase diagrams. The powders were mixed according the selected ratios of components to produce the blend. Blends were processed in high energetic "Fritsch" Planetary premium line ball mill for mechanical alloying, syntheses of new phases and ultrafine particles formation. The blends processing time was variable and change between: 1 to 10 hours. The optimal technological regimes of blend preparation were determined experimentally. Ball milled blends investigated in order to determine properties after milling and mechanical alloying. Ultrafine bland were consolidated using explosive compaction technology. Explosive consolidation technology was used for bulk composite formation. Consolidated samples were processed and prepared for the structural investigations. The paper includes structural investigations results of milling process and explosive compaction of compositions of Ti-Al-B-C powders, optimal technological parameters for explosive compaction and formation of bulk ultrafine-grained composites. The current article also includes the structural investigations of prepared samples.

1. Introduction

The increasing role and interest towards advanced materials is promoted and in direct connection with the development of engineering and materials science. Therefore there are number of investigations for the development of Ceramic and metal-ceramic composite materials by different conventional technologies [1-3]. The composite nanostructure materials are expected to be characterized with unique mechanical and physical properties which can work resist at high temperature and aggressive media. Majority of such materials represent the prospective materials for application in modern machine building, airspace, chemical and metallurgical industry and other fields. At the same time, it must be mentioned, that the wide application of composite materials is restricted due to the absence of effective technologies for the production of such materials. Industrial application of nanocrytalline materials requires the low cost production of the relevant quantity of nanopowder and simple technology for the consolidation of nanoparticles for obtaining bulk materials. In this point, it is very important to develop technologies which are orientated on industry and are characterized with resource-saving, environmentally friendly characteristics.

Several conventional methods are known for obtaining bulk ultrafine grained/nanostructured materials[4]. Some of those methods require use of high pressure and high temperature for long period of time. Because of significant coarsening of the ultrafine grains, nanostructure effects are decreased. Mechanical Alloying (MA) involves repeated cold welding, fracturing, and re-welding of powder particles in a high-energy ball mill. Because of the specific advantages, MA is used to synthesize a variety of ultrafine grained materials and nanocomposites. An important attribute of these nanocomposites is in preventing or minimizing grain growth till very high temperatures [5].

Technology preparing powders my Mechanical Alloying (MA) technique and synthesis of bulk materials from ultrafine grained powders of Ti-Al-Si-B-C system are described in this work. One of the main problems for production of bulk nanostructured samples are connected with following: limitations on the sizes and geometry of bulk material, energy consumption; needs for complicated facility, difficulties to control grains sizes; significant coarsening of structure upon high temperature conditions for extended period of time.

Therefore, main objectives of the work can be formulated as follow: a) MA for obtaining nanopowder materials as precursors for synthesis of bulk materials and b) Explosive Consolidation (EC) technology for fabrication of the bulk nanostructured materials.

2. Experimental procedure

Different compositions of Si-C-B, Ti-Al-B-C and Ti-Al-C were prepared for MA procedures at the first stage. Preliminary selection of blend compositions was made on the basis of theoretical investigations. Different initial compositions of Si-B-C and Ti–Al–B–C systems, including: 2Ti/Al/C, 3Ti/2Al/1C and 3Ti/6Al/4B/1C elemental molar ratios. Compositions were selected according to the phase diagrams for binary and ternary systems. Coarse powders of Ti, Al, C, Si and amorphous Boron were used as starting precursors. Different compositions (with different elemental molar ratios) of Si-C-B, Ti-Al-B-C and Ti-Al-C were prepared for MA. Compositions were selected according to the phase diagrams for binary and ternary systems. Precursors were classified by vibratory sieves. The particles size of Ti and Al powders was less than 200 μm.

For MA and nanopowder production, the high energetic "Fritsch" Planetary premium line ball mill was used. The mill was equipped with Zirconium Oxide jars and balls. Ratio ball to powder by mass was 5:1. The time of the processing was varied in range: 1; 3; 5, 10 hours. Rotation speed of the jars was 500 rpm. MA was applied for the Ti-Al-B-C powders for 1-10 h processing time and prepared for applying EC technique. Preliminary works showed that the EC of metal-ceramic compositions is not only feasible but can produce materials of almost theoretical densities [6]. The major advantages of EC for bulk nanomaterials production are realization of high pressure, short processing time, and super high cooling rate (adiabatic cooling). The powder blend was loaded in the steel tube container (Fig.1-b,c). Cylindrical container/tube was closed from the both sides. A card box was filled with the powdered explosive and placed around the cylindrical powder container (Fig. 1-a). The experiments were performed at room temperature. The shock wave pressure (loading intensity) was around 10 GPa. The explosive was detonated by electrical detonator.

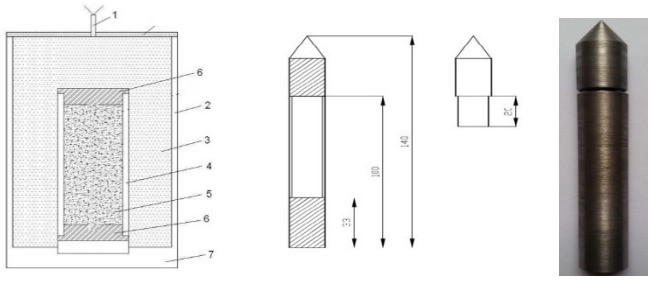

a b c

Fig. 1. a) Schematic view of assembly for fabrication bulk rod: (1) electrical detonator, (2) explosive's container, (3) explosive, (4) steel tube, (5) reaction mixture, (6) steel plugs, (7) base table, (8) detonator seizer; b) Schematic Container; c) Steel Container

The EC experiments were performed at the underground explosive chamber. For shock wave generation the industrial explosives were used in the experiments. The optimal shock wave loading pressure is varied in the range of (7-10) GPa. In these conditions the configuration of loading/unloading waves in powder and container allows one to initiate the syntheses in the reaction mixture, to simultaneously consolidate it and to fix the phase composition under adiabatic cooling.

Conclusions

- Different compositions of Ti-Al-Si-B-C were selected for formation of composites with nano structure. The optimal regimes for MA of Ti-Al-Si-B-C powders, such as ball to powder ratio, rotation speed, media conditions were established.
- The optimal shock wave loading pressure was selected and tested experimentally.
- Were established the following: if shock wave pressure and developed energy exceed the strength limits of the container the resulting effects are destruction.
- The microstructure and particle sizes were studied after MA and Before EC. By preliminary investigations is established, that the structure of bulk samples is not uniform. Structure is presented by nanosized and coarse grains.
- SEM investigations were carried out for EC samples.
- Regimes for obtaining nanocomposites in Ti-Al-Si-B-C composition has been elaborated.

Acknowledgment

This work was supported by Shota Rustaveli National Science Foundation (SRNSF) [grant #218008, Project Title: "Syntheses of Ceramic Nanocomposites in Si-B-C System by Mechanical Alloying and Explosive Compaction"]

References

[1] Mania M. Dabrowski et all. Some application of TiAl Micropowders Produced by Self-Propagating High Temperature syntheses, International Journal of Self-Propagating High-Temperature Synthesis. vol. 12 no. 3 s. 159–164, 2003.
[2] Levashov E.A., Senatulin B.R. et all. Peculiarities of the Functionally Graded Targets in Combustion Wave of the SHS-System with Working Layer Ti-Si-B, Ti-Si-C, Ti-B-N, Ti-Al-B, Ti-C, Book of Abstracts. IV Int. Symposium on SHS, Technion, Haifa, Israel, Feb. 17-21, p.35, 2002.
[3] Merzhanov A.G., Pityulin A.N. Self-Propagating High-Temperature Synthesis in Production of Functionally Graded Materials. Proceedings of 3 rd Int. Symp. on FGM, Lausanne, Switzerland, pp.87-94. 1995.
[4] Hebeisen J., Tylus P., Zick D., Mukhopadhyay D.K., Brand K., Suryanarayana C., Froes F.H. "Hot Isostatic Pressing of Nanostructured γ-TiAl Powders", Metals and Materials, Vol. 2. No. 2 (1996) pp. 71-74.
[5] Suryanarayana C. Mechanical alloying and milling, Progress in Materials Science 46 (2001) 1-184, 2001.
[6] Kecskes L.J., Woodman R.H., Chikhradze N., Peikrishvili A. Processing of Aluminum Nickelides by Hot Explosive Consolidation, International Journal of Self-Propagating High-Temperature Synthesis Volume 13, #1, 2004.
[7] Prummer R. Explosive Working of Porous Materials, Springer-Verlag Berlin Heldelberg, New York, 1987.

DIAGNOSIS OF DYNAMIC ECCENTRICITY FAULT IN INVERTER-FED PERMANENT MAGNET SYNCHRONOUS MOTOR BASED ON ZERO SEQUENCE VOLTAGE COMPONENT

Jawad Faiz[1,a], Mohamad Sadegh Bozorgian[1,b], Ehsan Mazaheri-tehrani[1,c]
[1]*School of Electrical and Computer Engineering, College of Engineering, University of Tehran, Tehran, Iran*
[a]jfaiz@ut.ac.ir, [b]ms.bozorgian@gmail.com, [c]ehsanmzht@gmail.com

Abstract— In this paper the finite element method is employed to simulate the healthy and faulty inverter-fed permanent magnet synchronous motor (PMSM). An on-line and non-invasive method based on zero sequence voltage component (ZSVC) for dynamic eccentricity fault diagnosis, which is independent of the load, for inverter-fed PMSM is proposed. The purpose of this method is to determine the frequency pattern due to dynamic eccentricity fault in the ZSVC signal for PMSM controlled by sensorless control ZSVC. Finally, some indexes are suggested for the fault detection.

Index Terms— PMSM, ZSVC, Inverter-fed, Dynamic eccentricity fault.

Introduction

The use of permanent magnet (PM) electrical machines in industry is rising due to their enormous advantages, such as high-power density, high efficiency and better dynamic performance compared to conventional machines, including induction machines. Eccentricity fault is an important fault in the PM machines in terms of occurrence rate and known as a progressive fault. Therefore, early detection of this fault is of paramount importance in order to prevent the fault expansion and further maintenance cost.

In [1], a fault detection method based on zero sequence voltage component (ZSVC) for induction machines has been presented. In addition, demagnetization fault detection method based on the ZSVC for PM synchronous motor (PMSM) has been introduced in [2]. Yet, there has never been a method introduced based on ZSVC for dynamic eccentricity detecting.

Fault diagnosis

To reduce the torque ripple and output current harmonics in PMSM, vector control with high precision can be implemented for control of the motor. This methods needs precise data of the rotor position which obtained through sensors fixed on the shaft of the motor. In addition to increasing the cost and geometrical size of the motor, this can decrease the reliability of the system. Therefore, many sensor-less methods have been introduced for more accurate control of the motor.

There are several sensor-less control techniques based on the 3rd harmonic of bemf (zero sequence voltage) [3, 4] which are very popular due to their simplicity and low cost. One problem of application of this technique is accessibility to the neutral in star-connected motor. Since current does nor pass the wire connected to the neutral, this wire is thin like signal wires and has no complexity.

Three methods have been introduced for measurement of the 3rd harmonic bemf and the most efficient and appropriate one is chosen for this measurement. Then mathematical analysis of the bemf under dynamic eccentricity fault in the PMSM is presented and the harmonics generated by the fault in the frequency spectrum of the bemf are determined.

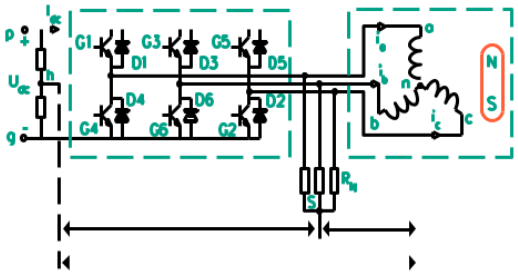

Fig. 1. Overall plan of the drive of a BLDC machines

Fig. 1 shows the overall plan of the drive of a BLDC machines with Y-connected resistance network in which measurement of the 3rd harmonic components of the bemf is possible. Three techniques are introduced for measuring the 3rd harmonic:

1. Voltage u_{sa} between the neutral of Y of the resistance network and neutral of the stator winding n.
2. Voltage u_{sh} between s and middle of DC bus.
3. Voltage u_{nh} between n and h.

The Table I summarizes the different measurement techniques of zero sequence voltage

Table I. different measurement techniques of zero sequence voltage

Voltage	BLDC Mode	BLAC Model
u_{sn}	3rd harmonic of bemf	3rd harmonic of bemf
u_{sh}	50% of 1st harmonic of bemf+PWM noise	PWM Noise
u_{nh}	Sum of 1st harmonic of bemf of two active phases+ PWM noise	3rd harmonic of bemf+PWM noise

The inverter switches on ZSV occurring at high frequencies has no impact upon fault diagnosi sidebands and can be filtered. PMSMs are analyzed and effects of stator slots and non-uniform air gap caused by dynamic eccentricity are also investigated. The following frequency pattern is introduced for dynamic fault detection:

$$f_{eccentricity} = \left[(2\chi - 1) \pm \frac{k}{p}\right] 3f_s \quad (1)$$

where χ is 1, 2, 3.. and fs is the supply voltage frequency

Two-dimensional finite element method (FEM) is used to model the healthy and faulty motor. Distortion and imbalanced in magnetic flux and flux density, stator current and bemf caused by dynamic eccentricity fault are addressed. This fault increases the amplitude of sidebands in the frequency pattern (1) in the ZSV spectrum. By comparing the sideband components due to the dynamic eccentricity fault in the stator current and ZSV voltage sensitivity and high reliability of the proposed indexes compared with MCSA method is studied.

Results

Fig. 2 illustrates the spectra of the ZSVC of a healthy PMSM and a PMSM with 25% dynamic eccentricity fault in rated load and speed. Since the fundamental frequency of the ZSVC is $3f_s$, and f_s at the rated speed is 200 Hz, the fundamental frequency of the ZSVC is 600 Hz. It is indisputable that the dynamic eccentricity fault leads to an increase in the amplitude at the frequencies of 150 Hz, 300 Hz, 450 Hz, 750 Hz, and so on.

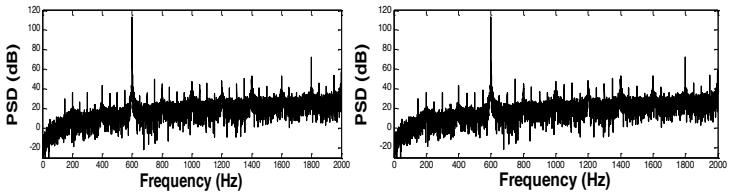

(a) (b)

Fig.2. Spectrum of ZSVC in nominal load and speed: (a) healthy PMSM and (b) 25% dynamic eccentricity fault

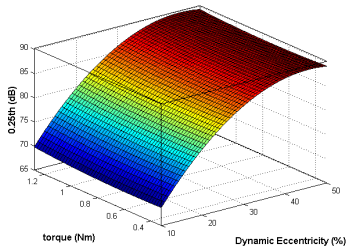

Fig.3. Effect of variation of load and eccentricity fault severity on amplitude of 0.25th harmonic

Moreover, in Fig. 3, the impact of variation of load and eccentricity fault severity on the amplitude of 0.25th harmonic is demonstrated. From Fig. 2, it can be inferred that the sidebands are independent of the load, which is one of the most prominent characteristics of this index. It is concluded athat.

1. The proposed index is independent of the load variations and it is constant by increasing the load.
2. The speed rising leads to the increase of the proposed side-bands used for the fault diagnosis.
3. Investigation of the faults severity and comparing the generated side-bands components due to the dynamic eccentricity fault in the stator current and ZSV indicates that the introduced indexes in the ZSV have higher sensitivity and reliability with compared with that of the stator current.

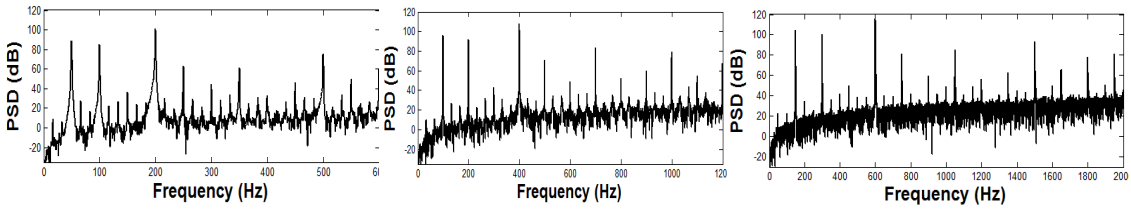

(a) (b) (c)

Fig.4. Spectrum of ZSVC in nominal load at speeds: (a) 1000 rpm, (b) 2000 rpm and (c) 3000 rpm.

References

[1] Garcia P., Briz F., Degner M.W., and Diez A.B. "Diagnostics of induction machines using the zero sequence voltage," in *Industry Applications Conference, 2004. 39th IAS Annual Meeting. Conference Record of the 2004 IEEE*, 2004, vol. 2, pp. 735–742.

[2] J.-R. Ruiz R., Rosero J. A., Espinosa A.G., and Romeral L. "Detection of demagnetization faults in permanent-magnet synchronous motors under nonstationary conditions," *IEEE Trans. Magn.*, vol. 45, no. 7, pp. 2961–2969, 2009.

[3] Emf T.B., Liu J.M., and Zhu Z.Q. "Improved Sensorless Control of Permanent-Magnet Synchronous Machine Based on," vol. 50, no. 3, pp. 1861–1870, 2014.

[4] Morimoto S., Sanada M. and Takeda Y. "Inverter-driven synchronous motors 98 for constant power," IEEE Ind. Appl. Mag., vol. 2, no. 6, pp. 18–24, 1996.

NONCONTACT IRON LOSS MEASUREMENT OF MOTOR STATOR CORE USING RADIATION THERMOMETER IN THE ATMOSPHERE

Daisuke Wakabayashi[1,a], Mohachiro Oka[2,b], Masato Enokizono[1,3,c]

[1] *Nippon Bunri University, Faculty of Engineering, Department of Mechanical and Electrical Engineering, Japan*
[2] *National Institute of Technology, Department of Information Engineering, Japan*
[3] *Vector Magnetic Characteristic Technical Laboratory, Japan*
[a]wakabayashids@nbu.ac.jp, [b]oka@oita-ct.ac.jp, [c]enoki@oita-u.ac.jp

Abstract. The use of a low iron loss motor core is required to develop the low loss and high efficiency motor. The main material of the motor core is electrical steel sheet. Usually, the magnetic properties of the steel sheet are measured according to standard measurement methods (IEC, JIS, etc.). On the other hand, it is difficult to evaluate the characteristics of the iron core state because of the complicated shape. In this paper, we report the result of noncontact measurement of iron loss of motor using thermal measurement method in the atmosphere.

1. Introduction

A non-oriented electrical steel sheet is used for the motor core. The iron loss measurement of a electrical steel sheet is evaluated from the relationship between the magnetic flux density and the magnetic field strength using a standard measurement method such as an Epstein flame or a single sheet tester[1]. On the other hand, iron loss measurement of a motor core is difficult due to its complicated shape, and in general, it is equivalently evaluated using a ring core or the like. Moreover, in the motor core, since it processes and laminates a single sheet, it is different from the iron loss characteristic at the time of single sheet in many cases. This is known as a building factor problem, and stress due to processing affects the magnetic properties and appears as an increase in iron loss[2]. In addition to the iron loss evaluation of the motor core, if iron loss increase by the manufacturing process can be performed more simply, it can contribute to high efficiency motor development.

One of the iron loss evaluation methods is a method of evaluating from the heat generation time gradient[3]. In recent years, radiation thermometers that can measure heat generation with non-contact and small spots have become inexpensive, and their use in research and development and manufacturing processes has spread. A system has been developed that can accurately measure iron loss that occurs during actual driving of an actual motor using a non-contact thermal method[4]. It is a vacuum environment to eliminate the influence of motor rotation. On the other hand, the cost of the equipment is high and the measurement is not easy. We aim to be able to evaluate motor iron loss in the atmosphere and in a short time so that it can be used in the manufacturing process as well.

In this paper, the iron loss generated in the motor stator core is compared with the iron loss obtained from the magnetic characteristics for measurement in air using a noncontact radiation thermometer, and the accuracy is shown.

2. Measurement method

Figure 1 shows a motor stator core. An excitation winding and a magnetic flux density detection B-coil are wound around the outer periphery. Figure 2 shows a measurement system. The magnetic field strength of the core is calculated from the terminal voltage of the shunt resistor connected in series to the excitation winding, and the magnetic flux density is calculated by integrating the induced voltage of the B-coil. Install a noncontact radiation thermometer (Keyence, FT-H20) near the core and record it with a data logger (GRAPHTEC, GL240).

The iron loss W_c due to heat is calculated by the following equation.

$$W_c = C\frac{\partial T}{\partial t} \tag{1}$$

where, C is specific heat, T is temperature, and t is time. The iron loss due to heat generation can be evaluated by measuring the temperature gradient.

3. Experimental Results

The measurement results are shown in Figure 3. Figure 3(a) shows a time change of heat generation generated in the motor stator core after the start of excitation. The third temperature measurement shows a similar temperature gradient. The result of having calculated the iron loss using this temperature gradient using Formula (1) is shown in Figure 3(b). The black plot shows the iron loss obtained from the average magnetic

properties of the core. Thermal iron loss increases with magnetic flux density as well as core loss obtained from magnetic properties. In the case of thermal iron loss, since it is a local iron loss measurement, it may increase or decrease compared with average iron loss.

Conclusions

In this paper, the thermal iron loss of the motor stator core using a non-contact radiation thermometer is measured in the atmosphere and compared with the average iron loss, and the accuracy is shown. In addition, in full paper, we will report on the results of comparisons by the location of the motor stator core surface and the evaluation of the lamination surface.

Acknowledgments

This work was supported by Tsugawa Foundation (Japan).

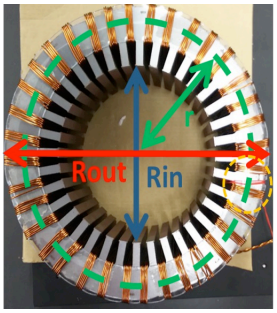

Rout[mm]	160
Rin[mm]	100
Tickness[mm]	65
r[mm]	72
Turn of Ex-coil	180
Turn of B-coil	3

Fig. 1 Specimen (motor stator core);

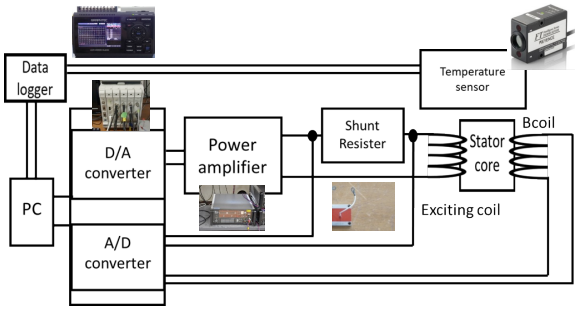

Fig. 2 Measurement system

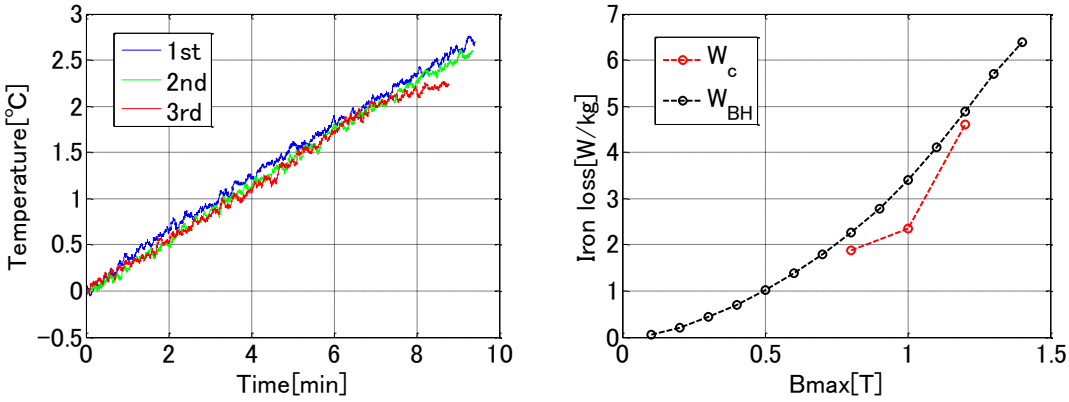

(a) (b)

Fig. 3 Experimental results: (a) Temperature gradient; (b) Iron loss

References

[1] Sievert J., The measurement of magnetic properties of electrical sheet steel – survey on methods and situation of standards, *Journal of Magnetism and Magnetic Materials*, Vol.215-216, 2000, pp.647-651

[2] Oka M., Kawano M., Shimada K., Kai T., Enokizono M. Evaluation of the Magnetic Properties of the Rotating Machines for the Building Factor, *PRZEGLĄD ELEKTROTECHNICZNY*, Vol. R87, 2011, pp.43-46

[3] Narita K., Imamura M. Studies on a thermometric method of measuring local iron losses in an electrical sheet, *Trans. IEEJ*, Vol. 94-A(4), 1974, pp.167–174

[4] Sato T., Enokizono M. Evaluation of stator core loss of high speed motor by using thermography camera, *AIP Advances 8*, 2017, 047609

SIMPLE METHOD FOR MICRO FLOW GENERATION USING MAGNETIC FLUID AND SMALL CUBIC PERMANENT MAGNET

Seiichi Sudo[1,a] and **Masahide Ito**[1,b]
[1]*Akita Prefectural University, Aza-ebinokuchil 84-4, Yurihonjo-shi, Akita-ken 015-0055, Japan*
[a]sudo@akita-pu.ac.jp, [b]itouera@gmail.com

Abstract. This paper proposes a simple method to generate some water micro flows. The method is a wireless energy supply system composed of a magnetic fluid and a cubic permanent magnet. The magnet—magnetic fluid element was submerged in the water. Immiscible magnetic fluid was adsorbed on the small permanent magnet in water. The system was driven by the external alternating magnetic field created by the coil. The interface of magnetic fluid responded to the alternating magnetic field with harmonic oscillation. The interfacial oscillation of magnetic fluid generated micro water flows. The generation of micro water flows was confirmed by visualization technique. The details of micro water flow and magnetic fluid interface response to the alternating magnetic field were revealed experimentally.

1. Introduction

Extensive studies on the flows induced by the vibration have been conducted for a long time. Such flows are especially of interest in fields such as acoustic streaming, acoustic levitation, heat exchanger, naval architecture, aerospace engineering, and civil engineering. For example, the vortex flows formed around a solid sphere or a cylinder in vibrating air were observed using smoke particles experimentally [1]. The flows around an oscillating cylinder in a fluid at rest were investigated by the visualization method [2]. Flow fields from transversely oscillating circular cylinders in water at rest were studied by numerical solution of Navier-Stokes equations [3]. Quantitative measurements on streaming flows forced by mechanical vibrations within a two-dimensionally confined geometry were presented [4]. In these studies, however, mechanical vibration generators such as electrodynamic shakers and diaphragms were used for excitation vibration. Wireless energy supply system for micro flow generation is important in microsystem applications such as μ-TAS, lab- on-a-chip, micro-mixer, and micro-reactor.

In this paper, a new simple method to generate micro water flows using wireless energy supply system was proposed. Water micro flows were driven by the interfacial oscillation of immiscible magnetic fluid adsorbed on a small permanent magnet in water. The interfacial oscillation of magnetic fluid was actuated by the alternating magnetic field with small intensity amplitude. Micro water flows around the magnetic fluid were visualized and the flow properties were revealed experimentally.

2. Principle of the proposed method

Schematic diagram of the proposed simple method for generation of micro water flow is shown in Fig.1. The flow generation system consist of small cubic NdFeB permanent magnet and hydrocarbon-based magnetic fluid. The permanent magnet is adhered to an acrylic resin flat plate. Magnetic fluid is adsorbed on the permanent magnet and it is immiscible with water. This magnet-magnetic fluid element is submerged in water. When the element is subjected to alternating magnetic field along the direction of magnetic pole of the permanent magnet, the interface of magnetic fluid responds in elongation and contraction [5]. This interface oscillation of magnetic fluid induces flows in the surrounding liquid (water).

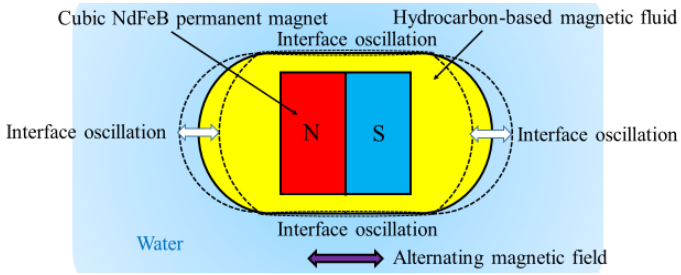

Fig. 1 Principle schematics of a simple method for generation of micro water flow

3. Experimental apparatus

The experimental apparatus was composed of magnet-magnetic fluid element, external alternating magnetic field generation system, and high-speed video camera analysis system. The NdFeB permanent magnet used in the experiment was a cube 5mm on each side. The sample magnetic fluid was synthetic hydrocarbon-based MSG P50 (Ferrotec Co.). The alternating magnetic field was generated by the Helmholtz

coil. The high-speed video camera analysis system was used to observe the flow phenomena. Fig.2 shows the photograph of the experimental apparatus.

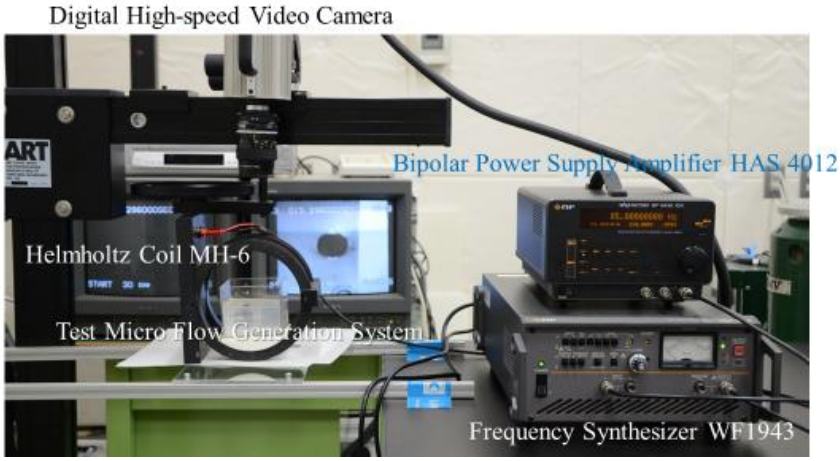

Fig. 2 Photograph of experimental apparatus

4. Experimental results and discussion

When the alternating magnetic field was applied to the magnet-magnetic fluid system in water, the interfacial oscillation of magnetic fluid was generated. The interface of magnetic fluid adsorbed on the permanent magnet showed a harmonic response to the external magnetic field. The interfacial oscillation generated flows around the magnetic fluid. A flow visualization picture is shown in Fig.3. In Fig.3, the volume of magnetic fluid is V_m=300μl, the frequency of alternating magnetic field is f_0=75 Hz, and the total amplitude of applied voltage to the Helmholtz coil is E_0=90 V. In Fig.3, the symbol t is the elapsed time after applying the external alternating magnetic field. It can be seen from Fig.3 that four flows are flowing out of the magnet-magnetic fluid element. The velocity of the water flow depends on the amplitude of magnetic field strength.

Fig. 3 A series of photographs indicating the progress of four flows produced around magnetic fluid element

Conclusion

Micro water flows were generated by the proposed system. The tip of flows grew with the elapsed time after applying the external alternating magnetic field.

References

[1] Andrade E. N. DA. C., and Filon L. N. G. "On the circulations caused by the vibration of air in a tube," *Proc. Roy. Soc. London,* vol. A134, pp.445-470, 1932.

[2] Tatsuno M., and Bearman P.W. "A visual study of the flow around an oscillating circular cylinder at low Keulegan-Carpenter numbers and low Stokes numbers," *J. Fluid Mech*., vol. 211, pp.157-182, 1990.

[3] Uzunoğlu B., Tan M., and Price W.G. "Low-Reynolds-number flow around an oscillating circular cylinder using a cell viscous boundary element method," *Int. J. Numer. Meth, Engng.*, vol. 50, pp. 2317-2338, 2001.

[4] Costalonga M., Brunet P., and Peerhossaini H. "Low frequency vibration induced streaming in a Hele-Shaw cell," *Phys. Fluids*, vol.27, pp. 013101, 2015.

[5] Sudo S., Asano D., Takana H., and Nishiyama H. "The dynamic behavior of magnetic fluid adsorbed to a small permanent magnet in alternating magnetic field," *J. Magn. Magn. Mater.,* vo. 323, pp. 2314-2338, 2011.

IRON LOSS EVALUATION FOR A SMALL HIGH-EFFICIENCY MOTOR STATOR CORE MADE OF AN ULTRATHIN ELECTRICAL STEEL SHEET UNDER PWM INVERTER EXCITATION USING THE STATOR WINDING EXCITATION METHOD

Mohachiro Oka[1,a], Masato Enokizono[2,b], Daisuke Wakabayashi[3,c], Hirofumi Kiyotake[1,d]

[1] *National Institute of Technology, Oita College, 1666 Maki, Oita-city, Oita, 870-0152, Japan*
[2] *Vector Magnetic Characteristic Technical Laboratory, 533 Joi Usa-city, Oita, 879-0442, Japan*
[3] *Nippon Bunri University, 1727 Ichigi Oita-city, Oita, 870-0397, Japan*
[a] oka@oita-ct.ac.jp, [b] enoki@oita-u.ac.jp, [c] wakabayashids@nbu.ac.jp, [d] kiyotake@oita-ct.ac.jp

Abstract. To develop a small high-efficiency motor for an aerospace machine, we developed a new stator core made of a 0.08-mm-thick ultrathin electrical steel sheet. The *B-H* curves and iron loss of the stator core were measured using the stator windings excitation method that we proposed. Experiments shows that when the excitation frequency was 2000Hz, the iron loss of the stator core was very low, and the eddy-current loss was especially low. Additionally, we measured the iron loss under pulse width modulation (PWM) excitation in the stator core. The stator core made of a 0.08mm-thick ultrathin electrical steel sheet for a small high-efficiency motor was deemed suitable for an aerospace machine.

1. Introduction

Motors used in space should be light and should generate little of heat. Small high-efficiency motors are being developed all over the world. In order to obtain a small high-efficiency motor, it is necessary to develop a high speed rotation motor. It is well established that the rotational speed of the motor is proportionate to driving frequency. However, when the rotational speed of the motor increases, it is understood that the iron loss in the stator core increases. Moreover, the drive by a PWM inverter increases the iron loss in the stator core of the motor [1, 2]. When the PWM inverter is used or a motor rotates at high-speed, the ensuing increase of iron loss in the stator core manifests as an eddy current. In order to decrease the eddy-current loss in the stator core of a small, high-efficiency motor, we developed a new stator core made of an ultrathin electrical steel sheet. Moreover, we compared the iron loss of the stator core that used this ultrathin electrical steel sheet and the iron loss of the stator core that used a conventional electrical steel sheet. In this paper, we report usefulness of the stator core made of an ultrathin electrical steel sheet.

2. Measurement Method

We prepared two small motor stator cores that were made of two kinds of electrical steel sheets including the 0.08-mm-thick ultrathin electrical steel sheet and a 0.35-mm-thick electrical steel sheet. The two stator cores were called the 0.08mm_Core and the 0.35mm_Core. Figure 1 shows the dimension and arrangement of a stator core, a dummy rotor, excitation coils and a search coil. The effective magnetic pass length shown in Fig. 1 occurred when the iron loss as measured. The dummy rotor was also made of the 0.08-mm-thick ultrathin electrical steel sheet. The stator cores and the dummy rotor were cut off of the laminated electrical steel sheet with a wire-electrical discharge machine and both laminated thicknesses were 12.5 mm. Figure 2 shows the schematic drawing of the magnetic property evaluation system under PWM wave excitation. When the iron loss was measured under PWM wave excitation, the excitation magnetic flux density controlled the maximum value (B_{ex1st}) of the fundamental wave of the measured magnetic flux density in the stator core.

3. Results

The iron loss W_i [W/kg] was evaluated using Eq. (1), where, ρ [kg/m^3] is the material density of stator cores and T [s] is the period of the excitation current (see below).

Figure 3 shows the measured the *B-H* curve of the 0.08mm_Core using the stator windings excitation method when the modulating signal frequency (f_m), the carrier frequency (f_c), B_{ex1st}, and modulation index (m) were 200 Hz, 5 kHz, 1.2 T, and 0.6, respectively. From this figure, the *B-H* curve was long and slender because there was a gap of 0.1 mm between the stator core and the dummy rotor. Moreover, the minor loop was observed through the influence of the PWM excitation wave form.

The comparison between the measured iron loss (W_{isin}) under the sinusoidal wave excitation and the measured the iron loss (W_{ipwm}) under PWM wave excitation when f_m, f_c , and m were 200Hz, 5 kHz and 0.6, respectively, is shown in Fig.4. As seen in Fig. 4, W_{isin} and W_{ipwm} of the 0.08mm_Core were smaller than those of the 0.35mm_Core. Moreover, the ratio of W_{ipwm} and W_{isin} (W_{ipwm}/W_{isin}) was 1.32 in the 0.08mm_Core, and

1.85 in the 0.35mm_Core. It is thought that the cause of the decreased iron loss of the 0.08mm_Core under the PWM inverter excitation condition was caused by a decrease in the eddy-current loss by a decrease in the electrical steel sheet thickness.

$$W_i = \frac{1}{\rho T}\int H_{ex} \cdot \frac{dB_{ex}}{dt}\,dt \tag{1}$$

Conclusions

We developed a new stator core made of a 0.08-mm-thick ultrathin electrical steel sheet. The magnetic properties of the new stator core were measured using the stator windings excitation method. The iron loss of the ultrathin electrical steel sheet clearly decreased at a excitation frequency (200Hz). The iron loss of the stator core was limited under PWM wave excitation as well. The stator core made of 0.08mm-thick ultrathin electrical steel sheet was suitable for the small high-efficiency motor well. The full paper shows the usefulness of the stator core made of an ultrathin electrical steel sheet..

Acknowledgments

We would like to thank the Japan Society for the Promotion of Science (grant no.17K06480) for partially funding our study.

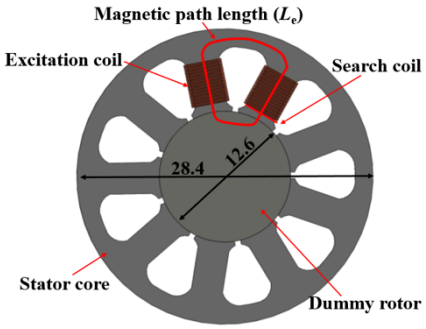

Fig.1. Arrangement of a stator core, a dummy rotor, excitation coils, and a search coil.

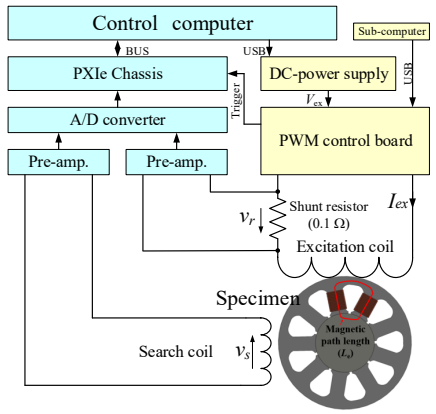

Fig.2. Schematic drawing of the magnetic property evaluation system under the PWM inverter excitation.

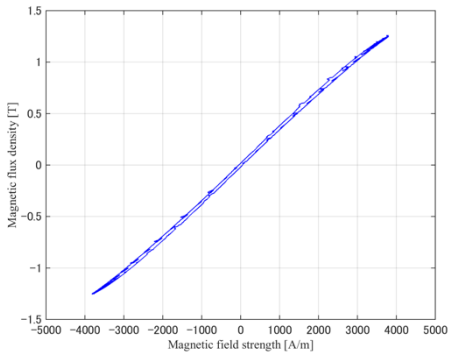

Fig.3. *B-H* curves (0.08mm_Core, f_m=200Hz, f_c=5kHz, m=0.6, B_{ex1st}=1.2T).

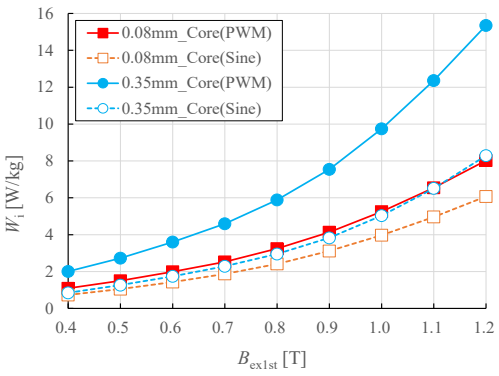

Fig.4. W_{isin} vs. W_{ipwm} (f_m=200Hz, f_c=5kHz, m=0.6).

References

[1] Kogi R., Odawara S., and Fujisaki K. Iron Loss Increase due to Increase of Carrier Frequency on Inverter, IEE Japan, MAG-13-150, 2013, pp. 7-12.

[2] Oka M., Enokizono M., Mori Y., Yamazaki M. Building Factor Evaluation of the Stator Core made of Ultrathin Electrical Steel Sheet for the High-speed Motor, Material Science Forum, Vol. 915, 2018, pp. 9-15.

CHARACTERISTICS COMPARISON OF SELF-PROPELLED ROTARY ACTUATOR IN CONSIDERATION OF SHAPE AND ROLLING DIRECTION OF STEEL SHEETS

N. Soda[1,a], T. Kawano[1], M. Enokizono[2,b]

[1] *Graduate School of Science and Engineering, Ibaraki University, Japan*
[2] *Vector Magnetic Characteristic Technical Laboratory, Japan*
[a]naoya.soda.magtec@gmail.com, [b]enoki@oita-u.ac.jp

Abstract. In this paper, in order to improve self-propelled rotary actuator, characteristics comparison of the actuator in consideration of shape and rolling direction of steel sheets used for the actuator is reported. A grain-oriented electrical steel sheet is used as the stator core of the actuator. The shape of steel sheets affects the characteristics of the actuator greatly. Moreover, the relation between a rolling direction of steel sheets and a direction of an exciting magnetic field is important for the starting torque and rotational stability of the actuator. Therefore, the relation between the shape and rolling direction of steel sheets in the stator of the actuator is investigated by finite element magnetic field analysis which introduced the complex E&S model which is one of a vector magnetic property utilization technique. Regarding the shape of steel sheets, a triangle and a rectangle are investigated. As a result, in order to improve the starting torque of the actuator, it is considered that a triangle is better than a rectangle as the shape of the stator core.

1. Introduction

In order to detect cracks and defects inside of a tube with complicated structure, it is necessary to develop an electromagnetic actuator self-propelled in a tube [1] [2]. An exciting magnetic field for moving an actuator is able to be easily supplied to the actuator in a tube from the outside of a tube by a solenoid coil which winded copper wire on the surface of a tube. In this case, the exciting magnetic field is induced in parallel to the axis direction of a tube by the coil. Therefore, the self-propelled rotary actuator whose rotational axis is parallel to the exciting magnetic field was fabricated as shown in Fig. 1 [3]. In this actuator, the pole pieces of the stator are made of a grain-oriented electrical steel sheet, and the rotor has permanent magnets. Moreover, as a feature of this actuator, the shape of steel sheets of the stator was not a rectangle, but a triangle as shown in Fig. 1. It was thought that a triangle steel sheet generates larger starting torque than a rectangle steel sheet, because magnetic flux distribution at the base of triangle steel sheet under an exciting magnetic field is asymmetrical to the rotational direction of the rotor as shown in Fig. 2 (a). However, as shown in Fig. 2 (b), by setting the rolling direction of a grain-oriented electrical steel sheet in the different direction from the exciting magnetic field direction, it was clarified that magnetic flux distribution at the end of the steel sheet becomes asymmetric even if the shape of stator is a rectangle [4] [5].

In this paper, the suitable setting direction of the rolling direction of triangle steel sheets is investigated by the magnetic field analysis. When carrying out magnetic field analysis in consideration of the rolling direction, it is effective to introduce the vector magnetic property utilization technique to the analysis. Therefore, the magnetic field analysis of self-propelled rotary actuator's stator is carried out by using the complex E&S model which is one of a vector magnetic property utilization technique.

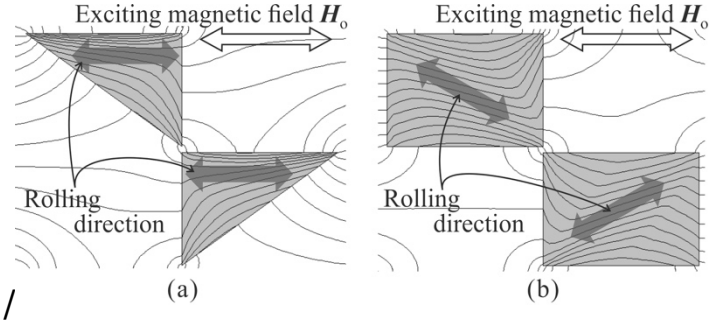

Fig. 1 The self-propelled rotary actuator.

Fig. 2 Magnetic flux lines in steel sheets of the stator under the exciting magnetic field.

2. Analysis results of stator core in the actuator

When the exciting magnetic field $\boldsymbol{H}_o$ is not applied, the rotor is stationary at the position stabilized by

the attractive force acting between the permanent magnets of the rotor and the steel sheets of the stator. As a result of experiment, the permanent magnets are stationary at the right-angle corner of the triangle steel sheets and are stationary in the middle of the rectangle steel sheets. The magnitude of starting torque of the actuator is dependent on the magnitude of y-axis direction of magnetic flux density over the magnet shown in Fig. 3 when the exciting magnetic field $\boldsymbol{H}_o$ is applied. Therefore, area-average of B_y (i.e., y-component of magnetic flux density) within the region of stationary position shown with the dashed line in Fig. 3 is calculated. The exciting magnetic field $\boldsymbol{H}_o$ is a sign waveform of the peak amplitude 500 Oe, and the frequency is 50 Hz. Fig. 4 shows the relation between the area-average of B_y within the region of stationary position and the inclination angle ϕ of the rolling direction in the triangle and rectangle steel sheets. The inclination angle ϕ of the rolling direction in the steel sheets is defined as shown in Fig. 3, and $\phi = 0°$ means the rolling direction of steel sheet is parallel to the direction of exciting magnetic field $\boldsymbol{H}_o$. In every inclination angle ϕ, the average of B_y of the triangle steel sheets is large than that of the rectangular steel sheets. The average of B_y in both the triangle and the rectangle steel sheets becomes large in accordance with increase of the inclination angle ϕ. The data enclosed with a circle in Fig. 4 denotes the maximum. The average of B_y of the rectangle steel sheets takes the maximum in $\phi = 30°$, however, that of the triangle steel sheets takes the maximum in $\phi = 35°$. The reason of this difference is effect of the shape of steel sheets. As shown in Fig. 2 (a), the magnetic flux lines bend at the end of the triangle steel sheets even if the rolling direction of the steel sheets is parallel to the direction of the exciting magnetic field $\boldsymbol{H}_o$. Furthermore, the maximum value of the average of B_y of the triangle steel sheets is about 1.7 times that of the rectangle steel sheets. These results indicate that a triangle steel sheet generates larger starting torque than a rectangle steel sheet.

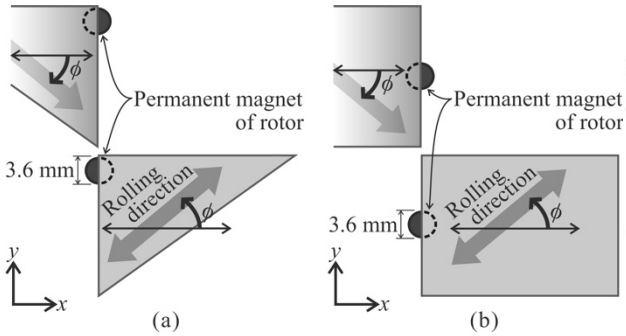

Fig. 3 The stationary position of the permanent magnet of the rotor when the exciting magnetic field $\boldsymbol{H}_o$ is not applied.

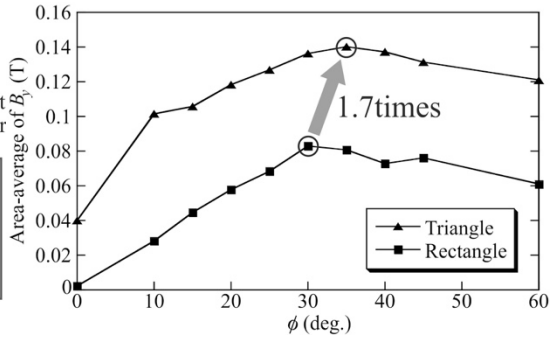

Fig. 4 The relation between the area-average of B_y within the region of stationary position and the inclination angle ϕ of the rolling direction

Conclusions

In this paper, the relation between shape and rolling direction of steel sheets in the stator of the self-propelled rotary actuator is investigated by finite element magnetic field analysis which introduced the complex E&S model. As a result, it is concluded that the starting torque of the actuator using a triangle steel sheet is larger than that of a rectangle steel sheet. It is important to optimize a shape of steel sheets in consideration of an inclination angle of rolling direction because an optimum inclination angle of a rolling direction changes with a shape of steel sheets.

References

[1] Qiao J., Shang J., and Goldenberg A. *IEEE/ASME Trans. on Mechatronics*, Vol. 18, No. 2, pp. 799-806, April 2013.
[2] Yaguchi H. *IEEE Trans. on Magnetics*, Vol. 51, No. 11, Nov. 2015, Art. no. 8205704.
[3] Enokizono M., Todaka T., Goto K., and Chew Y.S. *IEEE Trans. on Magnetics*, Vol. 35, No. 5, pp. 4016-4018, Sept. 1999.
[4] Soda N., and Enokizono M. *IEEE Trans. on Magnetics*, Vol. 52, No. 3, March 2016 Art. no. 7000404.
[5] Soda N., and Enokizono M. *2016 XXII International Conference on Electrical Machines*, pp. 918-923, Sept. 2016.

OSCILLATION AMPLITUDE REDUCTION OF A HIGH-TC SUPERCONDUCTING LEVITATION SYSTEM BY AN ELECTROMAGNETIC SHUNT DAMPER COUPLED NONLINEARLY

Toshihiko Sugiura[1,a], Keisuke Uchino[1], Issei Tanabe[1]

Department of Mechanical Engineering, Keio University, Yokohama, Japan
[a]sugiura@mech.keio.ac.jp,

Abstract. An electromagnetic shunt damper, consisting of an electric circuit, can work as a kind of dynamic vibration absorber for a mechanical system. It can convert a portion of mechanical vibration energy into electricity, and the vibration amplitude of the main system can be reduced as a result. This energy conversion can be achieved by electromagnetic coupling and no mechanical contact is required. Thus, this damper is convenient for a superconducting levitation system where a magnet, the target of damping, levitates with no contact support. However, since the natural frequency of such a levitation system is commonly much lower than that of an electric circuit, it is difficult to tune the parameter values of both systems. In this research, we introduced a different type of electromagnetic shunt damper, which is nonlinearly coupled with a high-Tc superconducting levitation system. Our experimental results, showing successful suppression of vibration, verified the effectiveness of this type for reducing the required value of the circuit to one fourth of the conventional one through internal resonance.

1. Introduction

A high-Tc superconducting levitation system can levitate a magnet stably with no control and has the advantage that its energy loss is extremely small and there is no deterioration due to friction because there is no mechanical contact. On the other hand, since the damping of such a levitation system is small, the vibration amplitude of a levitated body tends to increase. As a result, there is a risk of vibration beyond the pinning limit of the superconductor, and of the quenching phenomenon in which the superconducting state is broken by heat generation. One of the ways of avoiding such risks is to use an electromagnetic shunt damper. It can reduce the amplitude of a levitated body by converting its mechanical vibration to the electric vibration of a circuit coupled with the main system electromagnetically. With this damper, the non-contacting characteristics of the levitation system can be maintained, because it can damp the vibrations of the target body in a non-contacting manner by means of electromagnetic force. However, the required values for the circuit elements become so large that it is difficult to realize them. Therefore, instead of such dampers, control is often utilized in many studies [1]. In this research, in order to operate the electromagnetic shunt damper with the advantage of non-control, we focus on the mechanism that can relax the conditions required for the circuit elements by using the internal resonance phenomenon caused by nonlinear coupling [2], We experimentally verify the amplitude reduction.

2. Analysis model with nonlinear coupling

In our analysis model, a magnet is levitated over a high-Tc superconducting bulk placed on a shaking table. A coil is attached to the levitated magnet so that they can vibrate together, while this coil is connected to a capacitor and a resistance, forming an electric circuit. When the superconducting bulk excited vertically, with the vibration of the levitated magnet, the coil moves in the static magnetic field generated by magnets with an iron yoke fixed around the coil. The electric circuit and the fixed magnets with the yoke stated above can work as an electromagnetic shunt damper suppressing vibration of the main system.

With this setup, there exists coupling between motion of the levitated magnet and fluctuation of the electric charge in the circuit. The electromotive force is induced in the coil during vibration, while the electromagnetic force is exerted on the electric current in the coil by the static magnetic field. Let x be the displacement of the levitated magnet seen from the shaking table, and q be the electric charge of the capacitor. The induced voltage in the coil is proportional to both the velocity of the magnet dx/dt and the magnetic flux density B, while the electromagnetic force is proportional to both the electric current dq/dt and the magnetic flux density B. These are coupling terms in the governing equations describing this electromagneto-mechanical problem. This coupling is linear with respect to x and q if the magnetic field is uniform in the moving region of the coil. However, in our analysis we assume the magnetic flux density B varies linearly with x, which can be given by arranging the opposite magnetic poles along x. With this gradient magnetic field, the coupling terms become quadratic, and thus the governing equations for x and q can be coupled through these nonlinear terms.

Now we consider that the natural frequency of the subsystem for q is close to twice that of the main

system for x. According to the governing equations, once x starts to vibrate with its natural frequency, q also starts to oscillate with its natural frequency through the nonlinear coupling between them. This is called an internal resonance. In such a system, the vibration energy of the main system can be converted to the electrical energy of the subsystem, so the subsystem can work as a damper. The optimal design value for the product of the inductance L and the capacitance C can be reduced to one fourth of that for the linear coupling type.

3. Numerical calculation

Numerical calculations were carried out for the governing equations by using the fourth-order Runge-Kutta method. Obtained frequency response curves show that the amplitude of the main system is successfully reduced in the vicinity of primary resonance region, while the current oscillating at a frequency twice the excitation frequency is induced in the circuit. These results, indicating occurrence of internal resonance and conversion of the vibration energy to the electrical energy, predict effectiveness of the electromagnetic shunt damper using internal resonance.

4. Experiment

We carried out experiments by using a setup corresponding to the above model and by measuring the displacement and the electric current. Fig. 1 shows frequency response curves in a nondimensional manner. Fig. 1 (a) plots the amplitude of the excitation frequency component of the magnet vibration. It can be clearly found that the maximum amplitude near the primary resonance is reduced by 25.4% by using the electromagnetic shunt damper. It can be further confirmed from Fig. 1 (b) that the current oscillating at a frequency twice the excitation frequency is induced in the circuit when the excitation frequency is close to the natural frequency of the main system.

Conclusions

For the purpose of suppressing vibration of a levitated body in the high-Tc superconducting levitation system, this research focused on a method of using an electromagnetic shunt damper coupled nonlinearly with the main system. Our numerical calculations show occurrence of internal resonance and conversion of the vibration energy to the electrical energy, leading to effective reduction of the vibration amplitude. This numerical prediction was verified by our experiments using this type of electromagnetic shunt damper with reducing the required value of the circuit.

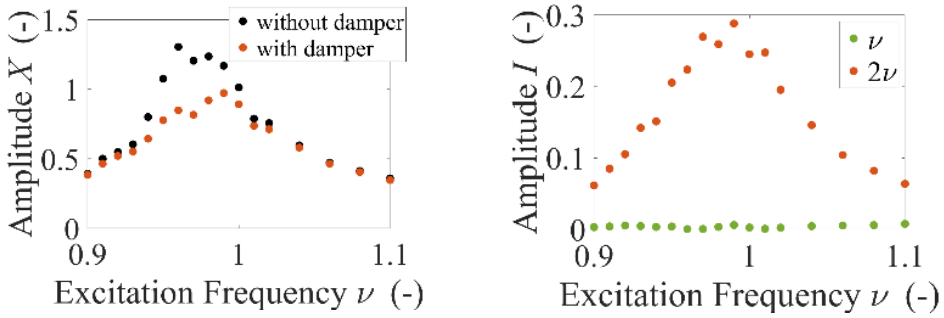

Fig. 1 Experimental results of nondimensional frequency responses: (a) levitated magnet; (b) electric current

References

[1] Takagi K., Inoue T., Miyachi T. Electromagnetic shunt vibration control using a digital Virtual impedance circuit, Proceedings of the Japan Society of Mechanical Engineers, 2012, 78, 474-488.

[2] Sasaki M., Kimura J., Sugiura T. Vibration suppression in high-Tc superconducting levitation system utilizing non-linearly coupled electromagnetic shunt damper, IEEE Transactions on Applied Superconductivity, 2015, 25-3, 1-5.

ESTIMATION SCINTILLATION INDEX ON A SUPERCONDUCTOR RECEIVER FOR GAUSSIAN LASER BEAM PROPAGATED TROUGH RANDOM PHASE SCREEN

N. Kh. Gomidze[1,a], I. N.Jabnidze[1,b], K.A.Makharadze[1,c], M.R.Khajishvili[1,d], L.G.Kalandadze[1,e], O.Nakashidze[1,f], E.N.Mskhaladze[2,g]

[1] Batumi Shota Rustaveli State University, Batumi, Georgia
[2]Batumi Maritime Academy
[a]gomidze@bsu.edu.ge, [b]izolda.jabnidze@bsu.edu.ge, [c]k.makharadze.01@gmail.com, [d]mirandukht@gmail.com, [e]lali.kalandadze@bsu.edu.ge, [f]omar.nakashidze@bsu.edu.ge, [g]eldar@mskhaladze.com

Abstract: The goal of the present work is to study the regulations of the changes of the characteristics of high frequency optical signals using both quantitative and qualitative terms, on the basis of changes statistical parameters of turbulent media on the random phase screen model. There is an analytical assessment of statistical moments of laser radiation via random phase screen by numerical modelling and comparison with known experimental results. The object of the study is a random inhomogeneous atmosphere with weak turbulence, as well as optically dense turbulent media. The model of a random phase screen is discussed and the distribution of the statistical moments of scattered laser radiation is studied. The dependence of the effective size of the laser beam and the scintillation index on the correlation radius of the phase screen in the plane of the detector for a random phase screen is estimated.

1. Introduction

In this paper, we will, based on the Rytov weak fluctuation method [1] and the thin phase screen model [2], research the statistical property of Gaussian beam propagation through an arbitrary thickness phase screen [3], establish the mathematic models of involving statistical quantities, and develop the analytical results. The application scope of our results will be discussed based on the comparison between the thin phase screen models and arbitrary thickness models.

2. Formulation of the problem

The case when the laser beam incident perpendicularly to the phase screen was studded in the work [4]. The phase screen is of a small thickness, scattered radiation is registered in the distant zone through the photo detector. The photo detector axis makes θ angle of the laser beam (fig. 1). Let's consider the case when phase screen model is with arbitrary thickness. Optical system detects the signal passing through a random phase screen (fig.2).

If it is known the statistics of deterministic coherent Gaussian laser beams, it is possible to calculate the scintillation index on the detector plane on the basis of averaging over the ensemble of intensity incident on the detector partially coherent beam.

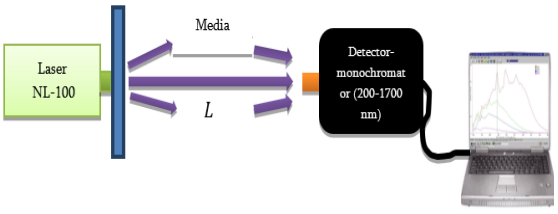

Fig 1. An experimental device scheme for studying partially coherent laser beam in the free space or in the turbulent media

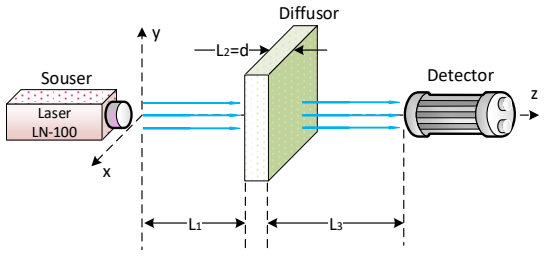

Fig.2. Propagation of a laser beam located at a distance L_1 from the optically dense medium (diffuser) with the arbitrary thick $L_2 = d$ to the detector (optical system) located at a distance L_3 from the diffuser.

3. Results of numerical experiments

The dependence of the effective normal radius $W_{1,d}/W_0$ ($W_0 = 2.5$ cm) of the laser beam on the correlation radius l_c via diffuser is shown on the Fig. 3. Fig.4 provides an effective scintillation index as the function of the correlation radius for different length from diffusor ($L = 200$ m – red line, $L = 500$ m – green line). Fig.5 shows impact of the detector area on the fluctuation intensity spectrum and on the Doppler spectrum for the Gaussian laser beam.

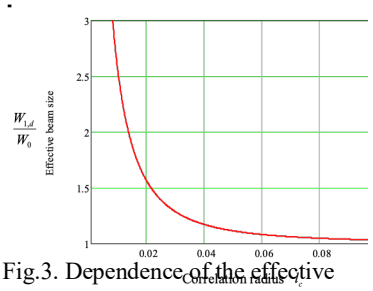

Fig.3. Dependence of the effective normal radius W_d/W_0 vs correlation radius l_c, when: $W_0 = 2.5$ cm, $L = 500$ m.

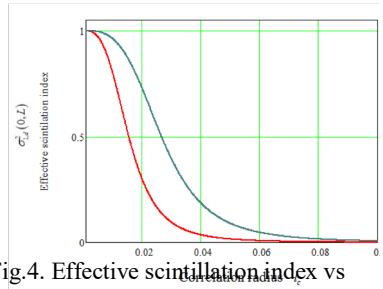

Fig.4. Effective scintillation index vs correlation radius l_c, for different distant from diffusor ($L = 200$ m – red line, $L = 500$ m – green line), when: $W_0 = 2.5$ cm.

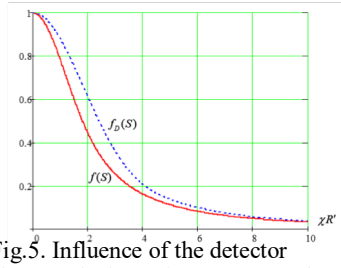

Fig.5. Influence of the detector surface on the intensity spectrum of the fluctuation $f(S)$ (dot line) and on the Doppler's spectrum $f_D(S)$ (line) for the Gaussian laser beam.

Conclusion

- The effective function of mutual coherence, consequently, the laser beam size, intensity, correlation radius and the expressions of the angle of fluctuations are obtained in the plane of the detector. It is shown that the laser beam size, the correlation radius and the average intensity of the radiation coincide with the results of Riklin's or other's works. However, the results obtained in the turbulence of the atmosphere somewhat differ from the classical results. The results obtained for the coherence radius are in good standing with the results obtained in Belenk's and other's works.
- In case of fast detectors, the scintillation index is obtained in the free space of laser beam, as well as in the weak turbulence atmosphere. In case of a strong diffuser, the model shows that the index is close to 1 and agrees with Akhmanov's and other's works. While considering the atmospheric effects, the influence of diffuser on the effect of scintillation in the receiving detector space is in compliance with the results obtained in Andrius' and other's works.
- The correlation function of the intensity is calculated which shows that the doppler spectrum dominance in the expression of the correlation function of intensity increases the value of the signal/noise ratio to the detector's outlet.

Acknowledgment

2019 Competition for Targeted Scientific Research Projects "Diagnostics of a liquid medium based on an estimate of the correlation function of the intensity of partially coherent waves scattered from the fluid volume". Batumi Shota Rustaveli State University (2019), project manager PhD of Physics Kakha Makharadze.

References

[1] Bernhardt, P., et al., "Ionospheric applications of the scintillation and tomography receiver in space mission when used with the DORIS radio beacon network," J. Geod, 80, 2006.
[2] Andrews L. C., Phillips R. C., Hopen C. Y. Laser beam scintillation with applications (SPIE Opt. Eng. Press, 2003).
[3] Tian Y., Guo J., Wang R., Wang T. Mathematic model analysis of Gaussian beam propagation through an arbitrary thickness random phase screen. Optics Express, vol. 19, no. 19, 2011
[4] Gomidze N. Kh, Khajisvili M. R., Jabnidze I. N., Makharadze K. A., Surmanidze Z. J. To the Problems of Detecting Signals Passing Through a Random Phase Screen. Journal "Recent Advances in Technology Research and Education" Springer International Publishing. Print ISBN: 978-3-319-99833-6, Electronic ISBN: 978-3-319-99834-3, pp. 177-184, 2018.

PARAMETER IDENTIFICATION OF NONLINEAR DYNAMIC SYSTEMS OF INDUSTRIAL PROCESSES

B. Shanshiashvili[a], N. Kavlashvili[b]

Georgian Technical University, Tbilisi, Georgia
[a]besoshan@hotmail.com, [b]nkavlash@gmail.com

Abstract. The problem of parameter identification of nonlinear dynamic systems of industrial processes on the set of continuous block-oriented models, the elements of which are different modifications of the Hammerstein and Wiener models, is considered. Method of parameter identification in steady state based on the observation of the system's input and output variables at the input sinusoidal influences is proposed. The solution of the problem of parameter identification is reduced to the solution of the systems of algebraic equations by using the Fourier approximation. The parameters' estimations are received by the least squares method. Reliability of the received results, at the parameter identification of the nonlinear system in industrial conditions at the presence of noise depends on the accuracy of the measurement of system output signals and mathematical processing of the experimental data at the approximation.

Keywords: nonlinear system, block-oriented model, identification, parameter, dynamic, sinusoidal.

1. Introduction

Basis of automatic control of any system of industrial processes is presence of the information on a condition of the system in the form of mathematical model. The majority of the real industrial dynamic systems are nonlinear and possess many "inconvenient" features from the point of view of their control. Such systems can be adequately characterized only by nonlinear models on all working area of change of variables.

The nonlinear systems are generally represented by the block-oriented models consisting of different modifications of the Hammerstein and Wiener models or general models, in particular, the Volterra and Wiener series and the Kolmogorov-Gabor continuous and discrete polynomials.

Despite their simplicity, block-oriented models are successfully used in many fields of the industrial processes (modelling of ball-tube mills of the concentrating factory, distillation columns, hydraulic actuators, electrical water-heater process, heat transfer process, etc.).

In the given work the problem of parameter identification of continuous nonlinear dynamical systems is considered on the set of continuous block-oriented models at the input sinusoidal signals.

2. Theoretical and experimental results

At the representation of nonlinear systems by the block-oriented models [1], most of the existing developed methods of parameter identification is developed for the simple Hammerstein and Wiener models (e.g. [1-4]). Comparatively small quantity of works is devoted to the identification of parameters of other block-oriented models (e.g. [5-7]). That can be explained by the fact that the majority of such models, except for the Hammerstein models (simple and generalized) are nonlinear relative to the parameters, and also because of the big number of estimated parameters. So, for example, the number of estimated parameters of the simple Wiener-Hammerstein cascade model with the nonlinear elements in the form of polynomial functions of n degree and linear dynamic elements described by the differential equations of the m_1 and m_2 order, is equal to $n + m_1 + m_2 + 3$. Therefore, the solution of the problem of parameter identification is analytically possible only for some block-oriented low order models.

In this work the problem of parameter identification is considered on the set of models, elements of which are different modifications of the Hammerstein and Wiener models with nonlinear elements in the form of polynomial functions of second degree and stable linear elements described by the ordinary differential equation of second order. Such models are widely used for the modelling of industrial processes.

Different modifications of the Hammerstein and Wiener models consist of different combinations of connections of linear dynamic and nonlinear static blocks.

When the harmonic signal acts on the input of the nonlinear block-oriented system, the forced oscillation with features for different models is obtained at the output of the system in the steady state after the termination of the transient process.

When a sinusoidal signal acts on the input of the linear element**,** then at the output of the element in the steady state the sinusoidal signal with same frequency and with amplitude and phase, which depends on the frequency, is obtained. In such case, the periodic signal is obtained on the output of nonlinear static element,

which is the sum of the sinusoidal signals with multiple frequencies. These facts were used to determine analytical expressions of the forced oscillations on the output of models.

Estimations of Fourier coefficients of the forced oscillations of the model output are obtained by the numerical harmonic analysis. The algebraic equations are taken to determine estimations of unknown parameters by equaling the estimations of Fourier coefficients to their theoretical values.

Below, for example, an estimation of one of the dynamic parameters of the simple Wiener model is given:

$$\hat{T}_{01} = \frac{\left(\sum_{i=1}^{n}\omega_i^2\right)\left(\sum_{i=1}^{n}\frac{\hat{a}_{1_i}^2}{\hat{b}_{1_i}^2}\omega_i^2\right) - \left(\sum_{i=1}^{n}\frac{\hat{a}_{1_i}}{\hat{b}_{1_i}}\omega_i\right)\left(\sum_{i=1}^{n}\frac{\hat{a}_{1_i}}{\hat{b}_{1_i}}\omega_i^3\right)}{\left(\sum_{i=1}^{n}\omega_i^4\right)\left(\sum_{i=1}^{n}\frac{\hat{a}_{1_i}^2}{\hat{b}_{1_i}^2}\omega_i^2\right) - \left(\sum_{i=1}^{n}\frac{\hat{a}_{1_i}}{\hat{b}_{1_i}}\omega_i^3\right)^2},$$

where a_{1i}, b_{1i}, a_{2i}, b_{2i} $(i = 1,2,\ldots,n)$ are values of the Fourier coefficients at the frequency ω_i.

The identification method is investigated by theoretical analysis and computer modelling. The reliability of the received results, at the parameter identification of nonlinear systems of industrial processes conditions, in the presence of noise and errors, depends on the measurement accuracy of the systems' output signals and on the mathematical processing of the experimental data at approximation.

Conclusions

Developed parameter identification method can be used for the modelling of nonlinear industrial processes when the model structure is known a priori. As the estimations of parametres are received by the least squares method, it can be used in the industrial conditions in the presence of the noise and measurement errors. The specification of the method of identification allows to use Fourier coefficients of various harmonics to estimate the parametres and compare the received results.

References

[1] Giri F., Bai E-W. (Eds). Block-oriented Nonlinear System Identification. Springer, Berlin, 2010.
[2] Giri F., Rochdi Y., Brouri A., Chaoui F.Z. Parameter identification of Hammerstein systems containing backlash operators with arbitrary-shape parametric borders. Automatica, vol. 47, no. 8, 2011, pp. 1827-1833.
[3] Hagenblad A., Ljung L., Wills A.G. Maximum Likelihood identification of Wiener models. Automatica, vol. 44, no. 11, 2008, pp. 2697–2705.
[4] Salukvadze M., Shanshiashvili B. Identification of nonlinear Continuous Dynamic Systems with Closed Cycle. International Journal of Information Technology & Decision making, vol. 12, no. 2, 2013, pp. 179-199.
[5] Wills A., Schön T.B., Ljung L., Ninness B. Identification of Hammerstein–Wiener models. Automatica, vol. 49, no. 1, 2013, pp. 70–81.
[6] Shanshiashvili B., Salukvadse M. Parameter identification of Hammerstein-Wiener systems in the frequency domain. Archil Eliashvili Institute of control systems of the Georgian Technical University. Proceedings. № 22. Tbilisi, 2018, pp. 130-135. (in Georgian).
[7] Li L., Ren X. Decomposition-based recursive least-squares parameter estimation algorithm for Wiener-Hammerstein systems with dead-zone nonlinearity, Inter. Jour. of Syst. Sc., 48(11), 2017, 2405-2414.

NOVEL ELECTRICAL APPROACH TO PROTECT PV MODULES UNDER VARIOUS PARTIAL SHADING SITUATIONS

Hamed Hanifi[1,2,*], Matthias Pander[1,2], Bengt Jaeckel[1,2], Jens Schneider[1], Afshin Bakhtiari[3], Waldemar Maier [3]

[1]Fraunhofer Center for Silicon Photovoltaics CSP, Halle (Saale), Germany
[2]Fraunhofer Institute for Microstructure of materials and systems IMWS, Halle (Saale), Germany
[3]Alternative Energy Solar (AE Solar), Messerschmittring 54, D-86343 Konigsbrunn, Germany
**Contact person: Hamed.hanifi@csp.fraunhofer.de*

1. Introduction

PV modules are highly sensitive to partial shading conditions. Partial shading over a PV module can be generated by consistent shadings such as placement of obstacles on the active area of the module or by partial shading during different time of the day such as shadow of a chimney over a PV module. Partial shading can influence the performance, lifetime, reliability and energy yield of PV modules depending on type, duration and pattern of the shade. In the most extreme case, hot-spots form in shaded PV modules which lead to the failure of the PV modules. To avoid hot-spots, every 20-24 solar cells in series (one string) are protected by a bypass diode in a standard PV module. Since the current of each string is limited to the shaded solar cell, by shading of one solar cell 33.3% of module power will be affected. In this work, a novel interconnection design is developed for PV modules to increase the reliability, power and energy yield of PV modules under different partial shading conditions. In this approach, instead of using one bypass diode for every 20-24 solar cell, every individual solar cell is protected by bypass diodes to reduce the power loss and chance of hot-spots in PV modules.

2. Experiment and simulation

A 60-cell hot-spot free and a standard PV module designs are measured by Sun Simulator. The modules are fabricated from identical materials and solar cells. The only difference is in hot-spot free module, each solar cell is protected by a bypass diode while in standard module, and every 20 solar cell is protected by one bypass diode. Different shading patterns are applied to the PV modules in different sizes and directions. The modules are measured when just one solar cell is shaded from 0% to 100% (see Fig.1). Then, one row of solar cells located in different strings and finally multiple rows in both modules are shaded step by step and then measured and simulated by sun simulator and SPICE.

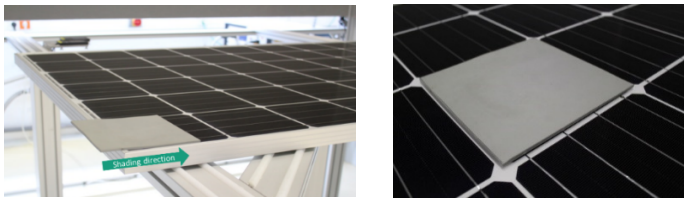

Fig.1. The shading direction and the shading object on a solar cell of a standard module (left) and a top view of a totally shaded solar cell of a hot-spot-free module by the shading object under sun simulator (right).

To ensure the reliability of the hot-spot free module, especially by considering the thermal expansion due to the high temperature of the module under partial shading conditions, a new testing setup is developed to measure the electrical properties and temperature of the module by switching the bias voltage and powering the module in forward and reverse bias.

3. Results

a) Partial shading conditions

The modules are shaded under partial shading conditions.

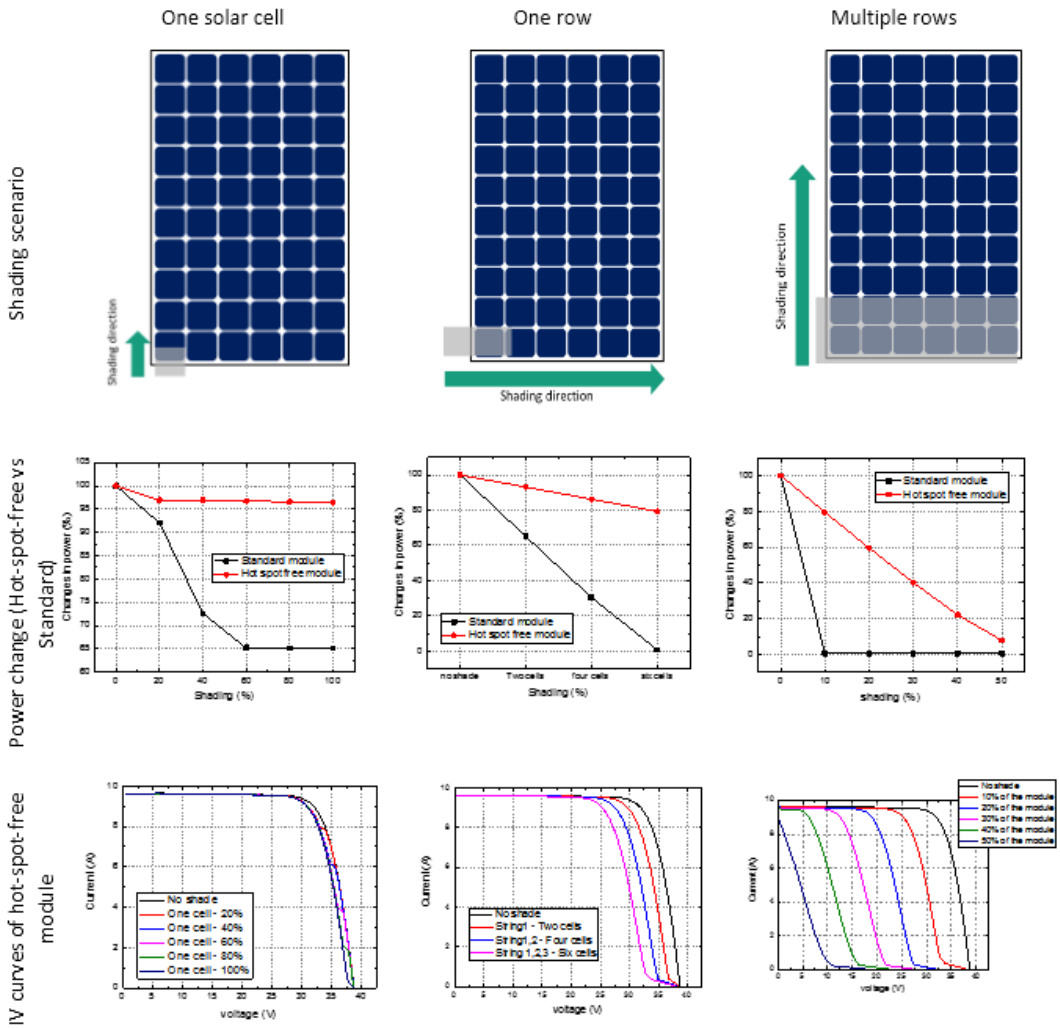

Fig.3. Comparison of shading scenarios, power change comparison in hot-spot free module and standard module and IV curve of hot-spot free module under different shading scenarios

The electrical measurement results with partial shading conditions show 32% and 80% extra power of hot-spot free module compared to the standard module by referencing the non-shaded module under partial shading conditions. By shading multiple rows, the standard module produce no power after shading of just 10% of the module while the hot-spot free module can produce power when almost 50% of the total module is shaded.

b) Stress test of hot-spot free module

To ensure the reliability of the module, the modules are tested in frequent switching between reverse and forward bias. In forward bias, the solar cells are in operation while in reverse bias the diodes are working. The PV modules are tested in 10000 cycles of 60 seconds in each direction. The IV measurement show 0.38% deviation from reference module before stress test and the EL test after the experiments show no visible defects on the module.

Conclusion

The results show that hot-spot free module with integrated bypass diodes for every single solar cell increases the performance and reliability of the module. In three different shading scenarios, the module show 32%, 80% extra power compared to standard module with reference of not shaded module under shading conditions of one solar cell, and one row. The hot-spot free can produce power even when almost 50% of total module area is shaded. We also show that the extra bypass diodes do not affect the reliability of the module and changes in power after 10000 bias cycles are below 1%.

INVESTIGATION OF THERMAL INSULATION FOR STATIC CRYOSTATS OF HTSC DEVICES

L.I. Chubraeva[1,2,a], S.S. Timofeyev[1,b]

[1] *Institute of Electrophysics and Electric Power Engineering of RAS, Saint-Petersburg, Russia*
[2] *Institute of Silicate Chemistry of RAS, Saint-Petersburg, Russia*
[a]lidiach@mail.ru, [b]sergio121@yandex.ru

Abstract. Experimental investigation of HTSC electro-technical devices may be simplified substantially due to application of multi-layer thermal insulation. Presented below are test results for the foamed rubber K-FLEX, applied as an external thermal insulation of static cryostats intended for cryogenic devices, in particular, HTSC alternators

1. Introduction

At present thermal insulation for cryogenic electro-technical devices comprises two main groups: screen-vacuum and multilayer insulation. Static cryostats may be either metallic or non-metallic ones. If the investigated device has an external alternating magnetic field, which may cause eddy-current loss in the inner shells of metallic cryostat, facing the cryogenic coolant, non-metallic cryostats are preferable. We possess a vast experience with the application of non-metallic cryostats. We used them on the 1-st stage of our experiments with HTSC devices, cooled by LN_2. Application of plastic cryostats with vacuum insulation shows they cannot keep the vacuum for a long time and need practically constant vacuum pumping out. As far as we have proved absence of external alternating magnetic fields in electrical machines with axial magnetic flux, we started to apply thermal insulation for the outer frame of model alternators.

2. Experimental investigation results

The foamed rubber K-FLEX sheets are chosen for a set of preliminary investigations. Main advantages of this thermal insulation are listed in [1]. The main range of its application lies in between -40 - +85 ^{0}C. The tests covered two main aspects: determination of the thermal insulation optimal thickness for LN_2 experiments and evaluation of K-FLEX ageing process in LN_2. The model cryostat is made of stainless steel [2]. It is wrapped with the insulation layers fixed with special glue.

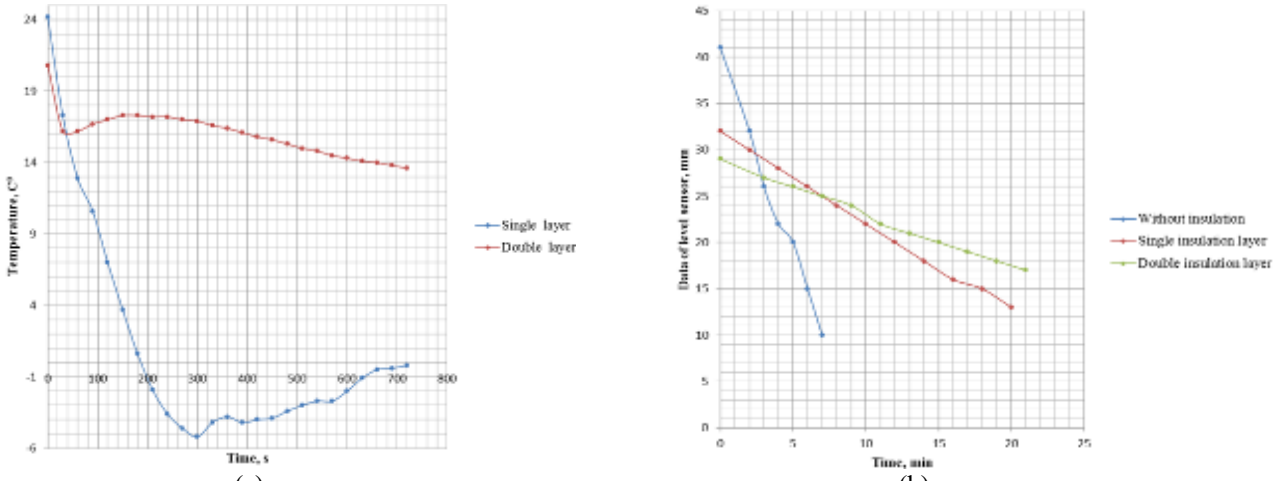

(a) (b)

Fig. 1 Test results: (a) - variation of the temperature on external cryostat surface, (b) - variation of LN_2 volume with a single and a double layer insulation

During the tests the ambient temperature was equal to +25 ^{0}C and the temperature of the coolant – appr. -196 ^{0}C. K-FLEX sheet thickness – 18 mm. The data presented in Fig. 1,a shows two layers of the thermal insulation are minimum for the static cryostat of electrical machine model in case of long-term experiments with LN_2 cooling. The velocity of LN_2 evaporation confirmed (Fig. 1,b) two layers are enough. The curve for 3 layers is practically similar to the one obtained with 2 layers of K-FLEX (36 mm).

Behavior of K-FLEX during thermo-cycling is as follows. Two layer sample (the layers were fixed by glue) was immersed in LN_2, cooled-down in it and then warmed up at ambient temperature 20 ^{0}C. The results

of thermo-cycling are shown in Fig. 1 b. The two layer glued sample before experiments is presented in Fig. 2, a. After the 1-st thermo-cycle there appeared cracks on the sample surface. It became less elastic and showed a tendency to crumbling. After the 3-d thermo-cycle there appeared a dent in the center of the sample (Fig. 2, b). The total amount of thermo-cycles equaled 10, but after the 3-d one there did not appear any visible changes.

The elasticity of the sample improves with the time, but not to the initial level. The material stays more rigid. It is necessary to be accurate during experiments with liquid nitrogen not to spoil the outer thermal insulation of the static cryostat of the device.

Experiments with a rotating electrical machine showed additional advantages of K-FLEX: it is a good acoustic insulation as well and damps the alternator vibrations [3].

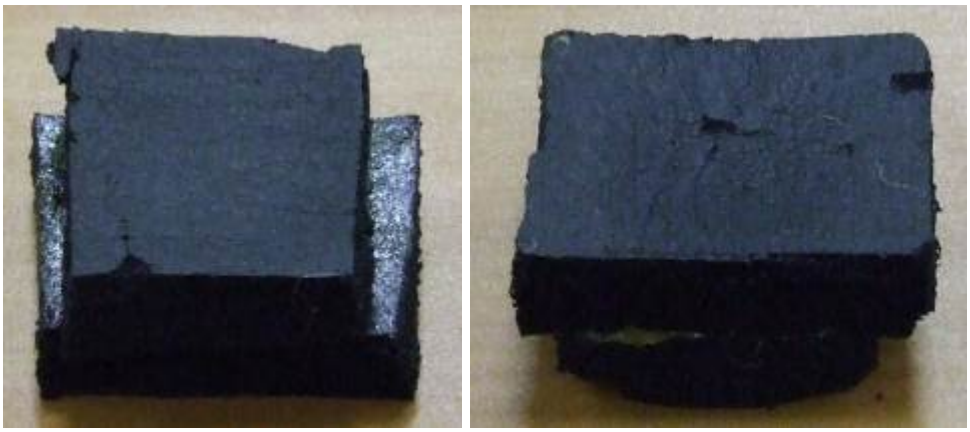

(a) (b)

Fig. 2 Thermo-cycling experiment: (a) - prior to thermo-cycling, (b) – after 3 thermo-cycles

Conclusions

The K-FLEX thermal insulation is applicable for static cryostats of cryogenic devices, operating with LN_2. It permits to simplify the design and to decrease the expenses for the cryogenic models investigations.

References

[1] L'ISOLANTE K-FLEX GmbH web-site: http://www.kflex.com/en/#

[2] Andreev Eu. N., et al., Use of materials on the basis of foamed rubber as a thermal insulation of high-temperature superconducting devices, International Conference on Electromechanics and Robotics "Zavalishin's Readings" 2013, pp. 1-6

[3] Chubraeva L., Timofeyev S., Project of Autonomous Power Plant with High-Temperature Superconductive Devices, International Multi-Conference on Industrial Engineering and Modern Technologies (FarEastCon), Vladivostok, Russia, 2018, pp. 1-5. doi: 10.1109/FarEastCon.2018.8602671

REFUNCTION TECHNIQUES OF ELECTRICAL STEEL SHEETS BY SECONDARY CURRENT HEATING FOR HIGH EFFICIENCY MOTORS

Y. Tsuchida[1,a], M. Enokizono[2,b]

[1] *Faculty of Science and Technology, Oita University, Oita, Japan*
[2] *Vector Magnetic Characteristic Technical Laboratory, Oita, Japan*
[a]*tsuchida@oita-u.ac.jp,* [b]*enoki@oita-u.ac.jp*

Abstract. This paper presents the newly proposed heating method names as "Secondary Current Heating Method" to reduce the iron loss on laminated electrical steel sheet cores for high efficiency electrical motors. It is well known that the magnetic properties of electrical steel sheets, which are used for electrical motor cores, are deteriorated by the residual stress during manufacturing the electrical motors, and then the iron loss of the laminated electrical steel sheet cores of the electrical motors increases inevitably. The newly proposed Secondary Current Heating Method can improve the magnetic properties on laminated electrical steel sheet cores and reduce the iron loss of them in the very short time in comparison with conventional methods. In this paper, the electromagnetic and heating characteristics of the specimens by proposed method were confirmed, and then it was applied into the laminated cores to reduce iron loss.

1. Introduction

This paper presents the newly proposed heating method names as "Secondary Current Heating Method" to reduce the iron loss on laminated electrical steel sheet cores for high efficiency electrical motors. Conventionally, the residual stress had been removed by the annealing process with a huge-size electric furnace after assembling electrical motors [1, 2]. However, a huge-size electric furnace itself is very expensive and the annealing process by it costs a lot and is very time-consuming (normally, it takes about 12 hours), therefore, the annealing process has been eliminated for the cost performance. Especially, the annealing process has never been applied into the "industrial electrical motors" in Japan for these twenty or thirty years. It means that the industrial electrical motors have been used with high iron loss for many years. In this paper, the electromagnetic and heating characteristics of the specimens by proposed method were confirmed, and then it was applied into the laminated cores to reduce iron loss. The measured results of the magnetic properties and iron loss are discussed for high efficiency electrical motors.

2. Secondary Current Heating Method

Fig. 1 shows the setup of the newly proposed heating method names as "Secondary Current Heating Method". It consists of the main yoke, exciting coils, auxiliary yoke and laminated core (specimen) from electrical steel sheets as shown in Fig. 1 (a). The cross section of the heating equipment and specimen by proposed method is shown in Fig. 1 (b). The exciting coils are connected to the normal commercial power source (200V, 60Hz) as shown in the both figures. The special and expensive power source which are essential for high-frequency induction heating is not needed in this proposed method. The exciting coils make the magnetic flux in the main yoke and

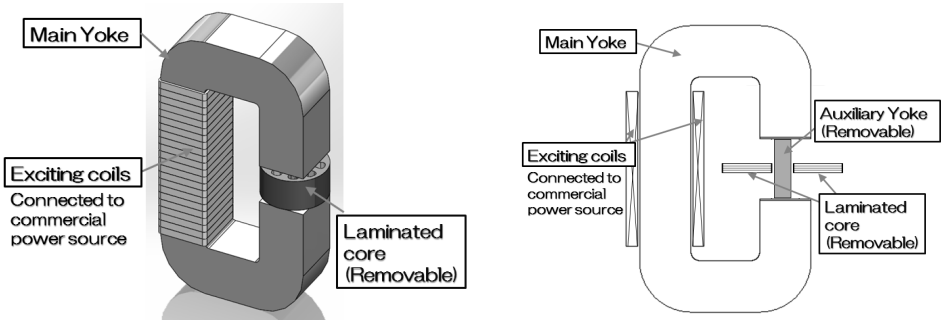

(a) Schematic view (b) Cross-section

Fig.1. Setup of Yokes and Specimens by Secondary Current Heating Method.

auxiliary yoke, and the secondary current is induced in the laminated core due to the variation of the magnetic flux across it. The laminated core can be considered as electrical shorten circuit, therefore, the induced secondary current occurs Joule's heat on the laminated core itself. This Joule's heat can increase the temperature of the laminated core, remove the residual stress, and reduce the iron loss of it. The high-frequency induction heating can heat the only surface on the specimen because of the skin depth. On the other hand, our

proposed method can heat the internal region of the specimen, too. The auxiliary yoke and specimens (laminated cores) are removable to assume to apply this method into the real industrial manufacturing line from the beginning.

3. Measurement of Magnetic properties and reduction of iron loss

Magnetic properties before and after the heat-treatment by proposed Secondary Current Heating Method were measured by the magnetic measurement system. Fig. 2 shows the measured magnetic properties before and after the heat treatment by the proposed Secondary Current Heating method. The B-H loops in Fig. 2 were measured under the 10-Hz excitation and the magnetic flux density, B, are controlled as to be 1.0 [T]. All electrical steel sheets were made by the punching process before lamination process, therefore, some residual stress must be on them by punching and lamination processes. As described above, the heating time is decided as 0, 2.5, 5.0, 7.5, and 10 [minutes]. By comparing these five B-H loops, the magnetic properties improved in the case of the 7.5, and 10 [minutes] processes. The total iron loss was decreased more in the case of the 10 [minutes] process than in the case of the 7.5 [minutes] process. Fig. 3 shows the total iron loss derived from the B-H loops shown in Fig. 2. The total iron loss can be decreased approximately 10 % in the case of the 10 [minutes] process by comparing the non-heat treatment specimen.

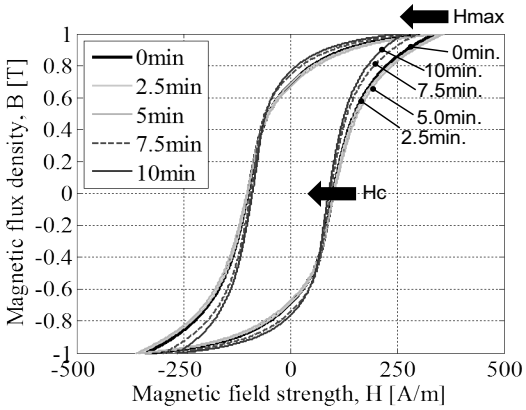

Fig. 2 Variation of B-H loops by secondary current method.

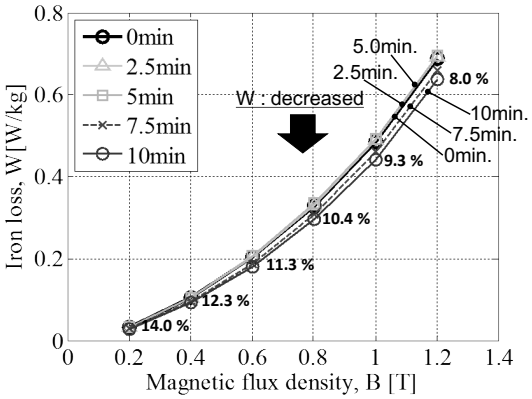

Fig. 3 Reduction of iron loss by secondary current method changing magnetic flux density.

Conclusions

The newly heat treatment name as "Secondary Current Heating" has been proposed, and the effectiveness of the proposed method were discussed in this paper. The Secondary Current Heating method was newly proposed. The proposed method was applied into the ring-shaped laminated electrical steel sheet cores, and then the total iron loss can be reduced by proposed method. And it was shown that the hysteresis loss could be mainly reduced because the proposed method can improve the magnetic properties of the specimens.

References

[1] Gokyu I., Abe H. "Electrical steel sheets", Corona Publishing Co. LTD, 1955.

[2] Huang B.Y., Yamamoto K., and Yamashiro Y. "Relationship between the Annealing Conditions and Magnetic Properties of Non-oriented Silicon Steel Sheets," *Journal of Magnetics Society of Japan*, vol. 22, No. 4-2, pp. 49-52 1998.

DEVELOPMENT OF TRAVELLING WAVE PROPULSION MECHANISM WITH PERMANENT MAGNET VIBRATION MOTOR

K. Kasuga[1, A], I. Murakami [1, B], M. Ono[1. C], Y. Ando [1. D]

[1] *Dept. of Mechanical Science and Technology, Gunma University. 1-5-1 Tenjin-cho, Kiryu. 376-8515, Japan*

[a]T181b019@gunma-u.ac.jp, [b]murakami@gunma-u.ac.jp, [c]t15305008@gunma-u.ac.jp, [d]ando@gunma-u.ac.jp

Abstract. Recently, the autonomous underwater vehicles use screw propellers as propulsion mechanisms. However, the screw propellers generate bubbles and affect acoustic measurement. Therefore, in recent years, there have been many researches on propulsion mechanisms using travelling waves imitating the permanent magnet vibration motor. By using permanent magnets for the vibration motor, it can save power consumption and drive with high thrust. This propulsion mechanism can reduce the sound during propulsion. We produced a propulsion mechanism with travelling wave and evaluated its basic structure and characteristics from the experiment.

1. Introduction

The propulsion mechanisms with travelling wave are studied for low power consumption [1] We developed propulsion mechanism with travelling wave in the past. [2] However, in past research, it is driving at high frequency and isn't known whether high frequency vibration is useful for promoting underwater. Therefore, we produced a travelling wave propulsion device of low frequency vibration. Fig.1(a) shows the geometry of the propulsion mechanism with travelling wave. It consists of a permanent magnet type vibration motor and a swing arm part. Travelling wave is generated by using three permanent magnets type vibration motors. By using a permanent magnet, the vibration motor is characterized by high thrust and low power consumption. Swing arm parts increase amplitude of vibration motor. The purpose of this study is to evaluate the basic structure and characteristics from experiment.

2. Structure of propulsion mechanism with travelling wave

The propulsion mechanism with travelling wave consists of permanent magnets vibration motor and swing arm parts. Fig.1(b) shows the geometry of the permanent magnets vibration motor. Vibration motor use two magnets with 4poles. One magnet is fixed to perform only rotational movement. The other magnet is limited only in the horizontal direction. By using springs, vibration motor utilizes spring forces. Moreover, it prevents excessive isolation between the magnets. By repeating suction and repulsion between permanent magnets, the linear motion side moves in the horizontal direction and vibrates. At the time of suction, torque is generated to promote rotation, but as the time of repulsion, counter torque is generated. By giving a phase different to the three vibration motors, it is possible to reduce the torque that hinders rotation when repulsion is generated. Fig.1(c) shows the geometry of the swing arm parts. Swing arm parts can increase the amplitude. It increases amplitude up to 36 times using principle of leverage. Also, a copper plate is attached to the tip as a fin. The copper plate has a width of 70 [mm], a height of 200 [mm], and a thickness of 0.3 [mm].

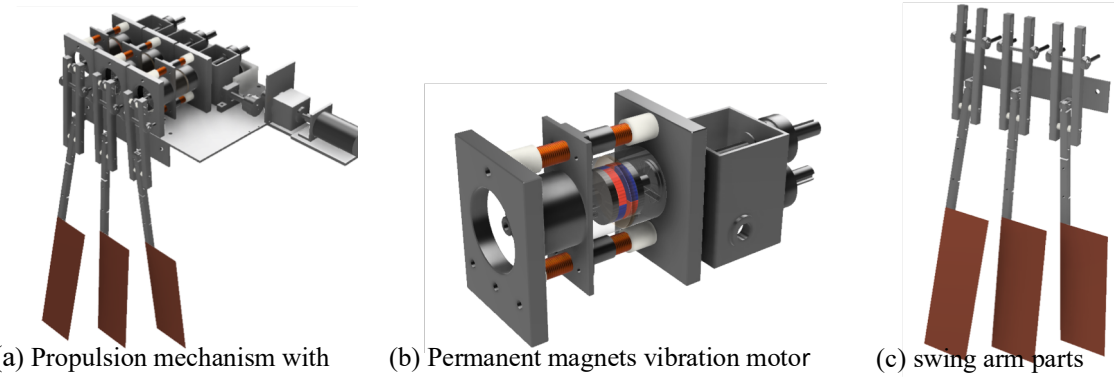

(a) Propulsion mechanism with traveling wave (b) Permanent magnets vibration motor (c) swing arm parts

Fig.1 Geometry of propulsion mechanism with travelling wave

3. Experiment

At first, we investigated the characteristics of only the permanent magnets vibration motor. When the spring balanced, the linear motion part was fixed and the thrust was measured. Fig.2 shows the relation between

thrust and frequency. When the spring with a spring constant is 24.5 [N/mm], the maximum repulsive force is 78 [N] and the maximum attractive force of the spring is -79 [N]. Fig.3 shows the relation between power consumption and frequency.

Fig.4 shows the relation between thrust and frequency in the water. We confirmed the driving from 0.2 [Hz] to 5.1 [Hz]. The maximum thrust was 1.3 [N] when the frequency was 1.8[Hz]. Fig.5 shows the relation between displacement and frequency in the water in the case of the swing arm parts and 36 times the displacement of the linear motion part. Although the amplitude sharply increases at 0.9 [Hz], this is considered to be resonance. Displacement of swing arm parts decreases when the frequency exceeds 2.3 [Hz]. It is thought that the water resistance increased by increasing frequency. Moreover, it was confirmed that the device is propelled in the water.

Conclusion

The propulsion mechanism with travelling wave of permanent magnet vibration motor was produced. When the maximum power consumption of vibration motor is 1.2 [W], the maximum repulsive force is 78 [N] and the maximum attractive force of the spring is -79 [N]. The maximum displacement of the swing arm parts in the water is 79 [mm]. As a result, the device is able to output sufficient amplitude to obtain thrust underwater. We confirmed that the maximum thrust of the propulsion mechanism with the travelling wave in the water is 1.3 [N]. We confirmed that the device can be propelled in the water.

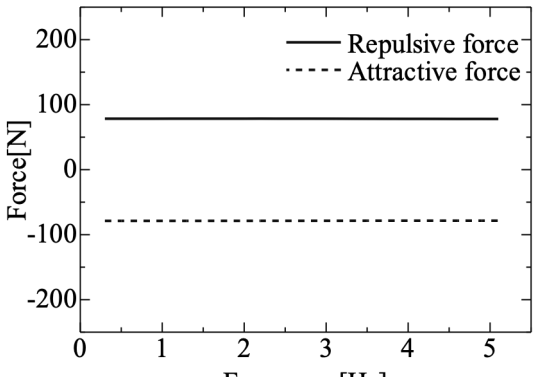

Fig.2. Relation between thrust and frequency (Only the permanent magnets vibration motor)

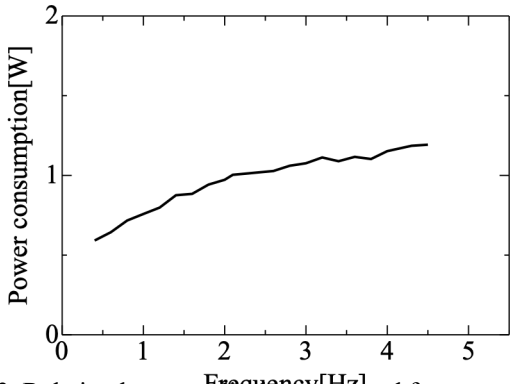

Fig.3. Relation between displacement and frequency (Only the permanent magnets vibration motor)

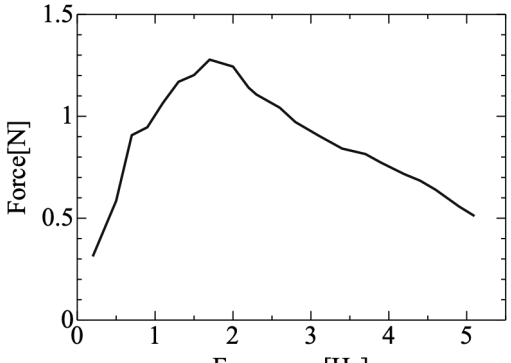

Fig.4. Relation between thrust and frequency in the water

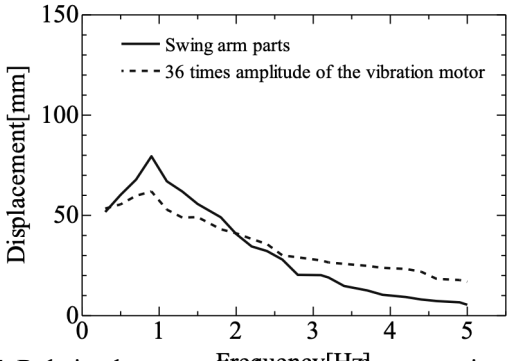

Fig.5. Relation between displacement frequency in the water

References

[1] Minoru Nagai (1999) Fluid dynamics learned from dolphins, Japan: Ohm Corporation.
[2] Iwanori MURAKAMI , Hiroto OCHIAI, Kensuke KANEKO, Shohei MORITO, Tenshiro TAGUCHI. The development of Permament Magnet Actuator for Travelling Wave Generator, Proceedings of MAGDA Vol.25 (2016.11), pp. 439-444

TRANSPORT CHARACTERISTICS OF A TRANSPORT DEVICE COMPOSED OF TWO MAGNETICALLY-DRIVEN SYSTEMS USING A TEMPERATURE-SENSITIVE MAGNETIC FLUID

Y. Ido[1,a], Y. Iwamoto[1,b], G. Ichinose[1], H. Nakasumi[1]

[1] *Department of Electrical and Mechanical Engineering, Nagoya Institute of Technology, Japan*
[a]*a,ido.yasushi@nitech.ac.jp,* [b]*iwamoto.yuhiro@nitech.ac.jp*

Abstract. The transport properties of fluid transport device composed of two magnetically-driven systems utilizing a temperature-sensitive magnetic fluid were investigated experimentally. Two driven systems were connected in tandem or in parallel. The flow rate of the two driving systems in parallel arrangement is larger than the flow rate of two driving systems in tandem arrangement.

1. Introduction

Magnetic fluids are colloidal suspensions composed of ferromagnetic particles covered with surfactant and mother liquid such as water and kerosene. Temperature-sensitive magnetic fluids are sensitive to temperature as well as applied magnetic field, i.e., magnetization of the temperature-sensitive magnetic fluids strongly depends on the temperature. The basic principle of the magnetically-driven system was proposed by Resler and Rosensweig [1]. The principle of energy conversion using this magnetically-driven system was proposed and many researchers have been studied [2-4]. When a non-uniform magnetic field is applied to the temperature-sensitive magnetic fluid by using a permanent magnet, the magnetic body force proportional to the gradient of the magnetic field acts on the fluid. When heat is applied to the fluid at the position displaced from the center of the arranged permanent magnet, a difference occurs in the balanced positive and negative magnetic body forces, which produces as a driving force and transport the fluid. The magnetically-driven system can be used for heat transport system, and this system is self-driven by applying magnetic field and heat, and its size can be reduced with a simple structure. In the previous research, it has been shown that using this system, the fluid is self-driven by applying magnetic field and heat, and heat transport of 6000 mm is possible [5]. In order to enhance the transport properties, it is conceivable to use multiple magnetically-driven systems connected in tandem or in parallel.

In this study, fluid transport characteristics of the transport device composed of two magnetically-driven systems using temperature-sensitive magnetic fluid is investigated experimentally. The flow rate of the transport device is measured when the magnetically-driven systems are arranged in tandem or in parallel.

2. Experiments

The experimental apparatus for investigating transport properties of transport device using the magnetically-driven system mainly consisted of a fluid driving part, a fluid cooling part, and a flow rate measuring part. Figure 1 shows the arrangements of the drive systems as the fluid driving part. In our experiments, the flow rate was measured and compared in the case of one drive system or the case when two drive systems were connected in tandem or in parallel. The test fluid was the temperature-sensitive kerosene base magnetic fluid (TS-50K, Ichinen Chemicals Co. LTD) whose magnetization strongly depends on the temperature in the normal temperature region. The diameter of the tube made of Teflon was 1.54 mm and the total length of the tube was 1730 mm. The maximum strength of applied magnetic field was 273 kA/m and the magnetic field was applied by using two permanent magnets whose width was 22 mm. The position of the magnets was changed and d is defined by the distance between the center of the magnets and the center of the heating area. When the number of drive system was 2, the distance d of one drive system was fixed to 25 mm. The heat flux was 5.0 kW/m^2.

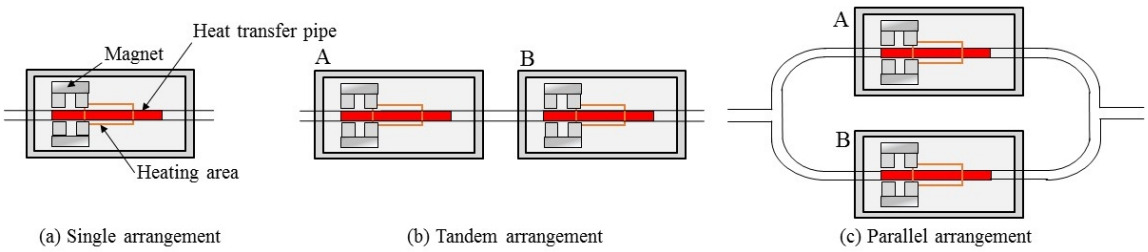

Fig. 1. Arrangements of the drive systems.

3. Results and discussions

Figure 2 shows the flow rates of the transport device when the distance *d* is changed. From Fig. 2, it can be seen that the flow rate is larger in the cases of using two magnetically-driven systems than in the case of using one magnetically-driven system. The flow rate is the largest when two magnetically-driven systems are connected in parallel. When two driving systems are connected in parallel, loss is generated at the junction part of the two flow paths, so it is considered that the flow rate is smaller than twice flow rate of the single system. In any case, when the magnet is arranged at 25 mm from the center of heating area, the flow rate becomes maximum. When two driving systems are connected in tandem, the flow rate is 1.55 times the flow rate of one drive system, while the flow rate of two driving systems in parallel is 1.75 times that of one driving system.

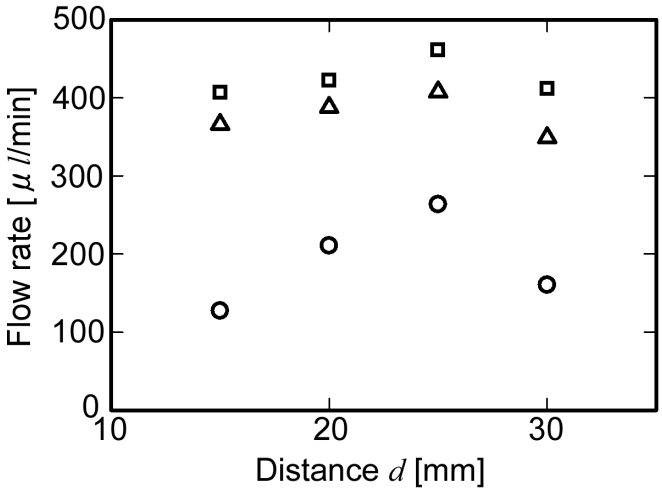

Fig.2. Flow rate of the transport device. The open circle: one drive system, the open triangle: two driving systems in tandem, and the open square: two driving systems in parallel. The distance *d* is defined by the distance between the center of magnet and the center of the heating area.

Conclusions

It has been found that the fluid transportation amount is increased when two driving systems are arranged than when only one driving system is provided. In the case of using two driving systems, the flow rate is larger in the case of connecting in parallel than in the case of connecting in tandem.

References

[1] Resler E.L., Rosensweig R.E. Magnetocaloric power, *AIAA Journal*, 1964, 2, 1418-1422.
[2] Aursand E., Gjennestad M.A., Lervag K.Y., Lund H. A multi-phase ferrofluid flow model with equation of state for thermomagnetic pumping and heat transfer, *Journal of Magnetism and Magnetic Materials*, 2016, 402, 8-19.
[3] Aursand E., Gjennestad M.A., Lervag K.Y., Lund H. Potential of enhancing a natural convection loop with a thermomagnetically pumped ferrofluid, *Journal of Magnetism and Magnetic Materials*, 2017, 417, 148-159.
[4] Iwamoto Y., Yamaguchi H., Niu X.-D. Magnetically-driven heat transport device using a binary temperature-sensitive magnetic fluid, *Journal of Magnetism and Magnetic Materials*, 2011, 323, 1378-1383.
[5] Iwamoto Y., Nakasumi H., Ido Y., Yamaguchi H. Long distance heat transfer using temperature-sensitive magnetic fluids, *International Journal of Applied Electromagnetics and Mechanics*, Submitted.

TORQUE PROPERTIES ANALYSIS OF MAGNETIC HARMONIC GEAR WITH STACKABLE STRUCTURE

Takahito Kurahashi[1,a], Yoshinori Ando[1,b], Ryohei Takei[1,c], Koichi Yonezawa[1,d], Iwanori Murakami[1,e], Akihiro Tomura[1,f]

[1]Dept. of Mechanical Science and Technology, Gunma University, 1-5-1 Tenjin-cho, Kiryu, 376-8515, Japan
[a]T171B034@gunma-u.ac.jp, [b]ando@gunma-u.ac.jp, [c]T181B043@gunma-u.ac.jp,
[d]15302118@ gunma-u.ac.jp, [e]murakami@ gunma-u.ac.jp, [f]T181b053@gunma-u.ac.jp

Abstract The magnetic harmonic gear has been studied because of its high magnet use efficiency. However, the magnetic harmonic gears are difficult to assemble. So, a new type of the magnetic harmonic gear was proposed. This magnetic gear has the stackable structure and is assembled easily. Thus far, it was studied its characteristics. In this study, we deal with dynamic torque properties of the proposed magnetic gear. As a result, the cause of torque properties are considered by frequency analysis.

1. Introduction

The magnetic harmonic gears (MHG) are studied because they have the high torque density and large transmission torque [1-4]. Fig.1 shows the structure of the MHG. It is structured of the three parts (an outer, a center and an inner). The outer and the inner consist of magnets. The center consists of pole pieces. The center has a role to modulate the magnetic flux. The authors study the MHG that has the stackable structure [4]. In this magnetic gear, the inner and outer have the two types of layers. It can adjust the transmission torque by changing the number of stuck.

The purpose of this study is to analysis a dynamic torque property by the frequency analysis. In this paper, we use a prototype and deal with the dynamic characteristics of it.

2. The MHG with stackable structure

In the MHG with stackable structure, the outer and the inner has two types of layers. Fig.2 shows the new structure. Layer1 (L1) is a set of radially magnetized segment magnets arranged on the circumference. The magnetic flux is directed in the radial direction and is directly related to the transmission of the rotation in this layer. Layer2 (L2) is a set of axially magnetized segment magnets arranged on the circumference. In L1 and L2, adjacent magnets are magnetized in opposite direction. In the outer and the inner, a Halbach array is formed by alternately stacking L1 and L2 (Fig.3).

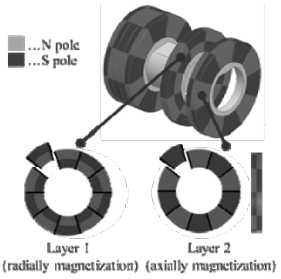

Fig.1. Magnetic harmonic gear

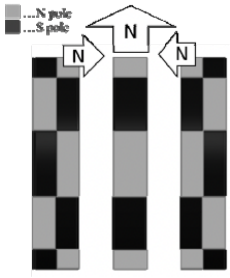

Fig.2. Stackable structure

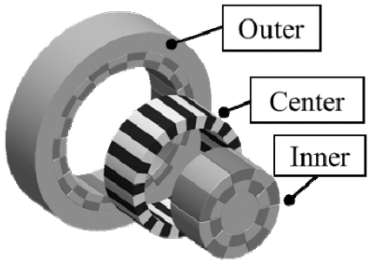

Fig.3. Halbach array

Table 1. Dimension of the magnetic gear

	outer	center	inner
No. of pole pair / pole pieces	13	16	3
The size of magnets for Layer1 [mm]	10×7×3	-	R30×R27×7×60°
The size of magnets for Layer2 [mm]	10×5×3	-	R30×R27×5×60°
The size of the pole pieces [mm]	-	R41×R31×11.25°×7	-
Outside and inside diameter [mm]	Φ120-Φ84	Φ82-Φ62	Φ60

Table 1 shows the dimension of the prototype. Fig.4 shows the parts of the MHG and prototype. In the prototype, the inner is an input and the outer is an output

3. Experiment

We measured input and output torque while rotating input shaft constantly and loading output shaft 3 Nm. Setting rotational speed from 50 rpm to 1000 rpm. The measurement data calculated by FFT to analyze

the frequency spectrum of the torque. The sampling frequency was 1,000Hz, and the measurement time was 8.192 seconds.

Fig.5 shows the FFT analysis of a dynamic torque. Fig.5 (a) shows input-side torque included rotational component proportional to rotational speed of outer from 1st-order to 3rd-order and high-order frequency spectrum proportional to rotational speed. Fig.5 (b) shows output-side torque included rotational component proportional to rotational speed of outer from 1st-order and 2nd-order.

Conclusion

In this report, we revealed some dynamic torque properties of the stackable MHG by frequency a nalysis.

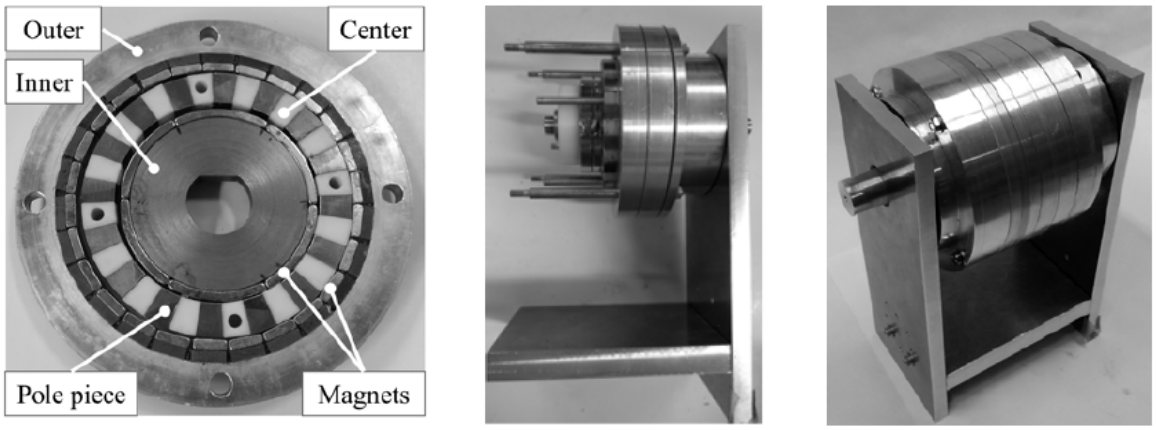

(a) Parts of magnetic gear (b) Stacking (c) Magnetic gear

Fig.4 Prototype

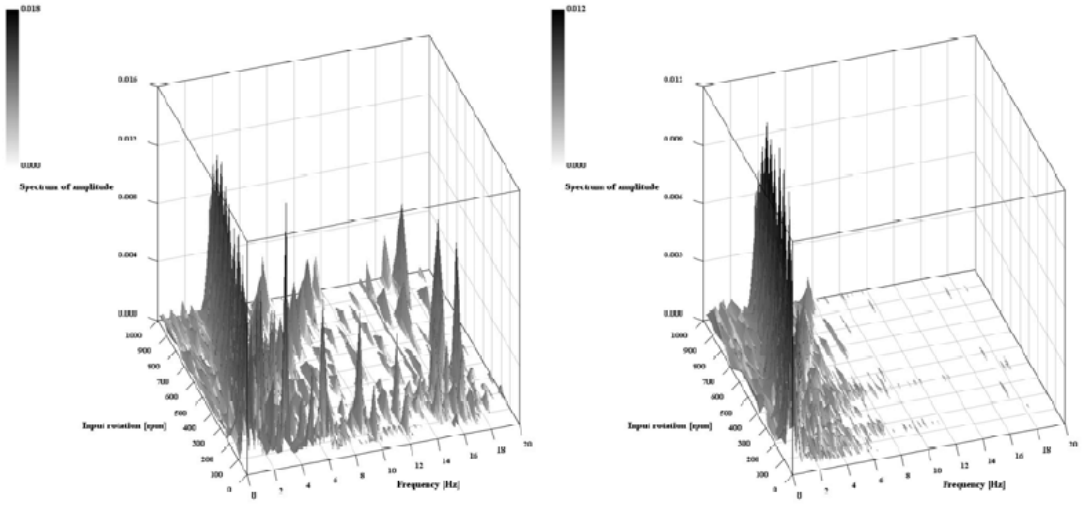

(a) Input side (b) Output side

Fig.5 FFT Analysis of a dynamic torque

References

[1]. Atallah K., and Howe D. Novel High-Performance Magnetic Gear, IEEE Transactions on Magnetics 37 (2001), pp.2844-2846

[2]. Ikeda T., Nakamura K. and Ichinokura W. Way to Improve Efficiency of Permanent-Magnet Magnetic Gears," Journal of the Magnetic Society of Japan, 33 (2009), pp.130-134.

[3]. Yamamoto M., Hirata K., and Muramatsu M. "Study of a New Magnetic Gear," Transaction of Japan Society of Applied Electromagnetics and Mechanics, 17 (2009), pp.188-193.

[4]. Ando Y., Kuroiwa S., Kobori K., and Murakami I. Development of Magnetic Harmonic Gear with Stackable Structure, International Journal of Applied Electromagnetics and Mechanics 52 (2016), pp.809-816.

DEVELOPMENT OF 2 DOF LINEAR OSCILLATORY ACTUATOR FOR VIBRATION CONTROL

F. Kitayama[1,a], R. Kondo[1,b]

[1] Department of Mechanical System Engineering, College of Engineering, Ibaraki University, Japan
[a]fumiya.kitayama.amayatik@vc.ibaraki.ac.jp, [b]ryou.kondo.piyashiri@vc.ibaraki.ac.jp

Abstract. In automobiles, multi axis vibrations were generated by many mechanical parts. So, vibrations were actively controlled by using some linear oscillatory actuators. In the paper, we propose a 2 degrees of freedom linear oscillatory actuator to reduce vibrations, that achieves downsizing and weight saving of the system. First, the basic construction and operation principle are described. Next, the characteristics are clarified through measurements on prototype.

1. Introduction

It is well known that an automobile is a multimode system that generates multidimensionally undesirable vibrations. Also, some 1 DOF active control devices [1] are set on the automobile to reduce one or some dimensional vibrations. In this study, a 2 DOF inertia mass shaker as 2 DOF active control devices, that generates two-dimensional inertia force expressed as a product of acceleration and mover's weight by a 2 DOF linear oscillatory actuator, are developed in order to reduce two-dimensionally undesirable vibrations in a smaller number of devices. In this paper, the 2 DOF linear oscillatory actuator with lightweight movers is proposed.

2. 2 DOF linear oscillatory actuator for vibration control

First, a target amplitude and drive frequency range of inertia force are determined as 30 N and 25-100 Hz at two dimensions, and limited current is 3A. The target inertia force is achieved by oscillating lightweight movers at large acceleration and strokes. Target mover's weight, acceleration and stroke are determined as 300g, 100m/s^2 and 10mm.

The proposed actuator is shown in Fig. 1. External dimensions of the main part are 78 x 78 x 61mm, that is almost the same as an actuator of the 1 DOF inertia mass shaker. The proposed actuator mainly consists of eight springs, a stator and two movers called as X mover and Y mover. Four springs are connected between the X mover and stator, and other springs are connected between the Y mover and stator. The stator is composed of two coils called as X coil and Y coil, yokes made from soft iron, and support parts made from non-ferromagnetic materials. The X mover is composed of yokes, eight square-shaped magnets, support parts and linear bearings that supports on the Y and Z axes. The Y mover is also configured like the X mover. Magnets magnetized at the positive Z direction and magnets magnetized at the negative Z direction are alternately arranged as shown in Fig. 1 (b) and (c). In order to constantly keep thrust at large stroke, relationships of position and size between magnets and the stator yoke are determined as referring to a 1 DOF actuator [2], and isosceles triangle-shaped notches are made in the stator yoke. Since current is applied to the X coil, a part of the stator yoke facing the X mover is magnetized, and it is repulsed and attracted with magnets of the X mover, consequently, the X mover is moved. Also, the stator yoke facing the Y mover is magnetized since current is applied to the Y coil, and it is repulsed and attracted with magnets of the Y mover, consequently, the Y mover is moved.

3. Experimental Evaluation by using prototype

A prototype was manufactured to experimentally evaluate the characteristics, as shown in Fig. 2(a).

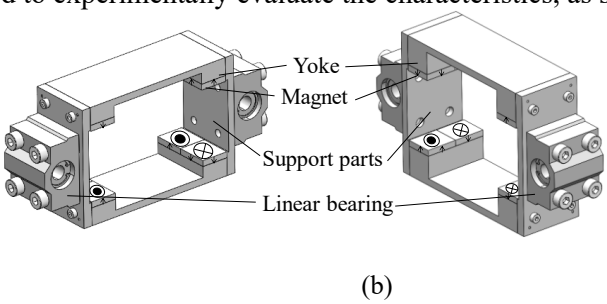

(a) (b) (c)

Fig. 1 Basic constructions: (a) overall; (b) X mover; (c) Y mover

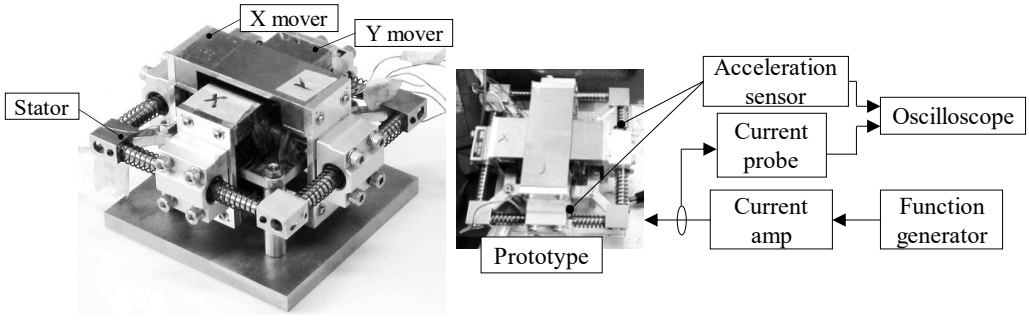

(a) (b)

Fig. 2 Experiments for measuring acceleration: (a) prototype; (b) experimental setup

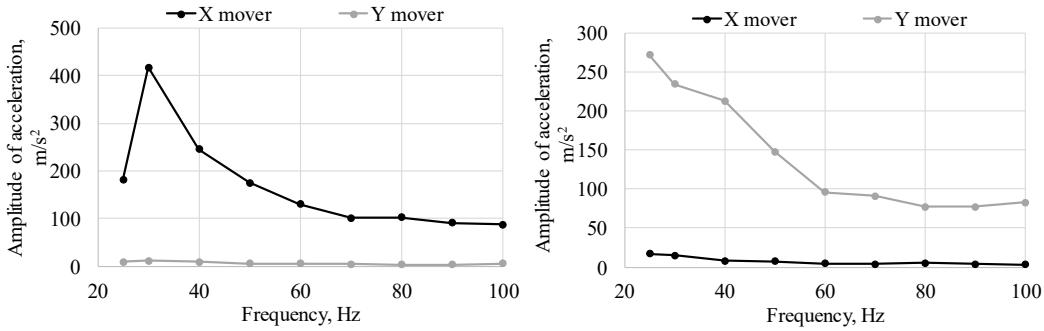

(a) (b)

Fig. 3 Measured acceleration: (a) current is applied to X coil; (b) current is applied to Y coil

The X mover's and Y mover's weight are 268 and 328 g. The experimental setup is shown in Fig. 2 (b). Sinusoidal current that an amplitude is 3 A and drive frequency is from 25 to 100Hz, was applied to the X coil or Y coil by a function generator (AFG1022, Tektronix) and a servo amplifier. Acceleration of movers and current of coils were measured by using acceleration sensors (NP-3211, Onosokki), current probes (3273-50, HIOKI) and an oscilloscope (LeCroy, 314A). The amplitude of measured acceleration when applying current to each coil was respectively shown in Fig. 3. The X mover was mainly oscillated when applying current to the X coil, and the Y mover was mainly oscillated when applying current to the Y coil. The acceleration amplitude was large at low drive frequency due to mechanical resonance, but minimum acceleration amplitude was 88m/s^2 on the X mover and 77m/s^2 on the Y mover. Also, it was observed that the maximum stroke is above 10mm. The inertia force of the X mover was maximum 112N and minimum 23N, and that of the Y mover was maximum 89N and minimum 25N.

Conclusions

- The 2 DOF linear oscillatory actuator that consists of two lightweight movers with surface permanent magnets and a stator yoke with notches, was developed.
- From measured results on prototype, it was verified that movers could be two-dimensionally oscillated at large strokes. Also, the calculated inertia force was satisfied the target value at the low drive frequency range, but the ratio of the calculated inertia force to the target value was from 78 to 90% at the high drive frequency range. In the future, it will be satisfied the target value at all drive frequency range by adjusting the mover's weight and coil conditions.
- In the presentation, measured results will be discussed in detail by comparing with analyzed results.

References

[1] Svaricek F., Bohn C., Marienfeld P., Karkosch H.J., Fueger T. *Automotive Applications of Active Vibration Control*, *Vibration Control*, IntechOpen, 2010, 303-318.
[2] Asai Y., Hirata K., Ota T. Dynamic Analysis Method of Linear Resonant Actuator with Multimovers Employing 3-D Finite Element Method, IEEE Transaction on Magnetics, 2010, 46 (8), 2971-2974.

FATIGUE CORROSION BEHAVIOR OF NITI SHAPE MEMORY ALLOY

Mahdi Mohajeri[1,2], Homero Castaneda[1], Dimitris C Lagoudas[1,2,a]

[1]Department of Materials Science & Engineering, Texas A&M University, College Station, TX 77843, USA
[2]Department of Aerospace Engineering, Texas A&M University, College Station, TX 77843, USA
[a]lagoudas@tamu.edu

Abstract

The fatigue process causes the protective passive film rapture, which accelerates the corrosion of metallic materials. The synergic interaction of fatigue and corrosion processes with variable thermal and mechanical loads cause the shorter fatigue lifetime. In this study, the thermomechanical fatigue of Nickel-Titanium shape memory alloy (SMA) undergoing thermally induced martensitic phase transformation in a physiological corrosive environment is investigated. The effect of the change in phases of Nickel-Titanium SMA on the electrochemical behavior at different load levels was characterized. Electrochemical techniques showed the global influence on the SMA surface during the change in crystallographic orientation and phase transformation due to the loading conditions. This change in crystallographic orientation affected the surface of Nickel-Titanium SMA locally. These local effects could be sensed by the global interfacial changes with electrochemical measurements, such as Electrochemical Impedance Spectroscopy (EIS), Open Circuit potential (OCP) and Linear polarization (LPR) methods.

The passive layer formation includes Ni and Ti oxide based composition following exposure in Ringer's solution. The increase in the loading parameter resulted in the breakdown of the passive layer while passivation stage could be reached due to the strain effect on the bonding or physical characteristics of the passive layer.

Keywords: Shape memory alloy; Corrosion fatigue; Martensitic phase transformation

MODELING OF INTERNAL DAMAGE EVOLUTION DURING ACTUATION FATIGUE IN SHAPE MEMORY ALLOYS

F.R. Phillips[1], D.T. Martin[1], and D.C. Lagoudas[1,a]

[1]Aerospace Engineering and Materials Science and Engineering, Texas A&M University, College Station, Texas, United States of America
[a]lagoudas@tamu.edu

Abstract

Shape memory alloys (SMAs) are unique materials capable of undergoing a thermo-mechanically induced, reversible, crystallographic phase transformation. As SMAs are utilized across a variety of applications, it is necessary to understand the internal changes that occur throughout the lifetime of SMA components. One of the key limitations to the lifetime of a SMA component is the response of SMAs to fatigue. SMAs are subject to two kinds of fatigue, namely structural fatigue due to cyclic mechanical loading which is similar to high cycle fatigue, and functional fatigue due to cyclic phase transformation which typical is limited to the low cycle fatigue regime. In cases where functional fatigue is due to thermally induced phase transformation in contrast to being mechanically induced, this form of fatigue can be further defined as actuation fatigue. Utilizing X-ray computed microtomography, it is shown that during actuation fatigue, in- ternal damage such as cracks or voids, evolves in a non-linear manner. A function is generated to capture this non-linear internal damage evolution and introduced into a SMA constitutive model. Finally, it is shown how the modified SMA constitutive model responds and the ability of the model to predict actuation fatigue lifetime is demonstrated.

Keywords: SMAs, low cycle fatigue, thermally induced, X-ray μCT, damage evolution

CERAMIC COMPOSITES BASED ON FUNCTIONALIZED GRAPHENE OXIDE AND ALUMINA

G.G. Bokuchava[1,a], E.E. Sanaia[1,b], T.N. Archuadze[1,c], T.V. Kuchukhizde[1,d], N.T Jalagonia[1,e]

[1]Ilia Vekua Sukhumi Institute of Physics and Technologies, Tbilisi, Georgia
[a]sipt@sipt.org.ge, [b]esaniaa@gmail.com , [c]tamari.tamriko@gmail.com , [d]tinikokuchukhidze@gmail.com,
[e]n.jalagonia@sipt.org.ge

Abstract. Improvement of the physical-mechanical properties of ceramics to a certain degree became possible by reducing the size of particles of sintered powders to nano sizes, also by doping different type structure containing compounds (Nanofibers, nanotubes, nanonets and other) and selection of consolidation optimal regimes. Homogenization of nanomaterials into ceramic composites have significantly influence on its' mechanical properties. For purpose, we have carried out functionalization of graphene oxide by organic compound and homogenization in alumina has conducted by grinding in nanomill during 24 h. Following ceramic composites have obtained by hot pressing method: α-Al_2O_3, α-Al_2O_3-GO, α-Al_2O_3- ZrO_2-Y_2O_3-GO, α-Al_2O_3- ZrO_2-Y_2O_3-GO_{mod}. Structure, morphology and mechanical properties of obtained materials have investigated. It is established, that mechanical characterization is improving by addition various nanoparticles into alumina.

1. Introduction

Recently obtaining of ceramic materials have a big attention, because they are characterized high physical-mechanical properties, corrosion ressitance, eqspluatation possibility at high temperature (1400-2000^{O}C) and other. Powdery technology are used often for fabrication a new materials, which implies elaboration of obtaining method of various type and purposes powdery and further fabrication of ceramic materials with high exploitation properties. Nowadays, main focus is to nanotechnologies for obtaining nanopowders and its' based on nanostructural materials. Materials physical-mechanical properties are depend on consolidation process of powdery. Several methods are using for consolidation of powdery, such as gradually increasing of consolidation temperature, consolidation method using microwave oven, spark-plasma sintering, consolidation in induction furnace and other [1-3].

It is known in literature, that graphene is most stsrength material, that's why increases physical-mechanical properties of materials addition of its' in ceramic [4-5]. We have used hot pressing method for obtaining of ceramics. Preparation of graphene monolayer is actual problem, which is related to cost, time and other, because of this graphene oxide are used mostly. For purpose, Obtaining of hard ceramic materials, graphene oxide was functionalized by organic compounds (polyvinyl alcohol (PVA), polyethylene glycol (PEG). Then functionalized graphene oxide was added in alumina and homogenization process carried out in nanomill during 24 h. Organic compounds are allocated form graphene oxide at high temperature during sintering, so being reduction of graphene oxide. This kind reduced graphene oxide has mostly similar properties as graphene, which have influence on physical-mechanical properties of ceramics.

2. Experimental procedure and sample preparation

Synthesis of graphene oxide. Synthesis of graphene oxide have conducted by intercalation method from graphite. Graphite flakes (2 g) mixed in 50 mL of H_2SO_4 (98%) and potassium permanganate (6 g) very slowly during 1 h. The flask kept under at ice bath (27-35°C) with continuous stirring. After 1 h 100 ml water was added in the mixture. Then continue stirring again about 1 h and 20 mL H_2O_2 was added. After washing and filtration, the mixture centrifugation has done. Stable graphene oxide suspensions have obtained which used as reinforcement materials in ceramic composite.

Functionalization of graphene oxide. 1 g graphene oxide was dispersed in 100 mL H_2O using ultrasound bath. Obtained stable suspension and added 1 g PVA (or PEG), mixture was treated by ultrasound bath again. Identification of materials have been done by modern research methods.

Preparation of pressing powdery composite. 65 g α-Al_2O_3 was mixed to functionalized graphene oxide (1.5% mas.). 100 mL H_2O was added into mixture and homogenization carried out by nanomill during 24 h. Then the mixture dried and placed in press form.

Sintering was performed using nanopowders hot pressing installation with direct current passage under a pressure 40MPa and holding for 2min at various temperatures. Further studies were performed on samples molded - tablets with a diameter of 20 mm and a height of 4 mm.

The phase composition of the samples was determined by X-ray diffraction X-ray diffractometer DRON-3M.

3. Results of hot vacuum pressing of nanopowders

Obtained graphene oxide was investigated by SEM, identification was carried out by Raman, FTIR and UV, particles sizes was measured by laser nanosizer.

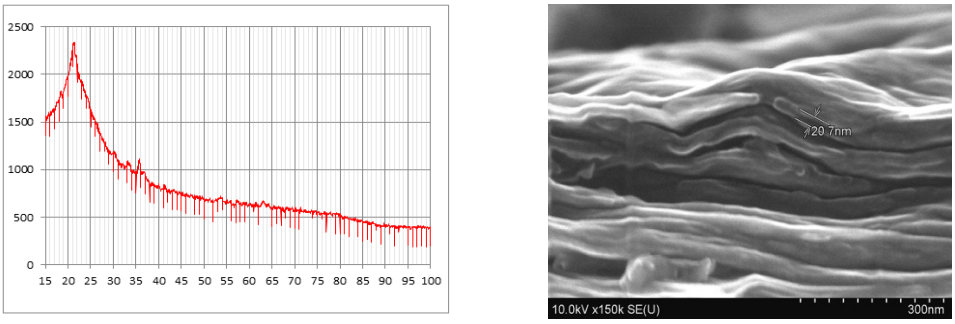

(a) (b)

Fig. 1Elecrtonic micrograph (a) and XRD (b) of graphene oxide

As electronic micrographs showed, average number of reduced graphene oxide layers are 20-40 nm and graphene oxide particles sizes are approximate 50-90 nm in suspension.

Various type ceramic composites have obtained by high temperature vacuum furnace (OXY-GON), such as: α-Al_2O_3-GO, α-Al_2O_3-ZrO_2-Y_2O_3-GO, α-Al_2O_3-ZrO_2-Y_2O_3-GO_{mod}. Graphene oxide was synthesized with particle sizes ~50-96 nm by proved method in the literature. Then graphene oxide modification was conducted by organic compounds (PVA, PEG).

Ceramic composites dopped functionalized graphene oxide was sintered in high temperature furnace with 50 mm dimeter sizes. Physical-mechanical and structural-morphological research has been conducted for obtained materials.

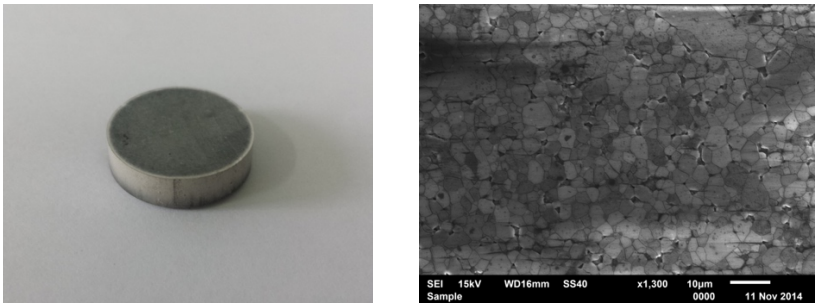

Fig. 2 Electronic micrograph and ceramic material

Corundum ceramic materials have obtained at 1600ºC (1h), which characterized with high hardness, crack and corrosion resistance. Their density reaches to 99,5-99,6% of theoretical.

Conclusions

In this work, reduced graphene oxide preparation method was developed. Matrix composites have obtained based on graphene structure and alumina. Following ceramics α-Al_2O_3-GO, α-Al_2O_3-ZrO_2-Y_2O_3-GO, α-Al_2O_3-ZrO_2-Y_2O_3-GOmod have fabricated at 1600^{O}C by high temperature vacuum furnace. Physical-mechanical properties, phase composition and microstructure of matrix ceramic materials have been established.

References

[1] Sheng-Tao Yang, Yanil Chang, Haifang Wang, Gangbo Liu, Sheng Chen, Yanwen Wang, Yuanfang Liu, Aoneng Cao. Journal of Colloid and Interface Science 351, 2010, 122-127;

[2] Harshit Porwal, Peter Tatarko, Salvatore Grasso, Jibran Khaliq, Ivo Dlouhy, Mike J. Reece. Carbon 64, 2013, 359-369;

[3] Jixin Zhu, Ting Zhu, Xiaozhu Zhou, Yanyan Zhang, Xiong Wen Lou, Xiaodong Chen, Hua Zhang, Huey Hoon Hng, QIngyu Yan. Nanoscale 3, (2011), 1084-1089;

[4] Kuchukhidze T., Jalagonia N., Sanaia E., Barbakadze K., Marquis F., Bokuchava G. Matrix Composites Reinforced with Modified GO Based on Alumina and Their Investigation. Proceedings of ICMSF 2018: 20th International Conference on Materials Synthesis and Fabrication, 2018, 1659-1662;

[5] Natia Jalagonia, Fernand Marquis, Karlo Barbakadze, Ekaterine Sanaia, Guram Bokuchava, Tinatin Kuchukhidze. Obtaining of Graphene Structure Containing Ceramic Composites in High Temperature Vacuum Furnace. Materials Science Forum, ISSN: 1662-9752, Vol. 900, 101-104; doi:10.4028/www.scientific.net/MSF. 900.101; © 2017 Trans Tech Publications, Switzerland.

STUDYING ELECTRO-PHYSICAL AND MECHANICAL PROPERTIES OF SNO2- SB2O3-C CERAMIC-BASED COMPOSITE MATERIAL

S. S. Dobromyslov[1,3,a], V. I. Kirko[1,2,b], V.A. Razumovskaya[1,c].

[1]Siberian Federal University
[2]Krasnoyarsk State Pedagogical University named after V. P. Astafyev
[3]Krasnoyarsk Scientific Center of the Siberian branch of the Russian Academy of Sciences
[ba]dobrosmislov.s.s@gmail.com, [b]director.nifti@mail.ru [c]veronica_raz@hotmail.com

Abstract

The materials based on tin oxide and antimony oxide are of great interest as they are conductive at high temperatures and possess high corrosion resistance in corrosive environment such as an electrolyte used in the aluminum electrolysis.

In connection with it these tin dioxide-based materials can find wide application as current-carrying anodes in the aluminum production. In this research the **SNO_2- SB_2O_3-C** ceramics electro-physical and physical mechanic properties have been studied.

The material has been synthesized by the following technology: preparing the mixture→ pressing the press-powder with 5% polyvinyl alcohol content → drying → firing. The pressed samples have been dried in a drying chamber at the temperature of 383 K up to the moisture content of 2 – 4 %. Firing has been done in a muffle furnace in the open air at the temperature of 1573 K. Specific electrical resistivity in the range of temperatures from 20 to 1000°C has been measured by a four-contact method. The thermophysical characteristics have been studied by a Netzsch LFA 457 laser flash method. The material phase composition has been controlled by an X-ray analysis at the XRD 6000 analyzer. Its microstructure has been studied at the JEOL JSM-6490 LV and JEOL JSM 7001-F electronic microscopes.

It has been proved that specific electrical resistance of the ceramics of 96%SnO_2 – 2%Sb_2O_3 – 2%MnO_2 – 2%C at the temperatures of 600-700 °C does not practically depend upon the temperature. At the temperature above 700°C the specific electrical resistivity of the material begins to increase disastrously that is caused by carbon oxidation. At the temperatures of 700-1200 °C the specific electrical resistivity of the ceramics becomes the same as a classical semiconductor and practically becomes the same as carbon-free ceramics with the composition of 96%SnO_2 – 2%Sb_2O_3 – 2%MnO_2.

The replacement of MnO_2 by Al_2O_3 in the material studied allows enlarging the temperature range of the material specific electrical resistivity stability up to 1200 °C.

INFLUENCE OF THE SIZE, SHAPE AND CONCENTRATION OF MAGNETIC PARTICLES ON THE OPTICAL PROPERTIES OF NANO NICKEL THIN FILMS

L.G. Kalandadze[1,a], O.M. Nakashidze[1,b], N.KH. Gomidze[1,c], I.N. Jabnidze[1,d]

[1] *Department of Physics, Batumi Shota Rustaveli State University, Batumi, Georgia*
[a]lali.kalandadze@bsu.edu.ge, [b]omar.nakashidze@bsu.edu.ge, [c]Gomidze@bsu.edu.ge, [d]izolda.jabnidze@bsu.edu.ge

Abstract. In the present paper, using the discontinuous Ni films as examples we consider theoretically and experimentally the influence of the structural parameters on the optical properties of the ultrafine structures. The optical spectra strongly depend on composition and dielectric constants of particles and matrix. In its turn the dielectric constants are functions of the structural and electronic parameters and can differ from those for corresponding bulk materials. Thus optical spectra investigations can give very useful information about structural parameters of the ultrafine structures. The behavior of the optical spectra of thin Ni films was explained in the framework of the effective medium approximation. These calculations proved a good agreement between the experimental and the theoretical results.

1. Introduction

It is known that the qualities of already explored materials change in the process of their transformation into nanocrystals. This was predictable because these structures contain from some atoms to thousands of atoms and take a middle place between atoms and massive substances, and subsequently, they have properties different from both of them. Consequently, they acquire the set of particular qualities, such as: giant magnetoresistance, giant magneto-impedance, anomalous Hall effect, anomalous optical and magneto-optical effects [1- 3] and etc.

In general, the optical properties of nano-dispersive structures are very different from the properties of the bulk materials and depend on the structural parameters: the occupancy of the volume of the ultrafine medium with nanoparticles (q), the size and shape of the particles (f), the order of the particles, the properties of the medium, surrounding nanoparticles (ε_m) [4-7].

In this paper we present theoretically and experimentally the influence of the structural parameters on the optical properties of the nano-dispersive nickel. We interpret the obtained optical spectra in the framework of the effective medium approximation [8].

2. Theory

We have modified the Maxwell-Garnett effective-medium theory to study nano-dispersive medium with optically anisotropic particles (ellipsoids). After generalization of the Maxwell-Garnett theory for nano-dispersive structure which composed of ellipsoidal particles with different dielectric permittivity $\varepsilon_i (i = 1,2,3\cdots,n)$ and matrix with dielectric permittivity ε_m we arrived at formula how to calculate diagonal elements of the dielectric tensor for non-spherical ultrafine particles.

$$\frac{\varepsilon_{ef} - \varepsilon_m}{\varepsilon_m + f(\varepsilon_{ef} - \varepsilon_m)} = q\frac{\varepsilon - \varepsilon_m}{\varepsilon_m + f(\varepsilon - \varepsilon_m)} \tag{1}$$

Where ε_{ef} is effective dielectric permittivity of nano-dispersive structure, q is the ratio of the volume, occupied by particles, to the total volume of the medium and f is the factor of the shape of the ultrafine particles.

The effective dielectric permittivity $\varepsilon_{eff} = \varepsilon_{1eff} - i\varepsilon_{2eff}$ is connected to reflective index n_{eff} and absorption index k_{eff} of nano-dispersive medium by formula

$$\varepsilon_{ef} = (n_{ef} + ik_{ef})^2 \tag{2}$$

3. Experimental

In this work we investigate the optical properties of discontinuous nickel films, the weight thickness d ($d = m/\rho S$, where m -film mass, ρ -metal density and S -film square) of which falls within the interval 4.8-30 nm. Discontinuous films were obtained by evaporation in vacuum of 10^{-5} Torr on glass substrates with a rate of 1 to 5 $\overset{0}{A}$/S. The optical constants were determined using the Avery method [9].

4. Results and discussion

Fig. 1 gives the dependences of optical constants on $\hbar\omega$, calculated for nano-dispersive nickel as given in eqns.(3) and (2). Note that n_m is reflective index of matrix.

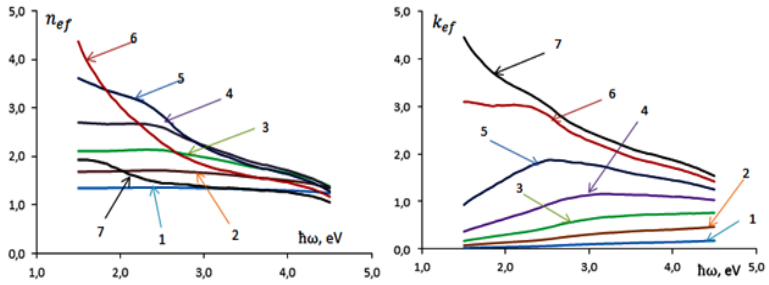

Fig. 1. Dependences of the equatorial Kerr effect on $\hbar\omega$ for ultrafine nickel, calculated by formulas (3) and (2) with q=0,1(1); 0,25 (2); 0,4 (3); 0,55 (4); 0,7 (5); 0,85 (6); 1,0 (7) and n_m=1.15; $f = 1/3$.

Comparing experimental results with the theoretical results of fig. 1, we observe that the spectra of the optical constants with weight thicknesses d =4.8 – 30 nm are similar to the spectra computed with different q =0,1-0,85. We have also calculated the dependences of n_{eff} and k_{eff} on the quantum energy of incident light $\hbar\omega$, for nano-dispersive nickel with different n_m. It is evident from the results of these calculations that the optical spectra of nano-dispersive medium strongly depend on the volume fraction of magnetic particles, shape of the particles and dielectric constants of matrix.

Conclusions

The behavior of the optical spectra of thin Ni films was explained in the framework of the effective medium approximation in two cases: q<0.5 and 0.5< q<1. In this approach effective refractive index (n+ik) of the nano-dispersive structures have calculated as a function of the ε_m, q, and particle shapes. Moreover, the experimentally derived data are well compatible with the above discussed theory.

References

[1] Mnh-Huang Phan, Hua-Xin Peng, // Progress in Materials Science 53 (2008) pp.323–420.
[2] Slonczewski J.C. //Physical Review B/ 1989.V.39.N10.P/6995-7002.
[3] Ganshina E., Granovsky A., Dieny B., Kumaritova R., Yurasov // Physica B 229, 2001,P260-264.
[4] Mitani S., Fujimori H., Takanashi K., Yakusiji K., Ha J.G., Takanashi S., Maekawa S., Ohnuma S., Kobayashi N., Masumoto T., Ohnuma M., Hono K., //JMM.1999.V.198-199/P.179.
[5] Kalandadze L. Journal of Sensor Letters. American Scientific Publishers. V5, Number 1, 2007, 13-14.
[6] Nakashidze O., and Kalandadze L. New Developments in Materials Science; Nova Publishers; 2013 pp. 119-126.
[7] Nakashidze O., and Kalandadze L. 2016IEEE 7th international conference on Advanced Optoelectronics and Lasers; (2016), pp. 17-20.
[8] Nikitin L.V., Kalandadze L.G., Akmedov M.Z., Nepijko S.A., Ostranica A.P. Journal of Magnetism and Magnetic Materials 148 (1995) 279-280.
[9] Maxwell J.C. Garnett. Phil. Trans. R. Soc. Lond. A 203, 385 (1904).
[10] Avery D.G., "An Improved Method for Measurements of Optical Constants by Reflection", Proc. of the Physical Society, section B, V. 65, 426 (1952).

RHEOLOGICAL PROPERTIES OF MAGNETIZED BIDISPERSE MAGNETORHEOLOGICAL FLUIDS CONTAINING NEEDLE-LIKE PARTICLES

Y. Iwamoto[1,a], T. Koroki[1,a], Y. Ido[1,b], H. Yamamoto[2,c], H. Nishida[2,d], Y. Fujii[3,e], T. Deguchi[3,f]

[1] *Department of Electrical and Mechanical Engineering, Nagoya Institute of Technology, Gokiso-cho, Showa-ku, Nagoya 466-8555, Japan*

[2] *Department of Electrical and Control Systems Engineering, National Institute of Technology, Toyama College, 13 Hongo-cho, Toyama 93908630, Japan*

[3] *KRI, Inc. Kyoto Research Park, 134, Chudoji Minmi-machi, Shimogyo-ku, Kyoto 600-8813, Japan*

[a]iwamoto.yuhiro@nitech.ac.jp, [b]ido.yasushi@nitech.ac.jp, [c]h.yamamoto@nc-toyama.ac.jp, [d]nishida@nc-toyama.ac.jp, [e]ya-fujii@kri-inc.jp, [f]deguchi@kri-inc.jp

Abstract. In the present study, a novel magnetic functional fluid, magnetized bidisperse magnetorheological fluids containing needle-like magnetic particles, was proposed to enhance magnetorheological effect. This is a fluid magnetized by a pulse-strong magnetic field of 8 T, before exposed to a weak external magnetic field for inducing the magnetorheological effect. The dynamic rheological measurements in the presence of a magnetic field using the magnetic field imposed-type rheometer (MCR302, MRD, Anton-paar) was carried out to investigate the effect of the initial magnetization on the rheological behavior. The results show that the storage modulus increases with the initial magnetization. Four element model fits the data well. The model shows that the magnetization increases the elastic elements of the fluid.

1. Introduction

Magnetic Functional Fluids (MFFs), dealt in the present work, are magnetic particle suspensions in which nm- and/or μm-sized magnetic particles disperse in proper carrier liquids. When such fluids are exposed to an external magnetic field, the magnetic particles are magnetized and forms chain-like structures along the magnetic field. These structures apparently increase the fluid viscosity. This effect is often called a Magnetorheological effect (MR effect). The effect can be regulated by magnetic field strength and direction [1]. Hence, the magnetic functional fluids have been applied to semi-active dampers and clutches [2]. The authors have been proposed a Bidispersed Magnetorheological Fluid (BMRF) containing Needle-like magnetic particles to enhance the MR effect [3]. The BMRF is a mixture MFF of nm- and μm-sized magnetic particles. Significant large clusters are known to be formed under an external magnetic field. The authors found that addition needle-like magnetic particles to BMRF render it more the MR effect. In the present work, to enhance further MR effect, we proposed a novel MFF, magnetized BMRF containing needle-like magnetic particles.

The proposed fluid is a fluid magnetized by a pulse-strong magnetic field of 8 T, before is exposed to a weak external magnetic field for inducing the MR effect. μm-sized magnetic particles have a multi-magnetic domain, in which magnetic moments randomly orients. Once a pulse-strong magnetic field applies to the particles, the magnetic moment orient to the field direction. After removing the magnetic field, the moments keep the orientation, which means that the particles are magnetized and have remanent magnetization and coercive force. Therefore, a significant enhancement of the MR effect is expected by applying a relatively weak magnetic field.

To understand the effect of the initial magnetization to the MR effect, most relevant are investigations of the rheological properties. In the present study, we carried out the dynamic rheological measurements in the presence of a magnetic field using the magnetic field imposed-type rheometer (MCR302, MRD, Anton-paar). And by fitting the obtained data by four element model, the effect of magnetization on the dynamic rheological properties was discussed.

2. Test fluids and dynamic rheological measurements

The test fluids are mixture magnetic functional fluids in which nm-, μm and needle-like magnetic particles disperse in polyalphaolefin. The nm-sized magnetic particle was maghemite with an averaged diameter of 10 nm (APG314, Ferrotec). μm-sized magnetic particle is carbonyl iron with an averaged diameter of 4~6 μm (OM grade, BASF). Needle-like magnetic particle is iron with averaged major axis length of 100 nm and an aspect ratio of 4.0 (MP-5, Dowa Electronics Materials Co., Ltd.). Their fraction was arranged to be 3.0 vol. % of nm-sized magnetic particle, 26.0 vol. % of μm-sized magnetic particles and 1.0 vol. % of needle-like magnetic particles, respectively. Smectite of 2.2 vol. % was added as an additive to increase fluid viscosity. We prepare two types of test fluids. One of them is magnetized fluid (Magnetized BMRF), which was initially

magnetized by a pulse-strong magnetic field of 8 T. Another is non-magnetized fluid (Non-magnetized BMRF).

The dynamic rheological properties were measured by the plate-type magnetic field imposed-type rheometer (MCR302, MRD, Anton-paar) in the presence of the magnetic field of 150 mT. The gap between rotor and stator was set to be 1.0 mm.

3. Results and discussion

In order to verify the influence of initial magnetization on the dynamic rheological behavior, Fig. 1 shows the storage and loss moduli, G' and G'', of the non-magnetized BMRF and the magnetized BMRF. The solid lines are the fitting data with the four-element model. The model fits the experimental data well in a range of 70 ~ 140 rad/s. Of particular interest is that the storage modulus is significantly enhanced by initially magnetizing the BMRF with a pulse-strong magnetic field of 8T. The four-element model is a combination of Voigt and Maxwell models. The Voigt model is often used to describe the solid behaviors, and the Maxwell model describes the liquid behavior. With fitting the experimental data by the four-element model, it was found that the elastic elements in Voigt and Maxwell models increases by the initial magnetization. The magnetic dipole interaction force acts on the magnetic particles and forms the chain-like structures in the presence of a magnetic field. This elastic variation is thought to be due to a change of structure morphology. The morphology depends on the particle shape, size and fraction [4]. Because the μm-sized and the needle-like particles have a multi-magnetic domain, the remanent magnetization is induced by initially magnetizing the BMRF, resulting in that the magnetic particle assemblage are formed in the absence of magnetic field. This relatively huge magnetic assemblage may form further huge structures along the applied magnetic field. Consequently, the storage modulus of the BMRF may be enhanced by the initial magnetization.

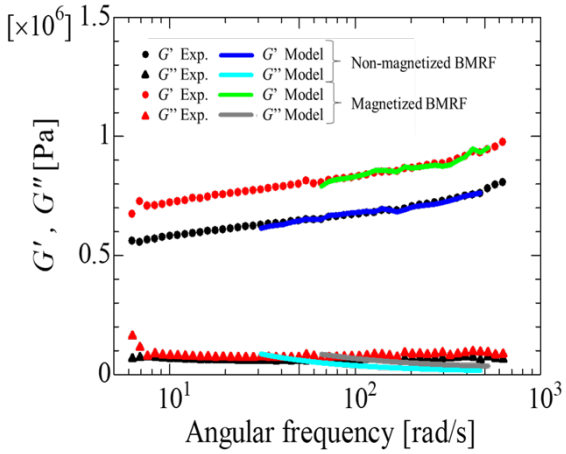

Fig.1. The storage modulus G' and the loss modulus G'' of non-magnetized and magnetized bidipsersed magnetorheological fluids. The plots are measured moduli. The solid lines are fitting data with the four element model.

Conclusions

We investigated the effect of the initial magnetization on the dynamic rheological properties of bidisperse magnetorheological fluids containing needle-like magnetic particles. The BMRF has an inherent potential to enhance the MR effect significantly. By initially magnetizing the BMRF to induce remanent magnetization, it was found that the MR effect is significantly increased. The analysis with fitting the four-element model shows that the initial magnetization enhances elastic properties.

References

[1] Yamaguchi H. *Engineering Fluid Mechanics*, Springer, 2008.
[2] Odenbach S. Ferrofluids -Magnetically Controllable Fluids and Their Applications, Springer, 2002.
[3] Ido Y., Nishida H., Iwamoto Y., Yokoyama H. Viscous properties of ferrofluids containing both micrometer-size magnetic particles and fine needle-like particles, Journal of Magnetism and Magnetic Materials, 2017, 431, 94-98.
[4] Iwamoto Y., Kondoh S., Ido Y., Yamamoto H., Nishida H., Yamasaki H., Yamaguchi H., Jeyadevan B. Influence of size on anisotropic thermophysical and rheological properties of magnetic suspensions, International Journal of Applied Electromagnetics and Mechanics, 2018, 58, 1-15.

GENERATING ANALYTICAL FRAGILITY CURVES FOR GYPSUM PARTITION WALLS WITH DIFFERENT ASPECT RATIOS

E. "Manos" Maragakis[1,a]

[1]Dean of College of Engineering,University of Nevada, Reno, Nevada, 89557, USA
[a]maragaki@unr.edu

Abstract

Since generating experimental-based fragility curves for gypsum partition walls are cost-consuming, such curves have been conducted for only limited aspect ratios of wall specimens. To fill this gap, a reliable numerical modelling methodology is necessary to generate comprehensive simulation-based fragility curves. As part of this study, a previously-verified experimental-based analytical model is adopted to develop a procedure to generate seismic fragility curves for the gypsum partition walls. Additionally, five categories of 36 wall specimens with aspect ratios of 0.5, 1, 1.5, 2, and 3 of the gypsum partition walls are modelled and, for the first time, their corresponding seismic fragility curves are generated. Besides wall aspect ratios, the effects of construction quality and connection variations are examined through these numerical simulations. Results from this methodology are then compared against values presented in FEMA P-58. This comparison showed that the medians of partition fragility curves obtained from this study are in close agreement with those in FEMA P-58 for the similar aspect ratios.

Keywords: Gypsum partition wall, Analytical study, Fragility curve, Aspect ratios, Risk assessment.

ELECTRICAL CONSOLIDATION UNDER PRESSURE FOR AL2O3 AND WC NANODISPERSE POWDERS

Edwin S. Gevorkyan[1, 2, a], Athanasios G. Mamalis[3, b], Yuriy G. Gutsalenko[4, c]

[1]Ukrainian State Univ. of Railway Transport, [2]Cermet-Ukraine Ltd., Kharkov, Ukraine
[3]Nat. Center Scientific Research "Demokritos", Athens, Greece
[4]Nat. Tech. Univ. "Kharkov Polytechnic Inst.", Kharkov, Ukraine
[a]edsgev@gmail.com, [b]a.mamalis@inn.demokritos.gr, [c]gutsalenko@kpi.kharkov.ua

Abstract

The features of hot pressing by the method of electrical consolidation under pressure of nanodispersed powders of two types of materials – electric current conductive (WC) and nonconductive (Al2O3) are considered. WC powder (Aldrich Co, Austria) with a particle size of <2 μm and α-Al2O3 powder (Sumitomo Chemical Co., Japan) with a particle size of <0.1 μm were used. The heating rate varied from 50 °C/min to 500 °C/min. Sintering was carried out in an electric field activated by a direct current lead to the vacuum processing chamber, with the implementation of the well-known FAST technical approach (Field Assisted Sintering Technique) using the well-known SPS method (Spark Plasma Sintering) on the original installation with longitudinal-axial pressing of the chamber contents.

With rapid heating, the density of the sintered powders to 99% after 2 minutes of exposure under a pressure of 40 MPa reached respectively at 1200 °C for Al2O3 and at 1650 °C for WC. At the same time, the order of grain size did not change. Intensive compaction and minimal grain growth in each of these materials are caused by the combined effect of electric current and mechanical pressure, which positively changes the mass transfer pattern, its intensity, uniformity and dispersion of the consolidated grain structure compared to conventional sintering, when large grain growth is characterized for both materials.

Direct action of electric current contributes to remove of impurities contaminants from the surface of the particles, activates their surface, changes the transboundary structure, provides direct physical contact between the grains, ensures cleanliness and flexibility of their boundaries, increases sensitivity to heat, intensifies their compaction, alleviates the necessitate problem of sealing for compacting bonding additives.

High-speed electric heating of powders reduces the time of change of grain boundaries, inhibits their growth and ultimately leads to the formation of fine homogeneous structures of high functionality.

The unified character and convergence of the geometric dynamics of the behavior of fine WC and Al2O3 structures in electrical consolidation under pressure with accelerated thermal loading of powders from these refractory materials made it possible to create their operational effective high density composites with a nanoscale grain structure.

DESIGN OF HIGH SPEED INTERIOR PERMANENT MAGNET TYPE MOTOR FOR TURBO-MACHINERY

Yohji Okada[1,a], Fumiya Kitayama[1,b] and Ryou Kondo[1,c]

[1]*School of Engineering, Ibaraki University, 3-14-6 Nakanarusawa, Hitachi, 316-8511, Japan*
[a]yohji.okada.spam@vc.ibaraki.ac.jp , [b]fumiya.kitayama.amayatik@vc.ibaraki.ac.jp,
[c]ryou.kondo.piyashiri@vc.ibaraki.ac.jp

Abstract. High speed Interior Permanent Magnet (IPM) motor is proposed. It is intended to apply to the turbo-machinery which is supported by magnetic bearings. Such a system usually requests a big UPS to support the rotor when the power supply stops suddenly. Just after the power supply stope, the motor generates electric power from the rotational energy. The regenerated energy is used to operate the magnetic bearing until the rotor speed slows down. The rotor is touch down to the emergency bearing (ball bearing). This paper is considering two pole IPM motor as a generator for such a sudden power stop. The rotating energy is regenerate the electric power to support the magnetic bearing until the rotor speed slow down.

Keywords: High speed motor, Magnetic bearing, Turbo machinery, Regenerative generation.

1. Developing tested motor

A laboratory model of two pole type IPM motor is developed which is expected to run up to 20,000 rpm. The analytical model is shown in Fig. 1. The motor yoke is made by thin non-oriented electrical steel sheet (15HX1000) with outer diameter of φ100. The detailed rotor is shown in Fig. 2. Inside the rotor six PMs (N32EX) are inserted in two lines to give N-S polarities. The detailed dimensions are determined using the commercial Finite Element Method (FEM) MagNet, as shown in Figs. 1 and 2.

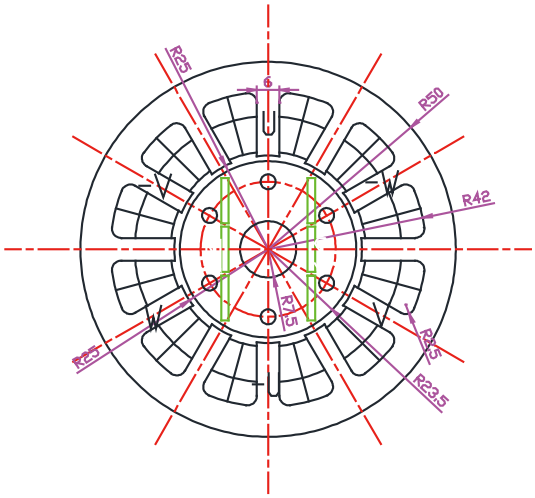

Fig.1. The analytical model of the IPM high speed motor.

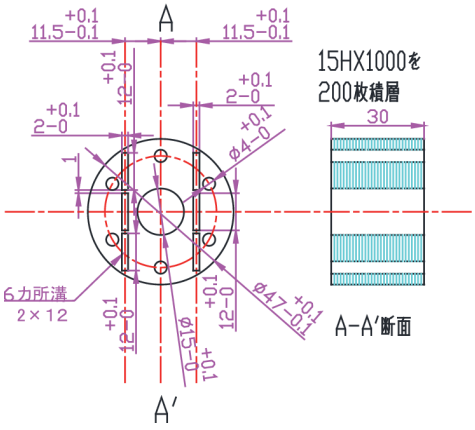

Fig.2. The construction of rotor

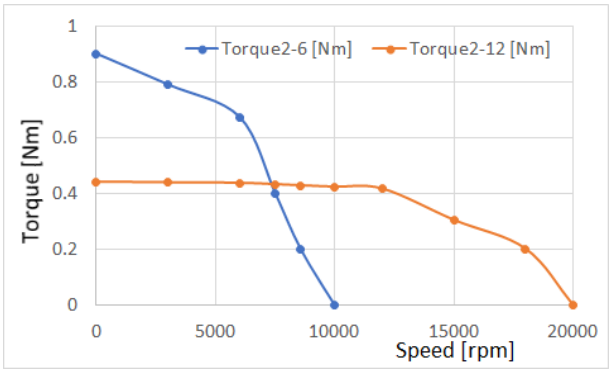

Fig.3. Torque versus speed curves (72 V)

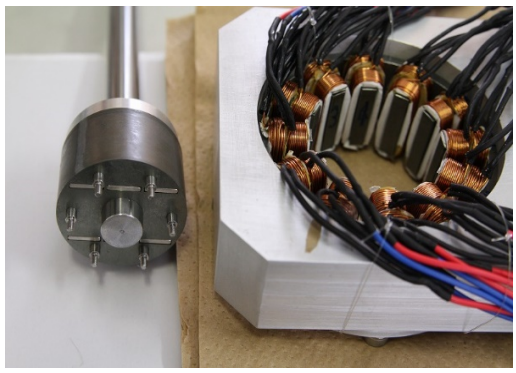

Fig.4. The manufactured rotor and stator

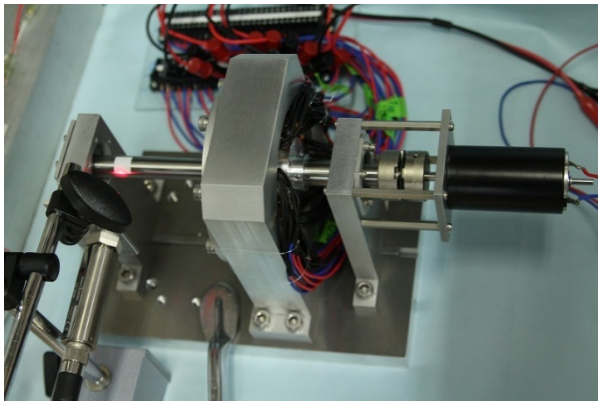

Fig.5. Photo of BEM voltage test

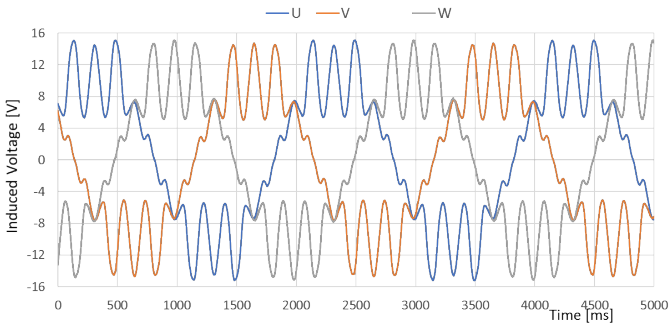

Fig.6. BEM test results of the motor

2. Fabricated motor and back-electro-motive (BEM) voltage test

From the analysis we get the torque and velocity properties shown in Fig. 3. There are two curves with six slot type and 12 slot type ones. The 12 slot type has higher speed property, we developed a 12 slot motor as shown in Fig. 4. The motor is driven by a DC motor and BEM voltage test is carried out as shown in Fig. 5. The three phase BEM voltage is measured at the rotating speed at 3000 rpm, as shown in Fig. 6. There are high frequency ripple, but we can recognize the fundamental frequency component. Further research work is continuing to get high speed rotation.

3. Concluding remarks

The research is just started to develop two pole high speed IPM motor. BEM voltage test is carried out. After we can succeed to get high speed, Active magnetic bearing is installed and the regenerative power is used to support the magnetic bearing until the speed is slow down.

Acknowledgement

The research is supported by Tsugawa motor research foundation. The authors would like to express sincere appreciation.

References

[1] Okada Y., Kitayama F., and Kondo R. Proposal of High Speed IPM Motor for Turbo Machinery, Proceeding of the 27th MAGDA Conference in Katsushika, pp. 74-77, Oct. 20-21, 2018 (in Japanese)

INFLUENCE OF PLASMA BASED ON IMPLANTATION AND DEPOSITION METHOD ON STRUCTURE, INTERNAL STRESS, MECHANICAL PROPERTIES OF NANO-CRYSTALLINE BIOINERT ZRN COATINGS

Anton Taran[1,a], Igor Garkusha[1,b], Valerij Taran[1,c], Renat Muratov[1], Vadym Starikov[2], Alexey Baturin[2], Svetlana Romaniuk[3] and Athanasios G. Mamalis[4,d]

[1]Institute of Plasma Physics of NSC KIPT, Kharkov, Ukraine;
[2]National Technical University "Kharkov Polytechnic Institute", Kharkov, Ukraine;
[3]National Technical University of Agriculture, Kharkov, Ukraine;
[4]Project Centre for Nanotechnology and Advanced Engineering, NCSR "Demokritos", Athens, Greece
[a]avtaran@ukr.net, [b]garkusha@ipp.kharkov.ua, [c]vtaran@kipt.kharkov.ua, [d]a.mamalis@inn.demokritos.gr

Zirconium nitride (ZrN) ceramic with cubic structure attracts considerable attention due to its high wear, fatigue and corrosion resistance properties. ZrN coatings are widely used as hard, refractory and bioinert coating in industry and medicine [1-4].

Plasma based PVD coatings have favorable residual stresses, higher density and better adhesion compared to other techniques. It was shown earlier that the utilization of vacuum-arc evaporation with RF discharge allows applying ZrN coatings onto dielectrics and termoliable instrument at low temperature decreasing the amount of macro-particles emitted from plasma flow [5]. The developed technology allowed producing coatings with hardness variation from 26.6 to 31.5 GPa.

The plasma based ion implantation and deposition method (PBII & D) provides the highest adhesion of all currently known PVD deposition methods. According to this technology, the processed object is immersed in the plasma and an impulse negative potential is applied to it. In this case, the product being processed becomes a part of a certain ion source in a more general sense. Here, the ion acceleration occurs in a dynamic self-organizing boundary layer, which is formed around the target surface under a pulsed negative potential. High adhesion is provided due to the formation of a thin transition layer between the substrate and the tool surface [6]. A significant decrease in the temperature of synthesis of coatings to 100-150°C was also achieved due to this method. The effective control of the compressive stresses in the coating during low-temperature synthesis conditions was also achieved due to ion implantation, even at relatively low energies (0.5-5 keV). The internal stresses were found to depend on the amplitude of the pulses and their repetition rate [7].

The nano-crystalline films of zirconium nitride have been synthesized using PBII&D technique on AISI 430 stainless steel at 150°C. Structure examinations – X-ray diffraction analysis (XRD), scanning electron microscopy (SEM) with microanalysis (EDX), nanoidentation method – were performed to study phase and chemical composition, surface morphology, microstructure and nanohardness of coatings. The stressed state was studied by the X-ray tensometry technique (a-$\sin^2\psi$ method) and its modified variants in application to condensates with a strong axial texture.

For ZrN coating application installation "Bulat-6" has undergone a corresponding modernization. For this purpose, a pulse voltage generator with adjustable pulse amplitude, their duration and repetition frequency was developed. ZrN coatings were applied on the surface of stainless steels 20 × 20 × 2 mm (AISI 430). Chemically pure zirconium (99.999) was used as a cathode material. Nitrogen at a purity of 99.999% was used as an active gas. Typical surface morphology of ZrN coating is shown in Fig.1a, b. The surface of the coating is cellular with so-called "honey-comb" type structure with a cell size of 0.5-2 μm (Fig.1a). A possible reason of cells formation is the non-uniform surface sputtering of a growing coating by ions from a gas-metal plasma accelerated by the negative potential of the substrate during the coating deposition. There is low amount of macro-particles with dimensions of about 0.1-5 μm (Fig.1b). According to EDX microanalysis, the relative content of elements in the coating was 5.36 wt% C, 16.60 wt% N, 2.27wt% O and 75.77wt% Zr.

XRD data revealed (111), (222), and (220) main reflections of ZrN phase with a crystal structure of B1 NaCl cubic lattice type (according to JCPDS 35-0753, a = 0.4577 nm lattice constant).The high intensity of the ZrN (111) Bragg peak, indicates that the ZrN grains grow with the [111] preferred orientation perpendicular to the growth plane.The average grain size in accordance with FWHM comprised 13 nm. According to X-ray tensometry data, the crystallites in the condensate are under the action of compression deformation in the film

plane and the action of compressive stresses in the system is about 1.94 GPa. The level of microdeformation comprises $\varepsilon \approx 4.85 \cdot 10^{-3}$. The maximal value of nanohardness reached 44 GPa with elastic modulus 500 GPa (Fig.2).

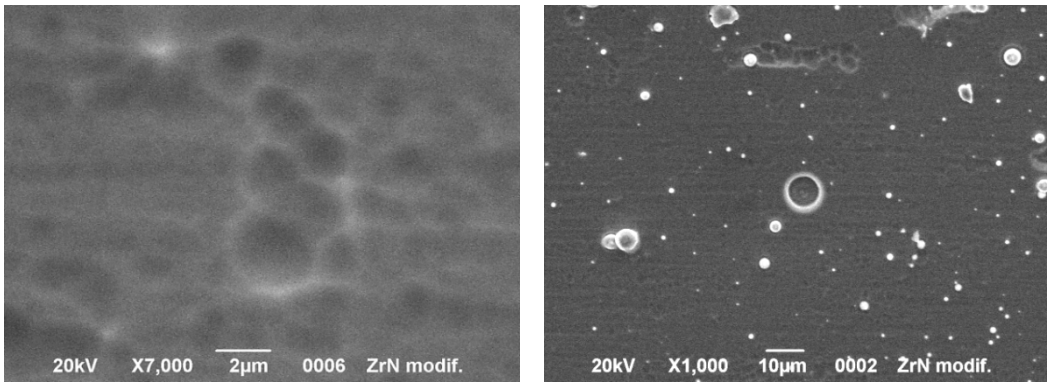

Fig.1. SEM images from ZrN coating on AISI 430 at various magnifications

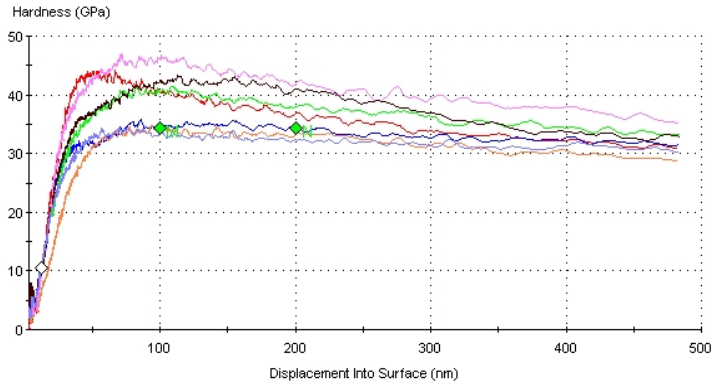

Fig.2. Hardness values in accordance with nanoidentation tests

References

[1] Jianxin D., Jianhua L., Jinlong Zh., Wenlong S., Ming N. "Friction and wear behaviors of the PVD ZrN coated carbide in sliding wear tests and in machining processes" Wear, vol.264,2008, pp. 298-307

[2] Han Cheol Choe, Chae Heon Chung and William Brantley. "Mechanical Surface Behavior of ZrN and TiN Coated Dental Screw by Ion-Plating Method" Key Engineering Materials Vol. 345-346, 2007, pp. 1201-1204

[3] Linkevicius T., Vaitelis J. "The effect of zirconia or titanium as abutment material on soft peri-implant tissues: a systematic review and meta-analysis". Clin Oral Implants Res, vol. 26, 2015, pp.139-147.

[4] Beniaa H. M., Guemmaza M., Schmerberb G., Mosserb A, Parlebas J. C. "Optical properties of nonstoichiometric sputtered zirconium nitride films", Journal of Applied Science, vol. 211, 2003, pp. 146-155.

[5] Taran A., Garkusha I., Taran V., Muratov R., Starikov V., Baturin A., Skoblo T., Romaniuk S., Mamalis A.G. "Structure and properties of nanostructured ZrN coatings obtained by vacuum-arc evaporation using RF discharge" Nanotechnology Perceptions Vol. 14, 2018 (in press).

[6] Pelletier J., Anders A. "Plasma-based ion implantation and deposition": A review of physics, technology and applications//IEEE Transactions on Plasma Science. vol. 33, 2005, No. 6, pp. 1944-1959.

[7] Bilek M.M.M, Moeller D.R., McKenzie W. "Use of low energy and high frequency PBII during thin film deposition to achieve relief of intrinsic stress and microstructural changes". Journal of Surface and Coatings Technology, vol. 186, 2004, pp. 21-28.

NEUTRON SENSORS BASED ON SILICON-GRAPHENE NANOSYSTEMS ENRICHED BY BORON10 ISOTOPE

P. Kervalishvili[1a], R. Turmanidze[1b], T. Berberashvili[1c], L. Chakhvashvili[1d]

[1]*Georgian Technical University, Tbilisi, Georgia*
[a]*kerval@global-erty.net*, [b]*inform@gtu.ge*, [c] *t.berber@mail.com*, [d] *lalichakhvashvili@gmail.com*

Abstract. The aim of the paper is elaboration of precise and fast neutron sensors using B isotopes. The work's objectives include: Development of physical principles of work of 10B isotopes doped semiconductor sensitive nanoelements and basis of their fabrication technology; By using of modern technologies of preparation of Boron isotopes enriched elementary semiconductor - Si based sensory elements development of high-efficient prototypes of nanosensors of the new construction; To study the peculiarities of technology of growth the semiconductor Si thin films doped by 10B isotopes and their properties and investigating the usage of the Graphene FETs (GFET), as instruments to increase the sensitivity of measurement leading due to the importance of the target of ultra-sensitive neutron detection.

1. Introduction

For neutron radiation safety there is need of development of sensory elements and sensory systems for instantaneous responding to variation of nuclear radiation. In order to be useful as a part of Artificial Intelligence systems, the sensors and sensory systems will be designed as a miniature instrument providing information transmission and processing about neutron radiation.

The appearance of new advances in nanotechnology and nanosystems preparation is very important for the development of neutron detectors. The development of new technologies and the corresponding development of the proper microstructure and nanostructure with the required characteristics can be enhanced by the newly appearing nanomaterials.

2. Theoretical and experimental results.

Recognizing this need, we built the next generation of neutron detectors for security requirements. The main proposed novelty of work is related to a Silicon-Graphene ultrasensitive advanced radiation detector, able to detect single neutrons [1-2]. This new family of ionizing radiation sensors is based on the exceptional electronic properties of Graphene.

In a case of Sillicon(Boron10)- Graphene based detector sensitive to thermal and even fast neutrons, a Si(B10) absorber material can be used in order to achieve conversion of neutron to heavy charged particles. Boron which is a shallow acceptor for Silicon changes its charge because of n,α nuclear reaction stimulated by neutron irradiation to Lithium, which is a shallow donor for Silicon. Charge carrier concentration changes (1 neutron reverses 1 charge) are easy to fix by electrical measuring instrument very precisely. These give us opportunity to measure neutron fluence up to neutrons very high density[3,4]. A Graphene nanolayer has to be deposited on the bottom of the Si wafer (Fig.1) to act as amplifier of electron-hole pars born in Si as result of nα nuclear-chemical reaction [5-7]. The added graphene monolayer is trapping the carriers of the B10 isotope doped thin Silicon layer which is following by generation of a "depletion" layer in the Graphene-Silicon layer interface. Graphene also reduces the thermal fluctuations (thermal noise) of the doped Silicon thin layer and whole detector accordingly.

The limits of the ^{10}B isotope content in materials, from which should be made neutron detectors, are too high: (0.1–2.5) $10^{23}/cm^3$. It means that, the neutrons will be rapidly stopped in a10B-enriched material. If we build the model of evaluation the key physical characteristics of the neutron detectors, when E - energy released during a single act of B10 – n interaction, is spent only on the thermal generation of the electron–hole pairs, consequently, the rate of rise in the temperature in process of neutron absorption in material will be $dT/dt=EW/C$. As for the neutron detectors' typical operation time, apparently it can be estimated from the following relation: $\tau = l/v$, where W is the rate of releasing of the nuclear reaction products, C is the heat capacity per unit volume of the irradiated material and v is the neutrons mean velocity.

Research which is performed in the work is unique. It applies to create new sensor elements and devices with high parameters, which is useful for precise neutron radiation measurements. These devices could be unite in electronic and intellectual networks. They will be able to function in harsh environment pollution. Compared to the analogies, these nanosensory elements and sensory devices have high sensitivity and resolution capacity, small dimensions, much smaller power consumption, low voltage and power

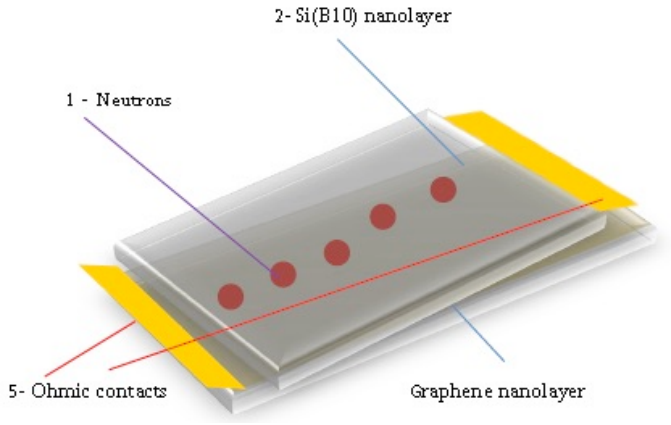

Fig.1. Scheme of Silicon(B10)-Graphene sensitive element of neutron detectors.

Conclusions

Among the main results of the work it is necessary to underline: development and characterization of the Boron nano-sensors; design and optimisation of the Graphene FET sensors; Investigations of parameters of testing of the Silicon –Boron- Graphene FET neutron sensor under different neutron flux conditions.

References

[1] Kervalishvili P, Boron10 isotope doped silicon-graphene nanosensory element for neutron detection, Extended abstract of 11th International conference on Advanced Nanomaterials (ANM 2018), July 18-20, 2018, Aveiro, Portugal.
[2] Kervalishvili P., Labunov V., Hristoforou E., Mostafavi M., Oliveira P., Yannakopoulos P., Boron isotope enriched graphene based neutron sensors International conference, Advanced Materials and Technologies, Ilia Vekua Sokhumi Institute of Physics and Technology (SIPT), Tbilisi, October 21-23, 2015.
[3] Kervalishvili P., Shavelashvili Sh., The Principle of recording neutrons with the AID of Sensitive Boron Elements", Soviet Atomic Energy, vol. 62, no. 5, 1987, pp. 412-414.
[4] Kervalishvili P., Karumidze G., Kalandadze G., Semiconductor Sensor for Neutrons, Sensors & Actuators, A: Physical, v.36, no.1, 1993, p.43-45.
[5] Bykovskii Yu A., Kervalishvili P., Nikolaev I.N., Neutron Fluence Sensor Based on Boron Carbide, Technical Physics Letters, vol. 19, issue 7, 1993, pp. 457-458.
[6] Kervalishvili P.J., Yannakopoulos P.H.. Nuclear Radiation Nanosensors and Nanosensory Systems, NATO Science for Peace and Security Series B: Physics, and Biophysics, Springer, 2016, 200p.
[7] Kervalishvili P., Berberashvili T., Chakhvashvili L. About some novel nanosensors and nanosensory systems, Nanostudies, vol.4, 2011, p.155-164.

THE EFFECT OF MAGNETIC FIELD ON THE DESTRUCTION PETROLEUM EMULSION

N. Mamulaishvili[1,a], G. Partskhaladze[1], G. Chavleshvili[1] , O. Janelidze[1]

[1]*Batumi Shota Rustaveli State Univefsity, Georgia*
[a]nora.mamulaishvili@bsu.edu.ge, [b] gizo.partskhaladze@bsu.edu.ge, [c]gocha.chavleshvili@bsu.edu.ge,
[d]otari.janelidze@bsu.edu.ge

Abstract. One of the main problems of the technology of oil extraction at the Supsa field includes oil emulsions and their demulsification. Emulsions are formed in different areas of the oil well operation: in the process of pumping water into the oil well to maintain reservoir pressure, the emulsion is formed in the bottomhole zone, in oil pipelines, and not in the productive zone. The stability of such an emulsion depends on the content of its own emulators in the reservoir oil: naphthenes, SAS-es, paraffin, resins. The greater the salinity of the formation water, the more stable the emulsion. The emergence of stable emulsions is associated with the turbulent movement of air and liquid. Therefore, the extracted petroleum needs to be pretreated to a state of production for further transportation and processing.

The article shows the effectiveness of the influence of the magnetic field on the process of destruction of the oil emulsion, which forms in the extraction of oil from the Supsa field. The results of the process of the demulsification of crude oil under the influence of a magnetic field with low and high frequencies (Hertz) and in the presence of the demulsifier Alkan De 202 are presented.

1.Introduction

The destruction of water-oil emulsions is successfully carried out by thermochemical method. To improve the efficiency of the demulsifier, especially for highly viscous and high-strength oil-water emulsions, various methods are used, among which the application of a magnetic field has a significant effect.[1].

In the modern period, demulsifiers of foreign origin are widely used. A: Most demulsifiers are very expensive and on average cost 1 ton. $ 3500. ALKAN DE 202 was chosen as a demulsifier [2].

Previously, we carried out work in the direction of oil-water demulsification using a demulsifier based on non-ionic SAS solution, which has the ability to reduce surface tension at the oil-water interface. [3]. [4] [5].

In order to reduce the dosage of the demulsifier and reduce the residence time of the oil-water emulsion in the settling apparatuses, the separation of aggregate-resistant water-oil emulsions under the influence of a magnetic field has been studied.

2. Experimental procedure and sample preparation

The experiments were carried out in the educational laboratory of the technological faculty of Batumi State University Shota Rustaveli. Initially, we prepared a petroleum emulsion (233 ml of petroleum was added 100-200 ml of distilled water). When mixing, the mixture was blended with a mixer for 5-7 minutes. As a result, a homogeneous emulsion was produced without any segregations. The experiments were carried out separately by the method**.**

Method 1. The method involved carrying out a demulsification process using magnetic solenoid, which was omitted in the test sample. The solenoid core was made of Ferrite, 140 mm long. diameter of 8mm. Top wrapped with copper conductor. A low-frequency current in the range of 20–50 hertzs was passed through a solenoid in the samples under study and observed during the process of water separation. see figure 1.

Samples were prepared in graduated cylinders of 100-250 ml each. Then we injected certain amounts of the demulsifier into each sample (0.5-1.0 ml). at T = 20-22ºC. Then, a low-frequency current of 20-40 hertz was suppressed and observed during the demulsification process. As a result, two separate phases were formed: the upper phase of petroleum and the lower phase of water.

Fig.1. processing of petroleum emulsion method 1

Fig. 2. processing of petroleum emulsion method 2

Method 2. This method involves processing samples at higher magnetic field frequencies. Graduated cylinders with the test solution were placed in a coil and a voltage of 150-180 volts was applied. The frequency of the magnetic field varied from 20 to 80 hertz. fig. 2. The amount of released water and the coefficient, the degree of demulsification were determined.

Conclusions

The results obtained when testing both methods revealed that the process of de-emulsification of the oil emulsion effectively takes place at the initial stage of the process within 30-40 minutes, at a magnetic field frequency of 30 Hertz. A further increase in the volume of allocated water was not observed.

It is shown that the low-frequency magnetic field significantly increases the rate of separation of the water-oil emulsion in the presence of a demulsifier, Alkan DE 202.

References

[1] Shaikhulov A.M., Bojchuk A. A., Dokichev V. A., Svirsky S. E., Singizova V. H., Kresteleva I. V., Telin A. G. Magnetik field effect on demulsificationof water –in-oil emulsion of Kiengorskoe field a4 formation.ж. Нефтегазовое дело. 2014, т. 12, № 1

[2] "Alkan202" https://elibrary.ru/item.asp?id=15229926

[3] Mamulaishvili N., Salimova N., Khitarishviliand T., Partskhaladze G.Regulation of filtration and reservoir features of oil stratum rock with use of compositesolutions of SAS. J.Pet Environ Biotechnol 2018, Volume 9 DOI:10.4172/2157-7463-C1-041; 3rd World Congress onPetroleum Engineering and Natural Gas Recovery. July 20-21, 2018. Sydney, Australia.

[4] Mamulaishvili N., Partskhaladze G., Chavleshvili G., Zoidze R.. International Journal of Engineering Innovation & Research. Volume 6, Issue 6, ISSN: (2277– 5668); Supsa Crude Oil Demulsification Technology Development by Usingnon-ionogenic Surfactant Solution.2017.

[5] Mamulaishvili N.D., Salimova N.A., Khitarishvili T.D., Baladze D.A. Effect of various classes SAS on hydrophobic surface of oil stratum.The "International journal of Appled and fundamental research'' №2, 15-21.11.2014 Munch. Germany; http://www.science-sd.com/457-24744

POLYVALENT IRON OXIDE MAGNETIC NANOPOWDERS SYNTHESIZED BY ELECTROEROSION DISPERSION FOR MICROWAVE ABSORBING COATINGS

T. Prikhna[1,a], M. Monastyrov[1,2,b], A. G. Mamalis[3,c], B. Halbedel[4,d], S. S. Ponomaryov[5,e], V. Moshchil[1,f], O. Prysiazhna[1,g]

[1]*Bakul Institute for Superhard Materials of the National Academy of Sciences of Ukraine (NASU), 2, Avtozavodskaya Str., Kiev 07074, Ukraine.*

[2] *Institute of Ecology and Alternative Energetic of the Open International University of Human Development "Ukraine", 23 Lvivs'ka Str., 04071 Kiev, Ukraine*

[3]*Project Center for Nanotechnology and Advanced Engineering, NCSR "Demokritos", Greece*

[4] *Department of Inorganic-Nonmetallic Materials, Institute for Material Engineering, Technische Universität Ilmenau, POB 10 05 65, D-98684 Ilmenau, Germany*

[5]*Institute of Semiconductor Physics of the National Academy of Sciences of Ukraine (NASU), 41, Nauky Ave., Kyiv 03028, Ukraine*

[a]prikhna@ukr.net.ua, [b]mmonastyrov@gmail.com, [c]mamalis@central.demokritos.gr , [d]bernd.halbedel@tu-ilmenau.de
[e]s.s.ponomaryov@gmail.com, [f]vik_ism@ukr.net, [g]orgenic.pris@gmail.com

Abstract. The method for simple preparation of polyvalent magnetic iron oxide nanopowders by electroerosion dispersion (EED) of carbon steel in water will be presented. The developed low cost masking coatings based on corrosion resistant polyurethane and acrylic-urethane priming, varnishes and paints of Ukrainian manufacture (InterGasSinthez) with the addition of EED nanopowders of polyvalent iron oxides, carbon, omega spheres (based on silica and alumina), basalt fibers demonstrated high absorption abilities (90-99%) of microwaves in the wide range of frequencies (10-70 GHz, wavelength 0,03-0,0043 m) and close to zero reflection of the microwaves (-10 Db - - 23 Db or 10% -0.5%).

1. Introduction

Magnetic nanoparticles (MNP) have attracted considerable interest in many fields of research and applied science due to their impressive properties. In the past, especially biomedical problems have promoted the development of MNPs. For technical applications e.g. wastewater treatment and absorption of electromagnetic waves, the existing synthesis approaches are too expensive and/or the producible quantities are too low. Modern applications with high-frequency electromagnetic fields (satellite-TV, mobile funk, WLAN technologies, radar for traffic and aerial supervision, microwave heating, drying, sintering, up to automotive and medical applications) require such low-cost absorbing materials in order to reduce the electromagnetic radiation exposure on biological systems or assure the safe operation of instruments and equipment as well as for their security (prevention of wireless signal leakages) or facilitate modern communication applications. We describe the synthesis method, the laboratory installation and discuss the structural, chemical and electromagnetic properties of the synthetized EED powders as well as their applicability for microwave absorption compared to other available ferrite powders. The electromagnetic properties of the EED powder allow microwave absorption values like that of hexaferrite powders and values considerably larger than that of the commercially available iron oxide powder Magsilica®. However, the production of the EED powder is much simpler [1].

2. Experimental procedure and sample preparation

The method of electroerosive dispersion (EED) is a physical process of instanta-neous evaporation-condensation of a metal in a liquid medium. The stoichiometry of the obtained powders depends on the quality of the raw materials (chips, cuttings, granules, etc.) and the working liquid medium, as well as the stoichiometry of the electrode material. Varying the above factors and controlling the parameters of electrical discharges (voltage, frequency of discharges, and shape of pulses) determine the powder quality: composition, size of grains (from several nanometers up to several microns), their shape (spherical or with a highly developed surface), phase state (amorphous, glassy, and crystalline). Changing the type and/ or the composition of the working liquid medium (water, spirit, kerosene) with suitable additions provides the possibility to synthesize pure metals, oxides, carbides or nitrides. In the present study, the iron chips and electrodes from structural grade carbon steels, e.g. St3 (composition see in data sheets DSTU 2651-94/ GOST 380-94, A568M/ ASTM or in 1.0116/ DIN EN 10025) were used for preparation of polyvalent ron oxides. The shape of the electrodes practically does not affect the EED process. The shape of the electrodes is determined by the shape of the reactor and can be cylindrical, trapezoidal, rectangular parallelepipeds, segments of the

discs etc. The quality of water is determined by the requirement for cleanliness of the obtained powders. In this study tap water was used.

To prepare the coatings we used polyurethane and acrylic-urethane priming, varnishes and paints of Ukrainian manufacture (InterGasSinthez). We mixed the polymer media with the EED nanopowders of polyvalent iron oxides, carbon, omega spheres (based on silica and alumina), basalt fibers in different proportions and then painted surfaces of the objects several times (using mixtures with different concentrations of the ingredients).

Results and conclusions

As a result the new cheap corrosion resistant coatings based on polyurethane and acrylic-urethane with nanopowders of polyvalent iron oxides (contained FeO, Fe_3O_4 and some Fe), carbon, omega spheres, basalt fibers have been developed. The thick coatings demonstrated high absorption abilities (90-99%) of microwaves in the wide range of frequencies (10-70 GHz, wavelength 0,03-0,0043 m) and close to zero their reflection (-10 Db - - 23 Db or 10% -0.5%). Polymeric bases of the developed coatings are used to protect against corrosion of metal structures in all macroclimatic areas, in sea and fresh water, in saline solutions, in oil and oil products, resistant to ultraviolet radiation, aggressive media. They demonstrate high mechanical performance (adhesion, strength, elasticity) and long service life. The coatings can be used for painting of ships, deck structures, containers, building constructions and buildings, auto and railway transports, parts and mechanisms, etc. The results of structural study using SEM with microprobe analysis of the coatings of different thicknesses and their absorbtion characteristics (estimated transparency and reflectivity in the special anechoic chambers) will be presented and discussed. The iron oxide powder density 5.175 g/cm^3, the average particle size is 20-50 nm. With the help of cerimetry or cerimetric titration it was found that the Fe^{2+} content in the powder was 53.83 ± 1.23% by weight. Prime cost of the powder is about 20 USD/kg (in fact the price of the used electricity), productivity of one EED installation which can be located on the area of 7 m^2 is 1 ton per month. The selling price of analogue is 400-500 USD/kg and the delivery is no more than 50 kg per month. Specific gravity of the developed coating is 1 g/cm^3, the weight of 1 m^2 of the coating with the maximal absorbtion ability in 10-70 GHz range is 9 kg and its prime cost is about 50-70 USD.

Reference

[1] Halbedel B., Prikhna T., Quiroz P., Schawohl J., Kups T., Monastyrov M. Iron oxide nanopowder synthesized by electroerosion dispersion (EED) – Properties and potential for microwave applications; *Current Applied Physics*, 2018, **18**, 1410-1414

CLUSTERS – PARTICLES BALANCE IN MATTER BY DYNAMIC FRACTALS

A. Bakhtiari[1a], T. Berberashvili[1b] P. Kervalishvili[1c]

[1]*Georgian Technical University, Tbilisi, Georgia*
[a]bakhtiari.habib@gmail.com, [b]t.berber@mail.com, [c]kerval@global-erty.net

Abstract. The aim of the paper is development of dynamic fractal concept which provides the possibility of study and elaboration of model of substances with small scale structures.

1. Introduction

Atoms and molecules as smallest blocks of the matter represents physical and chemical properties and then difference between materials, but not enough to explain all of their characters(fig.1). Matter structure also shows some properties like Ductility, Strength, Work Function and so on. Therefore, study more structure, more capabilities by aspects and applications.

Fig.1. Liquid water and Ice structure

Solid state studies structure as Crystallization via stationary approach that disregards time effect on lattice to investigate it as stable structure [1]. However, Nano particle motion average conducts lattice study to stationary network, but particles motion is certainty [2].

On the other hand, there are two other well-known states as liquid and gas what represent semi approach but exaggerated what shows more time effect on position changing [3].

Meanwhile, random motion of molecules in liquid or gas and their collision also, is conducted to chaotic or non-regular motion that rise contradiction with lattice and its balance, because according to thermodynamics, entropy and then temperature rising is expected [4].

2. Results and Discussion

As well as, attempts to explain molecular motion in classical mechanics was unsuccessful that represents its disability and then contradictions go to Non-linear system (not Chaos) what observes balance concept but needs new approach to describe.

Generally, any approach represents particles momentum and Balance; what full feed by symmetric particle distribution in stationary approach, via dimensions investigation as space and time. New approach observes all of the concepts as rules, but in Non-linear system and then new mathematical approach is inevitable.

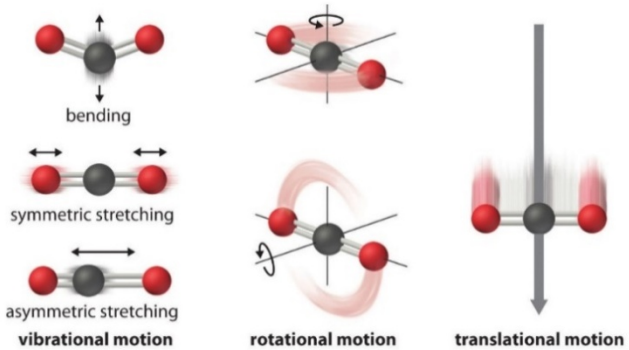

Fig.2. Nano Particle momentum possibilities

Up to now, particles are focused, but new approach consider space as clusters for particles motion as a serious part of momentum conversion study that goes to Balance target. Then, clusters as fractals (not fragment) in dynamic fractal concept defines Non-linear system reason at Nano scale (fig.2).

Also Balance seeking express unbalancing inside normally, what not only needs reason study but also finding a dynamic execution strategy that support all the above. In words, variable-function classic approach; $f(x) = y$, could not be acceptable and conducts study to Self-Control Closed Loop what describes momentum conversion repeatedly based on quantitated time to find dynamic Balance in Nano scale (fig.3).

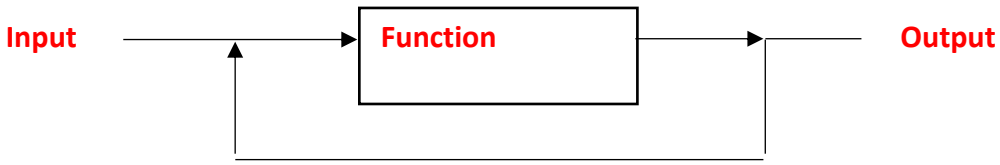

Fig.3. Self-Control Closed Loop

Conclusions

Therefore, Dynamic fractal concept not only provides more study of Nano Scale nature and then reasons explanation through rules observing, but also provides new way to find new and improved Nano Structure in many aspects as Energy, Semiconductors industries and so on.

References

[1] Kervalishvili P. On the growth mechanism of small particles of elemental boron. Solid State Physics (USSR), Vol. 29, No.-4, 1987
[2] Bakhtiari A., Berberashvili T., Kervalishvili P., Tseles D., Yannakopoulos P. Matter-Particle Approach Nanosystems Formation, e-RA 13 International scientific conference, University of west Attica, Greece, 2018
[3] Eisenberg D., Kauzmann W. The structure and properties of water, Oxford university press, First edition 1969, page 152
[4] Halliday, Resnick, Walker. Fundamentals of Physics. 8th edition. India: Winsome Books India, 2008.

PROSUMER COMMUNITIES PILOTING SMART CITIES DEVELOPMENT: THE CASE OF THE FIRST NEAR-ZERO ENERGY SMART HOME OF GREECE

Nikolaos T. Athanassoulis[1,a], Aggelos Tsakanikas[1,b], Dimitrios Tzovaras[2,c]

[1]Laboratory of Industrial and Energy Economics, Department of Chemical Engineering, National Technical University of Athens, Greece.
[2]Information Technologies Institute, CERTH, Center for Research and Technology Hellas, Thessaloniki, Greece.
[a] nathanas@central.ntua.gr ,[b]atsaka@central.ntua.gr, [c]Dimitrios.Tzovaras@iti.gr

Keywords: Prosumer; Sustainability; Smart Cities; Smart Home; nZEB; Energy Transition; Energy Storage

1. Introduction - Concept of Smart Homes / Smart Cities

Urban areas are responsible for the vast majority of the global GHGs, due to increased energy requirements, while trends towards urbanization are strengthened over time. The concept of smart citiesprovides new opportunities for the energy sector, where the energy efficiency and savings, as well as RESs further penetration in cities, can be significantly benefited from new technologies and approaches.Synergies achieved by multiple small-scale prosumers in microgrids, the induction of supportive legislations for energy communities, the trend of deregulation of energy markets, the emerging smart grid and ICT technologies, along with the trend of electrification of transportation systems and the upcoming generalized introduction of electric vehicles (EVs) in cities, are promising factors towards self-powered zero-emission smart cities [1, 2].

For the widespread of distributed renewable energy production in smart cities, in order to meet their environmental and energy objectives,the promotion of the small-scale so-called prosumers (residential/commercial) is crucial, i.e. an active concept of the classic passive consumer, who can also produces his own energy, see Fig. 1(a). EU is doing serious efforts towards this direction by promoting the liberalization of energy markets with the new "target-model" approach, as well as, the creation of energy communities/cooperatives and the improvement of buildings' energy performancetowards nearly zero-energy buildings. [2]. The near-Zero Energy Smart Home of CERTH/ITI, located in Thessaloniki, is the first house in Greece that combines enhanced construction materials and intelligent ICT solutions creating a future-proof, sustainable and active testing, validating and evaluating environment, see Fig. 1(b). In this paper, a techno-economic analysis of the CERTH/ITI nZEBis presented and discussed.

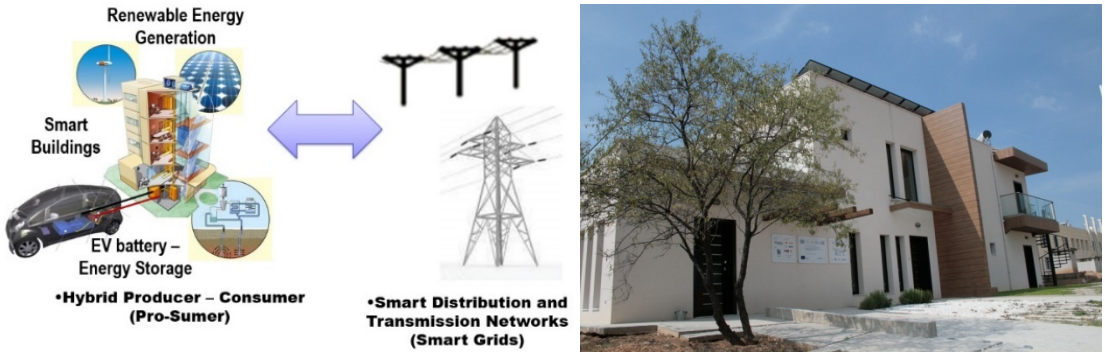

(a) (b)

Fig.1. (a) Concept of prosumer; (b) The first nZEB Smart Home in Greece

2. Techno-Economical Aspects

A commonly agreed energy calculation methodology and a consistent definition for ZEB concepts, is crucial before being fully implemented in the national building codes and international standards. A ZEB definition is mainly related with the following criteria:

(i) metric of the balance; (ii) balancing period; (iii) type of energy use included in the balance; (iv) type of energy balance; (v) accepted renewable energy supply options; (vi) connection to the energy infrastructure; (vii) requirements for the energy efficiency, the indoor climate and in case of gird connected ZEB for the building–grid interaction [3].

In this study the main technical parameters, as well as the energy and environmental performance of the nZEB of CERTH/ITI, are presented and discussed. ThenZEBs current economic attractiveness is examined, by calculating the NPV of different nZEB scenarios in comparison with the NPV of buildings that comply with current regulations in Greece.A construction analysis for thisspecific reference scenariois implemented and the influence on the E-level (a dimensionless unit which expresses the allowed primary energy use for a building)iscalculated. Furthermore, the NPV and the discounted payback period for all the nZEB scenarios, where sustainability prevails, are thoroughly examined.

Concluding remarks

The building sector is responsible for the vast majority of the total GHG emissions that cities produce. The challenge, which is now pressing, is to eliminate the energy-consumption building target to zero. In this direction, the energy efficiency and the rise of prosumers are expected to play a major role and, in that respect, EUs EPBD directive 2010/31/EU aims to increase nZEBs penetration in all state members including Greece. From our performed analysis it may be indicated that,investing in a nZEBin Greece is economically attractive and profitable, since multiple scenarios for all nZEB types proved to have a positive NPV.

References

[1] Papaioannou, D., Gakis, A., Athanassoulis, N.T., Rigos, A., Mamali, A.A., A review of urban sustainability criteria under global warming stress. Interdisciplinary Environmental Review, 2015. 16(1): p. 17-45.

[2] Athanassoulis, N.T., Tsakanikas, A., Kladas, A.G., Smart cities under electric energy trends: From autonomous building directive to prosumer target. Proc. SIPS 2018 Mamalis International Symposium on Advanced Manufacturing of Advanced Materials and Structures with Sustainable Industrial Applications; 2018 Sustainable Industrial Processing Summit and Exhibition, Rio de Janeiro, Brazil, November 2018.

[3] Marszal AJ, Hesiselberg P, Bourrelle JS, Musall E, Voss K, Sartori I, et al. Zero energy building - a review of definitions and calculation methodologies. Energy Build 2011; 43(4):971-979.

STATISTICAL ANALYSIS OF THE GLOBAL COMPETITIVENESS INDEX (GCI) OF GEORGIA

Raul Turmanidze[1,a], Predrag Dašić[2,3,b], Giorgi Popkhadze[1]

[1] Georgian Technical University (GTU), Tbilisi, GEORGIA, E-mail:
[2] SaTCIP Publisher Ltd., 36210 Vrnjačka Banja, SERBIA
[3] High Technical Mechanical School of Professional Studies, 37240 Trstenik, SERBIA,
inform@gtu.ge, dasicp58@gmail.com

Republic of Georgia is a Eurasia country in the Caucasus region, which consists of 7 regional territories, which unify 60 district and city centers. It borders with Russia in the north and northeast, Turkey and Armenia in the south and Azerbaijan in the southeast. In the west, it reaches the Black Sea shores of about 310 km. Georgia occupies an area of 69.700 km² with slightly less than 5 million people (according to estimates for 2018). The country's main and largest city is Tbilisi, with over a million people. Major cities in Georgia are: Kutaiszi, Batumi, Rusztavi, with over a 100 thousand people and etc.

Gross national income (GNI) of Georgia is 7.1 billion US$ and 37.64 billion PPP US$ and revenue per capita is 1350 US$. Georgia's exports are over 350 billion US$, and imports are more than 650 billion US$ for 2018.

Georgia is a member of the following international organizations: Council of Europe, Organization for Security and Co-operation in Europe (OSCE), EUROCONTROL, World Trade Organization (WTO), GUAM (Georgia, Ukraine, Azerbaijan and Moldova) Organization for Democracy and Economic Development, and is also a signatory to the NATO Partnership for Peace program and etc.

In the paper is given statistical and trend analysis of Georgia's global competitiveness index (GCI) for period 2004-2018.

Data on values of GCI of Georgia has been retrieved from Global Competitiveness Report (GCR) for period 2004-2018 [1], with a certain calculations from the part of the authors. The GCR with the data for each year for the countries of the world is issued by the World Economic Forum (WEF). The WEF coordinator for Georgia is BIRG (Business Initiative for Reforms in Georgia).

For the trend analysis, we used the following parameters: annual growth rate (AGR) and cumulative growth index (CGI). On Table 1 are given GCI data of Georgia for the period 2004-2018 and trend analysis for GCI with AGR is shown on Figure 1.

Table 1. Data of Global Competitiveness Index (GCI) for Georgia for the period 2004-2018

Year	Score	Rank	Position [%]	Q	AG	CI	AGR	CGI
2004	3.14	94/104	90.38	Q4	-	-	-	100.00
2005	3.25	86/117	73.50	Q3	0.11	103.50	3.50	103.50
2006	3.73	85/125	68.00	Q3	0.48	114.77	14.77	118.79
2007	3.83	90/131	68.70	Q3	0.10	102.68	2.68	121.97
2008	3.86	90/134	67.16	Q3	0.03	100.78	0.78	122.93
2009	3.81	90/133	67.67	Q3	-0.05	98.70	-1.30	121.34
2010	3.86	93/139	66.91	Q3	0.05	101.31	1.31	122.93
2011	3.95	88/142	61.97	Q3	0.09	102.33	2.33	125.80
2012	4.07	77/144	53.47	Q3	0.12	103.04	3.04	129.62
2013	4.15	72/148	48.65	Q2	0.08	101.97	1.97	132.17
2014	4.22	69/144	47.92	Q2	0.07	101.69	1.69	134.39
2015	4.22	66/140	47.14	Q2	0.00	100.00	0.00	134.39
2016	4.32	59/138	42.75	Q2	0.10	102.37	2.37	137.58
2017	4.28	67/137	48.91	Q2	-0.04	99.07	-0.93	136.31
2018	60.90	66/140	47.14	Q2				

Note: Quartile (Q), Annual Growth (AG), Chain Index (CI), Annual Growth Rate (AGR), Cumulative Growth Index (CGI).

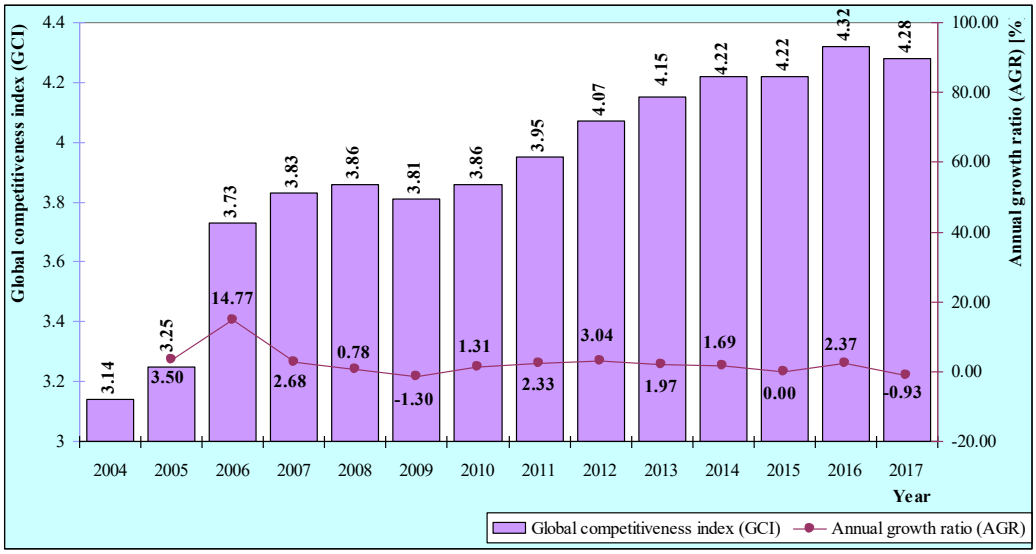

Fig. 1. Trend analysis for Global Competitiveness Index (GCI) with Annual Growth Rate (AGR)

Global Competitiveness Index (GCI) data for Georgia for the period 2004-2017 changed in intervals from 3.14 to 4.32. Maximum value was in 2016 and minimum in 2004 year. Highest growth of Annual Growth Rate (AGR) was by 14.77 in 2006 year, while the highest fall was by -1.30 in 2009.

Statistical descriptions parameters of Global Competitiveness Index (GCI) of Georgia for period 2004-2017 is given in Table 2.

Table 2. Descriptive statistics of the Global Competitiveness Index (GCI) of Georgia for period 2004-2017

Measures	Sign	CGI
Sample size	N	14
Minimum	Min	3.14
Maximum	Max	4.32
Range	Rx	1.18
Total	Sum	54.69
Mean	Aver	3.9064
Geometric mean	GM	3.8902
Harmonic mean	HM	3.8729
Median	Med	3.9050
Std. deviation	SD	0.3578
Variance	Var	0.1280
Coef. of variation	CV	9.1588
Skewness	Sk	-1.0516
Kurtosis	Ku	0.6709

References

[1] Schwab K., Sala-i-Martín X., Samans R., Blanke J., and etc. (editors): *The Global Competitiveness Report 2016-2017*. Geneva (Switzerland): World Economic Forum (WEF), 2016. – 382 pp. ISBN 978-1-944835-04-0.

[2] Dašić P. Statistical analysis and modeling of global competitiveness index (GCI) of Serbia. *Journal of Research and Development in Mechanical Industry*, Vol. 9, Issue 3 (2017). ISSN 1821-3103.

DYNAMIC SUSPENSION CHARACTERISTICS OF A COMPACT DOUBLE STATOR AXIAL GAP MOTOR WITH FULL MAGNETIC LEVITATION DURING ROTARY BLOOD PUMP OPERATION

M. Osa[1,a], T. Masuzawa[1,b], E. Tatsumi[2,c]

[1] *Ibaraki University, Japan*

[2] *National Cerebral and Cardiovascular Center Research Institute, Japan*

[a]masahiro.osa.630@vc.ibaraki.ac.jp , [b]toru.masuzawa.5250@vc.ibaraki.ac.jp , [c]tatsumi@ncvc.go.jp

Abstract. Compact magnetically suspended motors have been demanded to achieve miniature pediatric VAD which has long life expectancy and better hemocompatibility. An ultra-compact 5-degrees of freedom controlled self-bearing motor has been developed in this study. The motor consists of two identical motor stators and a levitated impeller sandwiched by both stators, and is driven as 6-slot and 4-pole synchronous permanent magnet motor. This paper investigated impeller suspension characteristics during centrifugal pump operation with closed circulation loop. The developed maglev pediatric VAD can produce enough flow rate to provide circulatory support for pediatric heart disease patients. The motor can completely levitate the impeller and sufficiently suppress the impeller vibration, that is indicating well suspension performance.

1. Introduction

Impeller suspension is one of the most significant components to achieve long life expectancy and better blood compatibility in rotary ventricular assist devices (VADs) development. There has been increasing research interest in magnetic suspension technology for next generation VADs, and magnetically levitated motors are being employed in several clinically available VADs for adult heart failure patients [1]. Currently, pediatric VADs which have durability and blood compatibility are strongly demanded [2]. However compact magnetically levitated VAD for use in pediatric patients are still not available due to difficulty of device miniaturization maintaining sufficient suspension performance and higher torque production. In this research, an ultra-compact 5-degrees of freedom (5-DOF) controlled axial gap self-bearing motor which has diameter of 22 mm and total height of 33 mm has been developed for pediatric VADs [3]. Magnetic circuit design and static suspension performance evaluation of the developed motor has been previously presented [4]. This paper investigated dynamic suspension characteristics during centrifugal blood pump operation.

2. Materials and Methods

The developed 5-DOF controlled self-bearing motor has two identical motor stators to suspend a levitated centrifugal impeller axially (Fig. 1). The motor is driven as synchronous permanent magnet motor. The double stator mechanism makes rotating torque double and can achieve 5-DOF control of levitated impeller postures. The levitated impeller has axially magnetized 4-pole neodymium permanent magnets on both surfaces. Thickness of the permanent magnet is 0.8 mm. The stator core made of soft magnetic iron (SUY-1) has 6-slot structure and concentrated windings for magnetic suspension and rotation are integrated and wound on each stator tooth. Turn numbers of control windings are 105. Magnetic gap between rotor and stator surfaces is 1.3 mm.

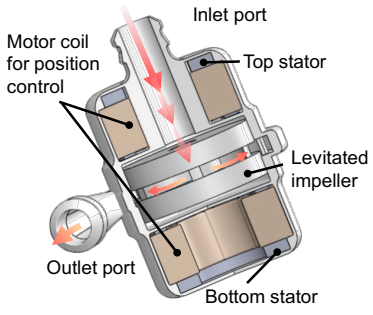

Fig.1. Schematic of the 5-DOF controlled self-bearing motor for pediatric VAD

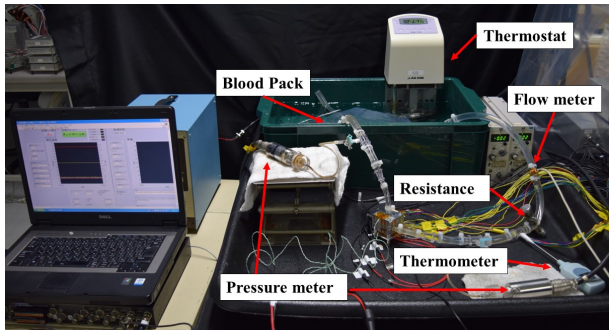

Fig.2. Closed circulation loop system for pump characteristics and suspension performance evaluation.

The developed motor was combined with centrifugal blood pump to evaluate dynamic impeller suspension characteristics during pump operation by using closed circulation loop as shown in Fig.2. 40wt % glycerol water solution at temperature of 37℃ was used as working fluid to mimic viscosity of blood. The centrifugal impeller was levitated with 3-DOF control (z, θ_x and θ_y) as a first step. HQ curve over a rotating speed range from 3500 rpm to 5500 rpm was evaluated. Axial oscillation amplitude and inclination angle around x and y axes were then evaluated. The axial oscillation amplitude was calculated as half of peak to peak value of impeller displacement.

3. Experimental Results

Pump performance and magnetic suspension performance are shown in Fig. 3. The developed maglev centrifugal pump can regulate the flow rate from 0.5-2.5 L/min with a head pressure of 100 mmHg at rotating speeds of 3500-5500 rpm as shown in Fig.3 (a). The achieved HQ curves indicate that the developed pump can applicable to 1-6 years old patients growing up. The levitated impeller was fully suspended with 3-DOF control over every rotating speed. The axial oscillation amplitude and the inclination angle were less than 0.03 m and 0.3 degrees, as shown in Fig 3 (b) and (c). The vibration of the levitated impeller was sufficiently suppressed with magnetic suspension force. As a next step the levitated impeller will be suspended with 5-DOF control and radial suspension performance will be evaluated. In addition to above, the frequency response evaluation of magnetic suspension system will also be carried out.

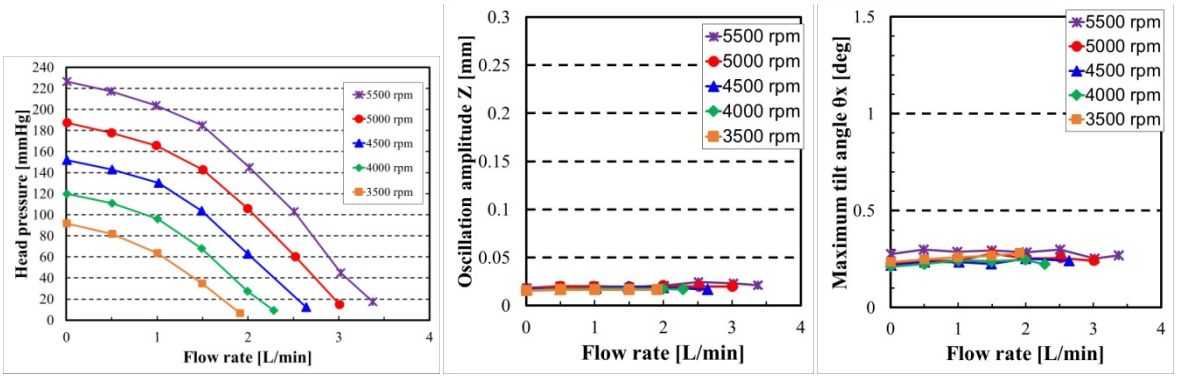

(a) (b) (c)

Fig. 3 HQ characteristics of centrifugal blood pump and dynamic impeller suspension performance of double stator maglev motor: (a) HQ curves with different rotating speeds, (b) maximum axial oscillation amplitude and (c) maximum inclination angle around x axis.

Conclusions

The miniaturized 5-DOF controlled self-bearing motor has been developed for pediatric VAD which has higher durability and better blood compatibility. The pump performance and dynamic impeller suspension characteristics during pump operation were evaluated with closed loop circulation circuit. The levitated impeller was completely levitated up to the rotating speed of 5500 rpm. The developed pediatric VAD achieved flow demand (0.5-2.5 L/min) for pediatric circulatory support, and indicated sufficient potential of stable magnetic suspension in VAD operation.

References

[1] Baldwin J.T., Borovetz H.S., Duncan B.W., Gartner M.J., Jarvik R.K., Weiss W.J., Hoke T.R. Weiss and Tracey R. Hoke, The National Heart, Lung, and Blood Institute Pediatric Circulatory Support, *Circulation,* 2006, 113, 147–155.

[2] Mehra M.R., Naka Y., Uriel N., Goldstein D.J., Cleveland Jr, J.C., Colombo P.C., Walsh M.N., Milano C.A., Patel, C.B., Jorde U.P., et al. A Fully Magnetically Levitated Circulatory Pump for Advanced Heart Failure. *N. Engl. J. Med.* 2017, 376, 440–450.

[3] Osa M., Masuzawa T., Saito T., Tatsumi E. Miniaturizing 5-DOF fully controlled axial gap maglev motor for pediatric ventricular assist devices. *Int. J. Appl. Electromagnet Mech.* 2016, 52, 191–198.

[4] Osa M., Masuzawa T., Orihara R., Tatsumi E. Characterizing A Compact 5-DOF controlled Self-Bearing Motor with Modified Magnetic Circuit to Improve Suspension Performance for Pediatric VAD. *J. Appl. Electromagnet Mech.* 2019, now printing.

GENETIC ANALYSIS OF STUDY DIAGNOSE MUTATIONS IN A GENE BRAF, NRAS, KRASAND RET GENE INTHYROID CANCER PATIENTS OF GEORGIA BY MATLABENVIRONMENT

Sahar Abd Elmogheth Madani[1,a], Irine Gotsiridze[1,b]

[1]*Faculty of Informatics and Control Systems,Biomedical Engineering,Georgian technical university, Georgia.*

[a]*a_sahar24@yahoo.com*, [b]*irgocci@gmail.com*

Abstract.

Objectives: Treatment decision-making in thyroidcancer is often guided by tumor tissue molecular analysis. The aim of this study is Study diagnose mutations in a gene BRAF, NRAS, KRAS in thyroid cancer patients of Georgia with determination of the frequency of these mutations in the populations and analyze it by matlab environment.

Setting: Diagnostic molecular laboratory located in Tbilisi, Georgia.

Participants: 135 patients with thyroid cancer participated in the study.

Primary outcome measures: the study on 150 samples divided into 135patients with thyroid cancer and represented the group of patients (Patients Group) and 15 blood samples from healthy people was set control (Control Group) extracted DNA for samples and detect two Mutations BRAF_475_mu and BRAF_476_mu for BRAF gene three Mutations HRAS_483_mu HRAS_486_mu and HRAS_499_mu to HRAS gene and five Mutations NRAS_580_mu, NRAS_584_mu, NRAS_573_MU, NRAS_562_mu and NRAS_564_mu to NRAS gene by using the TaqMan™ Mutation Detection Assays.

Results:

There are Mutation in 42 patients condition limitations are as follows (c.1799_1800TG>AA V600E c.1799T>A V600E) and mutations in 27 patient's condition palaces (Q61K , Q61R, G13V, G12C, G12D) and mutations in10 patient's condition palaces (G12V,G13R, Q61R). While only 4 patients for RET gene difference in the analysis of the genetic mutation. At comparable with the genetic mutation of the control group. In this study suggests that there is a link between the occurrence of mutations in this genes and the status of thyroid cancer.

COMPUTER SIMULATION STUDY OF PHYSICAL PROPERTIES OF NANOSIZED BIOSTRUCTURES

P.J. Kervalishvili[1,a], T.N. Bzhalava[2,b]

[1,2] *Georgian Technical University (GTU), Georgia*
[a] kerval@global-erty.net, [b] tamar.bzhalava@gtu.ge

Abstract. Computer simulation study of bionanoparticles' physical properties, method of estimation of electromagnetic (EM) spectrum and resonance wave-length ranges is considered. Solution of well-established classical electrodynamics boundary problem is applied to nanobioparticles characterization. Possibility of appreciation EM spectrum and EM field distribution is demonstrated for virion of Tobacco Mosaic Virus (TMV), which is modeled by the particle of cylindrical shape and definite geometrical, electrical and magnetic characteristics. A set of resonance wavelength is observed in ultraviolet (NUV-EUV) range of TMV particle's spectrum.

1. Introduction

Study of biostructure's physical characteristics, scattering and absorbtion properties, estimation of electromagnetic (EM) spectrum and resonance wave length ranges is important for characterization of nano-micro-scaled particles and determination of biostructures unique spectral signatures, so essential in bio-agents detecting and identification systems. Investigation of EM field distribution makes possible to have insight vision of the nanoparticles. Behavior of nano-micro sized pathogenic microorganisms such as bacteria, virus, organic and non-organic agents is selectively sensitive toward the electromagnetic (EM) field excitation. Elaboration of physical models of bioparticles, as well as computer simulation study of near and far EM field distribution in the areas of particles and surrounded medium is a possible way for investigation of physical properties of bio-particles of different morphology.

2. Method and approach

Method of estimation of spectral response on EM field & particle interaction is based on solutions of electrodynamics two (2D) or three (3D) dimensional boundary tasks [1, 2]. Obtained analytical expressions of EM fields are derived from rigorous solutions of Maxwell's and Helmholtz's equations and defined through the dimensionless parameters, diameters (d) over excitation wave-length (λ). It makes possible to apply the classical well-known approach to sub-micro particles characterization. Proposed method is used for investigation of viral particle's physical properties. EM near and far fields distribution, EM spectrum are proposed for viruses, having rod-like, prolate un-enveloped virions (e.g. Tobacco Mosaic Virus (TMV), bacteriophage M13). Virions, the extracellular infective forms of viruses are modelled by the particles of cylindrical shape of different structures, such as homogeneous dielectric particles and inhomogeneous through the radius, also particles of core-shell structure reflecting the properties of ribonucleic acids (DNA or RNA) of viruses and capsid's proteins. Shape, structure and the set of geometrical, magnetic and electrical characteristics are the main parameters defining the particles' EM spectral properties. Advantage of simulation study of complex molecular systems such as virions in contrast of measuring experiments associated with weak signals detection is noteworthy.

3. Results

Computer simulation (based on MatLabR2013b software) was carried out for TMV particles characterization. Parameters of TMV particle are obtained from scientific publications based on different measuring technics [3]. Length of TMV virion is 280-300 nm, outer and inner diameters of capsid are $d_2 = 18$ nm and $d_1 = 4\,\text{nm}$, correspondingly. Dielectric permittivitys of core (RNA) - ε_1, shell (capsids proteins) - ε_2, surrounded medium - ε_3. Two models are used for simulation study of TMV virion: homogeneous and core-shell structured cylinders. Computer simulation shows that expected resonant spectral response is observable on far-field ($r >> 2d_2^2/\lambda$) characteristics (Fig.1), resonant vibrational frequencies of whole TMV particle may be associated to scattering cross section maximums.

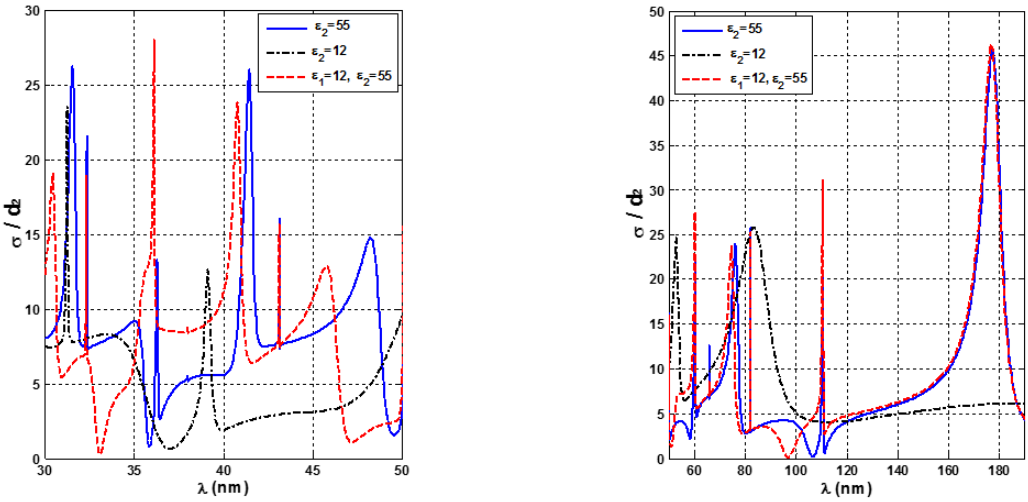

Fig.1. Forward scattering cross section (σ / d_2) vs excitation wave length (λ).
Cylindrical model: diameter d_2 =18 nm, dielectric permittivity $\varepsilon_2 = 55$ (solid blue), 12 (dash-dot black), Core-shell model (dash red): diameters $d_2 = 18$ nm (outer) and $d_1 = 4$ nm (inner), dielectric permittivitys: $\varepsilon_1 = 12$ (core), $\varepsilon_2 = 55$ (shell); $\varepsilon_3 = 1$ (surrounding medium).

Near-field distribution presented in a form of isolines of EM field amplitudes (Fig.2), indicates the locations of energy maximums inside and outside of particle.

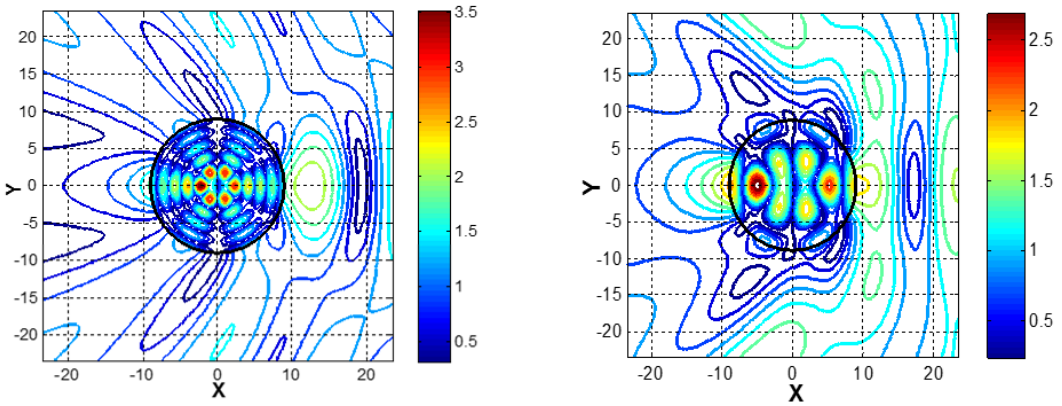

a) b)

Fig. 2 Isolines of EM field amplitudes for cylindrical model of TMV virion, in the range of (- λ ,+ λ).
Diameter of cylinder: d_2 =18 nm; dielectric permittivitys: of cylindrical particle - $\varepsilon_2 = 55$ (a), 12 (b), surrounding medium - $\varepsilon_3 = 1$, excitation wave length $\lambda = 23.5$ nm, (X,Y) plane is perpendicular to the axis of cylinder.

Conclusions

Method of estimation EM field characteristics and resonant wave ranges based on computer simulation is developed. Data analysis revealed the strong dependence of field characteristics on electromagnetic plus geometrical parameters and wave length in resonant wave range. Possibility of determination of resonant frequencies of virions is demonstrated. Simulated EM spectra as the specific signature of bio-particles of a given parameters is proposed for consideration.

References

[1] Bohren C. F., Huffman D. R. *Absorption and scattering of light by small particles*, 1983, John Wiley & Sons, 530 p.

[2] Bzhalava T. N., Kervalishvili P. J., Study of spectroscopic properties of nanosized particles of core-shell morphology, J. Phys., Conf. Ser. (IOP), 2018, 987, 012023, 1-6.

[3] Ermolina I., Morgan H., Green N.G., Milner J.J., Feldman Yu., Dielectric spectroscopy of Tobacco Mosaic Virus, Biochimica et Biophysica Acta, 2003, 1622, 57–63.

DESIGN AND THERMAL MANAGEMENT OF BATTERY PACK FOR MEDICAL DEVICES

Masoumeh Yaghoobi[1,a], Irina Gotsiridze[1,b]

[1]*Georgian Technical University, Tbilisi, Georgia*

[a]masoumeh.yaghoobi@gmail.com, [b]i.gotsiridze@gtu.edu.ge

Abstract

The health and medical industry must manufacture custom made battery solutions to meet requirements to work under extreme conditions. In this project we designed a battery pack using COMSOL Multiphysics with finite element analysis.

Our pack is containing 16 pieces of battery 38120 LiFePo4 and the cells kept together with special plastics. The mass of each cell is 330 grams with 38-millimeter diameter and 120- millimeter height. Each cell provides 3.2 volts of electrical energy and the electrical current is 100 A. The aluminum battery body with thickness of only 1.25 mm, keeping cells together and away from dust and rubbish.

The temperature of cells after few minutes of working, reach 47^{O}C and If the temperature of the device would be high, tissue damage may occur. So, we provide a cooling system to make it cold and near normal weather conditions.

With Thermal management analysis we put 50 mm SUNON fan on the battery pack. Two 15*80 mm canals made for transferring hot air to outside. The production of air by fan is 13^{CFM} and 1.4 wats is usage of electricity for this fan.

The price of whole battery pack including 16 battery cells will be 176 USD and price for fan and aluminum box is only 10 USD. The price for whole battery pack will be around 186 USD.

The thermal management of battery pack showed that the desired fan can cool the whole battery pack and control the temperature perfectly. This price can show that with just small amount of spending we can provide a reservoir electrical system for all our medical equipment's.

Keywords: Medical Devices, Thermal Management, Battery pack, Lithium Battery

POSTERS

OVERHEAD TRANSMISSION LINES IMPACT EVALUATION ON HUMAN PRESENCE

Tatiana Damatopoulou[1, a] and Antonios Kladas[1,b]

[1]School of Electrical and Computer Engineering, National Technical University of Athens,
9 Iroon Polytechneiou Street, 15780 Athens, Greece
E-mails: [a]damatat5@yahoo.gr, [b]kladasel@central.ntua.gr

Abstract. The paper presents an investigation of the impact on humans present in the vicinity of overhead transmission lines by the low frequency electric and magnetic fields generated. In particular the modeling procedures proposed in standards are reviewed and the precision obtained under the assumptions adopted are checked. The main interest is focused on electric field which is substantially distorted by the human presence.

Keywords: Low frequency electric and magnetic fields, finite element method, environmental impact, permissible limits.

1. Introduction

Electric and magnetic field analysis generated by overhead transmission lines are of great concern regarding the aspects of health, safety and environment. A large number of studies has been developed providing reference values of permissible limits for human activity in the vicinity of low frequency power equipment concerning both general public and working personnel [1]. Moreover, specific modeling procedures have been proposed in standards enabling efficient evaluation of these fields under human presence in the proximity of the respective power installations [2]. To that respect particular software techniques have been developed for the calculation of the fields and their impact on human organism undertaking appropriate compromises between computational speed and acceptable precision of the obtained results [3-5]. In the present paper an investigation is undertaken on the precision achieved by specific approximations proposed (Figs. 1-4).

2. Permissible limits of electric and magnetic fields

The permissible limits of low frequency electric and magnetic field intensities for human activities have been already extensively studied and specific values proposed by ICNIRP [1] have received international acceptance. In general, the electric and magnetic field intensity permissible limits at power frequencies are determined differently for general public and working personnel, due to unequal potential health sensitivities and duration of exposure. The generally accepted guidelines, which are actually adopted equally in EU concerning the maximal limits of acceptable human exposure to field intensities at the frequency of 50 Hz, are as follows:

- Electric field intensity of 5 kV/m for general public and 10 kV/m for working personnel, respectively.
- Magnetic field density of 200 μT for general public and 1000 μT for working personnel, respectively.

3. Modelling procedures proposed

The distributions of electric and magnetic field near the ground created by the overhead transmission lines can be easily evaluated by using appropriate analytical formulae. It may be noted however, that the consideration of objects such as towers or even the human presence may importantly affect mainly the electric field distribution thus necessitating introduction of numerical approaches [3-4]; to that respect appropriate modeling requires a trade off concerning 2D and 3D configurations and alternative methodologies depending on the effects to be accounted for. The developed techniques have been assessed and evaluated and particular guidelines for the modeling procedures to follow have been proposed by international standards [2]. As far as human presence is concerned a typical configuration of a man body has been adopted while 2D axisymmetric analysis by using the finite element method has been proposed providing accurate representation of the electric field distribution (Fig. 3). The present paper undertakes the assessment of deviations of such an approximation with respect to the more realistic 3D representation of the human body. To that respect a 400 kV rectilinear conductor case at a distance of 11 meters from a perfectly smooth planar ground surface has been considered in conjunction of the typical man body presence just below the conductor (Fig. 1). A 3D finite element model has been implemented for the simulation of this problem and the discretization adopted is shown in Fig. 2. The

maximum electric field intensity generated has been calculated along two lines at the level of the head positioned in parallel and orthogonal directions with respect to the conductor, as illustrated in Fig. 2. The obtained distributions of electric field intensity are shown in Fig. 4, indicating that the 2D axisymmetric representation provides the same results as the 3D one along the parallel direction of the conductor; in counterparts, it overestimates the electric field along the orthogonal direction with respect to the conductor, in particular at points situated distant to the man. A detailed investigation of the distance from the man that the 2D analysis provides sufficient accuracy will be presented in the extended paper.

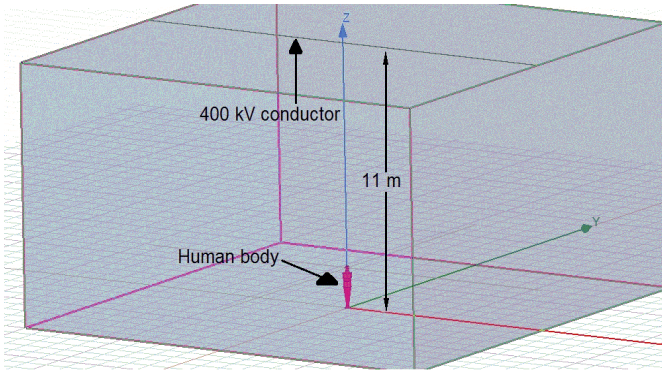

Fig.1. Considered position of the human body with respect to a 400 kV linear conductor.

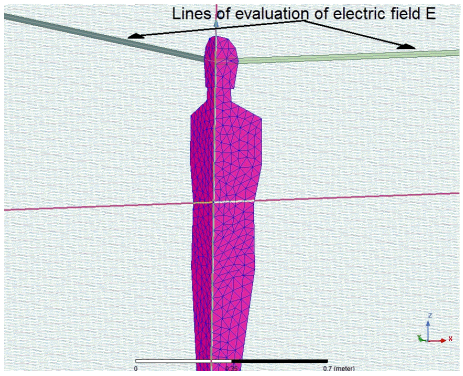

Fig.2. Finite element discretization of the human body in 3D representation.

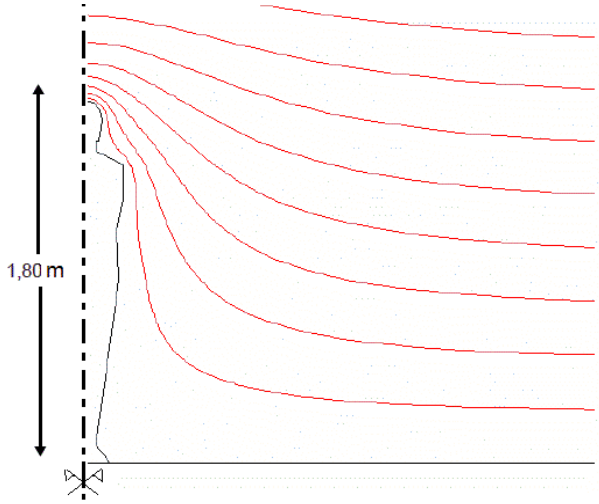

Fig.3. Axisymmetric 2D representation of the typical man body proposed in [2] and local electric field distortion.

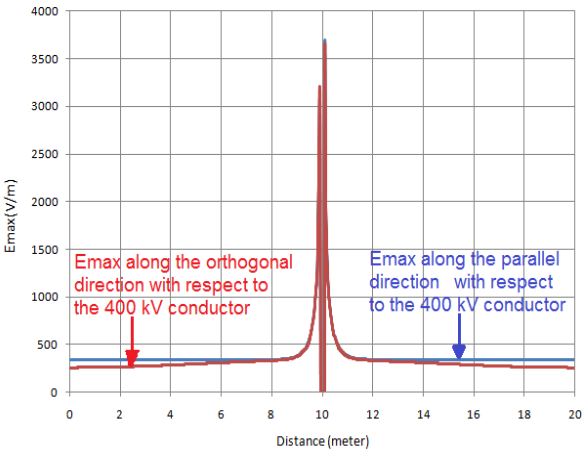

Fig.4. Electric field intensity E_{max} variations at the level of the human head along parallel and orthogonal directions with respect to the 400 kV conductor, respectively.

References

[1] ICNIRP, "Guidelines for limiting exposure to time-varying electric and magnetic fields (1 Hz to 100 kHz)", Health Physics, Vol. 99, No 6, December 2010, pp. 818-836.

[2] IEC 62226-3-1:2007, "Exposure to electric or magnetic fields in the low and intermediate frequency range - Methods for calculating the current density and internal electric field induced in the human body, Part 3-1: Exposure to electric fields - Analytical and 2D numerical models" (European Standard EN 62226-3-1, 2007, pp. 1-54).

[3] El Dein A.Z. "Calculation of the electric field around the tower of the overhead transmission lines," IEEE Trans. Power Del., vol. 29, no. 2, pp. 899–907, Apr. 2014.

[4] Xiao F., Yan J., Zhang B., and Wang Y. "Simplified approach of maximum electric field distribution on the ground near HVAC–HVDC shared tower transmission lines," J. Eng., vol. 2018, no. 17,pp. 1851–1854, Sep. 2018.

OPTIMAL DESIGN METHODOLOGY BASED ON SENSITIVITY ANALYSIS FOR MARINE ELECTRIC PROPULSION SALIENT POLE SYNCHRONOUS MOTORS

Angelos P. Moschoudis[1, a], Antonios G. Kladas[1,b] and George J. Tsekouras[2,c]

[1]School of Electrical and Computer Engineering, National Technical University of Athens, 9 Iroon Polytechniou Street, 15780 Athens, Greece
[2]Faculty of Engineering, Department of Electrical and Electronics Engineering, University of West Attica, 250 Thivon Avenue, 12244 Aigaleo-Athens, Greece
E-mails: [a]moshoudi@central.ntua.gr, [b]kladasel@central.ntua.gr, [c]gtsekouras@uniwa.gr

Abstract. In this paper the optimization procedure for a Salient Pole Synchronous Motor (SPSM) suitable for Marine Electric Propulsion Systems (MEPS) is presented involving preliminary and final design stages, respectively. The preliminary design is based on standard formulae while the final design implements sensitivity analysis investigation for several geometrical parameters by using finite element method.

Keywords: Marine electric propulsion systems, optimal design, salient pole synchronous motor, sensitivity analysis.

1. Introduction

In electrified ship's propulsion systems, synchronous motors can be considered as mature technological applications. In such applications low rotational speed salient pole synchronous motors connected to the propeller shaft directly are favored [1-4]. In this paper an optimization procedure based on sensitivity analysis investigation of several geometrical design parameters for a low rotational SPSM suitable for MEPS using finite element method is presented. The above mentioned design is accomplished by adopting a two step procedure for preliminary and final design stages, respectively, explained in the followings.

2. Preliminary Design Stage

Synchronous motor main dimensions are derived by using classical formulae. They are evaluated in order to fulfill the motor specifications such as nominal power, rotational speed, specific magnetic loading in the various parts, and electric loading in the windings. Additionally the temperature rise and the motor performance are equally approximately evaluated. The above mentioned main dimensions are then validated by using finite element analysis and the initial values obtained at the preliminary design stage are presented in Table 1.

TABLE 1: INITIAL AND FINAL VALUES OF THE MAIN DESIGN PARAMETERS

Parameter	Initial	Final	Dimension	Symbol	Initial	Final
Apparent Power (kVA)	1250	>>	Stator Internal diam (m)	*D int st*	2.65	2.05
Phases	3	>>	Air-gap length (m)	*Lgap*	0.009	0.0065
Nominal Voltage (V)	690 Y	>>	Active Part Length (m)	*L*	0.48	0.43
Nominal Current (A)	1045,9	>>	Teeth lip thickness (m)	h lip thick	0.004	0.003
Nominal Frequency (Hz)	35	>>	Stator slot height (m)	h slot stator	0.034	0.032
Nominal Speed (RPM)	140	>>	Rotor pole field height (m)	*h field*	0.175	0.149
Number of Poles	30	>>	Rotor pole width (m)	*b pole*	0.142	0.119
Maximum Torque (kNm)	71,6	104,2	Rotor pole shoe height (m)	*h pole shoe*	0.044	0.030
Efficiency n (%)	87,5	94,86	Pole arc / Pole pitch ratio	*Kf*	0.82	0.70
Total Harmonics Distortion (%)	13,3	2,33	Core Cutting Length (m)	-	49750	46162

3. Final Design Stage

Appropriate section of the motor geometry has been implemented in the solution domain in order to exploit the configuration symmetries corresponding to the different types of stator winding structures considered, as shown in Fig. 1. Analytical investigation of critical geometrical design parameters is accomplished leading to composite cost functions involving the following parameters extremum research: torque versus load angle and motor efficiency maximization, in conjunction with core cutting length, power losses and Total Harmonics Distortion (THD) minimization. The variations of the abovementioned quantities are shown in Figs. 2-4. The final values of the main design parameters derived by applying sensitivity analysis are given in Table 1.

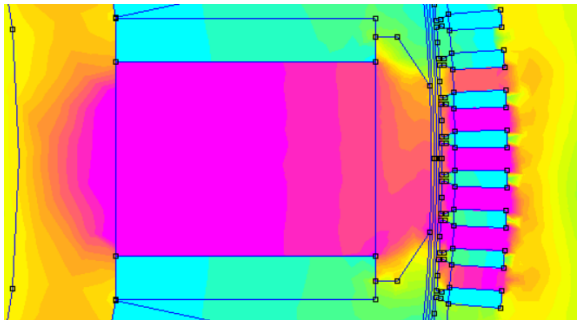

Fig. 1 Basic configuration of the proposed SPSM,

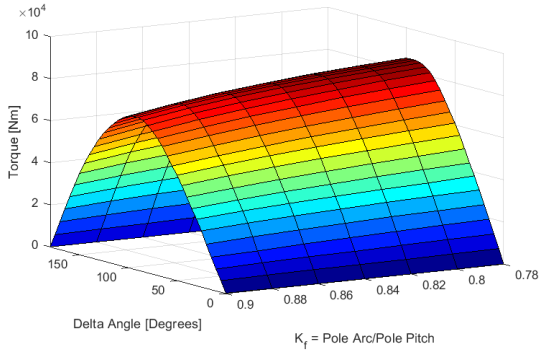

Fig. 2 Torque vs internal angle δ with K_f ratio variation.

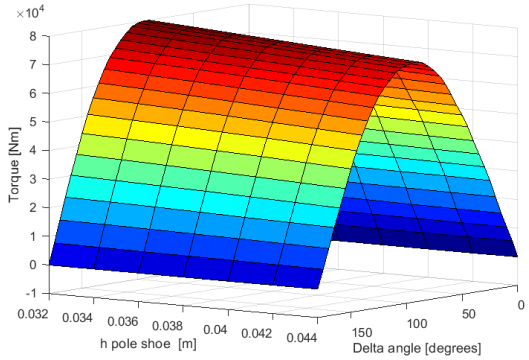

Fig. 3 Torque vs. internal angle δ with pole shoe height variation.

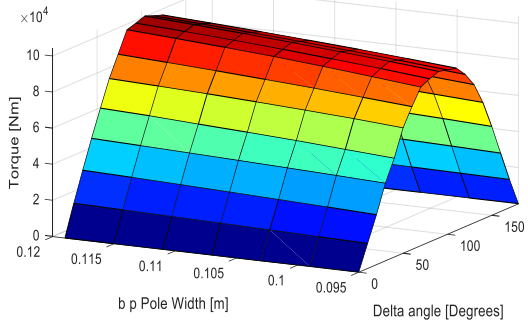

Fig. 4 Torque vs. internal angle δ with pole width variation.

Conclusion

By implementing the methodology proposed a substantial decrease of the rotor pole shoe height has been achieved with corresponding modification of the rotor pole width at the final design stage, through sensitivity analysis with respect to the initial values determined at the preliminary design stage. Moreover, this procedure resulted in a significant improvement of the developed torque and motor performance in conjunction with important reduction of the electromotive force THD.

References

[5] Moschoudis A.P., Filippou M.C., Tsekouras G.J. and Kladas A.G. "Geometry Investigation of L.R.S. Synchronous Machines using FEM," Materials Science Forum, vol. 792, pp. 266-271, 2014, doi: 10.4028/MSF.792.266.

[6] Moschoudis A.P., Tsekouras G.J., Kladas A.G. "Optimal Design of Marine Electric Propulsion Salient Pole Synchronous Motor," IEEE CEFC 2016, 13-16 Nov. 2016, Miami, Florida, USA, doi: 10.1109/CEFC.2016.7816370.

[7] Abdullin D.Sh., Vaganov M.A. "The Optimal Geometry of Salient Pole Synchronous Motors," 2019 IEEE Conference of Russian Young Researchers in Electrical and Electronic Engineering (EIConRus), 28-31 Jan. 2019, Saint Petersburg and Moscow, Russia, Russia doi: 10.1109/EIConRus.2019.8656878.

[8] Chu K.H., Pou J., Ramakrishna S., Gupta A.K. "Salient pole wound field synchronous machine for marine propulsors with outboard drives: Analysis and design," IECON 2017 - 43rd Annual Conference of the IEEE Industrial Electronics Society, 29 Oct.-1 Nov. 2017, Beijing, China, doi: 10.1109/IECON.2017.8216639.

DEVELOPMENT OF VEHICLE DETECTION SYSTEM USING GEOMAGNETIC LEVEL SENSOR

K. Oka[1,a], S. Kiyofuji[1,b], A. Harada[2,c], and Y. Kumagai[3,d]

[1] Intelligent Mechanical Engineering, Kochi University of Technology, Japan
[2] "Aerospace Engineering, Kochi University of Technology, Japan
[3] Research Organization for Regional Alliances, Kochi University of Technology, Japan
[a]oka.koichi@kochi-tech.ac.jp, [c]harada.akinori@kochi-tech.ac.jp, [d]kumagai.yasuhiko@kochi-tech.ac.jp

Abstract. This paper describes about a detection system for vehicle using a magnetic sensor. This system is used for detection of presence and traveling direction. The magnetic sensor system measuring geomagnetic level signal of a vehicle and is used as one of the sensor detecting a vehicle on a point. In this paper, we focus on the new detection method for traveling direction of a vehicle. First the concept of proposed sensor is explained. A new detection method of the traveling direction of the vehicle is proposed by analyzing the results. Experimental examination on the road was carried out and the results supports that the proposed method is valid for the detection of the direction.

1. Introduction

Magnetic sensor systems measuring geomagnetic level signal have been already investigated as one of the sensor detecting a vehicle on a point [1]-[4]. In this paper, a new type of sensor system is proposed. The sensor system can be considered as it is corresponding to the loop coil or supersonic system. It may have advantages in size and power consumption. Installation, cost, and maintenance can be considered to be superior. In the following especially the traveling direction of the vehicle will be focused on. First the concept of proposed sensor is explained and the proposed sensor system is introduced. Some basic experiment using a geomagnetism sensor is examined. A new detection method of the traveling direction of the vehicle is proposed by analyzing the results. Experimental examination on the road was carried out and the results supports that the proposed method is valid for the detection of the direction.

2. Proposed sensor system

If a vehicle has one magnetization as shown in Fig. 1, the presence and the traveling direction can be detected. In Fig. 1, a geomagnetic sensor which is indicated as a red rectangle is installed under the ground. The magnet on the vehicle is assumed as it is put in a horizontal position and the N pole is in the front. The green arrows indicate the directions of magnetic flux. When the vehicle travels in the direction according to the blue arrow, the flux densities in the x and z directions at the sensor point vary as shown in Fig. 2. First flux in the z axis is downward. So the value of the figure is minus. It becomes zero when the center of the magnet comes to the position just over the sensor. And after this point flux has positive value. Flux in the x direction indicates leftward during the magnet traveling. So the value is always minus. When the center of the magnet is just over the sensor, the flux value has local minimum. This flux variation can be used for detecting the vehicle traveling direction.

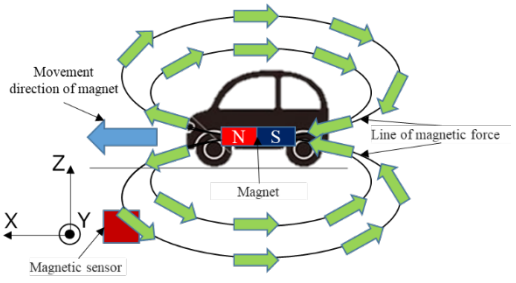

Fig.1. Basic concept of vehicle detection sensor using geomagnetic sensor

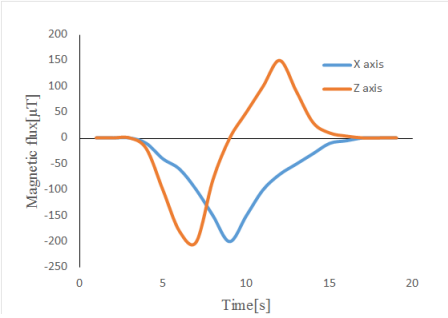

Fig. 2. Typical flux variation of z axis and x axis during vehicle traveling.

A basic experiment was carried out. The upper part of the experimental device is a path for a permanent magnet which is considered as a magnetized vehicle. A geomagnetic sensor is installed under the path. The magnet can be changed the pitch angle as it indicates various direction of the vehicle magnetism. A sensor measures the magnetic flux values in x axis and z axis.

We focus on the zero crossing points of each recorded line. At that time, we check the flux

value of the other direction indicates local maximum or local minimum. Combination of the direction at the crossing points and the extreme values can distinguish moving direction of the magnet.

3. Experiment on road

Using the proposed method, experiments on a real road were carried out. A photo of the vehicle which is examined is shown in Fig. 3. The sensor unit is buried just under the vehicle in the photo of Fig. 3. It is located about 10 cm under the ground. The positive direction x axis of the sensor is aligned as same as the vehicle in the figure travels. Sampling frequency of measurement is 100 [Hz].

The result of the Fig. 3 is shown in Fig. 4. As you can see in the figure, there are three zero crossing points. Two points are on the x axis line and one is on the z axis line. At the time of zero cross on x axis there are extremes. The moving directions can be determined and they were correct. However at the zero cross at z axis there is no apparent extreme. We ignored such a point without the extreme value.

The results of heavy vehicles have sometimes many zero crossing points, and they indicated unspecific variation and has small vibration. The reason is that the heavy vehicles have the middle part without ferromagnetic materials. The residual magnetism is very low level. As the magnetic flux of the middle part is very low. The data such one heavy vehicle may sometimes be recognized as two vehicles because the data is divided into the front and the rear.

We examined 81 cases on the road. As the results there is 8 cases that have wrong direction. These vehicles almost didn't pass through just over the sensor. More detail analyses of experimental will be provided in the final paper.

Fig. 3 A photo of experiment on road

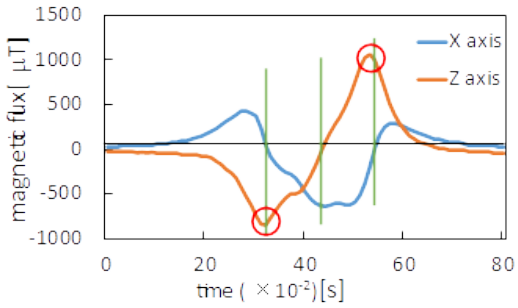

Fig. 4. Experimental result of vehicle shown in Fig. 3

Conclusions

A new type of the detection system for vehicle using a magnetic sensor has been proposed. This system is used for detection of the traveling direction. A prototype of the proposed sensor system has been introduced. Some basic experiments have been carried out and the detection method is verified that it was useful. Some experimental examination on the road carried out and the results supports that the proposed method is valid for the detection of the direction. However the system still has some problems. They are further study of this project.

References

[1] Ito H., Inamoto T., et al. Car Passing Measurements Using Two Amorphous Wire CMOS MI Sensor Built-in Disk Set on a Road (in Japanese), IEEJ, Vol. 122-D No. 2, 2002, pp. 176-181.
[2] Inamoto T., Iida T., and Mohri K. Car Passing Recording System Using Amorphous Wire CMOS MI Sensor (in Japanese), J. of Magnetics Society of Japan, Vol. 27, No. 4, 2003, pp616-619.
[3] Kamata K. et al. Magnetic Field Fluctuation Due to Movement of Automobile (in Japanese), IEEJ Transactions on Fundamentals and Material, Vol. 125 No. 2, 2005, pp. 92-98.
[4] Japan patent JP1998-172093.

C-V CHARACTERIZATION AND ELECTRIC PARAMETERS OF ZRO_2 RECEIVED BY UV STIMULATED PLASMA ANODIZING

Amiran Bibilashvili[1a], Zurab Kushitashvili[2,b]

[1]LEPL Micro and Nanoelectronics Institute, Chavchavadze ave.13, 0179 Tbilisi, Georgia.
[2]Ivane Javakhishvili Tbilisi State University, LEPL Micro and Nanoelectronics Institute, Chavchavadze ave.13, 0179 Tbilisi, Georgia,
[a]zurab_kush@yahoo.com, [b]amiran.bibilashvili@tsu.ge,

Abstract

Low temperature technologies creating metals oxides are promising solution for formation integral circuit elements. In this report have been investigated the electric properties of zirconia (ZrO_2) received by low temperature (~ 400^0 C) UV stimulated plasma anodizing. Zirconia is a potential high-k dielectric material with potential applications as agate insulator in transistors. This dielectricis distinguished by good electric parameters. For this purpose we used C-V characterization technic and calculate dielectric constant, flatband voltage, threshold voltage, bulk potential, work function, oxide effective charge, charge concentration. The C-V measurement was carried out on Keithley Instrument Semiconductor Parameter Analyzer 4200, oxide thickness was measured by reflectometer – MprobeVis System

Keywords: dielectric, anodizing, charge, capacitance.

RADIATION MODIFIED ION-IMPLANTED BALLS OF BALL BEARINGS

A.I. Guldamashvili[a], Yu.I. Nardaia[b], Ts.M. Nebierdze[c], , E.E. Sanaia[d] A.V. Sichinava[e]

Ilia Vekua Sukhumi Institute of Physics and Technologies, Tbilisi, Georgia
[a]anzor.guldamashvili@gmail.com,[b]nardaya@gmail.com, [c]tsiranebieridze@gmail.com, [d]esanaia@gmail.com,
[e]avtandil.sichinava@gmail.com

Abstract. A radiation-modified ion-implanted ball of 1/4 inch diameter ball bearings made of 440C steel was investigated. The tuning modification was carried out by ion beam-assisted/enhanced deposition (IBAD / IBED) methods. The surface of the samples was coated with a nanosize multilayer coating of VN-TiN- ... VN (11 layers with a thickness of 100 nm each layer, an energy of 30 keV and a fluence of ~10^{17} ions / cm^2. Hardness of the Modified Ion-Implanted Balls of Ball Bearings is more than the hardness of the original steel by 1.8 times. The results of the study show that IBAD / IBED methods can be used as an effective tool for improving the parameters of ball bearings.

1. Introduction

Various commercial processes of the production of new construction materials with improved mechanical parameters for the construction of various purpose items and devices with sophisticated operation parameters have found wide commercial application today. Among alternative methods of construction materials development for various purpose facilities and units with improved operation parameters quite successful are such innovation radiation technologies, as ion bombardment. Among them direct ion implantation (II), ion beam mixing/ (IBM), ion beam-assisted/enhanced deposition (IBAD/IBED), plasma source ion implantation (PSII) should be mentioned [1,2].

Radiation technologies are free from the limitations of equilibrium thermodynamics (exceed of impurity solubility limits, low temperature of the process, new phase nucleation and growth, etc). Therefore these methods, substantially differing from equilibrium thermodynamics conditions enable formation of modified surface composition layers of metals and alloys in equilibrium, non-equilibrium, metastable and nanocrystalline states [3-5].

Successfully proved method of ion beam assisted deposition is used to modify (hardening) nanosize surface layers of the balls for ball bearings with decreased friction features, made of 440 C steel. The process of ion-induced processing is used at the final stage of ball bearings making and does not change the rest bulk of the balls, their construction and bearing production processes. Applied radiation technology of balls modification is based on general theory of accelerated particles interaction with a solid body. Therefore, numerous complicated radiation processes, nano-physical phenomena and conditions of ion-induced processing of construction materials in many aspects define hardening and friction coefficient decrease in modified balls.

2. Materials and Experimental Methods

A martensitic stainless steel ball of ball bearing with¼" diameter was used as the starting material. Table presents chemical composition of hi-tech, high-alloy stainless steel 440C in percentage.

Grade		*C*	*Mn*	*Si*	*P*	*S*	*Cr*	*Mo*
440C	*min*	*0.95*	*-*	*-*	*-*	*-*	*16.00*	*-*
	max	*1.20*	*1.00*	*1.00*	*0.040*	*0.030*	*18.00*	*0.75*

The tuning modification was carried out by ion beam-assisted/enhanced deposition (IBAD / IBED) methods. The surface of the bullet was carried out by the nanosize multilayer coating VN-TiN- ... VN (11 layers with each layer thickness 100 nm 30 keV energy and fluence 10^{17} ion/cm^2.

Development of measuring procedures and study of microhardnes of initial (unprocessed) and radiation-modified ion-implanted 1/4' balls of ball bearings, made of 440C steel. A special ball-form specimen holder was designed and fabricated for measuring microhardness of balls of 1/4" diameter. A procedure for ball-form speciment microhardness testing was developed. Microhardness was tested using SHIMADZU Dynamic Ultra Micro Hardness Tester, DUH-211S.

Mechanical hardness was tested by microindentation under various loadings and constant deformation rates. The loads onto the indenter varied from 100 mN up to 1996 mN, which enabled microindentation at the

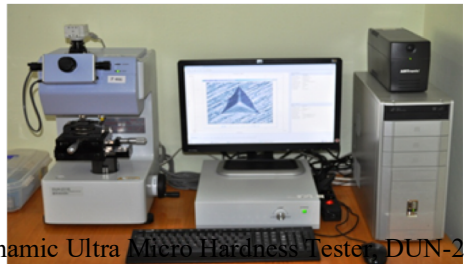

Fig.1. Dynamic Ultra Micro Hardness Tester, DUN-213S

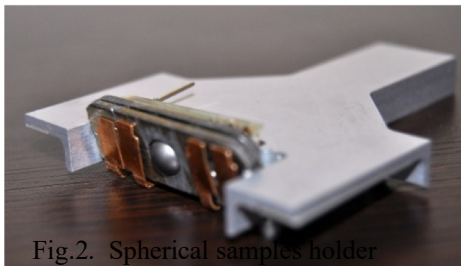

Fig.2. Spherical samples holder

depths of 350 nm up to 2000 nm. The following indentation parameters were selected for nicrohardness testing: loading speed – 13.324, $mN \cdot sec^{-1}$ at loads up to 200 mN, while at loads above 70.067, $mN \cdot sec^{-1}$, hold time at load -5, sec, hold time at unload - 3, sec and test count -5.

Nanomorphology of initial and ion-implanted samples was investigated on CMM-2000 microscope. Holder for spherical samples was created for scanning tunneling microscope CMM-2000.

Measurements were carried out on the scanning tunneling microscope, with high spatial resolution. Measuring range on the X and Y axis does not exceed $0.3\text{-}2x10^4$ nm, and on the Z axis $0.2 – 2x10^4$ nm. Measurement error is 10 nm ±10%.

Coefficient of dry friction the initial and modified samples was studied by non*destructive* pin on disc method [6].

Conclusions

Developed process and balls with improved strength by 1.7-1.8 times and friction coefficient can find application in the production of various purpose ball bearings with improved operation parameters. Radiation Modified Ion-Implanted Balls of Ball Bearings will be applied at the final stage of ball bearings manufacture, leaving unchanged the remaining bulk of the balls, structure and of ball bearings production processes.

References

[1] Was G.S."Fundamentals of Radiation Materials Science." In Metals and Alloys, Second Edition. Berlin: Springer, 2017..-1002 p.

[2] Ion Beam Modification of Solids: Ion-Solid Interaction and Radiation Damage (Springer Series in Surface Sciences. Vol. 61). Ed/Werner Wesch, Elke Wendler. ISSN 0931—51195. © Springer International Publicationsng Switzerland 1st ed. 2016.-547 p.

[3] Guldamashvili A., Nardaya Yu., Nebieridze Ts., Sanaia E., Sichinava A., Kadaria M. Mechanical properties of tungsten implanted with boron and carbon ions. Journal of Materials Science and Engineering: A. 2017, V.7, N. 3-4, p. 82-88.

[4] Guldamashvili A., Nardaya Yu., Nebieridze Ts., Sanaia E., Sichinava A., Kadaria M. Radiation Hardening of Molybdenum by Argon Ion Implantation. In: Kongoli F, Marquis F, Chikhradze N, editors. Sustainable Industrial Processing Summit SIPS 2017 Volume 5: Marquis Intl. Symp. / New and Advanced Materials and Technologies. Volume 5. Montreal (Canada): FLOGEN Star Outreach; 2017. p. 218-223.

[5] Guldamashvili A., Kutsia N., Nardaya Yu., Nebieridze Ts., Sichinava A. Surface Modification of AISI 310 and 440C Steels by Ion Implantation. International Conference Advanced Materials and Technologies Proceedings. (21-23 October, 2015, Tbilisi, Georgia). Tbilisi, Universal, 2015, p. 263-267.

[6] Popov V.L. Contact Mechanics and Friction: Physical Principles and Applications. Berlin, Heidelberg: Springer-Verlag, 2010. - 362p.

OBTAINING OF ULTRAFINE POWDER COMPOSITES OF TUNGSTEN, MOLYBDENIUM, TITANIUM AND BORON CARBIDES USING LIQUID PRECURSORS

Natia Barbakadze [1], Ketevan Sarajishvili [1], Roin Chedia [1], Levan Chkhartishvili [2, 3, *], Otar Tsagareishvili [2], Archil Mikeladze [2], Margalita Darchiashvili [2], Vakhtang Ugrekhelidze [4]

[1] Petre Melikishvili Institute of Physical & Organic Chemistry, Ivane Javakhishvili Tbilisi State University, 31 Anna Politkovskaya Street, Tbilisi, 0186, Georgia
[2] Boron-Containing & Powdered Materials Laboratory, Ferdinand Tavadze Metallurgy & Materials Science Institute, 10 Elizbar Mindeli Street, Tbilisi, 0186, Georgia
[3] Engineering Physics Department, Georgian Technical University, 77 Merab Kostava Avenue, Tbilisi, 0175, Georgia
[4] Quality Management Department, National High Technology Center of Georgia, 21 Petre Kavtaradze Street, Tbilisi, 0186, Georgia
** chkharti2003@yahoo.com*

True solutions and suspensions are widely used for obtaining the nano-sized ceramic composite powders. Selection of appropriate solvent depends on the nature of the initial substances. Usually, choosing of one solvent both for molecular and ionic compounds is impossible, since the solvent must simultaneously be an active carbon source. Previously, we have developed methods for preparing liquid and melt precursors, based on which ultrafine metal carbides and two-phase composite (WC, Mo_2C, TiC, B_4C, TiC–Ni, B_4C–TiB_2, WC–Co, Mo_2C–Ni, etc.) powders were obtained [1].

As for the technology developed here, it includes following steps:

1. (a) Preparation of true solutions by diluting / reacting the appropriate compounds and organic solvents; and (b) Obtaining of homogenized suspensions of insoluble compounds.
2. CVD (chemical-vapor-deposition) process of volatile compounds or their pyrolysis in preheated (at temperatures > 400 °C) furnace.
3. Grinding of precious precursors and subsequent thermal treatment (carbonation or boration) at temperatures > 1250 °C.

Solutions, as well as melts and suspensions, can be used for receiving of carbides or matrix ceramic composites. For example, by melting ammonium tungstate, ammonium molybdate, nickel chloride, cobalt chloride, and hexamethylene tetramine at 140 – 160 °C and further pyrolysis the WC, Mo_2C, WC–Co, and Mo_2C–Ni powders are obtained.

Presents work includes study of possibility to obtain boron carbides (B_4C) and B_4C-composites from various liquid precursors from boron and carbon compounds. In particular, boric acid esters (borates) with alcohol radicals of different structures (ROH, $R'(OH)_2$, $R'''(OH)_3$, polyols, oligomers, etc.) have been tested. In case of the use of volatile borates $B(OR)_3$ (R = CH_3, C_2H_5, and C_3H_7) the CVD process (at > 500 °C) was used in order to obtain boron carbide precursors.

Utilizing previously developed by us technology [2], the treatment of the viscous products obtained by interaction of boric acid with polyols and polymers was carried out by pyrolysis of liquids at 400 – 800 °C in preheated furnace in air. It is confirmed that viscous liquids can be diluted with water. The advantage of this technology is to get two- and multi-component ceramic composite powders in one stage, and in the powder the components are homogenized and are uniformly distributed throughout the powder. The same method is successfully used when small amounts of dopants are inserted. Our results are in full agreement with later reports [3, 4].

The composite with the same composition was received from various systems, e.g. B_4C–20%TiB_2 was obtained from $B(OR')_3$+$Ti(OR'')_4$ solution; and the same ceramic composite was obtained from suspension containing H_3BO_3–TiO_2–glycerine system (Fig. 1). It is established that particles size of B_4C–TiB_2 composite powder is within the range of 50 – 70 nm [5, 6].

In the well-known methods, this composition is made by mixing or sintering of finished powders. That is why their dispersion does not achieve the nano sizes. During the pyrolysis of organic components different quantities of active carbon are obtained. When using oxide components, carbon oxidation in air flow under controlled conditions (at 700 °C) was used to remove excess carbon from precursors or also well known methods used to produce active carbon (800 – 900 °C).

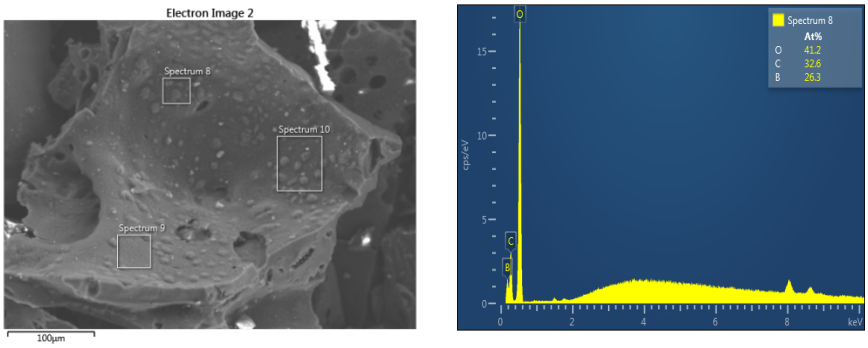

(a) **(b)**

Fig.1. SEM image **(a)** and EDX spectrum **(b)** of H_3BO_3–glycerine precursors, pyrolyzed at 800 °C in air.

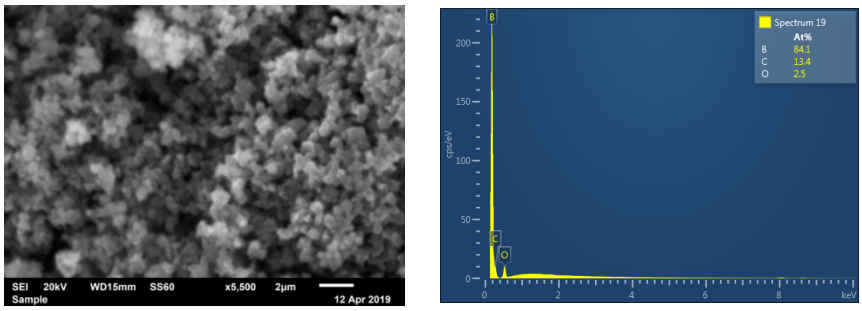

(a) **(b)**

Fig.2. SEM image **(a)** and EDX spectrum **(b)** of amorphous boron–glycerin precursors pyrolyzed at 500 °C under argon atmosphere.

Pyrolysis of homogenized suspensions obtained on the basis of amorphous boron is carried out at 350 °C in air or in the inert atmosphere at temperatures up to 800 °C (**Figure 2**). The optimum content of carbon is determined experimentally and in pyrolyzed precursor it reaches 18 – 25 %. After the grinding of the resulting product, its thermal treatment is performed under an inert atmosphere at temperatures up to 1250 °C. It is confirmed that adding of titanium and zirconium compounds (TiO_2, ZrO_2, TiH_2, ZrH_2, etc.) to the precursors promotes low-temperature synthesis of boron carbide.

Acknowledgement

This work was supported by Shota Rustaveli National Science Foundation of Georgia (SRNSFG) – Grant # AR–18–1045: Obtaining of boron carbide-based nanostructured heterophase ceramic materials and products with improved performance characteristics.

References

[1] ISTC Project # G–462: *New Hard Alloys with Nanocrystalline Components* (2001–2003).
[2] STCU Project # 4600: *Tungsten, Titanium, and Boron Carbide-Based Nanocrystalline Hardmetals* (2009–2011).
[3] Shawgi N., Li S.X., Wang S., Li Y. & Ramzi R. *Ceram. Int.* **44** (2018) 9887-9892.
[4] Watts J. *Controlled Synthesis of Boron Carbide Using Solution-Based Techniques*, PhD Thesis. Brisbane: Queensland Univ. Technol. (2018).
[5] Tsagareishvili O., Mikeladze A., Chedia R. & Chkhartishvili L. Method of obtaining boron carbide based hard nanocomposite materials. *National Center for Intellectual Property of Georgia "Geo Patent"* – Patent # GE P2018 6709 B, 2018 October 11.
[6] Mikeladze A., Tsagareishvili O., Chkhartishvili L., Chedia R., & Darchiashvili M. Production of titanium-containing metal-ceramic composites based on boron carbide in the nanocrystalline state. *Adv. Appl. Ceram.: Struc. Funct. & Bioceram.* (2019) – *in press*.

STUDY OF THE BEHAVIOR OF POLYMER CONCRETE TO SHOCK LOADING

N. Chikhradze[1,2,a], G. Abashidze[1,b], D. Tsverava[1,c], S. Kvinikadze[1,d]

[1]LEPL Grigol Tsulukidze Mining Institute., 7, E. Mindeli Str., 0186, Tbilisi, Georgia
[2]Georgian Technical University, Department of Engineering Physics, 77, Kostava Str., 0175, Tbilisi, Georgia
[a]chikhradze@mining.org.ge, [b]guramiabashidze@yahoo.com, [c]datotsverava@yahoo.com,
[d]sopiko.kvinikadze354@ens.tsu.edu.ge

Abstract.

The paper presents the results of the study of the basic physical-mechanical properties of polymer concrete produced on the basis of polyester resin. In the material, a mixture of fine- and coarse-grained andesite and teschenite are used as a filler and an aggregate, accordingly. Polymer concrete is reinforced with metal or non-metal fibers. The reinforced polymer concrete is a prospective material for manufacturing of the elements of building structures that are used in difficult conditions, including underground conditions. The reinforced polymer concrete with high mechanical properties may turn out to be effective materials under dynamic loading conditions. The results of testing of reinforced polymer concrete for compression, tension and shock resistance are given. It is revealed that the developed material, as compared with cement concrete, works better for tension and shock. Thus, the tensile strength of polymer concrete is seven-times higher than the tensile strength of ordinary concrete. Reinforcement of polymer concrete with basalt and steel fibers showed a noticeable increase in tensile strength. The advantage of reinforced polymer concrete in comparison with ordinary concrete in terms of shock resistance (10-12 times more) was also revealed. The opinion was expressed that the resistance of a material to dynamic effects is the best assessed not by shock resistance, but by explosion resistance.

KEY WORDS: polyester resin, andesite filler, teschenite aggregate, fibers, reinforced polymer concrete, shock resistance

MAGNETIC PARTICLES RETAINING ON OPEN AND CLOSED SYSTEMS

G. Banis[1,a], E. Mangiorou[1], P. Tselou[1], A. Ferraro[1,b], A. G. Mamalis[2,c] and E. Hristoforou[1,d]

[1]Laboratory of Electronic Sensors, National TU of Athens, Zografou Campus, Athens 15780, Greece
[2]Project Centre for Nanotechnology and Advanced Engineering, NCSR "Demokritos",Athens, Greece
[a]gbanis@mail.ntua.gr, [b]ferraro@eie.gr, [c] mamalis@ims.demokritos.gr,[d] hristoforou@ece.ntua.gr

Abstract: In recent decades the application of magnetic iron oxide micro- and nano-particles has been established in various technological fields, such as magnetic separation of biomolecules and ions, biosensors, biofuel production and others [1,2]. Working with iron oxide particles is becoming main stream subject thanks to the facility thatthis kind of materials can be functionalized with a variety of chemical groups which confer them specific selective or catalytic properties [3]. Furthermore, iron oxide nano-particles present magnetic properties, and in particular super-paramagnetism, which allows to remotely control them making their manipulation easy and cost-effective [4]. In addition, a new method of synthesis has been recently proposed, which can guarantee a cost-effective production of magnetic particles that may further reduce the running cost of separation methods based on magnetism [5]. Nevertheless, biotechnological applications of iron oxide particles are still confined to research level (lab scale devices) or for low throughput clinical applications [6]. Indeed, most systems based on the use of magnetic elements are designed to work with microfluid dynamic or can process samples in bath-based fashion, therefore discontinuously. The need of robust and high-productive methods is demanded especially in bioscience where, independently from the reaction or process involving magnetic particles, once such composite materials are mixed or added to a given solution, inevitably at the end of workflow they must be separated/harvested from the reaction vessel. Therefore, it is vital for a good productivity and processivity of reactions involving magnetic particles to ensure that large volumes of solution can be treated, and magnetic particles withdrew in the most fast and accurate way. The purpose of this paper is to compare an open and a closed type magnetic trapping system regarding their efficiency using two different types of magnetic sources.

Introduction

In both experiments [7,8], for the liquid solution we used ethanol ≥ 98% (Honeywell, Germany), oleic acid 90% (Alfa Aesar, Germany) and Iron oxide (Fe_3O_4) magnetic particles containing large polydomains with an average size of 200-400 nm, purchased from Chemical Store, USA.

We dissolved magnetic particles in ethanol containing 5% of oleic acid. Specifically, oleic acid was used to obtain a colloidal solution of dispersed magnetic particles. 0.1 grams of magnetite (Fe_3O_4) particles have been dissolved in 100 ml of alcoholic solvent by thoroughly shaking the flask. The resulting solution was homogenous, with magnetite particles well dispersed and showed an intense dark color; however, sedimentation of particles occurred when the solution was left un-stirred for long time.

Open system. Simulations in ANSYS were realized aiming to design, study and optimize the appropriate magnetic surface. An experimental setup was designed in order to verify the simulations. The setup is formed by an array of permanent magnets, a plastic surface, a peristaltic pump and silicon tube.

A 10x10 cm plastic foil was used together with 42 small neodymium magnets to realize the magnetic surface.

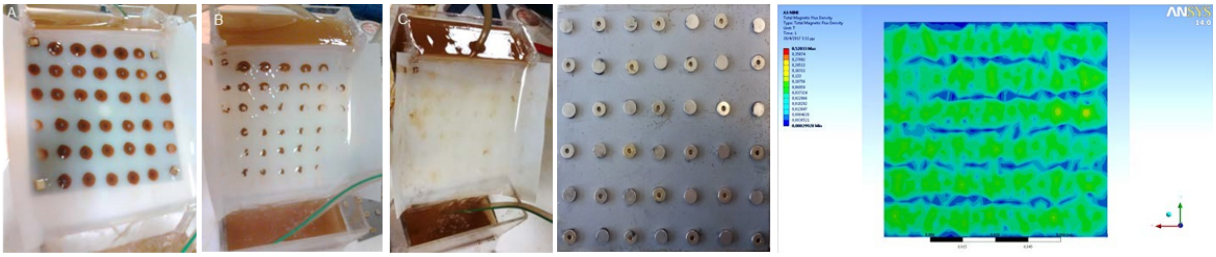

Fig.1. Open system setup A) the SPIONs are retained at the areas above the magnets B) after the magnets are removed, the flow gradually washes away the SPIONs C) after a few seconds the SPIONs are completely removed D) Neodymium magnets array and E) total magnetic field density produced.

The setup was consisted of a plastic surface (ABS) (120x100x1mm), the array of 42 neodymium magnets (N52) (2x5mm) underneath the plastic surface, a peristaltic pump, two tanks and a silicon tube (d=4mm).

The SPIONs were suspended in an ethanol-oleic acid mix in order to avert agglomeration and they were being circulated via the pump through the magnetic surface. From the first pass, the SPIONs were retained on the surface. After removing the magnetic array, the SPIONs started washing away with the flow. The same

experiment was repeated several times at different velocities in order to assert the max velocity allowing the SPIONs to be retained on the surface and they were in accordance with the simulations.

Closed system. A Teflon hose 100 mm length with a 4 mm external diameter and 3 mm internal diameter was used for the experiment. 80 mm of the Teflon hose were coiled into 8 turns around a 50 ml tube. The magnetic field was generated by striped North-South magnetic lines. The anisotropic flexible ferric magnetic strip (Neodymium Iron Boron, NdFeB) was 40 mm wide and has been purchased from Magnitech, Greece. The magnetic core can easily be inserted into the tube with the coiled Teflon hose. A peristaltic pump was used and a hose with a diameter of 4 mm, and a 3-way splitter with a manually adjustable valve (Figure 2).

We assumed that the magnetic particles that are close to the hose walls move slower than those in the center and thus, they can be retained easier by the magnetic field. However, since a spiral geometry was used, the mixing of the particles was allowed and statistically, most of the particles could be trapped. Thus, it can be assessed that the purity of the solution depends not only on the velocity of the fluid, but also on the number of the turns of the helical coil and the concentration of the particles in the solution.

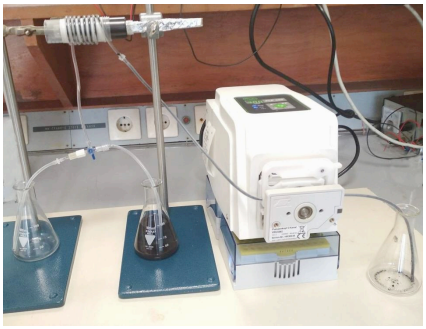

Fig.2. Experimental setup. Peristaltic pump, tube, magnetic core and valve are depicted

The peristaltic pump was set to a pumping rate of roughly 0.1 ml/sec and one side of the propelling hose was immerse in alcoholic solution containing particles, whereas the other side connected to the inlet pipe of the spiral. As the solution started to reach the pipe wrapped around the magnetic surface, the magnetic particles initiated to be trapped along the entire spiral. Once all alcoholic mixture was pumped through the spiral hose the peristaltic pump was let to run for a few seconds more in order to empty all the piping system. The solution deprived of magnetic particles was collect in a specific flask, and almost all magnetic particles were trapped by the spiral hose. Last, to elute magnetic particles from the system, we first separated the magnetic core from the spiral hose and subsequently used 20 ml of alcoholic solution to remove and collect magnetic particles in a separate flask. After passing the 20 ml of fresh alcoholic solution, the magnetic particles were completely removed from the spiral hose.

Comparison

In terms of efficiency, both systems provided a satisfying separation rate (up to 90%). Depending on the application, each process can provide some cos and pros. The open system is able to work for materials of various shape and size, something that is more restricted in the closed system. Such kind of materials could be the products from a mining process. However, the closed system can become fully automatic and provide a high throughput for biotechnological processes.

References

[1] Kouli ME, Banis G, Tsarabaris P, Ferraro A, Hristoforou E, A study on magnetic removal of sodium, calcium and potassium ions from seawater using magnetite/clinoptilolite-Na composite nanoparticles. J MagnMagn Mater 465: 692-699(2018).

[2] Rocha Santos TAP, Sensors and biosensors based on magnetic nanoparticles. Trends Anal Chem 62: 28-36(2014).

[3] An Hui ELS, Ferdi S, Magnetic Nanoparticles: Synthesis, Protection, Functionalization and Application. AngewChemie Int Ed 46: 1222-1244 (2007).

[4] Adamaki B, Karatza D, Chianese S, Musmarra D, Metaxa E, et al., Super-paramagnetic nanoparticles: Manufacturing, Structure, Properties, Simulation and Applications, p: 47 (2016).

[5] Aivazoglou E, Metaxa E, Hristoforou E, Microwave-assisted synthesis of iron oxide nanoparticles in biocompatible organic environment. AIP Adv, p: 8 (2017).

[6] Wegener C, Heber C, Min K, Novel cell washing device using spinning membrane filtration. Cytotherapy, p: 15(2013).

[7] Banis et al., An Innovative Application of Super-Paramagnetic Iron OxideNanoparticles for Magnetic Separation, Chemical Engineering Transactions Vol. 60 (2017).

[8] Banis et al, High-Flow System to Trap and Separate Magnetic Particles from Liquid Mixtures, J Bioprocess Biotech 8:5, DOI: 10.4172/2155-9821.1000340, (2018).

A FIRST COMPARISON BETWEEN THE MICROWAVE ASSISTED CO-PRECIPITATION TECHNIQUE AND THE TYPICAL SOLVOTHERMAL METHOD FOR THE TREPARATION OF Fe_3O_4/B-CYCLODEXTRIN CORE/SHELL TYPE NANOPARTICLES

M. Kourinou[1,a], I. Kokkinopoulos[1,b], M.-E. Kouli[1,c], A.Ferraro[1,d], A. G. Mamalis[2,e], E. Hristoforou[1,f]

[1]*Laboratory of Electronic Sensors, School of Electrical & Computer Engineering, National Technical University of Athens, Zografou Campus, Athens 1570, Greece*
[2]*Project Centre for Nanotechnology and Advanced Engineering, NCSR "Demokritos", Athens, Greece*
[a]mikour92@gmail.com, [b]ianiskokki@gmail.com, [c]mariliza@mail.ntua.gr, [d]ferraro@eie.gr, [e]hristoforou@ece.ntua.gr, [f]mamalis@ims.demokritos.gr

Abstract. In this work Fe_3O_4/β-Cyclodextrin core shell type nanoparticles are being prepared via two different synthesis methods and then the effectiveness of effectiveness of both methods is being discussed according to the resulting properties of the synthesized nanoparticles. The properties of the particles were characterized by FTIR, XRD SEM and VSM. The β-Cyclodextin (CD) grafted onto nanoparticle surface contributes to an enhancement of the adsorption capacity of Fe_3O_4 nanoparticles because of the strong complexation abilities of the β-CD polymer with metal ions and of the hydrophobic cavity with organic contaminants through host-guest interactions.

The research and development of coated magnetic nanoparticles, recently has found wide application in the field of biomedicine in the construction of sensing devices. However, the magnetic nanoparticle technology can be applied in various fields related to biomedicine and environmental engineering. In this research, Fe_3O_4/β-Cyclodextrin nanoparticles are being designed and synthesized via microwave assisted co-precipitation and are finally compared with the mainstream solvothermal method for the preparation of the specific type of magnetic nanoparticles. Referring to the size of the magnetic core of the nanoparticles (paramagnetic in micro scale / 0.1 to 1000 microns or superparamagnetic in nano-scale / 1 to 100 nanometers) and the size distribution of them, which is the backbone of the process, the synthesis can be performed by adapting the parameters of the aforementioned method.

The microwave co-precipitation method is a quite novel method which benefits from the uniform heating properties of the microwave technology. Microwaves are a region of the electromagnetic waves with a wavelength between 0.1 and 100 cm, corresponding to frequencies between 0,3-300 GHz. The operating principle of this method is based on the high power of microwave and the heating from the inside of the body which is penetrated by microwaves, which leads to oscillation of the bonds of the molecules. In fact the bonds which vibrate are those of the fluids even those inherent in the solid bodies and the outcome is the heat of the material.

In this work, the nano-particles designed are strictly magnetic and their core is magnetite with superparamagnetic properties. Magnetite is an iron oxide and a strong ferromagnetic material with the chemical formula Fe_3O_4. While obtained in nanoparticles <50nm it exhibits superparamagnetic behavior. In magnetite, the O^{2-} and Fe^{2+}, Fe^{3+} ions form an inverse spinel crystallographic structure [1]. As referring to the coating material, cyclodextrins (CDs) are oligosaccharide molecules deriving from the chemical processing of starch. β-CD is a cyclic oligosaccharide consisting of 7 glucopyranose units, which are joined together by α (1–4) linkage forming a torus-shaped ring structure with a hydrophilic exterior and a hydrophobic cavity. It can form inclusion complexes with a wide variety of organic compounds in its hydrophobic cavity through host-guest interactions [2,3]

These fascinating properties make them promising for applications in drug carrier systems, nanoreactors, bioactive supramolecular assemblies, molecular recognition, and catalysis For biomedical applications, the use of an organic coating compatible with human tissue is necessary and thus the use of materials such as cyclodextrins for coatings is considered more suitable. Considering modern water treatment technologies, functionalized magnetic nanocomposites have received many attentions recently for use in the adsorption of both organic and inorganic pollutants [4,5]. Magnetic nano-adsorbents have the advantages of

both magnetic separation techniques and nano-sized materials, which can be easily recovered or manipulated from complex multiphase systems with an external magnetic field.

Figure 1. illustrates the first characterization results (FTIR and VSM) for nanoparticles synthetized via both techniques. On the left scheme is depicted the effect of preparation time, and temperature modifications on the structure of the nanoparticles for both synthesis methods. From the results it is evident that both the microwave technique and the solvothermal method are quite effective for the preparation of Fe_3O_4/β-CD nanoparticles but the synthesized nanoparticles might occasionally not be fully coated if the preparation time and temperature are not precisely adjusted. The VSM results exhibit the superparamagnetic abilities of magnetite nanoparticles in both cases.

Fig.1. Left: FTIR characterization results for nanoparticles prepared via (a), (e) microwave assisted co-precipitation and (b), (c), (d) solvothermal method with stirring and ultrasound dispersion. Right: VSM characterization results for both types of nanoparticles

References

[1] Blaney Lee, *Magnetite: Properties, Synthesis and Applications,* (2007) Volume 15-2007, Paper 5

[2] Kenneth A. Connors, *The Stability of Cyclodextrin Complexes in Solution*, Chem. Rev., 1997, 97 (5), pp 1325–1358 DOI: 10.1021/cr960371r

[3] Uekama K., Hirayama F., and Irie T. *Cyclodextrin Drug Carrier Systems*, Chemical Reviews, Vol. 98, No. 5, 1998, pp. 2045-2076. doi:10.1021/cr970025p

[4] Rocher V., Siaugue J.M., Cabuil, V., and Bee A. (2008). *Removal of organic dyes by magnetic alginate beads*, Water Res. 42: 1290 – 1298.

[5] Zhang Y., Xu S., Luo Y., Pan S., Ding H., and Li G. (2011), *Synthesis of mesoporous carbon capsules encapsulated with magnetite nanoparticles and their application in wastewater treatment*, J.Mater. Chem. 21: 3664-3671

VISIBLE MCD SPECTROSCOPY AND NATURE OF ROOM TEMPERATURE FERROMAGNETISM IN HYDROGENATED CO - AND (CO+AL) - DOPED ZNO FILMS

Yu.E. Samoshkina[1,a], I.S. Edelman[1,b], D.A. Petrov[1,c], Hsiung Chou [2,3,d], S.G. Ovchinnikov[1,e]

[1] Kirensky Institute of Physics, Federal Research Center KSC SB RAS, 660036 Krasnoyarsk, Russia
[2] National Sun Yat-sen University, 80424 Kaohsiung, Taiwan, ROC
[3] National University of Kaohsiung, 81148 Kaohsiung, Taiwan, ROC
[a]uliag@iph.krasn.ru, [b]ise@iph.krasn.ru, [c]irbiz@iph.krasn.ru, [d]northpolebearchou@g-mail.nsysu.edu.tw, [e]sgo@iph.krasn.ru

Abstract. Co-doped ZnO and (Co+Al) - doped ZnO films were synthesized by the radio frequency magnetron sputtering in mixed atmosphere Ar+20% O_2 and Ar+20-50% H_2. The morphology, chemical composition, crystal structure, and magnetic circular dichroism of the films were investigated. It was established that the films thickness decreases several times when Ar replacing partly by hydrogen into the sputtering chamber. At the same time, the increase in relative Co content in the films with the increasing hydrogen concentration is observed. The hydrogenated films exhibit ferromagnetic behavior at room temperature. The nature of room temperature ferromagnetism in the hydrogenated Co - and (Co+Al) - doped ZnO films is discussed, as well as the mechanism of influence of hydrogen concentration on the magnetic properties of the samples.

1. Introduction

ZnO films doped with transition ions belong to the class of diluted magnetic semiconductors (DMS). Special attention is paid to the Co - and (Co+Al) - doped ZnO films due to possible room temperature ferromagnetism and high carrier concentration in the samples at a low content of the doped ions. However, it was established that the appearance of ferromagnetism in such materials depends strongly on the conditions of fabrication and treatment of the samples. To improve magnetic properties of the Co - and (Co+Al) - doped ZnO samples, many authors used the hydrogenation method, for example Refs. 1 and 2. However, in the works known to us, the hydrogen concentration in mixed-gas was up to 10-15%. In this work, the hydrogenated Co - and (Co+Al) - doped ZnO films are studied with 20-50% hydrogen concentration in mixed-gas.

2. Experimental procedure and sample preparation

The films were grown on glass substrate by the standard RF magnetron sputtering system using two inches $Zn_{0.95}Co_{0.05}O$ (CZO) and $Zn_{0.95}Al_{0.02}Co_{0.05}O$ (CAZO) targets. The CZO and CAZO targets were calcined at 1300 °C for 12 hours in atmosphere of flowing oxygen and 860 °C for 12 hours in atmosphere of flowing argon gas. The films were deposited at a total pressure of 30 mTorr and a forward RF power of 80W at the substrate temperature 450 °C for 20 minutes. Five samples of each composition were prepared with the following mixed gas in the chamber: Ar+20% O_2, Ar+(20%, 30%, 40%, 50%) H_2, samples CZO1, CZO2, CZO3, CZO4, CZO5, and CAZO1, CAZO2, CAZO3, CAZO4, CAZO5, respectively.

MCD was measured in the normal geometry: the magnetic vector and the light beam were directed normal to the films plane. The modulation of the polarization state of the light wave from the right-hand to the left-hand circular polarization relatively to the magnetic field direction was used. The MCD value was measured by the formula $MCD=(D_+-D_-)/d$, where D_+ and D_- are the optical density of the films for right and left polarized waves, and d is the films thickness. Measurements were carried out in the spectral range 1.2-4.5 eV in a magnetic field up to 13 kOe at the temperature 300 K.

3. Results

Data of the X-ray fluorescent analysis (XRFA) and electron probe microanalysis (EMP) for the CZO and CAZO films shown the increase of the Co content relative to the Zn content in the films. For the example, from 0.052 for CZO1 to 0.390 for CZO5 films. Such behavior is similar for the CAZO films. However, the growth of the Al content in them is also expected. At the same spraying time of the targets, a large difference in the thickness of the deposited films is noticeable. The films thickness decreases from 160 nm for CZO1 to 32 nm for CZO5, and from 99 nm for CAZO1 to 14 for CAZO5.

Special attention was paid to the MCD spectra measured in the visible range at the room temperature. The MCD spectra for the hydrogenated CZO and CAZO films are characterized by the intense signals of the different signs (for example, Fig. 1a). With increasing H_2 concentration a rearrangement of the MCD spectra is observed. At that, the MCD dependence on external magnetic

field is described by hysteresis loop in the whole investigated spectral range. Such behavior indicates the presence of room temperature ferromagnetism in the samples.

The MCD spectra and the MCD magnetic field dependencies for the Co - and (Co+Al) - doped ZnO films were compared with that for the Co particles [3] ion-synthesized in the amorphous matrix of silicon dioxide (Fig. 1b). The MCD spectra for the Co - and (Co+Al) - doped ZnO films were decomposed into several components. The intensity dependence of these components on hydrogen concentration was traced.

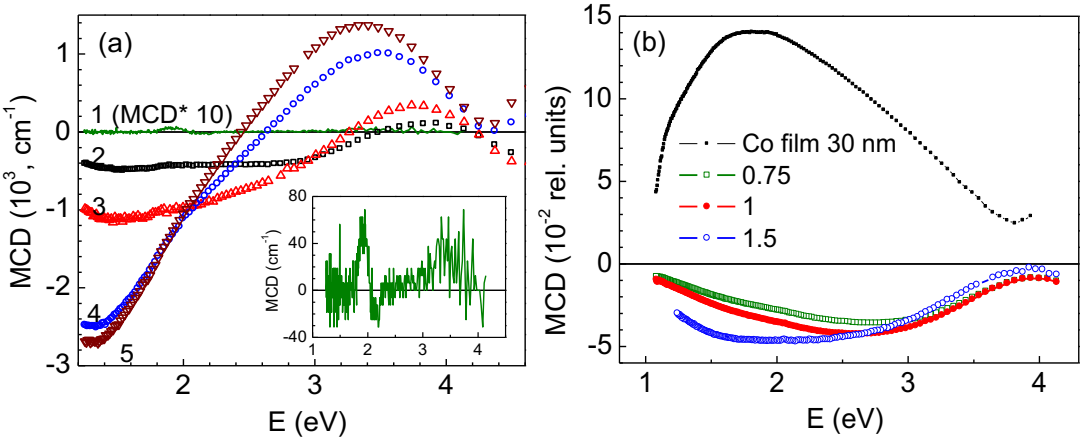

Fig. 1. a – MCD spectra for CZO1-CZO5 samples, curves 1-5, respectively, measured at H = 13 kOe and T = 300 K. Insert: the magnified MCD spectrum for CZO1. b – MCD spectra measured at H = 3 kOe and T = 300 K for the Co^+ implanted samples with ion current densities j=8 μA/cm^2. Black lines show MCD spectra for the thin films of Co measured at T = 300 K and H = 3 kOe.

Conclusions

An extremely strong effect of hydrogen on morphology, composition, and magnetic properties of the samples was revealed. The main tendency of the strong Zn content decrease in the films and their thickness with the growth H_2 concentration was observed. Unlike the CZO and CAZO films synthesized in atmosphere Ar+O_2, the hydrogenated CZO and CAZO films exhibit ferromagnetic behavior at room temperature. The complex nature of magnetism with a combination of the intrinsic ferromagnetism (due to the formation of the Co-H-Co complex) with the ferromagnetic inclusions is assumed in the investigated films. The nature of these ferromagnetic inclusions as well as the mechanism of influence of hydrogen concentration on the magnetic properties of the samples are discussed.

References

[1] Lee S., Cho Y.Ch., Kim S.-J., et al., Reproducible manipulation of spin ordering in ZnCoO nanocrystals by hydrogen mediation, Appl. Phys. Lett. 2009, **94**, 212507

[2] Park J.H., Lee S., Kim B.-S., et al., Effects of Al doping on the magnetic properties of ZnCoO and ZnCoO:H, Appl. Phys. Lett., 2014, **104** 052412

[3] Petrov D.A., Edelman I.S., Ivantsov R.D., et al., Magneto-optics of cobalt and nickel nanoparticles implanted in SiO_2: comparative study, Sol. St. Phen., 2014, **215**, 214-217

DEVELOPMENT OF FLEXIBLE FINGERTIP USING MAGNETIC FUNCTIONAL FLUID

N. Yamashita[1,a], I. Murakami[1,c], Y. Ando[1,b], Long Bui Si[1,d]

[1]Dept. of Mechanical Science and Technology, Gunma University. 1-5-1 Tenjin-cho, Kiryu. 376-8515, Japan
[a]t15302114@gunma-u.ac.jp, [b]murakami@gunma-u.ac.jp [c]ando@gunma-u.ac.jp,
[d]t181b063@gunma-u.ac.jp

Abstract. In manipulators, grippers using flexible materials have beendeveloped extensively. By using a flexible material, it is possible to grasp easily breakable objects and objects with different shapes. In this research,we developed two grippers withfingertips thatrespective used two kind of magnetic functional fluid. Then, we checked its performance by making it grasp various objects. This aims to grasp objects of various shapes without breaking them.

1. Introduction

Recently, there are many studies using flexible materials for the gripperattached to the tip of the manipulator. This is because, by using a flexible material for the gripperit is possible to grasp easily breakable objects and objects with different shapes. In addition, by using a flexible material, even if there is an error in the position of the object, the gripper's fingertipscan be flexibly deformed to enable grasping.

In this research, we developed two types of grippers that used two respective types of magnetic functional fluid, namely magnetic fluid and Magnetorheological(MR) Fluid.. In which, a flexible fingertip control by magnetic field is developed and used for gripping. This aims to grasp objects of various shapes without breakage or damage them.

2. The flexible fingertip structure

Fig. 1 shows the structure of the created flexible fingertip. The flexible fingertip consists of ①upper jig, ②rubber bag containing magnetic functional fluid, and ③electromagnet. Here, two types of flexible fingertips were created: one in which magnetic fluid is enclosed in a rubber bag and one in which MR fluid is enclosed.

Next, Fig. 2 shows the structure of the used electromagnet. This electromagnet is installed with a permanent magnet at the center, and when current is applied in the direction to weaken the magnetic force of this permanent magnet (negative direction), the magnetic flux density on the surface decreases. On the other hand, when the current is applied in the direction to strengthen the magnetic force (positive direction), the magnetic flux density on the surface increases. Here, in order to confirm the performance of the electromagnet, the absolute value of the magnetic flux density was measured when the value of the current supplied to the electromagnet was changed at the center of the surface of the electromagnet.The measurement result is,the absolute value of the magnetic flux density was minimum around -2.5 [A], and reached maximum175.3 [mT] at 3 [A].

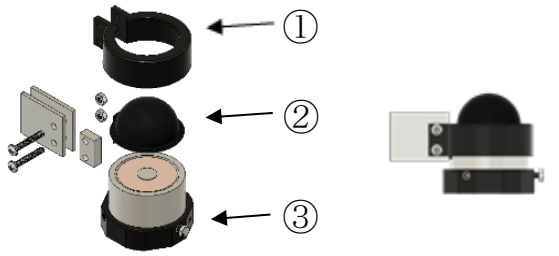

(a) deal drawing (b) assembly drawing

Fig.1. Strucrure of gripper'sflexible fingertip

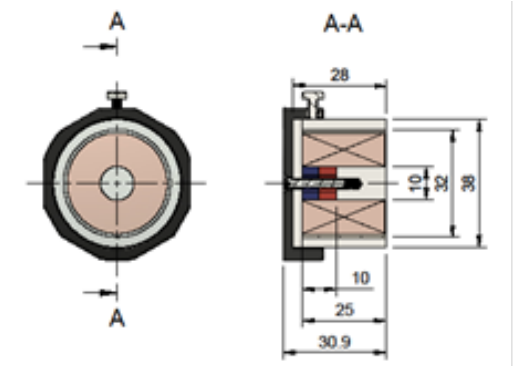

Fig.2. Structure of electromagnet

3. Experiment with robot hand using flexible fingertips

We made a 3-finger gripper using the created flexible fingers. The appearance is shown in Fig.3. An experiment was conducted to confirm whether the developed flexible fingertip cangraspobjects using this gripper. In order to confirm that objects of various shapes can be grasped, we performed gripping experiments of 10 types of objects summarized in Table 1. Fig.4 shows the overview of the experiment.

In this grasping experiment, first, a current of -2.5 [A] was supplied to the flexible fingertip to reduce the magnetic field applied to the flexible fingertip. In that state, it moved on the object and pulled a wire for opening and closing the gripper with a constant force by a motor. Next, after the gripper stopped moving further, the current was switched from -2.5 [A] to 2.5 [A]. Finally, the gripper was lifted, and if the object did not fall, the object was grasped successfully.

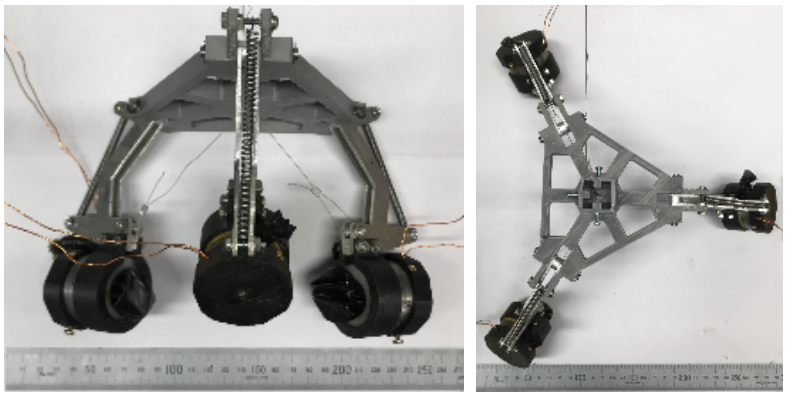

(a) Sideview (b) Topview

Fig.3. Gripperusing soft fingertips

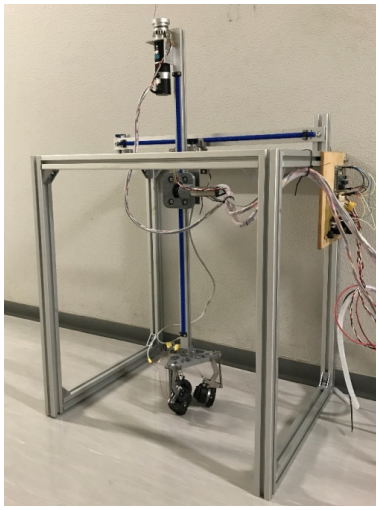

Fig.4. Overview of the experiment

Table 1 Objects gripped by robot hand

	Object Name	mass [g]	Use magnetic fluid	Use MR fluid
(a)	Hard tennis ball	57	○	○
(b)	Soft tennis ball	30	○	○
(c)	Empty plastic bottle	24	○	○
(d)	OPP tape	119	○	○
(e)	Paper cup	5	○	○
(f)	Resin spur gear	180	○	×
(g)	Raw egg	58	○	○
(h)	Strawberry	23	○	○
(i)	1/4 cut squish	280	○	○
(j)	Broccoli	248	×	×

Conclusion

In this research, we have successfully developed fingertips that used magnetic functional fluid.Then, the experiment to investigate the influence of the magnetic fluid and checked its performance by making grippers using those fingertips. It was confirmed that various objects can be lifted using the developed gripper.

References

[1] Brown E., et al. Universal robotic gripper based on the jamming of granular material, *PNAS,* Vol. 107 No. 44 (2010), pp. 18809-18814.

[2] Deimel R., Brock O.A. Compliant Hand Based on a Novel Pneumatic Actuator, 2013 IEEE International Conference on Robotics and Automation, (2013).

DOES EVOLUTIONARRY IMPROVEMENT OF CARS IS SUFFICIENT TO NEUTRALISE THEIR IMPACT IN POLLUTION AND CLIMATE CHANGE OR DO WE NEED A JUMP TOWARD NEW TECHNOLOGIES?

Konstantinos N. Spentzas[1,a]

[1]*Chief Academician Secretary of the EuroMediterranean Academy of Arts and Sciences*
[a]k.n.spent@gmail.com

Pollution of the environment and climate change reached a dramatic point last years because of the increas of emissions of combustion gases, and mainly of CO2.

According to data published in the web page of OICA (International Organisation of Automobil Manufacturers) Road Transport (use of cars, trucks and buses) is responsible for the 15.9 % of total CO2 emissions [1].

Public authorities as well as the automotive industry are trying to reduce the emissions comming from the use of vehicles. For this, regulations specifying the emission limits become stricter and an evolution technique is used in the production of newer models of cars: the new models have lower emissions, but are coming from the previous ones, without a revolution in the applied technology.

However, the effect of this (slow evolving) policy is partially neutralised:

a) By the increase of the fleet of road vehicles in use. Statistical data are given in the following References: paseenger cars [2], commercial vehicles [3] and all vehicles [4]. We can notice that between 2005 and 2015 the number of vehicles in use has incresed by more than 40% [4].

b) By the very low subtitution rate of older vehicles by vehicles of lower emissions. The average age of vehicles in use is really despointing for many EU countries [5].

In the present paper the author discusses the above problems and supports the opinion that we do not have anymore time to loose by applying policies that are facing the problem slowly. We need to take the following drastic measures:

a) Make a jump towards new technologies in order to design and produce non polluting cars.

b) Give attractive incentives in order to boost the substitution rate of all vehicles in use by vehicles designed on the basis of absolutely new technologies and not by evolutionary improvement of pre-existing cars.

A technological jump has already been made by the author and his team since 2005, when they have presented the prototype of a revolutionary car [6-11]: it is a very light solar/battery electric car that uses linear motors for its motion and which, with the exception of the body and the wheels, most of the other mechanical sytems have been substituted by electronic ones. For example there are no transmission axes, no differential and no gear box, because they are substituted by the linear motors system and an electronic box that functions also as an electronic differential [12]. The steering can be realised by variation of the turning speed of the wheels: for example, to turn left, the right wheels are made to turn faster than the left ones. In the limit, we can even make the left wheels to turn backwards in order to turn on the spot and reach unthinckable levels of manouvering ability.

The car presented above uses existing technologies which have never been previously applied in cars. For example, linear motors are already in use in trains, and *on the spot turning* is used in belt driven vehicles since very long time. The electronic differential concept has been introduced by the author and his team already since 2001 [12].

References

[1] http://www.oica.net/category/climate-change-and-co2/
[2] http://www.oica.net/wp-content/uploads//CV_Vehicles-in-use.pdf
[3] http://www.oica.net/wp-content/uploads//CV_Vehicles-in-use.pdf
[4] http://www.oica.net/wp-content/uploads//Total_in-use-All-Vehicles.pdf
[5] https://www.eea.europa.eu/data-and-maps/indicators/average-age-of-the-vehicle-fleet/average-age-of-the-vehicle-8 ; https://www.eea.europa.eu/downloads/5d71ba46be6d498197ddc66a880032e8/1520597309/average-age-of-

the-vehicle-8.pdf;
[6] Konstantinos N. Spentzas & Georgios Michael, A minimalist approach to the design of electric vehicles, Proceedings of the 21th International Electric Vehicle Symposium (EVS 21), Monaco, 2-6 April 2005, paper No 41.
[7] Spentzas K.N. and Michael G.: A minimalist approach to the design of electric vehicles, WSEAS / IASME Transactions, Vol. 2, Issue 3, pp. 400-405, May 2005.
[8] Spentzas K., Michael G. and Demić M.: A minimalist approach to the design of electric vehicles, Invited paper in the International Scientific Congress Motor Vehicles and Motors MVM 2006, Kragujevac, Yugoslavia, 4-6 October 2006.
[9] Spentzas K., Michael G. and Demić M.: A minimalist approach to the design of electric vehicles, Mobility and Vehicle Mechanics-The International Journal for Vehicle Mechanics, Engines and Transportation, Vol. 32, No. 3 & 4, pp. 30-36, September-December 2006.
[10] Spentzas K.N., Michael G., and Ioannou D.S.: A minimalist approach to the design of electric vehicles – what can vehicles be in the future?, International Advanced Mobility Forum, organized during Geneva International Motor Show, Geneva, 9-10 March 2010.
[11] Mamalis A.G., Spentzas K.N., Pantelelis N., Michael G., Vrouvakis T., Kouzilos G.: On the design and structural analysis of electric vehicles, Proceedings of the International Crashworthiness Conference ICrash 2012, Milano, Italy, 18-20 July 2012.
[12] Spentzas K.N., and Alkhazali I.: Generalisation of the concept of electronic differential, International Journal Forschung im Ingenieurwesen, Band 66, Heft 6, Oktober 2001, pp. 273-278, Springer-Verlag.

EFFECT OF HEAT TREATMENT ON THE STRUCTURE, MAGNETIC AND THERMOELECTRIC PROPERTIES DY0.2SR0.8COO3-Δ

Viacheslav Dudnikov[1,a], Yuri Orlov[1,b], Leonid Solovyov[2,c], Sergei Vereshchagin[2,d], Sergei Novikov[3,e], Victoria Kuznetsova[3,f], Sergei Gavrilkin[4,g], Sergei Ovchinnikov[1,h]

[1]Kirensky Institute of Physics, Federal Research Center KSC SB RAS
[2]Institute of Chemistry and Chemical Technology, Federal Research Center KSC SB RAS
[3]Ioffe Physical-Technical Institute
[4]Lebedev Physical Institute, RAS
[a]dudnikov@iph.krasn.ru, [b]jso.krasn@mail.ru, [c]leosol@mail.ru, [d]snv@icct.ru, [e]S.Novikov@mail.ioffe.ru, [f]v.kuznetsova@mail.ioffe.ru, [g]gavrs@sci.lebedev.ru, [h]sgo@iph.krasn.ru

Abstract

Magnetic and thermoelectric properties of perovskites Dy0.2Sr0.8CoO3−δ, with ordered and disordered states of Dy and Sr in the A-sites of the crystal lattice have been studied revealing remarkable differences in the physical properties of the ordered and disordered states. The ordered samples have larger oxygen nonstoichiometry, abnormal temperature dependence of the magnetization around 350 K and more thermoelectric stability at high temperature region. A number of transformations from the perovskite structure into a composite material consisting of the Ruddlesden-Popper family (n=2, RP-2) phase and cobalt oxide, as well as from the RP-2 phase and metallic cobalt, were investigated. The physical properties of these materials have also been investigated.

STUDY OF GENETIC ANALYSIS OF MUTATIONS IN BRAF, NRAS AND HRAS GENE IN THYROID CANCER PATIENTS OF GEORGIA BY USING PROGRAMMING LANGUAGE

Sahar Abd Elmogheth Madani[1,a], Irina Gotsiridze[1,b]

[1]Faculty of Informatics and Control Systems, Biomedical Engineering, Georgian technical university, Georgia.
[a]a_sahar24@yahoo.com, [b]irgocci@gmail.com

Abstract

Genetic change is the main force of thyroid tumor development, based on new methods of managing thyroid cancer. The latest significant genetic discovery in thyroid cancer is the BRAF-T1799A (V600E) transformation (the gene for B-type RAF kinase, BRAF). Since the initial report of this breakthrough in thyroid cancer years ago, rapid progress has been made. The BRAF mutation is the most common genetic change in thyroid cancer. We evaluated BRAF, NRAS and HRAS mutations in Georgian patients with indeterminate cytology or diagnosed with papillary thyroid cancer (PTC).

BRAF (V600E), NRAS (G12C, G12D, Q61R, and Q61K) and HRAS (G12C, G13R, and Q61R) were determined in the DNA extracted from fine needle aspirate specimens. In total, 130 patient samples were analyzed using TaqMan PCR (Cast PCRTM). In these samples, 45 were diagnosed as papillary thyroid carcinoma, and 85 were indeterminate by Bethesda System for Reporting Thyroid Cytopathology (BSRTC III-V).

BRAF (V600E) mutation was the most frequent genetic alteration found in 31% of all analyzed samples. Specifically, this mutation was present in 61% of PTC cases and 18% of cases classified as indeterminate (BSRTC III-V). NRAS mutations were present in 16% of PTC and 30% of indeterminate cytology samples. NRAS G12D and Q61R were most prevalent at 22% and 25% of all NRAS mutations. BSRTC IV category of indeterminate cytology had the highest frequency of NRAS mutations at 43%. From analyzed samples, HRAS (Q61R) mutation was present in one PTC case. Finally, 29 out of 45 PTC cases were positive for the mutations indicating 81% of diagnostic sensitivity of the test.

SUSTAINABLE DESIGN OF MOBILE TRANSILLUMINATOR VEIN FINDER DEVICE

Tohid Talebifar[1,a], Irina Gotsiridze[1,b]

[1]*Georgian Technical University, Department of Biomedical Engineering, Tbilisi, Georgia.*
[a]*tohid.biomedeng@gmail.com*, [b]*i.gotsiridze@gtu.ge*

Abstract- around Up to 80% of all patients admitted to hospitals worldwide will have a peripheral intravenous line inserted in the forearm or hand to administer fluids, medications, and blood products. Because PIVC is a common procedure, it is easy to forget the potential for serious complications and safety risks to the patient, as well as to the medical staff. Vein finder devices drastically reduce the amount of time it takes to find a vein. They eliminate wasting needles, syringes, PICC and midline trays on stick after stick. They are non-invasive because all they do is make use of light so you can see veins in subcutaneous tissue. In this article we try to show our work in sustainable design of this type of devices. Our desire is to have Echo-design with low price for Georgian medical market. We use Minimal and simplicity design theory in our structural model to strip down our design to fundamental elements as possible as we can, to reduce material and manufacturing cost of our device.

Keywords: Product Design- Sustainable Design-Transilluminator Vein Finder -Ecodesignn-Minimal Design

1. Introduction

Around Up to 80% of all patients admitted to hospitals worldwide will have a peripheral intravenous line inserted in the forearm or hand to administer fluids, medications, and blood products. Sometime this procedure can be difficult for paramedics or others in such cases like infants and elderly people [1]. Vein finder devices drastically reduce the amount of time it takes to find a vein. They eliminate wasting needles, syringes, PICC and midline trays on stick after stick. They are non-invasive because all they do is make use of light so you can see veins in subcutaneous tissue [2]. The important thing is that because this type of devices are not mandatory in PIVC procedure our device must be have economic price. If the price will be too much maybe medical parts do not want to buy it. So price has an important issue for presenting this devices to medical part especially in developing countries medical market.

Theory of Transilluminator Vein Finder device:

Fact 1: As you can see in Figure 1-left Here we have Absorption spectra of the oxygenated and deoxygenated hemoglobin molecules. So in region between 600 nm to 800 nm deoxygenated hemoglobin (Hb) absorbs more light compare to oxygenated one (HbO_2).

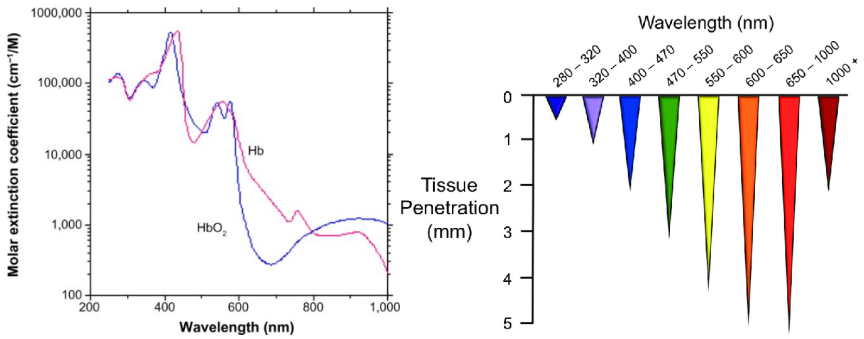

Figure 1. Left: Absorption spectra of the oxygenated and deoxygenated hemoglobin molecules, Right: Penetration depth of light of different wavelengths in skin tissue.

Fact 2: In Figure 1-right. You can see penetration depth of light of different wavelengths in skin tissue. So infrared red light has penetration about 4-5 mm in skin.

Result: Infrared red light is a good candidate for visualization of superficial veins for PIVC procedure.

2. Methodology

Engineers follow a process to make new products.[3] The engineering design process is a series of steps that engineers follow to come up with a solution to a problem.

The steps of the engineering design process are to: [3]

- Define the Problem
- Do Background Research
- Specify Requirements
- Brainstorm Solutions
- Choose the Best Solution
- Do Development Work
- Build a Prototype
- Test and Redesign

Also we use Minimal and simplicity design theory in our structural model to strip down our design to fundamental elements as possible as we can, to reduce material and manufacturing cost of our device.
Minimal design [4]:

- Strip down our design to fundamental elements.
- Simple functionality and user interaction.

3. Results & Conclusions

Now we present our design model. It is necessary to mention that this is primary design and it will be developed and improved in future work. As we mentioned in minimal design we try to strip down our design to fundamental elements. So here we strip down our device element into 2 main parts;
1- Arms: LED Transilluminator, Illustrate Red LED light to locate Veins as a shadow line between two arms.
2- Body structure: this part has 2 main function; first it contain electrical charging part and second it help users to handling device in comfortable and proper manner.
Now here in Figure 2-left. We can see our first structural model of our device. In the figure 2-midle first physical model for experiments and in figure 2-right we can see shadow of veins in picture when we use devices on arm in dim light room.

Figure 2. Left: Structural model of device, Middle: First physical model, Right: First experiment of device on case

We use 2 coin battery (Sonny 3 volts lithium cell- CR2032) and 2 red LED (LED 614 LD08-R HU-B 8000.MCD 30`) with 8000 MCD for illumination.

Conclusion

We use minimal design to reduce materials (in production and also when we use disposal plastic cover for operating our device in patient cases) to have an ecodesign. Device can work in dim light situation but the maximum penetration in about 4-5 mm. For future work we hope we can work on NIR device with cheap price and in most effective practical way.

References

[1] Peripheral vein locating techniques/ Gali Cantor-Peled, Moshe Halak & Zehava Ovadia-Blechman/ Department of Medical Engineering,Afeka Tel Aviv Academic College of Engineering, Tel Aviv, Israel/Department of Vascular Surgery, Sheba Medical Center.-
[2] https://thingsnurseslike.com, June 2018.
[3] https://www.sciencebuddies.org/science-fair-projects/engineering-design-process-guide /Jan. 2019.
[4] https://designshack.net/articles/layouts/minimal-design-how-to-design-more-with-less/ June 2019.

MEDICAL SIMULATION TRAINING SYSTEM WITH APPLICATION OF UNITY

Donghak Kim[1,a], Irina Gotsiridze[1,b], Zviad Gurtskaia[1,c]

[1]*Georgian Technical University, Georgia*
[a]donghak.kim@gtu.ge, [b]irgocci@gmail.com, [c]z.gurtskaia@gtu.ge

As computer technology advanced, the computer-based simulation has become popular and computer-based simulation training has been adopted in training professionals in other industries such as military, law enforcement, transportation and athletics. Healthcare was not an exception.

Simulation training was adopted to train medical professionals for many procedures and surgeries. Coronary angiography is one of the procedures and surgeries that have been simulated for training medical professionals. Traditional training of coronary angiography happens in a catherization lab, which requires physical resources such as space for lab, C-arm and X-ray intensifier, as well as human resources such as experienced trainers, and patients. The simulation training system was developed to reduce the physical and human resources and training time.

Another purpose of the development of this system was for an affordable training system for medical schools and institutions. For this purpose, it is essential to use free development tools.

Unity is the best development tool to achieve these purposes. Unity is a free cross-platform game engine and used for video games, simulations for computers, consoles and mobile devices. For the development of simulation training system for coronary angiography, Unity provides a physics engine in addition to a game engine. Its game engine offers easy programming for GUI and computer graphics. The movements of catheter and guidewire in arteries was simulated with the physics engine that provides a mass-spring model.

The computer-based simulation training system was developed with Unity for coronary angiography. The catheter and guidewire were modelled after a mass-spring model. Their movements were simulated with the physics engine of Unity. The contrast dye injection was also simulated in the coronary arteries. The flow of the contrast dye in coronary arteries is recorded so that the results of coronary angiography can be reviewed later. This system is capable of serial communication with other control devices through which catheter and guidewire can be controlled.

This simulation training system can be used in medical schools and hospitals to train medical students and refresh medical professionals' knowledge and skills. It is also useful for educators to teach medical students. For students, this system can be a learning tool to prepare themselves for coronary angiography.

Key words: Simulation Training, Coronary Angiography, Unity

ESTIMATION OF PARAMETERS FOR A MODEL OF POLYCRYSTALLINE SOLAR CELLS

J.J. Shainidze[1,a], L.G. Kalandadze[1,b], O.M. Nakashidze[1,c], N.KH. Gomidze[1,d]

[1]*Department of Physics, Batumi Shota Rustaveli State University, Batumi, Georgia*
[a] jabashainidze@gmail.com , [b] lali.kalandadze@bsu.edu.ge , [c] omar.nakashidze@bsu.edu.ge ,
[d] gomidze@bsu.edu.ge ,

Abstract. In many countries of the world the main factor for increasing energy potential and saving environment is applying non-conventional energy. Renewable energy is mostly connected with solar radiation. Above all, mastering solar energy depends on technological advancement. Main goal of scientists is to increase efficiency of photoelectric converting system and decreasing its cost. The parameters are required to be correctly computed from solar cell characteristic or a set of experimental data for control of the photovoltaic (PV) system. However, experimental data or accurate characteristic data (i.e. current-voltage or I-V curve) of a PV module may not be readily available. The present paper describes calculations of solar cell parameters, based on polycrystalline silicon, using experimental and theoretical approaches. Finding appropriate circuit model parameters of solar cells is crucial for performance evaluation, control, efficiency computations and maximum power point tracking of solar PV systems. Based on the conducted review, some suggestions are provided.

1. Introduction

Mastering of solar energy is directly connected with development of technology. Main goal of scientists is to increase efficiency and decrease price of photoelectric converter. New structures are introduced based on Silicon, which makes possible to decrease optical and recombination losses [1-3]. A solar cell or photovoltaic (PV) module is electrically represented by an appropriate circuit model with specific parameters. The parameters are required to be correctly computed from solar cell characteristic and a set of experimental data control of the PV system. Efficiency of photoelectric converter is defined by its current-voltage characteristics and it is one of the most important parameters. Based on polycrystalline Silicon, using theoretical and experimental methods we studied following parameters of solar cell: current-voltage dependence, short circuit current (I_{SC}), open circuit voltage (V_{OC}), fill factor (FF) and conversion efficiency [1-5].

2. Theory

Theoretical calculations were made based on standard parameters of crystalline silicon. I_{SC}=350 μA, V_{OC}=0,67 V. Assuming that the solar cell behaves as an ideal diode, the fill factor can be calculated as a function of open circuit voltage V_{OC} [4-7]:

$$FF = \frac{v_{oc} - \ln(v_{oc}+0{,}72)}{v_{oc}+1} = 0{,}84 \quad (1)$$

where

$$v_{oc} = V_{oc} \Big/ \frac{k_B T}{q} = \frac{0{,}67\ V}{0{,}0258\ V} = 26{,}8 \quad (2)$$

is normalized voltage.

The conversion efficiency is calculated as the ratio between the maximum generated power and incident power:

$$\eta = \frac{I_{SC} \cdot V_{OC} FF}{I_{in}} = 19{,}7\% \quad (3)$$

where I_{in} is irradiance of incident light in AM1.5 spectrum.

3. Experiment

Experiments were performed on regular solar cell, found on market, with following characteristics: sample manufacturer – NUZAMAS, dimensions - 90x60x2mm, V_{max}=6 V, P_{max}=0,6 W. Using multi meter we measured V_{OC}, I_{SC}, I_{mpp} (current at maximum power point), V_{mpp} (voltage at maximum power point) and by changing resistance measured current voltage at different values of external resistance.

As a result: I_{SC}=49,9 μA, V_{OC}=5,3 V, I_{mpp}=34,8 μA, V_{mpp}=3,9 V. Using these results fill factor and conversion efficiency (η) were calculated:

$$FF = \frac{(V_{mpp} \cdot I_{mpp})}{(I_{SC} \cdot V_{OC})} = \frac{3{,}9 \cdot 34{,}8}{49{,}9 \cdot 5{,}3} = 0{,}51 \quad (4)$$

$$\eta = \frac{I_{SC} \cdot V_{OC} \cdot FF}{I_{in}} = \frac{49{,}9 \cdot 5{,}3 \cdot 0{,}51}{1000} = 0{,}13 = 13\% \quad (5)$$

Volt-ampere characteristics of the solar cell are shown on Fig.1:

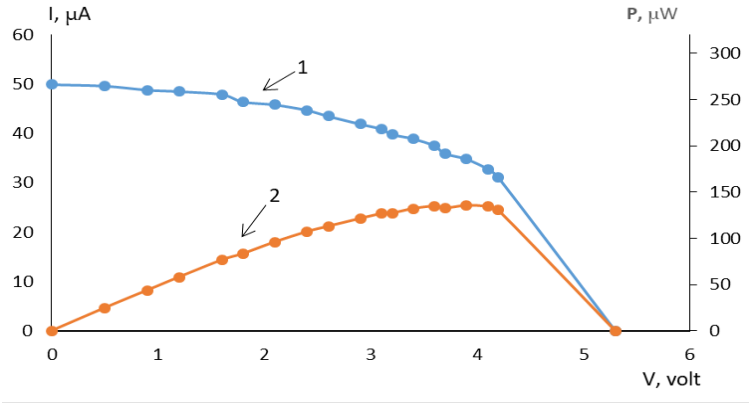

Fig.1. Dependences of the Electric Current (1) and Power (2) on the Voltage for the polycrystalline solar cell.

Conclusions

Solar cell parameter's dependence on photoelectric properties of semiconductor were studied. Using experimental results, volt-ampere characteristic chart was created and from this chart short circuit current, open circuit voltage, fill factor and conversion efficiency were defined. Polycrystalline Silicon Solar Cell parameters were calculated theoretically. Theoretical and experimental results showed that, ordinary solar cells, found on market, have low fill factor and conversion efficiency and in most cases they produce less electric current and voltage than according to the model description from the manufacturer datasheet. The manufacturer of a PV system usually provides information on open circuit voltage, short circuit current and maximum power points. Though knowing specific parameters (fill factor (FF) or conversion efficiency) of PV cells is crucial for performance evaluation, control, efficiency computations and maximum power point tracking of solar PV systems.

References

[1] Smets A., Jäger K., Isabella O., Swaaij R. V., Zeman M., Solar Energy UIT Cambridge, 2016
[2] Avsajanashvili G., *Solar energy and Helioresources*, TSU, Tbilisi, 2014
[3] Shockley W, Electrons and holes in semiconductors with applications to transistor electronics, New York, 1950
[4] Green M.A., *Solar cells: Operating principles, technology, and system applications* (Prentice-Hall, Inc., Englewood Cliffs, NJ, USA, 1982)
[5] Afanassiev V.V., Terukov E.I., Sherchenkov A.A., *Silicon Based Thin Film Solar Cells*, Moscow, 2016
[6] Bessel V.V., Kucherov, V.G., Mingaleeva R.D., *Study of Solar Photoelectric Cells*, Moscow 2016
[7] Kosiachenko L.A., Grushko E.V., *Open circuit voltage, fill factor and conversion efficiency of Cds/CdTe – solar cell, physics and technology of semiconductors*, 2010

IMPACT OF ELECTROHYDRAULIC PROCESSES UPON LIGHTNING PROTECTION OF THE BUILDINGS CONSTRUCTED ON HIGH WATER GROUNDS AND ONSHORE FACILITIES

Maia Tugushi[1,a], Gizo Partskhaladze[2,b], Madona Loria[3,c], Gocha Chavleshvili[4,d], Boris Karasiev[5,e]

[1]Batumi State Maritime Academy, Batumi, Georgia;
[2]Batumi Shota Rustaveli State University, Batumi, Georgia
[a]tugushi@mail.ru, [b]gizopar5@yahoo.com, [c]madona.loria@bsu.edu.ge, [c]gocha.chavleshvili@bsu.edu.ge, [d]kara-boris@yandex.com

Abstract. Many international lightning protection standards allow and even require to connect electrical circuitry of grounding circuits/contours with grounding of lightning conductors ([5], [6], [7], [8]). Appropriate grounding and connection are based on the system, which contains grounding (dispersing electricity in the soil) and connecting network (minimizing the difference of electrical potentials and decreasing magnetic field).
The novelty of the research described in the paper is presented by study related with correlation between a famous physical phenomenon the Yutkin (EHB) effect and lightning protection, which may take place in case of lightning at the construction sites, equipped with the outer lightning protection and being constructed on high water grounds or along the shores.

1. Introduction

The contents and moisture of the Earth are not homogeneous. The electrical resistivity of the Earth changes horizontally and in depth.

Depending on the importance of the site, existence and classes of explosion and fire sensitive zones in the industrial buildings, and also taking into consideration possibility of lightning, one of three existed categories of lightning protection is applied ([2], [3], [4]).

The categories of lightning protection standards do not foresee the peculiarities of the buildings constructed on high water grounds or along the shores. Concrete in dry ground is a good insulator. However, concrete buried in the ground has a resistivity that does not exceed several hundred Ohm.m.

Between the grounded pedestal (being in water or in liquid bog soil) and soil basement lighting may through water (bog soil liquid) cause high-voltage discharge provoking electro hydraulic blow (EHB) [1]. Pressure of tens and hundred thousand atmosphere is immediately created at the place of discharge [9]. The foundations of the buildings constructed on high water grounds or along the shores are badly damaged due to electro hydraulic blow.

When fulfilling the requirements for lightning protection, without the recognition of specific (local) climatic conditions and physical processes / phenomena when lightning strikes, the installed lightning rod can cause unexpected destruction of the protected object.

2. Experimental procedure

For the experiment, the foundation models were prepared: Model N1 - 400x400x230 mm^3; Model N2 - 500x490x190 mm^3; Model N3 - 290x290x180 mm^3; The model is -210x190x190 mm^3. As shown experiment in dry ground with a multiple high-voltage discharge (10kV) in the basement of the foundation, no special damage was detected.

A similar experiment was carried out in a wet environment - the foundation model was immersed in fresh and salty (0.6%) water and a high-voltage electric discharge was applied to it. If the foundation is wet and a few millimeter water medium forms between the reinforcement bars and the concrete, there is a danger of formation of an EHB. The same effect is obtained if the lightning is discharged in the water near the basement. The water surrounding the spark spreads with great rapidity to the sides, creating the first hydraulic impact. A void is formed - a cavity that is immediately filled with water; another powerful hydraulic shock is produced - cavitation. The electric discharge of a lightning, thus, can provoke an explosion capable of destroying the foundation.

3. Results of experiments

The results show that the closer the high-voltage wire / electrode to the foundation the damage is larger: rod of armature received strong oxidation; damage to the surface of the concrete model increases; the foundation reinforcement fixed washer broke away from the foundation (fig.1).

(a) (b) (c)

Fig.1.Foundation model befor (a) and after (b,c) high voltage discharge

Conclusions

The experiments were carried out at a voltage of 10 kV. With a real thunderstorm lightning, we have a voltage of several million volts, and accordingly the discharge power is much higher than in the cases considered.

Based on the results of the experiment, one can draw conclusions:

1) In the instructions / rules for the device of lightning protection of buildings and structures, it is necessary to separate the category for shore structures or for buildings in high-water grounds;

2) For shore structures or for buildings in high-water soils, it is necessary:

- apply a separately standing lightning conductor - a lightning conductor, lightning receivers and current collectors are located in such a way that the lightning current path does not have contact with the protected object;

- Observe the safe distance between the foundation and the metal objects around the foundation, which can provoke the EHB.

References

[1] Bekaev A.A., Sokovikov V.K., etc. "The use of L.A. Yutkin's effect in electrohy-draulic devices". Proceedings of the international scientific and technical confe-rence "Automotive and tractor construction in Russia: development priorities and training of personnel", Section 7, "Technologies and equipment of mechanic-assembly production" 2010, p. 27.

[2] Earthing devices, protective conductors and protective equipotential bonding conductors- ГОСТ Р 50571.5.54-2013/МЭК 60364-5-54:2011;

[3] Federal Standard No. S24.802, General requirements for ground electronic equipment;

[4] Federal Standard No. S24.809 (USA), Grounding Standard;

[5] Instruction for the device for the universal protection of buildings, structures and industrial communications, co 153-34.21.122-2003. http://www.sonel.ru/ru/biblio/standards/so_153-34.21.122-2003/;

[6] Instruction for the device for the protection of buildings and structures, РД 34.21.122-87 http://www.zandz.ru/pravila_zazemleniya/rd-34-21-122-87.html;

[7] IEEE Std 142-2007, Recommended Practice for Grounding of industrial and Commercial Power Systems (Institute of Electrical and Electronics Engineers);

[8] IEEE Std 602-1996, Recommended Practice for Electric Systems in Health Care Facilities (Institute of Electrical and Electronics Engineers);

[9] Yutkin L.A. "Electrohydraulic effect and its application in industry", 1986г. УДК 621.7.044.4.

IMPACT OF THIN NANOTECHNOLOGY COATINGS ON THE STRESS-STRAIN STATE OF THE CYLINDRICAL CLADDING MADE FROM ZR-BASED ALLOYS FOR NUCLEAR FUEL ELEMENTS

Yu. V. Romashov[1,2,a], E.V. Povolotskii[2,b], A.G. Mamalis[3,c]

[1] V.N. Karazin Kharkiv National University, Ukraine
[2] National Technical University "Kharkiv Polytechnic Institute", Ukraine
[3] Project Center for Nanotechnology and Advanced Engineering, NCSR "Demokritos", Greece
[a]yu.v.romashov@gmail.com, [b]povolotsky91@gmail.com, [c]a.mamalis@inn.demokritos.gr

Abstract. The actual problem about using the thin nanotechnology coatings for increasing operability of the cladding of nuclear fuel made from the Zr-based alloys is considered from the point of view the mechanical elastic interaction between the coating and the cladding. The mathematical model of thin coatings of the cylindrical cladding is presented in the form of especial boundary conditions for considering the equations of theory of elasticity, defining the stress-strain state of the cladding. It is shown, that thin coatings can decrease noticeably the stresses in the cladding made from the Zr-base alloys, widely used in fuel elements for nuclear reactors.

1. Introduction

Using thin nanotechnology coatings is one of the ways widely discussed to increase the operability of the cladding made from Zr-based alloys for fuel elements of nuclear reactors [1]. The main effects of application the thin coatings are connected both the properties of the coating materials as well as mechanical interacting between thick-walled and thin-walled structures, representing the cladding made commonly from the Zr-based alloys and its coatings respectively. The purpose of this research is to propose the mathematical model of mechanical interaction between the widely used cylindrical cladding from the Zr-based alloys and its thin coating made from the stainless steel as well as to estimate using this model the impact of the thin coatings on the stress-strain state of the cladding.

2. The stress-strain state of the cylindrical cladding considering with the thin coating

The cladding is commonly made from the Zr-based alloys as the cylinder with such length and ratio between the average diameter and the width of the wall, that the cladding can be considered as long and thick-walled. It can be assumed that the external impacting factors of the cladding are reduced to the internal pressure of the gases in the gap between the nuclear fuel pellets and the cladding and to the external pressure from the moving heat carrier. Considering these, the cladding is schematized as the long thick-walled axial-symmetric cylinder, like in the well-known plane problem of the theory of elasticity [2].

The thin coating of the cladding can be considered as the thin cylindrical shell, which is in the equilibrium under the radial stresses s_r from the cladding, the pressure p_a of the moving heat carrier and the circumferential forces N_t in the coating as it shown on fig. 1a. Displacements of the all point of the coating are equal to the radial displacement of the external surface of the cladding due to the thick of the coating is small. Thus, considering equilibrium of the segment of the coating (fig. 1a) with the Hooke's Law relation between the circumferential stress and strain, the radial stress on the external radius of the cladding is represented as the linear combination of the external pressure and of the radial displacement of the cladding; the multiplier at the radial displacement is depended on the Young's modulus of the material and the thick of the coating, as well as the external radius of the cladding. This representing of the radial stress on the external surface of the cladding must be considered as the boundary condition for equations of the theory of elasticity, defining the stress-strain state of the cladding. It is possible to find the analytical solutions for stresses and displacement in the cladding, considering the plane problem with this boundary condition [2], representing the model of mechanical interaction between the cladding and the coating.

3. Results for impact the thin coatings on the stress-strain state of the cladding

For researching the impact of thin nanotechnology coatings on the stress-strain state it is considered the cladding made from the Zr+1% Nb alloy with the different thick of the coatings from the stainless 18-10 type steel. The internal and external diameters of the cladding are 7,71 mm and 9,1mm respectively; the internal and external pressures are 10MPa and 16MPa; the Young's modulus of the materials of the cladding and the

coating are 96GPa and 210GPa. This data are corresponded to the VVER-1000 type nuclear reactors, widely used in the Eastern-European countries. The results for the circumferential stresses and the radial displacements in the cladding corresponded to the different thick of the coatings are presented on the fig. 1b and on the fig. 1c. These results show that the thin coatings can decrease noticeably the stresses and displacements in the cladding, which is not contradict the known data about increasing the yield strength of the cladding with coatings comparing the cladding without coatings.

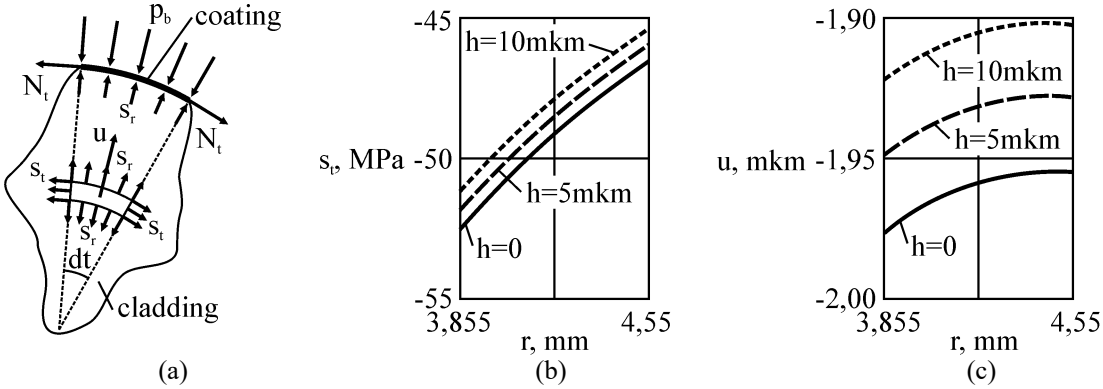

Fig.1. Schematizing of the cladding with the coating (a) as well as circumferential stresses (b) and radial displacements (c) in the cladding made from Zr-based alloy with different thick h of the coating made from the stainless 18-10 type steel

Results, presenting on the fig. 1b and fig. 1c for stresses and displacements in the cladding without the coating (h=0) are equal to well-known Lame's solution [2]. The boundary condition on the external surface of the cladding, representing the model of mechanical interacting between the cladding and the coating, reduces to well-known in the theory of elasticity boundary condition in the case of cladding with zero thick. Obtained and presented results are not contradicted with the known results [3] about impacting the coatings on the mechanical properties of the Zr-based alloy.

Conclusions

Obtained results demonstrate possibilities of noticeable impact of the thin nanotechnology coatings on the stress-strain state of the cylindrical cladding of fuel elements of nuclear reactors due to the specific of mechanical interacting between thick-walled and thin-walled structures. Using the thin nanotechnology coatings allows to noticeable decrease stresses, strains and displacements in the cylindrical claddings made from Zr-based alloys. At present, only particular results are well-known about the mechanical interactions between thick-walled and thin-walled structures. At the same time, it is necessary to fully solve the common fundamental problem about the mechanical interactions between thick-walled and thin-walled structures for realizing the all opportunities of the nanotechnology coatings on improving the cladding of fuel elements. Thus, it is necessary to develope the approaches for assessments the operability of the claddings of fuel elements considering with impact of the thin nanotechnology coatings for further widely industrial using of these coatings.

References

[1] Bischoff J., Delafoy C., Vauglin C., Barberis P., Roubeyrie C., Perche D., Duthoo D., Schuster F., Brachet J.-C., Schweitzer E. W., Nimishakavi K., AREVA NP's enhanced accident-tolerant fuel developments: Focus on Cr-coated M5 cladding, *Nuclear Engineering and Technology*, 2018, 50(2), 223-228.

[2] Timoshenko S. P. and Goodier J.N. *Theory of elasticity*, New York – Toronto – London: McGraw-Hill Book Company, 1951, 222 p.

[3] Stoev P.I., Belous V.A., Voyevodin V.N., Kuprin A.S., Leonov S.A., Ovcharenko V.D., Tikhonovsky M.A., Khoroshih V.M., Mechanical properties and acoustic parameters tubes of zirconium alloy Zr1%Nb with a protective coatings, **,** *Problems of Atomic Science and Technology*, 2015, **2(96)**, 87-97.

ELECTRODYNAMIC LEVITATION EFFECT IN VERTICAL HTSC ALTERNATORS WITH AXIAL MAGNETIC FLUX

L.I. Chubraeva[1,a], S.S. Timofeyev[1,b], V.A. Lazerko[1,c]

[1]*Institute of Electrophysics and Electric Power Engineering of RAS, Saint-Petersburg, Russia*
[a]lidiach@mail.ru, [b]sergio121@yandex.ru, [c]lazerko-vitl@mail.ru

Abstract. Vertical electrical alternators with axial magnetic flux and disc geometry of the rotor and the stator are characterized by the presence of electrodynamic force, which is acting perpendicular to the active zone elements. It depends mainly on the load angle value, magnetic flux density in the air-gap and armature current value. The presence of this force is to be accounted for during the alternator development and testing.

1. Introduction

Electrodynamic levitation in electrical alternators is based on the processes in the active zone and electromagnetic fields in the air gap. The idea of electrodynamic levitation in linear motors for trains was first discussed in [1, 2]. In [3] theoretical investigations were confirmed by experiments on a disc motor. Several years of our experimental investigation of HTSC vertical disc generators and motors shows the presence of this effect in electrical alternators with axial magnetic flux.

2. Bases of electrodynamic levitation effect

Cross-section of the disc alternator with two HTSC solenoidal armature windings positioned on both sides of the rotor with circular permanent magnets is presented in Fig. 1 and shows the levitation zone of the rotor. It represents two air-gaps between the rotor and two armatures. The 3-phase HTSC armature windings are settled on a cylindrical magnetic core of metallic glass tape. The rotor of the generator is fixed on a shaft, but presented below are general positions of its possible levitation in the air gap.

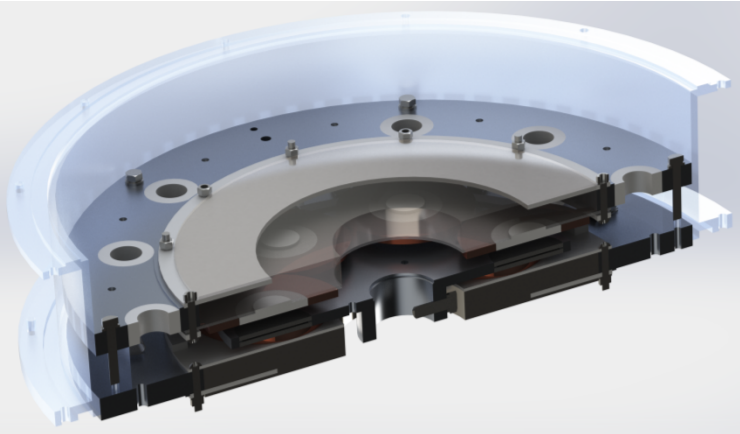

Fig.1. Presentation of the rotor levitation zone

The rotor electrodynamic levitation effect in disc alternators appears with the load angle δ. It equals zero in the no-load mode. The load angle δ depends on the armature synchronous reactance. Its maximum corresponds to $\delta = 90^0$, but from the point of view of stability synchronous alternators do not operate with the limiting load angle [4].

The density of electromagnetic forces influenced by electromagnetic fields of the alternator is determined as

$$\mathbf{f} = [\mathbf{jB}], \tag{1}$$

where j – vector of current density, B – vector of magnetic flux density.

The value of electromagnetic force Fem depends on the value and the rate of deformation of electromagnetic field in the air-gap. The latter is dependent on the load angle. The components of electromagnetic force, acting perpendicular to the air-gap F_{emx} and along it F_{emy} equal:

$$F_{emx} = iw\int_0^l B_{\delta y}dl\,, \tag{2}$$

$$F_{emy} = iw\int_0^l B_{\delta x}dl\,,$$

where i – armature winding current, w – number of turns in the armature winding, $B_{\delta x}$, $B_{\delta y}$ – components of the total magnetic flux density in the air-gap, l – armature winding coil length.

Components of magnetic flux density are determined as:

$$B_{\delta x} = B_{\delta} \sin \delta , \quad (3)$$
$$B_{\delta y} = B_{\delta} \cos \delta .$$

where B_{δ} is the sum of the rotor and stator magnetic fields under load.

3. Results of magnetic field and levitation force modeling

To calculate the levitation force of the rotor, a full-scale model of synchronous electrical alternator (the ELCUT software) was performed, the parameters of the model blocks were set, accounting for the real properties of the materials used, such as high-coercive permanent magnets, HTSC, metallic glass, etc. The finite element mesh was optimized to reduce the error of the calculations. The element of the involute of the active zone with calculation results is presented in Fig.2.

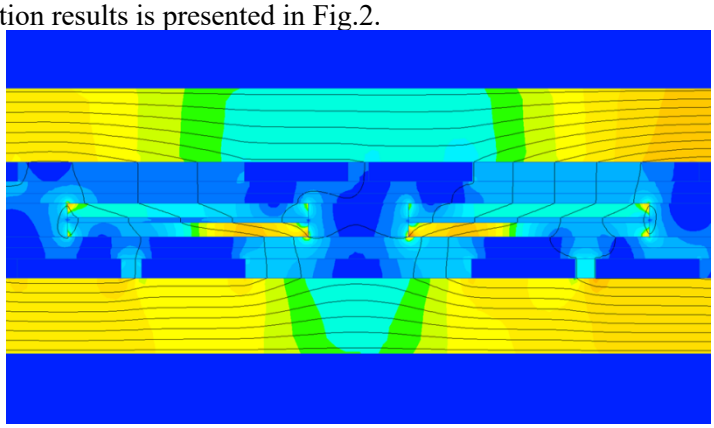

Fig.3. Magnetic field modeling of the levitation zone

Conclusions

- Electrodynamic levitation effect in electrical alternators with HTSC armature winding, high magnetomotive force of the armature and big load angle may cause problems during assembly and balancing processes. But it also opens way to an interesting version of electrical machine with a levitating rotor.

References

[1] Pawell I.R., Damby G.T. Mechanical engineering. 1967.
[2] Sloman G.R. et al. A linear synchronous motor for high speed ground transport // IEEE Trans on MAG. Vol. MAG-10, №2, February 1974. P. 435-438.
[3] Atherton D.L. et al. Superconducting linear synchronous motor tests // IEEE Trans. on MAG. Vol. MAG-13, № 1, January 1977. P. 1268-1282.
[4] Handbook on Electric Machines. S.A. Nasar. New York: McGraw-Hill Book Company, 1987. 460 p.

PREPARATION AND RELATIVE MECHANICAL STRENGTH OF ERBIUM MONOSELENIDE FILMS

Z. Jabua[1], A.Gigineishvili[1], K. Davitadze[1a], T. Minashvili[1], G. Iluridze[1]

[1]The Georgian Technical University, Department of Engineering Physics. Tbilisi, Georgia, Kostava, 77
[1a] ketevand@gmail.com

Abstract. For the first time was developed the technology of preparation of thin crystal films ErSe by method of vacuum-thermal evaporation from two independent sources of components and pre-synthesized ErSe volume material. The relative mechanical strength of the prepared films is studied by method of the complete attrition. It is shown that the relative mechanical strength of films depends on the method of preparation. Films prepared with method of discrete evaporation have considerably (30-35%) high mechanical strength, than films prepared with evaporation from two independent sources. It is possible, that it is connected to the fact that the crystalline structure of the films prepared with discrate evaporation is more perfect.

Compounds of rare-earth elements with elements of the sixth group of the chemical elements'periodic table have an interesting electrophysical, optical and other properties [1,2], but their mechanical properties have not been studied. Recently, massive attention has been drawn to the mechanical properties of films since films with interesting electrical properties often exhibit low mechanical strength, which limits their practical application. The aim of the present work has been developing a technology for preparing thin ErSe crystal films on different substrates by vacuum-thermal evaporation from two independent sources of erbium and selenium, and by the method of discrete vacuum-thermal evaporation, pre-synthesized ErSe compound and to study their relative mechanical strength using the full erasure method.

ErSe films were deposited on a substrate rectangular parallelepiped glass-ceramic with dimensions of 8x15x1 mm. Before the preparation of the films, the substrates were chemically cleaned in a mixture of nitric and hydrochloric acid and then washed with distilled water and heated in a vacuum at 650 K for 30 minutes. Experiments showed that films with good adhesion were formed on substrates treated in this way.

While the preparation of films by vacuum-thermal evaporation from two independent sources, the evaporation of Er and Se was carried out respectively at temperatures of 1250 K and 645 K, the distances from the evaporators to the substrates were 50 mm and 35 mm. The angle of slope between Er evaporator axes to the normal of the substrate surface was 25^0,of the Se evaporator - 40^0. The rate of deposition varied within ~ 35-45 Å / sec, the substrate temperature was the 650 K. The thickness of the prepared films was 1.5-1.9 μm. The source of Er was metal erbium, marked ErM-1 in which the total content of Dy, Ho, Tm and Y was 0.1%, the source material also contained Fe 0.01%, Ca 0.01%, Cu 0.03%, Ta or Mo 0.02%. The source of Se was material high purity with a Se content not less than 99.999 at%. According to X-Ray amd electron diffraction studies the films have the structure of NaCl type with lattice constant a = 5.62 ± 0.05 Å.

ErSe films were also obtained by the method of discrete vacuum thermal evaporation of a pre-synthesized material. Temperature of the evaporator was 2700K, the substrate temperature - 570 K. As well as in the first method a substrate was polycrystalline glass-ceramic. The deposition rate was ~40-50 Å/sec, the film thickness was 1.6-2.0 μm. Analysis of X-ray diffractograms and electron diffraction patterns showed that all films have the structure of NaCl with a lattice parameter a = 5.66 ± 0.05 Å, which is close to date for films obtained by vacuum-thermal evaporation from two independent source components.

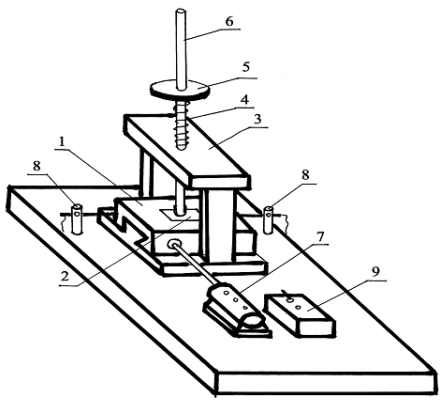

Fig.1. The scheme of installation for measurement the relative mechanical strength of films

In the presented work we investigated the relative mechanical strength of the prepared films by an complete attrition method. The essence of this method lies in the fact that the mechanical strength of the film and the degree of its adhesion to the substrate can be judged from the work that must be spent in order to completely erase the film from the surface of the substrate.The device for studying the relative mechanical strength of thin films by this method is shown in the fig. 1.

The test film (2) is attached to a massive plate (1). On the film, a rod (6) is supported from above, at the lower end where working material- a piece of suedeis attached, which is covered with diamond paste. Load on the rod is carried out by different weights placed on the disk (5). The film moves forward and backward with a special mechanism (7, 8) and counts the quantity of passes that are needed to completely erase the film. For the reliability of the result obtained, the investigations were carried out on films of the same thickness and under identical loads. The thickness of the all the studied films had the same thickness - 1.1 μm, and the load was also the same and amounted to 400 g. The data of the study of the relative mechanical strength of ErSe films prepared by a different technique on a glass-ceramic substrate are given on Table 1.

As seen from the Table, relative mechanical strength of the films prepared by the discretevacuum-thermal evaporation of the pre-synthesized material is almost 35% greater than the mechanical strength of the films prepared by vacuum-thermal evaporation from two independent sources.

Table. Relative mechanical strength of ErSe films

Method of film preparation	Film thickness, μm	Load, g	Quantity of passes to complete abrasion
Evaporation from two independent sources	1,1	400	62-67
Discrete evaporation Of pre-synthesized compound	1,1	400	112-120

Such a difference can be caused by the fact that, the crystal lattice of films prepared by discrete evaporation is more perfect than the structure of films prepared by evaporation from two independent sources.

References

[1] Gasgnier M. Rare Earth Compounds (Oxides, Sulfides, Silicides, Boron,..) as Thin Films and Crystalls. Phys. Status Solidi A. 1989. vol.114, №11, P. 11-71.

[2] Verna A.S. Electronic and optical properties of rare earth chalcogenids and pnictides.African physical review.2009,vol.3, P.11-29.

ULTRASONIC PROPAGATION WAVE VELOCITY IN MR FLUID AT MAGNETIC FIELD SWEEP RATES

Ryo Kanasashi[1,a], Yuya Tanaka[2,b] and Tatsuo Sawada[3,c]

[1]Department of Mechanical Engineering, Keio University 3-14-1 Hiyoshi, Kohoku-ku, Yokohama 223-8522, Japan
[a]ryo-kanasashi@keio.jp, [b]yuya_tanaka@keio.jp, [c]sawada@mech.keio.ac.jp

1. Introduction

MR (Magneto-Rheological) fluid consists of micrometer-scale magnetic particles, surfactant and a carrier fluid such as hydrocarbon oil. MR fluid is a magnetic functional fluid in which magnetic particles gather and form clustering structures when external magnetic field is applied. We need more force to yield the clustering structure, so viscosity and yield stress increases as a whole fluid. By taking advantage of this characteristics, MR fluid is applied to the absorber and dumper. However, the mechanism of formation of the clustering structures is not fully discovered because MR fluid is opaque. Since the ultrasonic propagation velocity is faster when it propagates in the clusters, we can make a quantitative analysis on the clusters in MR fluid by measuring the ultrasonic propagation velocity. In this study, we analyze how the formation of the clustering structures differs depending on sweep rate of the magnetic field. Sweep rate is a parameter which shows how fast we apply external magnetic field on the MR fluid. Bramantya et al. [1] measured ultrasonic propagation velocity for different sweep rates in DC magnetic field. Fujita et al. [2] examined characteristics of MR fluid under the effect of external AC magnetic field. We measured the ultrasonic propagation velocity for different sweep rates in both DC and AC magnetic fields.

2. Experiment

Figure 1 shows the experimental apparatus. The change rate of the ultrasonic propagation velocity $\Delta V/V_0$ is calculated by the following equation.

$$\frac{\Delta V}{V_0} = \frac{V - V_0}{V_0} = \frac{L/T - L/T_0}{L/T_0} = \frac{T_0 - T}{T_0} \tag{1}$$

where V_0 and V are initial ultrasonic propagation velocity without and with magnetic field, respectively. L is the ultrasonic propagation length, and T_0 and T are the ultrasonic propagation time without and with magnetic field, respectively.

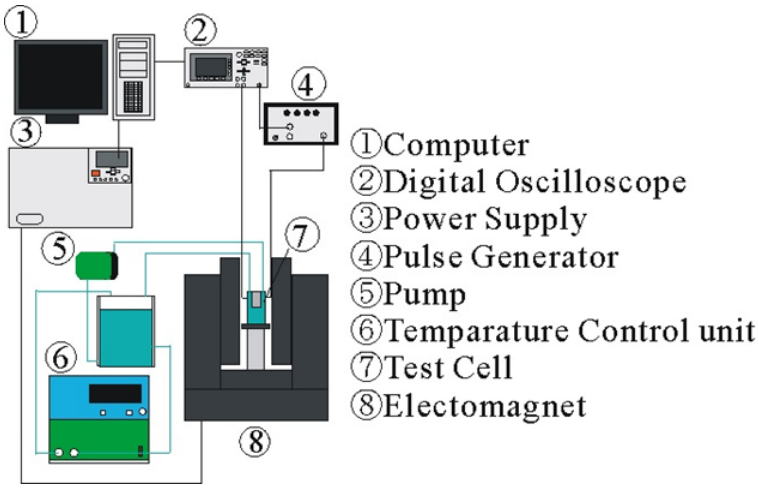

Fig. 1 Experimental apparatus

3. Experimental Results

The change rate of the ultrasonic propagation velocity increases with the magnetic field intensity. Figures 2 and 3 show the time-dependent change rate of the ultrasonic propagation velocity when DC and AC magnetic field intensity increases gradually. B_{dc} is the intensity of the DC magnetic field. B_{ac} and f are the root mean squared value of the AC magnetic field intensity and the frequency

of the AC magnetic field, respectively. Increase of the ultrasonic propagation velocity changes is delayed in comparison with the increase of the magnetic field intensity for both DC and AC fields. This delay is connected with cluster formation of magnetic particles.

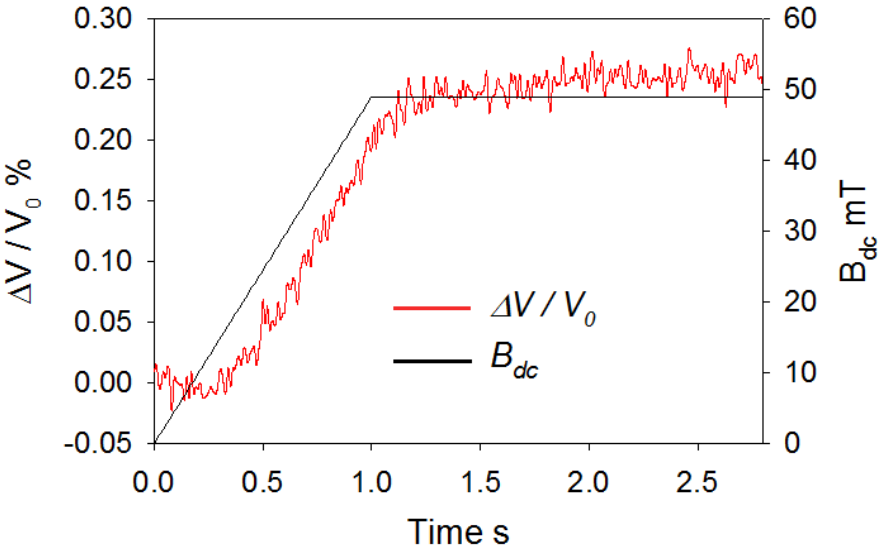

Fig.2. Change rate of the ultrasonic propagation velocity under DC magnetic field

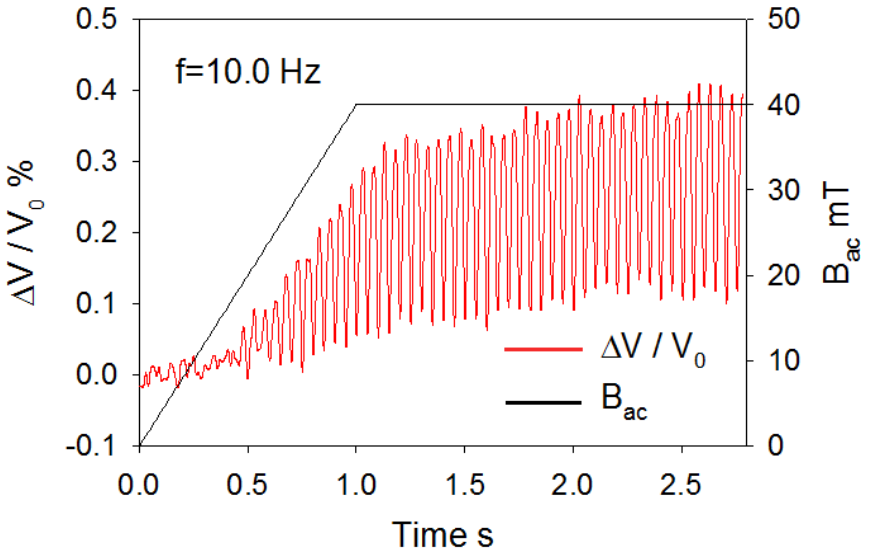

Fig.3. Change rate of the ultrasonic propagation velocity under AC magnetic field

References

[1] Bramantya M.A., et al., "The influence of magnetic field swept rate on the ultrasonic propagation velocity of magnetorheological fluids". Journal of Magnetism and Magnetic Materials, vol. 323 (2011), pp. 1330-1333.

[2] Fujita Y., et al., "Ultrasonic propagation characteristics of a magnetic fluid under AC magnetic fields". International Journal of Applied Electromagnetics and Mechanics, vol. 45 (2014), pp. 667-673.